DEVELOPMENT OF NOVEL PROXIMAL TUBULE *IN VITRO* MODELS TO PREDICT DRUG-INDUCED NEPHROTOXICITY

Thesis submitted in accordance with the requirements of the University of Liverpool for the degree of Doctor of Philosophy

By

Agnès Tort Piella

May 2016

DECLARATION

This thesis is the result of my own work. The material contained within this thesis has not been presented, nor is currently being presented, either wholly or in part for any other degree or qualification.

Agnès Tort

This research was carried out in the Department of Pharmacology and Therapeutics, The University of Liverpool, UK in collaboration with the NephroTools FP7 Marie Curie Initial Training Network.

CONTENTS

ABSTRACT

Drug-induced nephrotoxicity is a dose limiting factor and a common side effect of many drugs such as antibiotics, cancer chemotherapeutics or diagnostic agents and represents 20 – 25% of all cases of acute kidney injury (AKI). Due to a lack of representative animal models and metabolically competent renal cell lines, only 10.5% of the drug-induced nephrotoxicity cases can be predicted in preclinical studies. Furthermore, it has been recently accepted that mitochondria represent an important target for a broad spectrum of renal toxins. However, the supraphysiological glucose concentrations used in many culture conditions favour an energetic metabolic change known as the Crabtree effect, based on using glycolysis as the main route for ATP production and hence producing cell lines highly resistant to mitochondrial impairment. Therefore, there is a need for better physiologically-based renal *in vitro* models that can better assess drug-induced nephrotoxicity.

Conditionally immortalised proximal tubule epithelial cells (ciPTECs) had been previously postulated as a novel renal model with good transporter expression that could produce reliable nephrotoxicity data for pharmacological studies. In order to confirm the applicability of the received ciPTECs for further drug transporter and toxicity studies, the transporter expression was assessed and compared with other cell lines such as HEK 293 cells as well as isolated cells from a proximal tubule (PT) fraction. The functionality of some transporters that are crucial in drug-induced nephrotoxicity such as megalin, MRP2, MRP4 and P-gp were assessed via CMFDA accumulation. Data revealed a very close mRNA expression of ciPTECs compared to the PT fraction and better transporter functionality than HEK 293 cells. Therefore, it was confirmed that ciPTECs hold the necessary transporter functionality to be a valuable nephrotoxicity model.

The Crabtree effect had been previously circumvented in other cell lines by replacing glucose for galactose in the medium for 8 weeks. As a result, cells became highly aerobically dependant and more susceptible to mitotoxins. A recently developed strategy with only a 4 h pre-incubation period in galactose conditions was implemented in ciPTECs. As hypothesised, ciPTECs cultured in galactose medium displayed a significant upregulation of mitochondrial OXPHOS compared to glucose-grown cells, which caused a higher susceptibility in front of mitotoxins (rotenone EC_{50}ATPglu / EC_{50}ATPgal > 3125, $p < 0.001$ and antimycin A EC_{50}ATPglu / EC_{50}ATPgal > 14925, $p < 0.001$). Furthermore, when exposed to adefovir, a postulated mitotoxin in the clinic, galactose-cultured ciPTECs showed a significantly lower EC_{50} (EC_{50}ATPglu / EC_{50} ATPgal > 6.12, $p = 0.0049$, 3 days). Tenofovir (TFV), a lower toxic analogue of adefovir, was also submitted to the glucose *vs.* galactose model ATP depletion did not reach 50%.

Causes of mitochondrial dysfunction are variable but they all eventually trigger a perturbation of the respiratory parameters. Hence, to further explore the molecular mechanisms behind adefovir and TFV mitochondrial toxicity, ciPTECs bioenergetics were interrogated. After a 24 h adefovir exposure, a decrease in oxygen consumption linked to ATP production was detected as well as a 40% reduction of the coupling efficiency at 100 µM. Electron transport chain (ETC) complexes were also quantified and results revealed a depletion of complex I (45%) and complex IV (20%). These are the only two complexes with an important mtDNA encoded core. Furthermore, reactive oxygen species (ROS) levels increased 2 fold after adefovir exposure (48 h). In conclusion, these data evidenced that adefovir targets either mitochondrial RNA or protein synthesis, impeding a correct protein assembling of ETC complexes and therefore hampering cell respiration. However, other factors such as ROS might also play an important role. No decrease in oxygen consumption

was detected after ciPTECs were exposed to TFV for 15 days. In contrast, a dose-dependent increase in extracellular acidification rate (ECAR) was observed, which could be an initial sign of mitochondrial dysfunction.

Although ciPTECs exhibit most of the necessary features to investigate nephrotoxicity such as good transporter expression, they cannot take into account different people's pharmacokinetics or transporter polymorphisms that alter drug-induced toxicity. In contrast, urine-derived progenitor cells (UPCs) represent a non-invasive and limitless source of kidney cells that could be differentiated into PT cells. Even though the PT-differentiation was not fully achieved, we successfully isolated three colonies of UPCs that reached passaged 10 with similar clonogenicity values to cancer cell lines (31%) at the exponential growth phase. Therefore, if the differentiation process could be optimised, urine-derived cells could have the potential to be used as a patient-specific nephrotoxicity model as well as being applied in personalised medicine and regenerative studies.

In summary, the data presented in this thesis demonstrate that drug-induced mitochondrial dysfunction responsible for nephrotoxic events can be detected using the ciPTECs glucose *vs*. galactose *in vitro* model. Furthermore, in addition of screening for mitotoxic compounds, it has been shown that the model can also be used as a tool to investigate the molecular events preceding adefovir toxicity as well as other undisclosed mitotoxicities. Finally, the work undertaken has also demonstrated that UPCs and PT-differentiated UPCs hold promising answers to tackle and prevent drug-induced nephrotoxicity.

ACKNOWLEDGEMENTS

I would like to start thanking my supervisors Dan and Trish for giving me the opportunity to undertake a PhD and trusting me as a candidate. Thank you Dan for encouraging me throughout the whole project, giving me confidence and make me grow as a scientist. I would also like to thank the NephroTools Marie Curie Initial Training Network for the funding, training and incredible experience.

When I look back at this challenging 4-year journey, I not only see the ups and downs of PhD life, but mainly I see all the incredible people I have met along the way.

To my initial office team - Bhav, Jack, Oisín, James and Luke. Thank you guys for welcoming me, teaching me valuable lessons about weird facts and developing my hearing for a northern accent. Gosh understanding you guys was hard! Thanks for the patience.

I don't want to brag but, my girls, you are the most amazing friends and hottest PhD bunch that anyone could have ever asked for. Abby, Áine, Ali, Alix, Amy, Fiazia, Harriet, Holly, Jo, Liz, Nathalie, Pika and Sophie you became my Liverpool family. Holly, what would I have done without you? Thank you for being there in the hard times and making the good ones memorable. Harriet, you are the most selfless, quiet loving thing. Well, not that quiet depending on the subject… You definitely took my slang knowledge to a whole different level! I Nathalie tú tampoc te n'escapes, no sé com t'ho has fet però amb molt poc temps t'has convertit en algú imprescindible. I la millor companya de birres! A final special thanks goes to you Jo, my newfound soulmate. We have laughed, cried, danced and walked together for two solid years. Thank you for understanding me and making me a better person. Not to mention the crazy night outs, I can't keep up with you girl!

A special thank you to my ego-boosters Ross, Darren and Jonny, you are irreplaceable! And I am not forgetting about you Jon, the font of lab knowledge! Thanks for being so kind and supportive. Also, to my gym buddies Andy and Sully, thanks for making me laugh and for the mean (loving) banter! And James, you are just lovely.

Cris, Eva, Febrer, Jud, Serrano i Soler, gràcies per fer-me sentir com si mai hagués marxat. La vostra amistat és un luxe! També vull donar les gràcies als meus pares per creure en mi, recolzar-me i ensenyar-me que puc arribar fins allà on em proposi.

And last but not least, thank you Oriol. Moltes gràcies per la paciència, per fer-me costat quan els experiments surten del revés, compartir els meus moments d'eufòria i creure cegament que jo sempre faig les coses bé!!

I dedicate this thesis to all of you! THANK YOU!

PUBLICATIONS

Papers *(*Joint first author)*

Agnès Tort Piella, Amy E. Chadwick, Rosalinde Masereeuw, B. Kevin Park, Daniel J. Antoine. New mechanistic insights into adefovir and tenofovir toxicity using a galactose cultured conditionally immortalized proximal tubule epithelial cell line as a novel model to screen for mitotoxicity. (*In preparation*)

Agnès Tort Piella, Paul Jennings, Daniel J. Antoine. Integrated novel *in vitro* models and biomarkers for drug-induced kidney injury. Book chapter for Predictive Discovery Toxicology. Wiley and Sons. (*In press*)

Heslop JA*, Hammond TG*, Santeramo I*, **Tort Piella A***, Hopp I, Zhou J, Baty R, Graziano EI, Proto Marco B, Caron A, Sköld P, Andrews PW, Baxter MA, Hay DC, Hamdam J, Sharpe ME, Patel S, Jones DR, Reinhardt J, Danen EH, Ben-David U, Stacey G, Björquist P, Piner J, Mills J, Rowe C, Pellegrini G, Sethu S, Antoine DJ, Cross MJ, Murray P, Williams DP, Kitteringham NR, Goldring CE, Park BK. Concise Review: Workshop Review: Understanding and Assessing the Risks of Stem Cell-based Therapies (2015). Stem Cells Transl Med., 4(4):389-400.

Fanny Oliveira Arcolino*, **Agnès Tort Piella***, Elli Papadimitriou, Benedetta Bussolati, Daniel J. Antonie, Patricia Murray, Lamberthus van den Heuvel, Elena Levtchenko. Human Urine as a Noninvasive Source of Kidney Cells (2015). Stem Cells International, 2015:362562.

ABBREVIATIONS

ABC	ATP-binding cassette
ADP	Adenosine diphosphate
AG	Aminoglycoside
AKI	Acute kidney injury
AQP	Aquaporin
ATP	Adenosine triphosphate
BCA	Bicinchoninic acid
BCRP	Breast cancer resistant protein
BMP	Bone morphogenetic protein
bp	Base pairs
BSA	Albumin
°C	Degrees centigrade
cDNA	Complementary DNA
CKD	Chronic kidney disease
Cl	Chloride
ciPodocytes	Conditionally immortalised podocytes
ciPTECs	Conditionally immortalised proximal tubule epithelial cells
CMFDA	Carboxy dimethyl fluorescein diacetate
CO_2	Carbon dioxide
CSA	Cyclosporine A
Cu	Copper
Da	Dalton
DFBS	Dialysed FBS
DHE	Dihydroethidium
dH_2O	Distilled water
DMEM	Dulbecco's modified eagle medium
DMSO	Dimethyl sulfoxide
DNA	Deoxyribonucleic acid
dNTP	Deoxynucleotide
EC_{50}	Half maximal effective concentration
ECAR	Extracellular acidification rate
ECL	Electrochemiluminescence reagent
ECM	Extracellular matrix
EDTA	Ethylenediamineteraacetic acid
EGF	Epidermal growth factor
ETC	Electron transport chain
FACS	Fluorescence-activated cell sorting
FAD	Flavin adenine dinucleotide
FBS	Fetal bovine serum

FCCP	Carbonyl cyanide-4-phenylhydrazone
FITC	Fluorescein isothiocyanate
GFR	Glomerular filtration rate
GTP	Guanosine triphosphate
G418	Geneticin
h	Hour
H^+	Proton
HEK	Human embryonic kidney
HIV	Human immunodeficiency virus
HK	Human kidney
HMG-CoA	Hydroxymethylglutaryl coenzyme A
H_2O	Water
hTERT	Human telomerase reverse transcriptase
IC_{50}	Half maximal inhibitory concentration
ICC	Immunocytochemistry
IF	Immunofluorescence
Ig	Immunoglobulin
IMM	Inner mitochondrial membrane
iPSCs	Induced pluripotent stem cells
ITS	Insulin-transferrin-sodium selenite
K^+	Potassium ion
Kb	Kilobases
kDa	Kilodalton
KSPCs	Kidney stem/progenitor cells
LDH	Lactate dehydrogenase
L-glut	L-glutamine
LLC-PK_1	Proximal-like pig kidney
M	Molar
µCi	Microcurie
MeOH	Methanol
MDCK	Renal distal-like dog kidney
mg	Milligrams
µg	Micrograms
mL	Millilitres
µL	Microlitres
mM	Millimolar
mm	Milimeters
µM	Micromolar
mRNA	Messenger ribonucleic acid
mtDNA	Mitochondrial DNA
mV	Millivolts

Na	Sodium
NAD	Nicotinamide adenine dinucleotide
nDNA	Nuclear DNA
ng	Nanograms
nm	Nanometers
NMR	Non-mitochondrial respiration
NTP	Nucleoside triphosphate
NRTIs	Nucleoside reverse transcriptase inhibitors
NtRTIs	Nucleotide reverse transcriptase inhibitors
O_2	Oxygen
OAT	Organic anion transporter
OCR	Oxygen consumption rate
OCT	Organic cation transporter
OK	Opossum kidney
OMM	Outer mitochondrial membrane
O/N	Overnight
OXPHOS	Oxidative phosphorylation
p	Probability
PBS	Phosphate buffered saline
PCR	Polymerase chain reaction
PFA	Paraformaldehyde
pg	Picograms
P-gp	P-glycoprotein
Pi	Phosphate
pmol	Picomols
PPARα	Peroxisome proliferator-activated receptor –alpha
PT	Proximal tubule
Pyr	Pyruvate
qPCR	Quantitative PCR
RAP	Receptor-associated protein
REGM	Renal epithelial growth medium
RIPA	Radioimmunoprecipitation assay
RNA	Ribonucleic acid
RPTEC	Renal proximal tubule epithelial cell
ROS	Reactive oxygen species
RT	Room temperature
SCID	Severe combined immunodeficiency
SD	Standard deviation
sec	Seconds
SEM	Standard error of the mean
SLC	Solute carrier

SV40T	Simvian virus 40 T antigen
TBS	Tris-buffered saline
TERT1	Telomerase reverse transcriptase
TFV	Tenofovir
T_M	Melting temperature
UPCs	Urine-derived progenitor cells
UPK	Uroplakin
USCs	Urine-derived stem cells
UV	Ultraviolet
V	Volts
v/v	Volume/volume
ZO	Zona occludens

CHAPTER ONE

General Introduction

CONTENTS

1.1 THE KIDNEY

1.1.1 Structure and function

The mammalian urinary apparatus is composed of two kidneys, which are connected to the ureters, bladder and urethra. A single mammalian kidney is a bean-shaped organ with a concave renal hilum, where blood vessels connect and the ureter exits (Deshmukh 2009). The kidney has distinct zones forming a cone shaped renal lobe comprising the cortex at the top widest region, adjoined to the medulla and followed by the papilla at the inner tip (Hebert 2008). The kidney has important homeostatic functions which are essential to maintain the acid-base balance and an adequate blood pressure (Witzgall 2008). Specifically, the kidney receives 20 – 25% of the cardiac output and processes approximately 100 litres of filtrate per day. This filtrate contains high concentrations of metabolites which will ultimately be reabsorbed, leaving only 2 litres of filtrate to be excreted via the urethra as urine daily (Nagai and Takano 2010, Rahmoune et al. 2005).

The basic structural and functional unit of the kidney is the nephron, a tubular-like structure spanning from the cortex to the medulla (Frank 2012). The physiological function of the nephron is to regulate blood entering the kidney by adjusting its water and salt content, volume and pH and the removal of toxins and unwanted substances (Hebert 2008). Remarkably, it is estimated that each human possesses more than 1 million nephrons (Witzgall 2008). A nephron is composed of several structures, each with a specific function including the glomerulus and Bowman's capsule, the proximal tubule (PT), the loop of Henle and the distal tubule which adjoins the collecting duct (Deshmukh 2009), see Figure 1.1 .

The renal corpuscle is the initial section of the nephron, formed by the glomerulus and the Bowman's capsule, filters the blood supply from the renal circulation. The glomerulus is a tuft of capillaries located in the cortex that receives and filters blood from the afferent

arteriole. The fenestrated capillary walls facilitate the passage of molecules of up to 70 kDa (Deshmukh 2009) and pressure is created by the difference in diameter between the afferent arteriole and the narrower efferent arteriole, which can also be hormonally regulated. Collectively, the glomerulus, the basement membrane and the podocytes from Bowman's capsule selectively filter small molecules such as water, ions, low molecular weight proteins, glucose and amino acids whilst excluding blood cells and platelets as well as high molecular weight and anionic proteins (Hebert 2008), producing an ultrafiltrate.

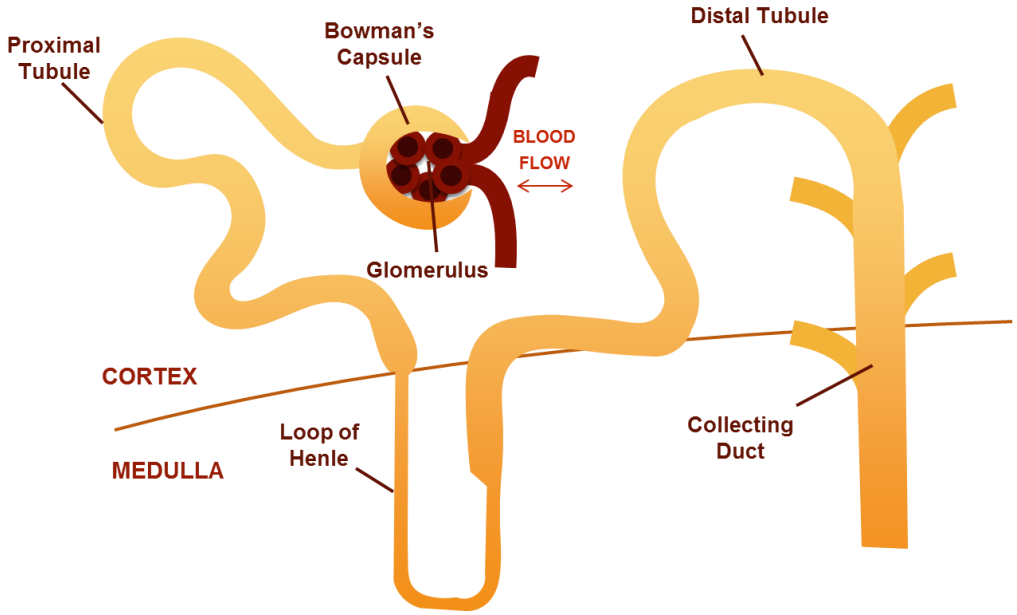

Figure 1.1 Nephron: the basic functional and structural unit of the kidney.
Each nephron is composed of an initial filtering section (formed by the glomerulus and the Bowman's capsule) and a tubule specialized section in reabsorption and secretion of metabolites. The renal tubule is attached to the Bowman's capsule and starts with the PT, followed by the loop of Henle, the distal tubule and finally the collecting duct.

The ultrafiltrate is further processed to produce urine upon entering the PT in the cortex, which has resorptive (glucose, salt, water, proteins) and secretive (creatinine) functions (Deshmukh 2009). The loop of Henle extends into the medulla from the PT and facilitates water and salt exchange. The remaining filtrate enters the distal tubule which mediates the uptake of calcium, phosphate, sodium and potassium from the filtrate (Deshmukh 2009) before it reaches the collecting duct, draining towards the ureter.

1.1.2 Drug-induced nephrotoxicity

Drug-induced nephrotoxicity is a type of kidney injury where functional or structural damage to the organ, pre-renal, intrinsic or post-renal, is caused by exposure to one or several therapeutic agents. It is a common clinical adverse event and, although the true incidence is difficult to determine, US hospital data suggests that drug-induced kidney injury accounts for 18-27% of all acute kidney injury (AKI) cases in the US (Taber and Pasko 2008). This number can rise to 66% in older adults (Nagai and Takano 2010). Some examples of pathogenic mechanisms caused by drugs range from altered intraglomerular hemodynamics, tubular cell toxicity, inflammation, crystal nephropathy and rhabdomyolysis (Naughton 2008).

As drug-induced kidney toxicity is a common side effect amongst many drugs, it is considered an important attrition factor during drug development. Nephrotoxicity accounts for 2% of drug failures in preclinical studies (Jang et al. 2013), however, on moving into clinical trials, this rises to 19%. Such a high fraction of drug-induced renal toxicity in human studies generates concern, and lays the need to improve nephrotoxicity models to better predict the incidence of toxicity at a preclinical stage. A more accurate prediction would decrease AKI prevalence and could reduce hospital interventions (Vaidya et al. 2010) as well as provide a reduction of costs for compounds which trigger nephrotoxicity levels that are considered too high to allow the drug onto the market.

1.1.3 *In vivo vs. in vitro* nephrotoxicity models

Pre-clinical studies are performed in both *in vivo* models, involving animals, and *in vitro* models, which include well-established cell lines. Although variable, animal studies have shown to be a valuable model to predict certain human toxicities produced by pharmaceutical agents. Nevertheless, they have a poor prediction of renal toxicity due to

producing 30% false negatives (Olson et al. 2000). In addition, the animal of choice and the compliance with the 3Rs are crucial detecting truly human hazard. *In vivo* studies are also time consuming, expensive and not suitable for performing mechanistic studies at a molecular level (Table 1.1).

Table 1.1 *In vivo vs. in vitro* models: advantages and disadvantages.

	ADVANTAGES	DISADVANTAGES
In vivo **models**	3D models Definite methodology Highly reliable to predict some toxicities: - Haematological - Gastrointestinal - Cardiovascular	Poor nephrotoxicity prediction (30% false negatives) Ethical regulations (3Rs) Expensive and time consuming Not useful for mechanistic studies at a molecular level
In vitro **models**	No ethical problems Cheaper and quicker than animal models High-throughput analysis Potentially useful for mechanistic studies at a molecular level 3D cultures in development	Experiments can only be conducted using one cell type (mainly) Lack expression of key functions/transporters Spheroids and chip devices are still far from mimicking kidney processes

In *in vitro* models, it is critical to choose the adequate cell line to study the mechanism of interest. As any other organ, the kidney is assembled with different cell types that execute different functions and express different transporters. Altogether, it influences the drug uptake and consequently the toxicity. In particular, the clearance and reabsorption of drugs is primarily conducted in the PT, thus this structure can be subjected to high concentrations of toxic compounds (Naughton 2008, Bonventre et al. 2010). As a result, PT cells are the most affected cells by drug-induced injuries and thus, the cell line of choice to monitor renal drug toxicity (Bonventre et al. 2010). *In vitro* models also offer the opportunity to

perform high through-put drug screening that produce large amounts of data at a molecular level, and are generally cheaper and quicker than carrying out animal studies (see Table 1.1). PT cells are usually seeded in 96 well plates and drug screening is performed. After exposure to the compound, OMICs, kinetic and functional data can be collected and integrated in a cell model to elucidate different nephrotoxicity pathways (Wilmes et al. 2013, Jennings et al. 2012).

In vitro cultures in 2D lack the organ architecture and complexity of the mammalian kidney. Hence, spheroids (Heuser et al. 2003, Buzhor et al. 2011) and renal chip devices (Jang et al. 2013) represent a bridge between the two strategies. In particular due to the fluidic flow the cells are exposed to, chip devices are able to mimic key PT functions (Jang et al. 2013). Despite the expense and bio-complexity of development, they have the potential to recover more sensitive information and provide the ability to study drug-induced nephrotoxicity in preclinical studies. Nevertheless, there is an inverse relationship between through-put analysis and the level of complexity.

1.2 THE PROXIMAL TUBULE

1.2.1 Structure and function

The PT is the region of the nephron between the Bowman's capsule and the loop of Henle. Initially, the PT forms several coils known as *pars convoluta* which are followed by a straight segment known as *pars recta* that descends towards the medulla (Levy et al. 2006). Regarding ultrastructure, three sequential segments can be differentiated named S1, S2 and S3, each of which is characterised by a unique cell type. The *pars convoluta* includes S1 and most of S2. A sudden transition takes place in the upper section of the *pars recta* to S3. Each segment has distinct cellular characteristics such as a longer brush border microvilli in S3 and S1. Moreover, mitochondria in S1 are long and perpendicularly stacked to the cellular axis, and get progressively shorter and more randomly distributed in S2 and S3 (Venkatachalam et al. 1978).

Generally, cells of the PT are characterised by their dense microvilli on the apical surface known as brush border, which increases their surface area to facilitate reabsorption and sense the flow within the lumen (Wang 2006).

The PT reabsorbs approximately 67% of the filtered water, Na^+, Cl^-, K^+ and other solutes (Levy et al. 2006). In addition, the PT is responsible for reabsorbing glucose (Wright 2001), low molecular weight proteins (Maack 1975) and other molecules to restore the plasma balance of these compounds. Essentially, the Na^+/K^+-ATPase located in the basolateral membrane is key in the reabsorption process, as any form of reabsorption, including water, is linked to the operation of this pump (Levy et al. 2006).

Another important function of the PT is the secretion of organic cations and anions. Many of these are secreted as end products of metabolism that circulate in the plasma. Other exogenous organic compounds are also secreted including penicillin and other toxic

chemicals. Many of them are bound to plasma proteins and hence not readily filtered through the glomerulus. Therefore, the PT contains powerful transport systems to remove the organic anions and cations from the plasma to the tubular fluid (Levy et al. 2006).

1.2.2 Transporters of the PT

The PT is the main contributor to endogenous and exogenous xenobiotic elimination due to its large selection of transporter proteins that hold diverse substrate specificities. It is worth noting that whilst transporters of the PT, as well as transporters in general, might possess a broad and overlapping substrate specificity, they may also display different affinities and turnover properties for specific compounds (Lee and Kim 2004). These renal transporters are categorised into families based on their selectivity and molecular properties: organic anion transporters (OATs), organic cation transporters (OCTs) and ATP-binding cassette (ABC) superfamily (Gallegos et al. 2012). Some PT transporters that play a crucial role in

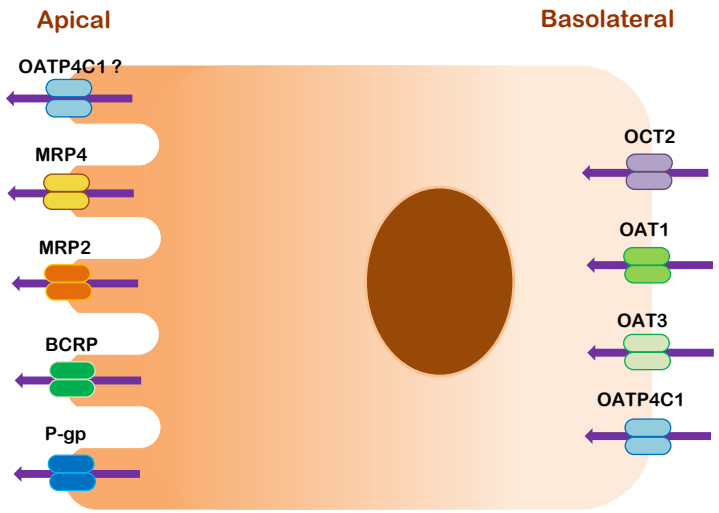

Figure 1.2 Localisation of some PT transporters involved in xenobiotic elimination. OATs and OCTs are located on the basolateral side and in contact with the blood flow. Due to the intracellular negative potential, OATs can only uptake the negatively charged anions through an energy-dependent active transport (Lee and Kim 2004). In contrast, ABC superfamily transporters are found on the apical side and secrete xenobiotic compounds to the tubular lumen.

drug clearance and toxicity are specifically outlined in the next section (see Figure 1.2).

A summary of some important PT transporters can be seen in Table 1.2.

Table 1.2 A selection of transporters of the PT

Transporter (Superfamily)	Site of expression	Substrates	Function	References
MRP2 (ABC)	Apical membrane	Endogenous and xenobiotic organic anion compounds. e.g. Tenofovir (TFV), adefovir, glutathione	- Efflux pump key to cellular protection against drug accumulation - Regulation of drug pharmacokinetics	(International Transporter et al. 2010, Jedlitschky et al. 2006, Russel et al. 2008)
MRP4 (ABC)	Apical membrane	Endogenous and xenobiotic organic anion compounds. e.g. TFV, adefovir, glutathione	- Efflux pump key to cellular protection against drug accumulation - Regulation of drug pharmacokinetics	(International Transporter et al. 2010, Jedlitschky et al. 2006, Russel et al. 2008)
P-gp (ABC)	Apical membrane	Endogenous and xenobiotic organic cation compounds. e.g. Digoxin, doxorubicin, steroids, lipids	- Efflux pump key to cellular protection against drug accumulation - Exerts great influence in drug pharmacokinetics	(Thiebaut et al. 1987, Schinkel and Jonker 2003, International Transporter et al. 2010)
BCRP (ABC)	Apical membrane	Endogenous and xenobiotic organic compounds. e.g. Statins, sulphate conjugates, methotrexate	- Efflux pump key to cellular protection against drug accumulation - Exerts great influence in drug pharmacokinetics	(International Transporter et al. 2010, Vlaming et al. 2009)
OAT1 (Solute carrier (SLC))	Basolateral membrane	Organic anions including many drugs and potential nephrotoxic endogenous compounds. e.g. TFV, adefovir, cidofovir	- Rate-limiting step to clear organic anion drugs and other metabolites from blood - Involved in drug-drug interactions	(International Transporter et al. 2010, Gallegos et al. 2012, Eraly et al. 2006, Sweet et al. 2002)
OAT3 (SLC)	Basolateral membrane	Organic anions including many drugs and potential nephrotoxic endogenous compounds. e.g. TFV, adefovir	- Rate-limiting step to clear organic anion drugs and other metabolites from blood - Involved in drug-drug interactions	(International Transporter et al. 2010, Gallegos et al. 2012, Eraly et al. 2006, Sweet et al. 2002)

OATP4C1 (SLC)	Basolateral (apical?) membrane	Organic anions including many drugs and uremic toxins. e.g. estrone-3-sulfate, digoxin, methotrexate	- Involved in the uptake of anionic oligopeptides and various drugs from blood	(Bleasby et al. 2006, Yamaguchi et al. 2010, Mikkaichi et al. 2004, Kuo et al. 2012).
OCT2 (SLC)	Basolateral membrane	Organic cations and many drugs as around 40% of drugs are cationic at their physiologic pH. e.g. metformin	- Regulates the entrance of endogenous and exogenous organic cations from blood - Involved in drug-drug interactions	(Motohashi et al. 2002, Belzer et al. 2013)
AQP1	Apical and basolateral membranes	Water	- Provides the chief route for proximal nephron water reabsorption - Functions as a water-selective transporting protein that excludes small solutes - Represents more than 25% of membrane proteins	(Nielsen et al. 1999, Ma et al. 1998).

1.2.3 Megalin and cubilin endocytic system

Megalin and cubilin are defined as endocytic receptors with multiligand properties that are co-expressed in the apical membrane of the PT, and play an important role in the receptor-mediated endocytosis of proteins and peptides (Christensen and Birn 2002, Nagai and Takano 2010, Christensen et al. 2009). Specifically, they are fundamental for the reabsorption of albumin (Figure 1.3), which is the most abundant protein in plasma (Cui et al. 1996, Zhai et al. 2000). In healthy adults, the daily glomerular filtration rate is 150-180 litres and therefore the daily filtered load of albumin is in the range of 3300 - 5760 mg (Renal Tubule Albumin Transport, Gekle 2005). Hence, without an efficient recovery system, the human body would eventually face proteinuria. Other ligands include insulin, vitamin D-binding protein, haemoglobin, and epidermal growth factor amongst other important carrier proteins, hormones and enzymes (Christensen et al. 2009). Thus, its

presence in the PT is critical to recover a wide range of proteins and peptides that would otherwise be discarded in the urine. Nonetheless, megalin and cubilin scavenger capabilities are also responsible for the uptake of exogenous substrates such as aminoglycoside antibiotics that, when accumulated in the PT, can induce nephrotoxicity (Nagai and Takano 2010).

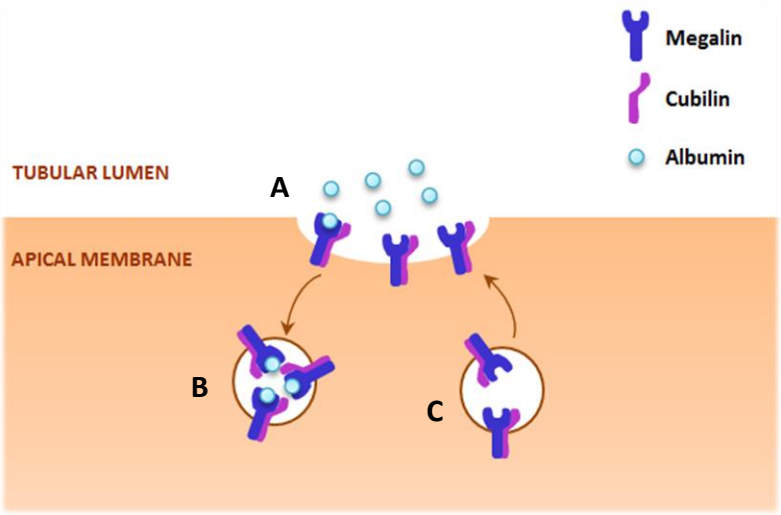

Figure 1.3 Schematic of albumin endocytosis via megalin and cubilin endocytic system. During the process of endocytosis, (A) small invaginations in the plasma membrane are formed that contain cubilin and megalin receptors bound to albumin. The endocytic invaginations detach from the membrane (B) to form endocytic vesicles that will eventually merge with lysosomes. Finally, (C) the receptors are recycled and brought back to the plasma membrane (Gekle 2005).

1.2.4 PT toxicity

The elimination of drugs and their metabolites from the system depends on three developments: glomerular filtration, tubular secretion and tubular reabsorption. (Nagai and Takano 2010). First, the unbound drugs escape from the glomerular filtration barrier and arrive at the PT. This is the main elimination route for most compounds. Additionally , if the drugs are hydrophilic they are uptaken from the blood flow and pass directly to the PT via OATs and OCTs (Inui et al. 2000). In contrast, the drugs already filtered by the glomerulus might be reabsorbed by active transporters or via receptor-mediated

endocytosis from the luminal side of the renal PT, causing an accumulation of potential damaging drugs in this section of the nephron. As a result, drug-induced nephrotoxicity is a significantly important event in the PT, and a limiting factor for the use of several drugs (Nagai and Takano 2010).

1.2.5 Classic PT cell lines

In order to obtain a reliable *in vitro* cell model that can mimic the metabolic and molecular processes in the PT, various cell lines have been developed over the years. These cell lines vary from animal kidney lines with poor transporter expression, to human PT lines that have retained most of their differentiated characteristics. This is due to the development of new isolating and immortalising techniques, and better culture conditions with hormonally supplemented media.

1.2.5.1 Animal PT cell lines

Proximal-like pig kidney (LLC-PK_1) and renal distal-like dog kidney (MDCK) cells are spontaneously transformed animal cell lines that contain a mixture of proximal and distal cells (Gstraunthaler 1985) and have been described to maintain some features typical of the kidney epithelium (Perantoni and Berman 1979). They have been a useful model to assess protein trafficking and heterologous transporter expression (Bens and Vandewalle 2008).

Another important animal *in vitro* model is the opossum kidney (OK) cell line, originally developed to study chromosome X inactivation (Koyama et al. 1978). However, although it originated from the whole kidney, it was later identified to possess typical PT properties (Malstrom et al. 1987). OK cells have been shown to recreate a dome formation and paracellular permeability in culture, typical PT features not found in other animal renal cell

lines such as LLC-PK_1 (Liang et al. 1999). Furthermore, OK cells have been demonstrated to be a valuable PT model to study the functionality of some receptors and transporters. Megalin and cubilin were successfully identified as the receptors responsible for the albumin uptake in OK cells (Olson et al. 2000) and later used to develop a therapeutic strategy to prevent aminoglycoside-induced nephrotoxicity (Antoine et al. 2010) amongst other studies.

Yet, these are animal-derived cell lines and as such they have important variations in pharmacokinetics and pharmacodynamics compared to human cells (Ito 2008). To better predict and understand drug-induced nephrotoxicity, a more translational human PT model is required (Gunness et al. 2010).

1.2.5.2 HEK 293 cells

Human embryonic kidney (designated 293) cells (HEK 293 cells) were derived from exposing a primary HEK cell to sheared fragments of adenovirus type 5 (Graham et al. 1977). The transformation resulted in the incorporation of approximately 4.5 kb from the viral genome into human chromosome 19 of the HEK cells (Louis et al. 1997). Since then, they have been used in a vast number of transfection and recombinant expression studies, due to the high responsiveness and efficiency of transfection via different methods (Thomas and Smart 2005). Furthermore, it has been speculated that HEK 293 cells do not have a kidney origin, but a neuronal one. Particularly, Shaw *et al*. claimed that HEK 293 cells are not typical kidney cells and so cannot be used to study normal kidney-related function. The same study showed that this adenovirus transformed cell line had mRNA constructs and gene products typically found in neurons (Shaw et al. 2002).

Nonetheless, HEK 293 cells have efficiently been used to study drug uptake after the overexpression of PT and other cell transporters through transfection (Biermann et al. 2006, Jong et al. 2011, Qadir et al. 2005).

1.2.5.3 HK-2 cells

In 1994, the first human immortalised PT cell line, human kidney-2 (HK-2), was developed by Ryan MJ *et al.* by infecting primary PT cells from the renal cortex with a human recombinant retrovirus containing the E6/E7 genes of the human papilloma virus. The cell line was described to retain characteristics of well-differentiated PT epithelium, such as staining positive for alkaline phosphatase and Na^+ dependent/phlorizin sensitive sugar transport (Ryan et al. 1994). Further characterisation was performed and it was demonstrated that HK-2 cells were a good model to study drug efflux associated with transporters from the ABC family, since the cell line exhibited expression and functionality of some of its members such as MRP4 or P-gp (Tramonti et al. 2001). However, no expression of BCRP or MRP2 was observed and the presence of drug uptake transporters was defined as limited, with no detectable levels of OAT1, OAT3 and near zero levels of OCT2 (Jenkinson et al. 2012).

In general, despite shedding some insight into drug transport and drug-induced nephrotoxicity (Sohn et al. 2013, Wang et al. 2007, Romiti et al. 2002, Matsui et al. 2013), HK-2 cells poorly predict *in vivo* clinical toxicity, mainly due to a lack of metabolic competence and transporter expression (Jenkinson et al. 2012).

1.2.5.4 Primary isolated cells

In 1998, Pfaller & Gstraunthaler pointed out that primary cultures of fresh isolated cells represented an attractive alternative to study long-term effects of nephrotoxins. Compared to their immortalised counterparts, they possess an optimum level of differentiation and

express the key functions and transport systems, such as gluconeogenesis and OATs. Nevertheless, on top of being time-consuming to develop, these cultures had a limited life span (days to weeks) and tended to suffer a quick loss of their *in vivo* metabolic properties in culture (Pfaller and Gstraunthaler 1998). However, despite of their disadvantages, when a good availability of kidney tissue is attainable, some research groups can afford to perform *in vitro* studies in primary PT cells. Their large array of transporters associated with major classes of important drugs is crucial in studying drug transport and drug-induced nephrotoxicity (Brown et al. 2008, Lash et al. 2006).

1.2.6 Newly immortalised PT cell lines

Although prior attempts to immortalise PT cells have been made (Kowolik et al. 2004, Orosz et al. 2004, Ryan et al. 1994), currently RPTEC/TERT1 (renal PT epithelial cells immortalised by the human telomerase reverse transcriptase (hTERT)) (Wieser et al. 2008) and ciPTECs (a conditionally immortalised PT epithelial cell line by hTERT and the simian virus 40 T antigen (SV40T)) (Wilmer et al. 2010) are considered superior options when assessing drug-induced nephrotoxicity *in vitro* due to their greater level of xenobiotic transporters, compared to alternative renal lines, and other typical markers of PT cells. Both cell lines have the advantages of being able to continuously grow with a high differentiation status, expressing endogenous receptors and transporters that mimic renal developments. As a result, they are considered a powerful tool for compound transport studies in pharmacology and physiology, as well as for drug screening and toxicology (Wieser et al. 2008, Wilmer et al. 2010, Gorvin et al. 2013).

1.2.6.1 RPTEC/TERT1 cell line

RPTEC/TERT1 cells are a commercially available cell line developed by Weiser *et al*. in collaboration with Evercyte in 2008. Initially, RPTECs cells were isolated from a kidney

biopsy and split once before being infected with retroviral particles encoding the essential catalytic subunit of telomerase (hTERT). A resistance cassette for geneticin (G418) was also encoded, which is essential to select for positive transfectants. The immortalisation procedure is explained in detail in Figure 1.4.

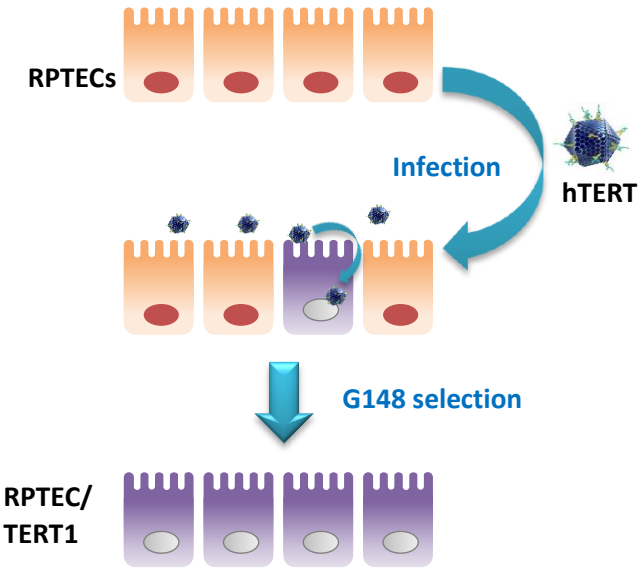

Figure 1.4 RPTEC/TERT1 cell line immortalisation procedure.
Primary RPTECs from kidney tissue were infected with retroviral particles containing hTERT-coding cDNA and a resistance cassette to G418. After 24 h of infection, cells were passaged and cultured in a medium containing G418. Therefore, only the clones resistant to the antibiotic, and as a consequence also transfected with hTERT, were selected.

Weiser *et al*. demonstrated that hTERT transfection was sufficient to circumvent replicative senescence and avoid terminal growth arrest as well as DNA damage linked to senescence. RPTEC/TERT1 cells gained the ability to grow up to 70 population doublings without slowing down cell division. Importantly, they exhibited comparable excretory capacity to primary RPTECs, and better expression of transporting systems than HK-2 cells. A typical PT morphology was also observed, including microvilli, solitary cilia, tight junctions and domes. Furthermore, intact sodium-dependant phosphate uptake and a functional megalin/cubilin transport system were confirmed (Wieser et al. 2008).

1.2.6.2 ciPTECs

ciPTECs were established by transfecting RPTECs isolated from the urine of a healthy volunteer. The PT origin of the collected cells was first confirmed by cell morphology and typical transporter activity characteristic of that region of the nephron. In this case, the immortalisation procedure was much more elaborate. Following the same procedure carried out by Saleem *et al*. to immortalise podocytes, two temperature-sensitive mutants of the hTERT and SV40 large T antigen (SV40T) were used to transfect the cells using viral vectors (see Figure 1.5). While hTERT expression enables the continuous elongation of the telomeres, SV40T expression promotes cell division (Saleem et al. 2002). However, since the promoters of both genes were temperature-sensitive, their expression is restricted to the permissive low temperature of 33°C. Therefore, the subcloning and further culture of these cells is performed at 33°C and they are only transferred to 37°C to inactivate gene expression, and induce cell differentiation (Wilmer et al. 2010).

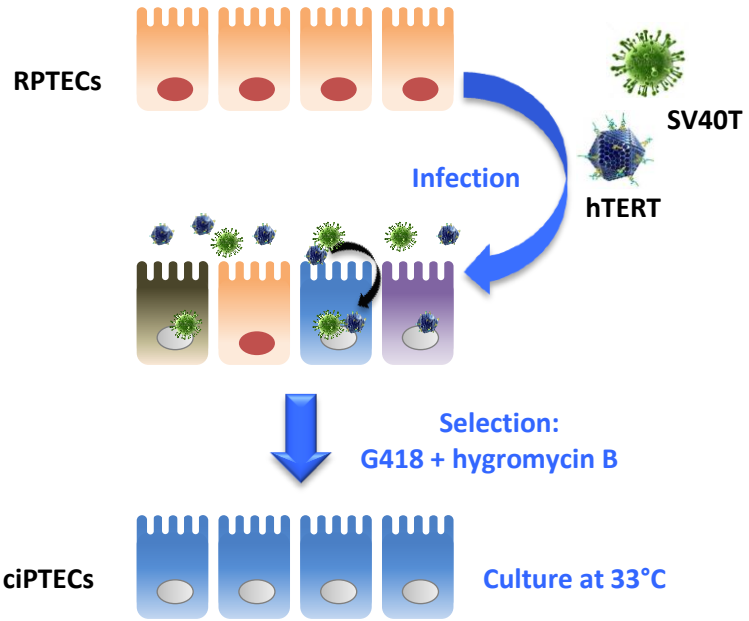

Figure 1.5 ciPTECs immortalisation procedure.
RPTECs collected from urine were infected with retroviral vectors containing hTERT and SV40T-coding cDNA plus a resistance cassette to G418 and hygromycin B respectively. After 24 h of infection, cells were passaged and cultured in a medium containing G418 and hygromycin B for 10 days. Therefore, only the clones resistant to both antibiotics, and as a consequence also transfected with both hTERT and SV40T, were selected.

After immortalisation, further characterisation was performed to verify that the DNA insertion into the genome had not modified the cell phenotype. Expression of CD13, ZO-1 and AQP1 was detected using antibody labelling techniques. The presence and/or absence of AQP1 was decisive in confirming that no other cell types, such as distal tubule cells, had been immortalised, as it is a PT specific transporter (Nielsen et al. 1999). Wilmer *et al.* also demonstrated that ciPTECs had a maintained expression of PT transporters involved in xenobiotic excretion and metabolite reabsorption for up to 45 passages. Specifically, they claimed to have developed the first human cell line to express active MRP4 combined with OCT2 and P-gp. In addition, despite being unable to provide evidence of the presence of the multi-ligand receptor megalin via western blotting or immunofluorescence (IF), they showed albumin uptake, competitive albumin uptake inhibition using non-labelled albumin and non-competitive inhibition using a receptor-associated protein (RAP), an inhibitor of prenylated GTP-binding proteins such as megalin (Ranghini et al. 2013). Other functional assays verified the activity of the sodium-dependent transporters NaPi-II and NaPi-IIc. The experiments were performed after 10 days maturation at 37°C. After this period, the expression of the oncogenes had completely ceased and hence, the influence of the transfection on cellular metabolism was minimised (Wilmer et al. 2010).

Shortly after the creation of the first ciPTEC line, another line was developed from patients with cystinosis, an autosomal-recessive disorder that produces an abnormal accumulation of the amino acid cysteine in the lysosomes. Therefore, providing the opportunity to investigate in detail the cell metabolic changes involved in the pathogenesis of cystinosis (Wilmer et al. 2011, Peeters et al. 2011).

1.3 RENAL MITOCHONDRIAL TOXICITY

1.3.1 Structure and morphology of the mitochondrion

Mitochondria range from 0.5 to 1 µm in size and are composed of two organelle compartments. The inner compartment, the mitochondrial matrix, is enclosed by the inner mitochondrial membrane (IMM), an extensively folded membrane in which invaginations are known as cristae. PT cells have a densely packed cristae (Kohler et al. 2009) correlating with the high energy requirements of these cells. However, the density varies for each tissue and cell type as a result of the different roles played by the mitochondria in each case. The outer compartment is known as intermembrane space as it is situated between the IMM and the outer mitochondrial membrane (OMM). This second membrane is smooth and separates the mitochondrion from the cytosol (see Figure 1.6) (Dykens and Will 2008).

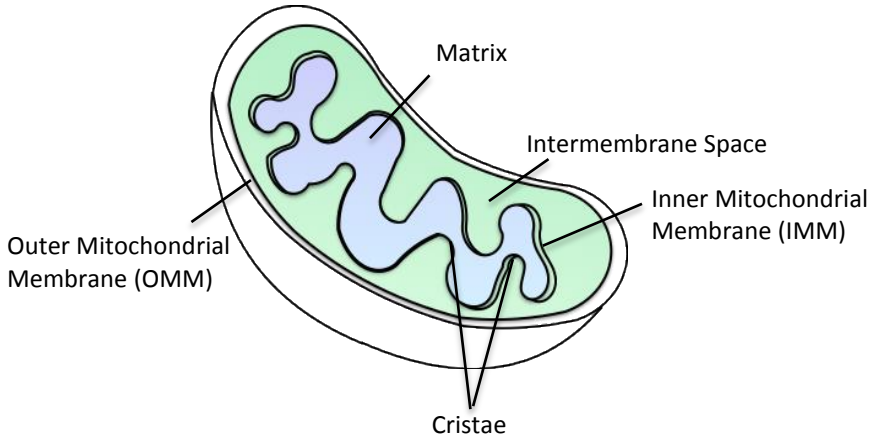

Figure 1.6 Parts of the mitochondrion.
The knowledge of the different parts of the mitochondria and its inner structure was mainly derived from electron microscopy techniques.

Mitochondria are partially autonomous organelles that harbour their own mitochondrial DNA (mtDNA), which is found in the matrix sub-compartment. The mtDNA has a circular shape and encodes 37 genes with few non-coding regions. It is also highly conserved amongst species, which supports the endosymbiotic theory (Dykens and Will 2008). These organelles are also able to replicate their genome independently of cell division thanks to a

self-encoding replication system. Mitochondrial half-life varies from days to weeks depending on the tissue (Dykens and Will 2007). They also have their own RNA and protein synthesizing machinery, but only 1% of their proteins are formed on ribosomes in the mitochondrial matrix and the bulk of mitochondrial proteins are translated in the cytosol and imported into the mitochondria (Endo and Yamano 2009).

1.3.2 Mitochondrial composition and electron transport chain (ETC)

The basic structure of both membranes is a phospholipid bilayer housing transporter proteins and enzymes. The OMM is the only membrane where cholesterol is found, and has a protein-to-phospholipid ratio similar to that of the cell membrane. It also contains a large number of integral membrane proteins known as porins or voltage-dependant anion channels (VDAC) that allow the free passing of compounds up to 5 kDa to the intermembrane space. As a result, the composition of the intermembrane compartment has a high similarity to the cytosol regarding low-molecular weight particles. However, the majority of these molecules cannot go through the impermeable IMM and reach the matrix, which only contains a highly selected set of molecules. The IMM is highly specialised, and it contains cardiolipin in high proportions, which contributes to the membranes impermeability to ions. Finally, the machinery responsible for energy production, the main mitochondrial function in the PT, is also found in the IMM. This machinery is composed by the entire ETC including the ATP synthase complex (see Figure 1.7). In operational normal conditions, the respiratory chain pumps protons to the intermembrane space creating a voltage gradient on both sides (membrane potential) ranging up to 180 mV (Dykens and Will 2007, Alberts B 2002) .

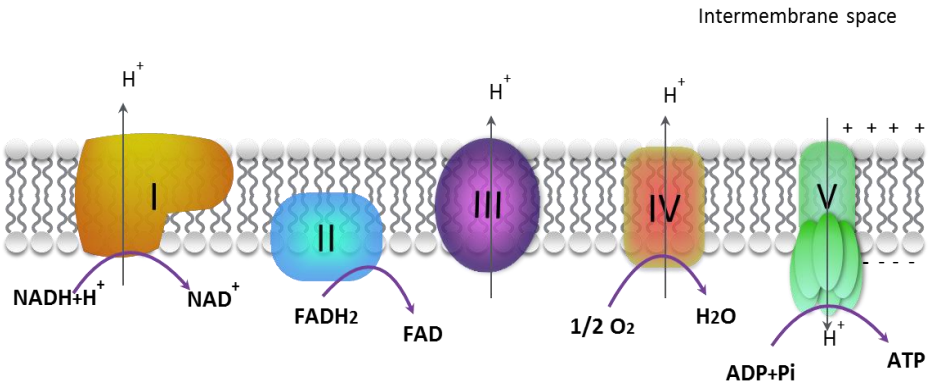

Figure1.7 Schematic of the ETC electron transfer.
The ETC or mitochondrial respiratory chain catalyses electron transfer from the reduced donors NADH (nicotinamide adenine dinucleotide) and $FADH_2$ (flavin adenine dinucleotide) to molecular oxygen (O_2) from complex I to complex IV. The final product of this pathway is water (H_2O). The energy derived from this process is used to pump protons (H^+) across the IMM towards the intermembrane space, creating a membrane potential. This membrane potential eventually drives H^+ through the ATP synthase (complex V), generating ATP from ADP and becoming the driving force of ATP production (Dykens and Will 2008).

1.3.3 Distribution of the mitochondria

These organelles form a mitochondrial network, and can be observed forming elongated threads when cells are transfected with a mitochondrial-targeted green fluorescent protein (Benard et al. 2007, Rossignol et al. 2004). Particularly, in the PT they are arranged forming a striated basolateral distribution (Hall et al. 2009). Nonetheless, it is not a static network and mitochondria are in continuous movement, migrating throughout the cell, constantly splitting and fusing with each other. These dynamics allow the mitochondrial recruitment to different cell compartments, a communication between mitochondria and cytosol, mitochondrial content exchange and mitochondrial quality control. As a result, fission and fusion mechanisms are highly regulated and essential to maintain a healthy mitochondrial population by quickly adapting to changes in cellular requirements, triggered by physiological needs (Chen and Chan 2009).

1.3.4 Mitochondria in the PT

Mitochondria consume 98% of the O_2 taken in by the human body and have been described as the "powerhouse of the cell" due to their prime role in cellular bioenergetics (producing >90% of the cell energy) (Duchen 2004). Mitochondria are also involved in calcium signalling, regulation of cell death pathways, generation of reactive oxygen species (ROS) and the regulation of intracellular pH and redox state (Hall et al. 2009). In the PT, the mitochondria represent 33% of the volume in cells from the S1 segment, 39% in cells from the S2 segment and 22% in cells from the S3 segment. Along the segments, S1 and S2 have a different cell metabolism compared to other parts of the nephron, which are characterised by the complete absence of glycolysis (Weinberg and Molitoris 2009). This dependence on aerobic metabolism for energy supply is believed to be the main reason of PT high vulnerability to mitochondrial dysfunction from a wide variety of insults such as xenobiotic toxicity (*e.g.*, antiretroviral drugs) (Hall et al. 2009, Izzedine et al. 2005). Only S3, although to a lower extent than distal tubules, can contribute to ATP production through glycolysis when there is an impairment in mitochondrial function (Weinberg and Molitoris 2009).

1.3.5 Mitochondria: a drug target

Organ toxicity is one of the main issues jeopardising novel compounds during the pre-clinical stages of drug development, and it is finally now recognised that mitochondrial impairment, as an "off-target" effect of drug exposure, will most likely lead to it (Dykens and Will 2007). As a result, drug-induced mitochondrial toxicity has recently become a focal interest by pharmaceutical companies to increase the probability of survival of a new compound during the process of drug discovery and development (Swiss et al. 2013).

1.3.6 Nucleotide reverse transcriptase inhibitors (NtRTIs) induce PT mitochondrial toxicity

The most aerobically poised tissues or the ones that receive high drug concentrations, such as the kidney, are classically the most affected by mitochondrial impairment. In particular, the PT is the main section affected by drug accumulation and therefore, mitochondrial dysfunction will be of a greater concern in this area. Moreover, PT cells have an extensive mitochondrial density that is fundamental to satisfy their elevated energy demand, as well as a limited capacity to generate ATP anaerobically (Bagnasco et al. 1985). Consequently, mitochondrial impairment will highly distress the PT cell metabolism and trigger nephrotoxicity.

For known renal toxins such as cisplatin, gentamicin, tobramycin, cyclosporine A or ifosfamide, the mitochondria has been shown to play a role in their mechanism of toxicity (Servais et al. 2008, Lopez-Novoa et al. 2011, Yao et al. 2007). However, only in specific compounds such as nucleoside and nucleotide reverse transcriptase inhibitors (NRTIs and NtRTIs) the mitochondria appear to be the primary target (Tanji et al. 2001, Herlitz et al. 2010). Interestingly, it was not until the release of these compounds onto the market that drug-induced mitochondrial dysfunction as the main cause for organ toxicity was accepted (Dykens and Will 2007).

Combinations of NRTIs and NtRTIs have been used for many years in the treatment of human immunodeficiency virus (HIV), with the name of highly active antiretroviral therapy (HAART), causing mitochondrial toxicity as an adverse effect (Kakuda 2000). Many NRTIs are known to inhibit the polymerase that replicates mtDNA (polymerase-γ), hence impeding mitochondrial replication and reducing mitochondrial function (Dykens and Will 2007). However, the mitotoxic pathogenic mechanism for the NtRTIs adefovir and tenofovir (TFV) (see Figure 1.8) remains to be elucidated.

1.3.6.1 Adefovir

Adefovir dipivoxil, the oral prodrug of adefovir, was the first NtRTI drug of its class, and was initially developed to treat HIV. However, its elevated nephrotoxicity halted the approval of this drug for this indication (Valle and Haragsim 2006). The incidence in adefovir PT toxicity

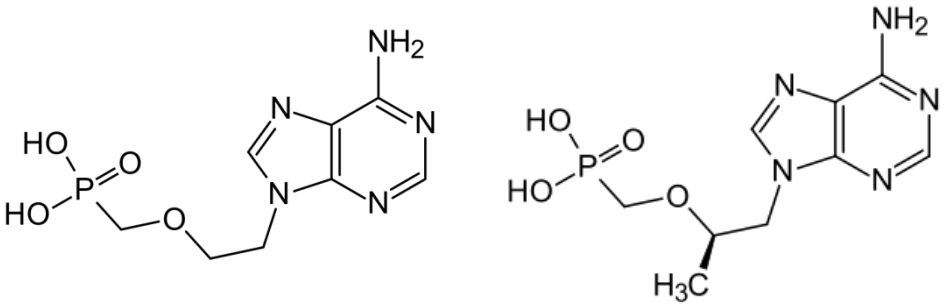

Adefovir **TFV**

Figure 1.8 Chemical structure of adefovir and TFV.
TFV and adefovir are two NtRTIs described to induce mitochondrial toxicity. Adefovir is a non-chiral adenine derivative while the stereochemistry of its lower toxic acyclic nucleotide analogue TFV is crucial for its activity (De Clercq and Holy 2005).

ranged from 27 – 50%, and was the most important dose-limiting toxicity in patients with HIV (Izzedine et al. 2005). Nevertheless, it has been used since 2002 as a retroviral therapy against Hepatitis B in highly controlled doses (De Clercq and Holy 2005, Song et al. 2012).

The antiviral mechanism of action relies on the incorporation of one molecule of adefovir at the 3' end of the growing DNA chain to prematurely terminate DNA elongation. Therefore, it serves as a substrate for the reverse transcriptase enzyme. Additionally, as a NtRTI, it only requires two phosphorylations to be converted to its active form (De Clercq and Holy 2005).

The proximal renal tubule is, in fact, the target of high drug concentration as a consequence of active adefovir uptake from circulating blood directly into the basolateral side of PT cells. This transport is, for the most part, dependent on OAT1 uptake (Ho et al. 2000), although

OAT3 has also been shown to be involved in adefovir renal transport, albeit to a lesser extent (Uwai et al. 2007). Adefovir has also been shown to be a substrate for MRP2 and MRP4 transporters, which modulate the excretion of the intact drug molecule to urine (Imaoka et al. 2007). These transporters are located in the apical side of PT cells and are responsible for the transport of anionic compounds into urine (Vigano et al. 2011). Both influx and efflux transporters mediate adefovir accumulation, and therefore nephrotoxicity (Fu et al. 2012).

An *in vivo* study revealed that adefovir causes PT necrosis with enlarged and dysmorphic mitochondria, as well as a loss and disorientation in their cristae. Moreover, they showed a deficiency in cytochrome C oxidase (complex IV of the ETC), which is in part encoded by mtDNA. On the contrary, no deficiency was observed in succinate dehydrogenase (complex II of the ETC), which is entirely encoded by nuclear DNA (Valle and Haragsim 2006). Therefore, it was suggested that adefovir induced nephrotoxicity via an inhibition of the mitochondrial DNA replication, hence polymerase-γ (Tanji et al. 2001). However, this study was highly criticised as it was performed on kidney biopsies from a single patient on multiple medications including staduvine and hydorxyurea, which are known to cause mitochondrial toxicity and impairment of tubular function respectively (Bendele and Richardson 2002). In conclusion, adefovir nephrotoxicity mechanisms remain undisclosed although evidence suggests that renal tubule transporters, apoptosis and/or mitochondrial toxicity in the PT may be involved (Vigano et al. 2011).

1.3.6.2 TFV

One of the most extensively used NtRTIs for HIV-1 (human immunodeficiency virus 1) is tenofovir disoproxil fumarate (TDF) (Herlitz et al. 2010), which is the oral prodrug of TFV. Despite nephrotoxicity being a rare complication (0.02% incidence) (Izzedine et al. 2005), several studies have described PT toxicity with significant loss of kidney function with long

term TFV exposure (Cooper et al. 2011, Hall et al. 2011, Herlitz et al. 2010). Fanconi syndrome has also been described in some severe cases with a general incidence of <1% (Hall 2013).

As described for adefovir, TFV mechanism of action is also based on early termination of retrotranscription, via the incorporation of one molecule of TFV at the 3' end of the growing DNA chain (De Clercq and Holy 2005).

The basolateral uptake of TFV is also regulated by OAT1 and OAT3, with OAT1 playing a quantitatively crucial role (Uwai et al. 2007). Subsequently, the efflux of TFV from the PT to the lumen is mediated by the apical membrane transporters MRP4 (Ray et al. 2006) and MRP2 (Rodriguez-Novoa et al. 2010).

TFV nephrotoxicity is dose-dependent and characterised by reversible acute tubular necrosis that reveals swollen and misshapen mitochondria when renal biopsies are analysed by electron microscopy (Herlitz et al. 2010). Whilst severe PT toxicity with detectable changes in glomerular filtration rate (GFR) is relatively uncommon, sub-clinical PT dysfunction with no GFR abnormalities has a prevalence that could be greater than 20%. However, the pathogenic mechanism by which TFV causes PT dysfunction remains to be elucidated (Hall 2013). Two possible mechanisms have been postulated but definitive conclusions are yet to be established. Animal studies support that mitochondrial injury is the primary mechanism of TFV-induced tubular damage (Kohler et al. 2009). It was first suggested that TFV could act as a weak inhibitor of mtDNA synthesis. Despite being able to induce mitochondrial toxicity in a similar way to adefovir or cidofovir, the potential to interfere with mitochondrial function is low (Rodriguez-Novoa et al. 2010, Cihlar et al. 2002). The second mechanism proposes that TFV could interfere with the normal function of transporter proteins such as MRP2/4 and trigger a reduced efflux of TFV and other toxic

compounds, which would eventually accumulate and cause cell damage (Rodriguez-Novoa et al. 2010).

1.4 URINE AS A SOURCE OF KIDNEY CELLS

Given the massive tubular network present in the kidney, it could be anticipated that cells could be detached and detected in urine. In fact, it is calculated that approximately 5×10^5 – 35×10^5 cells are dissociated from the renal system daily and can be collected in urine (Linder 1976). The first successful attempt to culture exfoliated epithelial-like cells from urine was carried out by Sutherland and Bain, who established cell cultures from neonatal urine (Sutherland and Bain 1972). Since then, numerous research groups have been able to reproduce this and have established renal cultures of different cell types from newborn babies, infants and adults (Linder 1976, Felix et al. 1980, Racusen et al. 1991, Dorrenhaus et al. 2000, Zhang et al. 2008, Wilmer et al. 2010). Hence, urine represents a limitless source of cells that have brought and will continue to bring new insights into renal toxicity and development.

1.4.1 Initial urine cell classification *vs.* today

Urine contains exfoliated cells from different sources of the renal system, starting from the kidneys, following with the ureter, bladder and finally urethra (Dorrenhaus et al. 2000). However not all these cells are viable, with many already degenerating and thus do not form attach with the surface when placed in culture (Felix et al. 1980). Cells were initially classified in two categories depending on their morphology. Type I cells were defined as randomly arranged and with irregular edges, whereas type II cells were characterised by smooth-edge contours and cobblestone-like appearance, resembling a renal tubular epithelium (Felix et al. 1980). Another classification was described in 1983 when Detrisac *et al*. distinguished five different morphologies, and suggested that urine could hold a diagnostic value as a biomarker for nephropathy in diabetes mellitus patients. This was also the first time that the kidney was proposed as the site of origin due to indirect evidence (Detrisac et al. 1983). Racusen *et al*. later showed that they could isolate PT cells from the

urine of patients with nephropathic cystinosis and hence confirmed the already postulated kidney origin. They published electron microscopy images of the brush border (Racusen et al. 1991) and used histochemistry to stain for the brush border enzyme gamma glutamyl transpeptidase (Racusen et al. 1995). The initial classification was applied again in 2000 by Dorrenhaus, who attributed a urothelial origin to type I cells and a renal origin to type II cells. Additionally, they added a type II subclassification: spindle-like and cobblestone-like type II cells, which were able to form domes, a feature typical of the PT) (Dorrenhaus et al. 2000). In summary, these classifications gave only a vague idea of the site of origin. However, it was evident that urine was becoming an interesting non-invasive source of renal cells for *in vitro* studies in toxicological and preclinical research.

Currently, cells isolated from the urine are characterised using gene and protein expression assays in order to classify them as specific cell types. For instance, cells expressing CD13 and AQP1 could be defined as renal PT cells (Wilmer et al. 2010), whereas cells expressing uroplakin 3A (UPK3A) and uroplakin 1A (UPK1A) could be defined as urothelial (Rahmoune et al. 2005). Nevertheless, recalling the initial classification, Zhou *et al*. established a protocol to generate induced pluripotent stem cells (iPSCs) from urine samples and renovated the idea. It was stated that type I colonies have smooth-edged contours and cobblestone-like morphology, whereas type II colonies are randomly arranged. Based on mRNA and IF analysis, it was established that both types expressed renal epithelial markers, with no expression of the urothelial marker UPK3A (Zhou et al. 2012). Consequently, based on the gene expression profile, they stated that even though urine cells most frequently originate from the renal epithelium, urothelial origin is still possible and has been detected in other studies (Rahmoune et al. 2005).

1.4.2 Diversity of cells in urine - applications

The diversity of cells from various regions of the renal system has allowed the formation of different cell lines from urine cultures (Figure 1.9). The culture of podocytes and PT cells has been key in understanding the molecular mechanisms behind genetic diseases such as nephropathic cystinosis (Peeters et al. 2011), performing toxicological studies and gaining a better understanding of basic renal cell biology (Sakairi et al. 2010b, Zhang et al. 2013, Rahmoune et al. 2005), including the discovery that podocytes are able to endocyte albumin (Eyre et al. 2007). However, further improvements are necessary in cell transformation and/or culture conditions to fully reproduce the *in vivo* characteristics of podocytes (Sakairi et al. 2010b). Stable urine-derived PT cell lines have been used as a tool to investigate uremic excretion in kidney disease models (Gorvin et al. 2013, Mekahli et al. 2012). In particular, Gorvin *et al*. have used conditionally immortalised PT epithelial cells from the urine of Dent's disease patients to identify impaired endosomal acidification and receptor-mediated endocytosis. Nevertheless, the most revealing finding so far has been the detection of urine-derived stem/progenitor cells (USCs/UPCs).

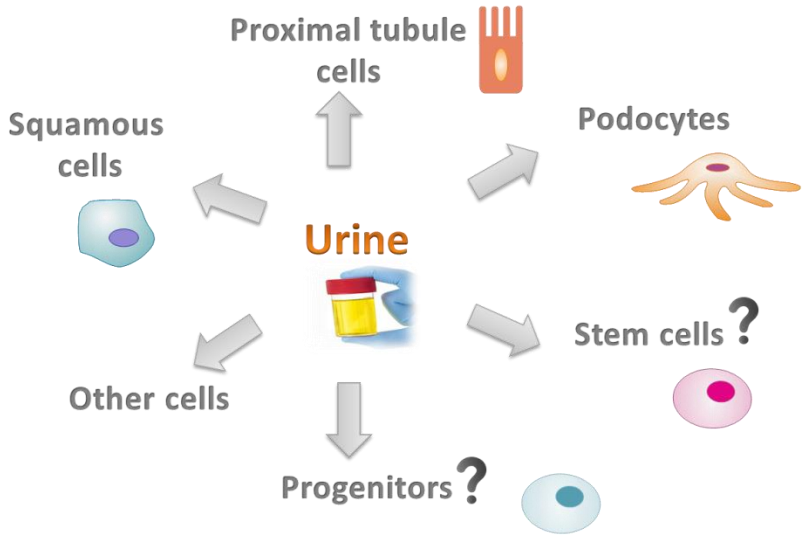

Figure 1.9 Cell types available in voided urine.
Urine collects different types of cells that for different reasons may detach from the site of engraftment. Amongst them we can find podocytes, PT cells, squamous cells (differentiated cells that do no attach in culture), non-renal cells and putative renal progenitor/stem cells.

1.4.3 Urine-derived progenitor cells (UPCs)

UPCs were isolated for the first time by Zhang *et al*. from healthy individuals and patients with vesicoureteral reflux. The isolating frequency of UPCs was calculated to be 0.2%, colonies formed from a single cell and they were capable of extensive expansion. Additionally, they were described as progenitors since they expressed progenitor cell surface markers, and demonstrated differentiation potential towards various cell lineages such as osteocytes, adipocytes and chondrocytes. However, Zhang *et al*. did not classify them as stem cells due to a lack of proof for unlimited self-renewal capability, and suggested a urothelial origin. Notwithstanding, in the following years other groups were able to reproduce the findings and defined the isolated cells as USCs (Bharadwaj et al. 2011, Wu et al. 2011). These studies were all able to use the urine-derived cells to give rise to urothelial-like cells, which displayed typical markers, such as UPK3A. Therefore, highlighting the potential of using UPCs/USCs as a cell source for urological tissue engineering (Zhang et al. 2008). Most recently, a renal origin for USCs was demonstrated by Bharadwaj *et al*., who also stated that different degrees of undifferentiated cells could be found in human urine (Bharadwaj et al. 2013).

In summary, these studies confirmed the importance of urine as a non-invasive source of viable cells with potential for cell therapy, cytotoxicity and pharmacological studies. Furthermore, the use of these cells would entail less ethical concerns and, most importantly, reduce the immune response and rejection for autologous cell-based approches (Bharadwaj et al. 2013, Wu et al. 2011).

1.5 AIMS

There is a significant predictive gap between preclinical (2%) and clinical studies (19%) in terms of drug-induced nephrotoxicity incidence, which may result in drug attrition or market withdrawal. Additionally, it has recently been revealed that mitochondria play an important role in organ toxicities. It is therefore important to identify nephrotoxicity early during the drug development process and to investigate the underlying pathologic mechanisms for this or that could predispose individuals to a safety risk. This would facilitate the development of risk mitigation and minimisation strategies to reduce the likelihood of nephrotoxicity during development and after marketing authorisation of the drug.

Consequently, the aims of the research presented within this thesis were to:

- Characterise the recently developed ciPTEC cell line to revalidate its potential as a nephrotoxicity model for further experiments.

- Implement the glucose replacement strategy for galactose in ciPTECs in order to develop a sensitive *in vitro* model to detect renal mitochondrial impairment.

- Interrogate ciPTECs cellular bioenergetics when exposed to adefovir and TFV as a strategy to uncover the molecular events responsible of renal mitochondrial toxicity triggered by these two NtRTIs.

- Isolate UPCs and derive them into PT cells to establish a novel patient-specific model to identify diverse nephrotoxicity events.

Chapter Two

Phenotypic and functional characterisation of a novel human conditionally immortalised proximal tubule cell line

CONTENTS

2.1 INTRODUCTION

Nephrotoxicity *in vitro* studies require suitable cell models that accurately reflect *in vivo* functionality and express a high range of transport systems to extend our knowledge in drug metabolism and to deliver rigorous toxicity information. Therefore, validation of *in vitro* PT models is essential to enable accurate interpretation of drug-induced nephrotoxicity experiments.

To be able to prove that ciPTECs are an alternative model that is fit for purpose to study nephrotoxicity and that the received cell line from our collaborative partners holds the same expression levels reported in the literature (Wilmer et al. 2010), a phenotypical and functional validation is required as well as a comparison of these data with appropriate controls (Figure 2.1). Comparator renal derived cell lines reported in the literature include,

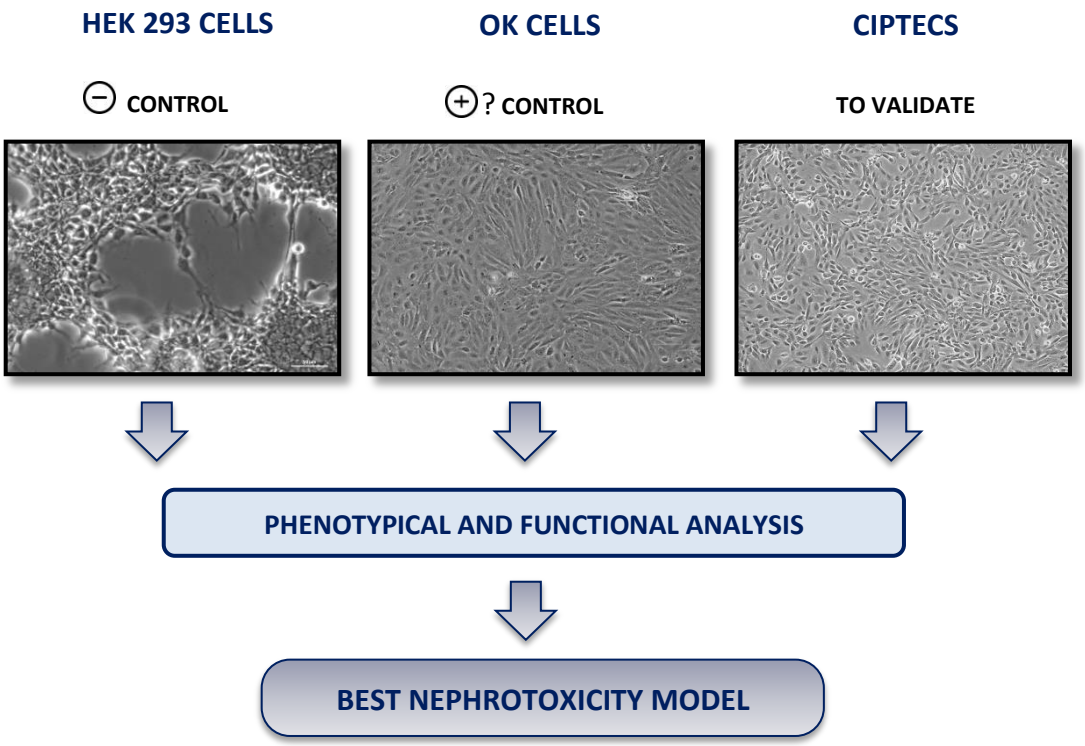

Figure 2.1 Diagram representing the validation process implemented in Chapter 2 to confirm the reliability of ciPTECs as a nephrotoxicity model.

HEK 293, LLC-PK1, OK and MDCK cells. HEK293 cells have been derived from primary cultures of human embryonic kidney but have been reported to barely retain any characteristics of a PT cell (Shaw et al. 2002). To date, most drug transport studies have focused on immortalised renal epithelial cell lines such as pig kidney cells (LLC-PK1), dog kidney cells (MDCK) or opossum kidney (OK) cells. These cell lines are of non-human origin and there might be rate-limiting factors that could influence the drug transport and metabolites (Verhulst et al. 2004, Ito 2008). However, they have been well studied regarding the albumin uptake mechanism through megalin and cubilin endocytic system. Albumin is the main protein in human plasma and has the important physiological role of maintaining an oncotic pressure difference between plasma and the interstitial space. Moreover, albumin also serves as a carrier for different metabolites and drugs (Gekle 2005). As a result, a good PT cell model (see Table 2.1) should hold this uptake mechanism on top of other important PT transporters involved in drug kinetics mentioned previously in Chapter 1. In the literature, ciPTECs appear to comply with most of these just defined standards. However, functional experiments are only performed after cells have spent 8 – 10 days at 37°C. The rationale for this decision is that at 37°C ciPTECs undergo a maturation

Table 2.1 List of desirable characteristics for a good nephrotoxicity model. A comparison between different cell lines.

CELL LINE	MORPHOLOGY	EXPRESSION OF PT GENES	PT MARKERS (*Ex. CD13*)	DRUG TRANSPORTERS	FUNCTIO-NALITY	HUMAN ORIGIN	CHARACTE-RISTICS MAINTAINED IN CULTURE
HEK 293	dissimilar	poor	✘	✘	✘	✓	✓
OK	comparable	too high	--	✓	✓	✘	✓
ciPTECs	**comparable**	**good**	✓	✓	✓	✓	✓
Primary PT cells	ideal	ideal	✓	✓	✓	✓	✘

that enables cells to reach a higher stage of PT differentiation while the expression of SV40T is downregulated and therefore cell division slows down. Nevertheless, no functional data is shown when the cells are at 33°C (Wilmer et al. 2010). Consequently, it would be interesting to interrogate ciPTECs at both temperatures.

In summary, phenotypical and functional assays will be a focus of the worked presented within this chapter with the specific interest of verifying the uptake of key substrates for drug uptake transporters to define which PT model would be fit for purpose to investigate the mechanistic basis of clinically relevant drug-induced nephrotoxicity *in vitro*.

2.1.1 Aims and hypothesis

Hypothesis:

Based on the specific aims of this chapter, our objective was to test the hypothesis that ciPTECs display a higher resemblance to the PT complexion than HEK 293 and OK cells, and that they would represent a more valuable and specific model to study clinically relevant nephrotoxicity *in vitro*.

The aims of this chapter were to:

- Phenotypically and functionally characterise the parent ciPTEC line at 33°C and 37°C and to compare the results with other established kidney cell lines.
- Confirm that ciPTECs express the necessary functional transporters to be a valuable nephrotoxicity model.

2.2 MATERIALS AND METHODS

2.2.1 Materials

The HEK 293 line was obtained from American Type Culture Collection (Manassas, VA, USA). The OK cell line was purchased from the European Collection of Cell Cultures (ECACC) and ciPTECs were received from the Department of Pharmacology and Toxicology in Radboud University Nijmegen (Nijmegen, Netherlands). RNA from human kidney tissue and a human kidney tubular fraction at passage 2 were received from the Department of Cellular and Molecular Physiology in University of Liverpool (Liverpool, UK). Tissue culture reagents Dulbecco's modified Eagle's medium (DMEM)/F-12 (1:1), fetal bovine serum (FBS), phosphate buffered saline (PBS) as well as Hoechst 33342, ProLong® Gold Antifade Mountant, CellTracker™ Green carboxy dimethyl fluorescein diacetate (CMFDA) Dye, qPCR reagents and primers, DNase treatment and reverse transcription reagents were purchased from Life Technologies (Paisley, UK). The HotStarTaq Master Mix Kit for PCR and QIAzol Lysis Reagent were purchased from QIAGEN (Manchester, UK). Cover slides (13 mm ∅) were purchased from VWR (Lutterworth, UK). Microscope slides, chloroform, isopropyl alcohol (IPA) and absolute ethanol were obtained from Thermo Fisher Scientific (Loughborough, UK). 100 bp DNA Ladder and 6x Gel Loading Dye were purchased from New England BioLabs (Ipswich, MA, USA). Precision Plus Kaleidoscope Standards (molecular weight markers) and non-fat milk were purchased from Bio-Rad Laboratories Ltd (Hemel Hempstead, UK). Amersham Hybond ECL membrane and Amersham Hyperfilm ECL were purchased from GE Healthcare (Little Chalfont, UK). Western Lightning Plus-ECL was purchased from Perkin Elmer (Beaconsfield, UK). Rap1A antibody was purchased from Santa Cruz (Ca, USA). All other reagents and chemicals were purchased from Sigma Aldrich (Dorset, UK).

2.2.2 Cell culture

HEK 293 cells and OK cells were cultured at 37°C in 5% CO_2 in DMEM and DMEM/F-12 (1:1) respectively. Both media were supplemented with FBS (10% v/v) and penicillin-streptomycin solution (1% v/v). HEK 293 cells were used up to passage 20 and OK cells used up from passage 48 to passage 54.

ciPTECs were maintained at 33°C under humidified air containing 5% CO_2 in their growth medium prepared with DMEM/F-12 (1:1) medium supplemented with FBS (10% v/v), penicillin-streptomycin solution (1% v/v), hydrocortisone (36 ng/ml), insulin-transferrin-sodium selenite (ITS) (I=5 µg/ml; T=5 µg/ml; S=5 ng/ml), epidermal growth factor (EGF) (10 ng/ml) and 3,3',5-Triiodo-L-thyronine sodium salt (40 pg/ml). Cells were used up from passage 39 to passage 45.

2.2.3 RNA isolation

From a 90% confluent T75, cells were washed with PBS, tripsinized and spun down to get a pellet. The pellet was resuspended in PBS and cells were spun down twice. After the second time, the PBS was removed and cells were resuspended with QIAzol lysis reagent and the solution was transferred to pyrogen-free microcentrifuge tubes. Then, 0.2 ml of 100% chloroform per 1 ml of QIAzol were added. Tubes were shaken intermittently for 2 minutes and then left still at the upright position for 5 minutes. After 15 minutes of centrifugation at 12,000 xg at 4°C, the top phase was carefully transferred to new microcentrifuge tubes. Then 0.2 ml of 100% IPA per 1 ml of QIAzol were added. Again, the solution was centrifuged at 12,000 xg for 10 minutes at 4°C. RNA precipitated as a gel droplet on the side of the tube, hence the supernatant was removed and then the pellet was washed with cold 75% ethanol. The RNA solution was spun down for the last time at 7,500 xg, the supernatant

was removed and the pellet was air dried to remove last ethanol traces. Finally, the pellet was dissolved in RNase free dH_2O.

2.2.4 DNase treatment of RNA

To remove any traces of DNA, a DNase treatment was performed on the RNA solution (see 2.2.3 section). A ratio of 44 : 5 : 1 µl (RNA solution : 10x DNase buffer : DNase) was prepared and left at 37°C for 30 minutes. Then, 5 µl of DNase inactivation reagent were added and the solution was spun down for 1 minute at 14,000 xg. The inactivation reagent precipitates and the supernatant containing purified RNA was transferred into a new tube. RNA quantification was performed using a NanoDrop (Labtech International Ltd).

2.2.5 Reverse transcription

The synthesis of complementary DNA (cDNA) from RNA was achieved using a reverse transcription procedure. Up to 5 µg of DNase treated RNA were incubated for 5 minutes at 65°C with random primers and a deoxynucleotide (dNTP) solution mix. Then, the solution was placed on ice for 1 minute. After the ice treatment, 5x first strand buffer, dithiothreitol solution (0.1 M) and the superscript III enzyme were added in this order. RNAse free dH_2O was used to get to 20 µl of final volume. Finally, samples underwent the following temperature treatment in a PCR System 9700 block (GeneAmp):

25°C – 5 minutes
50°C – 50 minutes
70°C – 15 minutes
4°C – 10 minutes and then storage

cDNA quantification was performed using NanoDrop (Labtech International Ltd, UK). NanoDrop analysis also gives information about the purity of the samples through the

260/280 absorbance ratio. Only samples with a ratio higher than 1.8 were selected to use for PCR (polymerase chain reaction) or qPCR (quantitative real-time PCR).

2.2.6 Design of the PCR primers

A set of primers for each PT marker of interest plus a housekeeping gene (GAPDH) were created (see Table 2.2).

Table 2.2 List of primers used for PCR to detect mRNA expression of PT genes plus GAPDH as a positive control

Gene	Primer pairs	Amplicon (bp)	T_M (°C)
AQP1	Fwd: 5' TTGTCTTCATCAGCATCGGTTCTG 3'	620	61.2
	Rev: 5' GATGAAGTCGTAGATGAGTACAGC 3'		61.2
LRP2	Fwd: 5' ATGCTTGCAACTATCCGACCTG 3'	600	60.3
	Rev: 5' GGAAGCTCCTTCCATGAATATCAC 3'		60.6
Cubilin	Fwd: 5' CATGGCTAAGTTCAGTGCTGAG 3'	806	60
	Rev: 5' GAGCTGTGGTAATAGGGCATC 3'		59.9
MRP2	Fwd: 5' ACTGAAGCTAGTGAATGACATCTTC 3'	730	59.9
	Rev: 5' CTATCCACCAGGACATAACCAG 3'		60.3
MRP4	Fwd: 5' TGACTCATCAGTTGCAGTACCTC 3'	366	60.6
	Rev: 5' TCCAGTGAGCACCAGCTCTG 3'		61.4
OAT1	Fwd: 5' GCACAGAAGCCAATGGCACAG 3'	487	61.8
	Rev: 5' GAGACCAGTAGCTGCAGGTG 3'		61.4
OAT3	Fwd: 5' AACAGCACCAAGGACTCCATTG 3'	559	60.3
	Rev: 5' CTTCCTTCTTGCCATTGAAGACAG 3'		61
OATP4C1	Fwd: 5' GCTATGTATTGGGAGGACAACTG 3'	891	60.6
	Rev: 5' GCAGTTTCGCACAATGAGTTTCAC 3'		61
GAPDH	Fwd: 5' GAGTCAACGGATTTGGTCGTAT 3'	435	58.5
	Rev: 5' CAGGAGGCATTGCTGATGATCT 3'		60.3

Both forward (Fwd) and reverse (Rev) primers were designed with a GC percentage higher than 40% and lower than 60%. The length of the amplicon or amplification product is represented in base pairs (bp) and T_M refers to the primers melting temperature.

To ensure a good amplification and annealing, the primers were designed with the following considerations:

- A GC percentage higher than 40% and lower than 60%.
- Avoiding several nucleotide or sequence repetitions.

- Ensuring that there were no other complementary regions in the genome.
- A similar melting temperature to be able to run them all in the same PCR reaction.
- A number of base pairs longer than 19 and shorter than 24.
- Ensuring that there was a guanine (G) or cytosine (C) at the 3' end to improve the annealing.

Oligo Calc: Oligonucleotide Properties Calculator Software was used for the primers design and the mRNA sequence of each gene was taken from the NCBI Reference Sequence Database. See Table 2.2.

2.2.7 PCR to detect PT genes expression

PCR reactions contained 100 ng of cDNA, 0.2 µM forward and reverse primers, 2.5 units of HotStarTaq DNA Polymerase, 1x PCR Buffer and 200 µM of each dNTP. The total reaction volume was readjusted to 50 µl with dH_2O. Thermal cycling parameters used can be found in Table 2.3. and the amplification was performed using the heating block from an ABI PRISM 7000 Sequence Detection System (Applied Biosystems).

Table 2.3 Steps and cycles using a HotStarTaq DNA Polymerase amplification from cDNA sequences

Steps	Time	Temperature	Cycles	Process
1	15 minutes	95°C	1	Heat activation
2	30 sec	94°C	2 - 34	Denaturation
3	30 sec	55°C		Annealing
4	1 minute	72°C		Extension
5	10 minutes	72°C	35	Final extension

2.2.8 DNA electrophoresis

The PCR products were resolved in a 2% agarose gel dissolved in 1x Tris/borate/EDTA (TBE) buffer, supplemented with a 1:20,000 dilution of ethidium bromide, at 100 V for 1 h. The

PCR product (5 µl) was combined with 5 µl of 1x Gel Loading Dye prior to loading onto the gel. PCR samples were resolved alongside a 100 bp DNA Ladder to enable estimation of DNA band sizes. Bands were visualized using a UV Transillumination system (Syngene Bioimaging System).

2.2.9 qPCR

TaqMan technology was used to perform the qPCR experiment. In contrast with other qPCR methods, this technology is characterized by an extra probe (TaqMan probe) that is also complementary to the gene fragment amplified by a specific set of primers. TaqMan probes contain a covalently attached fluorophore at the 5'-end and a quencher at the 3'-end. Therefore, when Taq polymerase starts synthetizing the nascent strand, its 5' to 3' exonuclease activity is able to degrade the annealed TaqMan probe. As a result, the quencher and fluorophore are released, breaking their close bond and thus allowing the fluorescence of the fluorophore. Consequently, the amount of fluorescence becomes directly proportional to the amount of amplified DNA.

The qPCR reactions contained 50 ng of cDNA, 1x TaqMan Gene Expression Assays (see Appendix 1) and 1x TaqMan Universal Master Mix II. The total reaction volume was readjusted to 20 µl with dH_2O and the thermal cycling parameters can be found in Table 2.4. The experiment was performed in a Viia 7 qPCR machine (Applied Biosystems).

Table 2.4 Thermal cycling parameters for qPCR experiments

Steps	Time	Temperature	Cycles	Process
1	10 minutes	95°C	1	Heat activation
2	15 sec	95°C	2 - 40	Denaturation
3	1 minute	60°C		Annealing

2.2.10 PPARα agonist treatment to increase megalin mRNA levels

ciPTECs were seeded in a 6-well plate at $1.2x10^5$ cells/well. After 24 h, they were treated with WY 14643, a peroxisome proliferator-activated receptor –alpha (PPARα) agonist, at 100 µM in their own medium with different concentrations of FBS (1%, 5% and 10%). The exact same design was repeated but cells were treated with a vehicle instead (DMSO, final volume lower than 1% v/v). The treatment lasted another 24 h and then RNA was isolated, followed by a DNase treatment, reverse transcription and qPCR (see 2.2.3 - 5 and 2.2.9 sections).

2.2.11 Western blotting – simvastatin treatment and whole cell lysates

To evaluate if simvastatin was functional and therefore could inhibit the prenylation of Rap1A, ciPTECs were seeded in a 6-well plate at $5x10^5$ cells/well. After 48 h at 33°C, ciPTECs were treated with simvastatin at different concentrations (0 µM, 0.01 µM, 0.03 µM, 0.1 µM, 0.3 µM, 1 µM, 3 µM and 10 µM) for 24 h. After the drug treatment, cells were washed twice with 1 ml of cold PBS before lysis in 100 µl of RIPA buffer.

2.2.12 Western blotting – protein quantification

For western blotting, the total protein content of whole cell lysates was measured using the bicinchoninic acid (BCA) assay. This assay relies on the fact that protein peptide bonds reduce Cu^{+2} ions to Cu^{+}. Therefore, the amount of reduced Cu^{2+} is proportional to the amount of protein and when the molecules of BCA chelate with each Cu^{+} ion, they form a purple-coloured product that absorbs at a 562 nm wavelength. A standard curve ranging from 0.125 – 2 mg/ml of albumin was prepared and 9 µl of each concentration were transferred in duplicate into a new 96-well plate as well as 3 µl of dH_2O (blank) and 3 µl of lysed cells from each well. Freshly prepared BCA reagent solution was added into each well

(200 µl/well) and the plate was incubated for 35 minutes at 37°C. The absorbance was read at 570 nm on a plate reader (Varioskan, Thermo Scientific). The blank reading (dH_2O with BCA reagent) was subtracted from all sample and standard readings and the protein concentration was extrapolated from the equation of the linear regression.

2.2.13 Western blotting – Rap1A

To detect the amount of unprenylated Rap1A in the whole cell lysates, 20 µg of cell lysate from each condition were mixed with reducing agent and sample buffer and then denatured at 85°C for 5 minutes. Samples were then loaded onto 10% acrylamide gels and proteins separated by electrophoresis in a Tris-Glycine running buffer. Proteins were then electro-transferred onto a nitrocellulose membrane using 20% MeOH buffer for 1 h at 80 V. Successful transfer and even loading was checked using Ponceau Red. Membranes were washed with 0.1% Tween-TBS and blocked with 10% non-fat milk for 1 h. Then, the membrane was cut in two parts around 30 kDa, leaving the expected band for Rap1A (22 kDa) in one half and the expected band for β-actin (41.7 kDa) in the other half. The membrane containing proteins up to 30 kDa was incubated overnight with a goat polyclonal antibody raised against unprenylated Rap1A (1/1,000 in 10% milk) while the other membrane was left in blocking solution also overnight, both with shaking at 4°C. Next day, the membrane containing proteins from 30 kDa was incubated for 1 h with mouse monoclonal anti-actin (1/10,000 in 10% milk). Membrane was then washed (4x 5 minutes) with 0.1% Tween-TBS and the secondary antibody anti-mouse IgG (1/10,000 in 10% milk) was incubated for 1 h at room temperature (RT). Meanwhile, the other part of the membrane was washed (4x 5 minutes) with 0.1% Tween-TBS and later incubated with the secondary antibody anti-goat (1/10,000 in 10% milk) for 1 h at RT. After the secondary antibody incubation, both membranes were washed again with 0.1% Tween-TBS and treated with enhanced chemiluminescence (ECL) reagent for 1 minute. Proteins were

visualised using exposure to X-ray film. After developing, films were scanned using a densitometry scanner (GS800, Bio-Rad).

2.2.14 Densitometry

ImageJ software was used to calculate the area and density of each protein band from the image obtained with the scanner. The software represented each band with a density peak and gave the percentage of that peak compared to the sum of the peaks from all selected bands. Results were then corrected by normalizing them to the percentage values from β-actin. Finally, the relative density was calculated by comparing the percentage of each band to the percentage of the control one (0 μM).

2.2.15 Megalin and cubilin albumin uptake assay

The assay was performed based on the work that Zhai *et al.* (2000) and Ranghini *et al.* (2013), published in OK cells and mouse developing nephrons respectively using albumin–fluorescein isothiocyanate conjugate (FITC-BSA) (Zhai et al. 2000, Ranghini et al. 2013). HEK 293 cells were seeded at $5.5x10^4$ cells/well, OK cells were seeded at $2.5x10^4$ cells/well (both cultured at 37°C) and ciPTECs were seeded at $5x10^4$ cells/well (cultured at 33°C) in 12-well plates. Cells were left to grow to confluence in their own medium, which took 4-5 days. However, to analyse the functionality at 37°C, two extra 12-well plates at $5x10^4$ cells/well of ciPTECs were cultured for 24 h at 33°C and then transferred at 37°C for 5 or 10 days. Then, cells were washed 3x with PBS and cultured overnight with their own medium without FBS and with their own medium without FBS plus 1 μM of simvastatin. Next morning, cells were incubated with 20 μg/ml of FITC-BSA, 20 μg/ml of FITC-BSA plus 4 mg/ml of unlabelled BSA or 20 μg/ml of FITC-BSA plus 1 μM of simvastatin (added to the ones that had been pre-treated overnight) for 15 minutes at 37°C. A negative control was also added where no FITC-BSA was used.

2.2.16 Assessment of FITC-BSA fluorescence - microscope

Previously to seeding the cells, to be able to analyse them under the microscope, cover slides (13 mm ∅) were placed in wells of a 12-well plate and coated with 0.5% of gelatine for 30 minutes. The gelatine was removed and cells were seeded at the designated concentration in 2.2.15. Then, megalin and cubilin functionality assay was performed also following 2.2.15 section. Right after, cells were washed 3x in warm PBS and fixed with 2% paraformaldehyde (PFA) for 15 minutes at RT in the dark. After cells had been fixed, 2x PBS washes were performed. Then, the nuclei were stained with 2 µg/ml of Hoechst 33342 for 10 minutes at RT protected from light. Finally, after 3x PBS washes, the cover slides were mounted onto a microscope slide with Prolong Gold. Results were visualized at 40x magnification using an inverted fluorescence microscope (Axio Observer.Z1, Zeiss).

2.2.17 Assessment of FITC-BSA fluorescence – flow cytometry

Flow cytometry is a laser based technology that allows to simultaneously analyse in real time different physical and chemical characteristics of particles and cells. A single cell suspension is required, as the flow cytometer analyses every single particle but it can process thousands of particles or cells per second. Here, flow cytometry was used to detect the fluorescence of cells. FITC has an excitation and emission spectrum with peak wavelengths of approximately 495/519 nm. If cells have uptaken the FITC-BSA, when the laser hits them they will release fluorescence that will be measured by a detector.

After the megalin and cubilin functionality assay (see 2.2.14 section) cells were washed in warm PBS, trypsinized and spun down. The pellet of cells was resuspended in PBS and cells were spun down again. Cells were again resuspended in PBS and transferred to FACS tubes. The voltage parameters in the flow cytometer (FACSCalibur, BD Biosciences) were set up

using the negative control sample and FL1-H channel was selected to measure cell fluorescence.

2.2.18 Flow cytometry data analysis

Data was analysed using Flowing Software. From the general cloud of particles, the population that represented single cells was selected, excluding debris and duplets of cells. Then, the median of the peaks for each condition in the FL1-H channel was measured. The fluorescence data from cells only treated with FITC-BSA (control) was established as 100%. Finally, data was compared with the positive control and expressed as a percentage.

2.2.19 CMFDA dye as a method to analyse MRP2/4 and P-gp functionality

This fluorescent assay relies on the fact that CMFDA can freely enter inside the cells but once inside, undergoes what is believed to be a glutathione S-transferase–mediated reaction (Barhoumi et al. 1993), producing a cell-impermeant reaction product that can only be excreted by selected transporters such as MRP2, MRP4 or P-gp (see Figure 2.2 A). Furthermore, CMFDA is non fluorescent until its acetate groups are cleaved by intracellular esterases; hydrolysis of the acetates yields a product with an excitation/emission spectra of (492/517 nm). As a result, the analysis of CMFDA fluorescence can be used to study the activity of specific membrane transporters upon inhibition (see Figure 2.2 B) (Jenkinson et al. 2012).To perform the assay, cells (HEK293, OK cells or ciPTECs) were grown in a T75 and left until 90 – 95% confluence. Then, cells were split and 1/3 of the total pool of cells was seeded in a 96-well plate (ciPTECs and HEK cells had a concentrations of 9,000 cells/well while OK cells had a concentration of 4,500 cells/well). HEK 293 and OK cells were cultured in the 96-well plate for 72h at 37°C, and the same was done for ciPTECs at 33°C. However, to analyse the functionality at 37°C, an extra 96-well plate of ciPTECs was cultured for 24 h

A. CMFDA uptake and metabolism

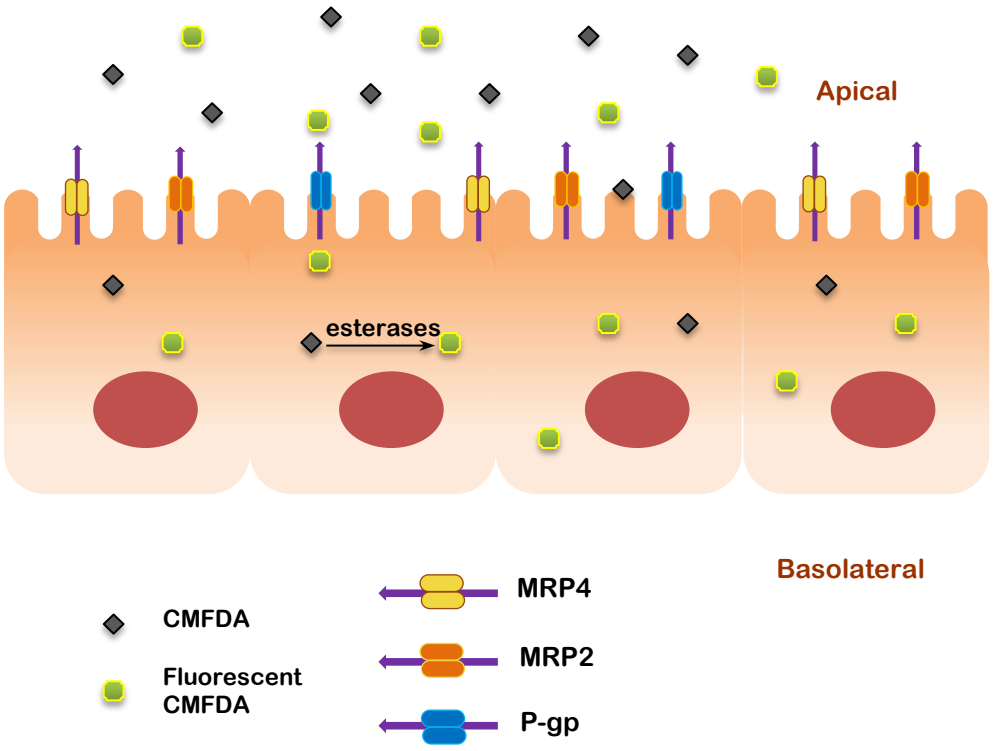

B. Inhibition of MRP2/4 and P-gp

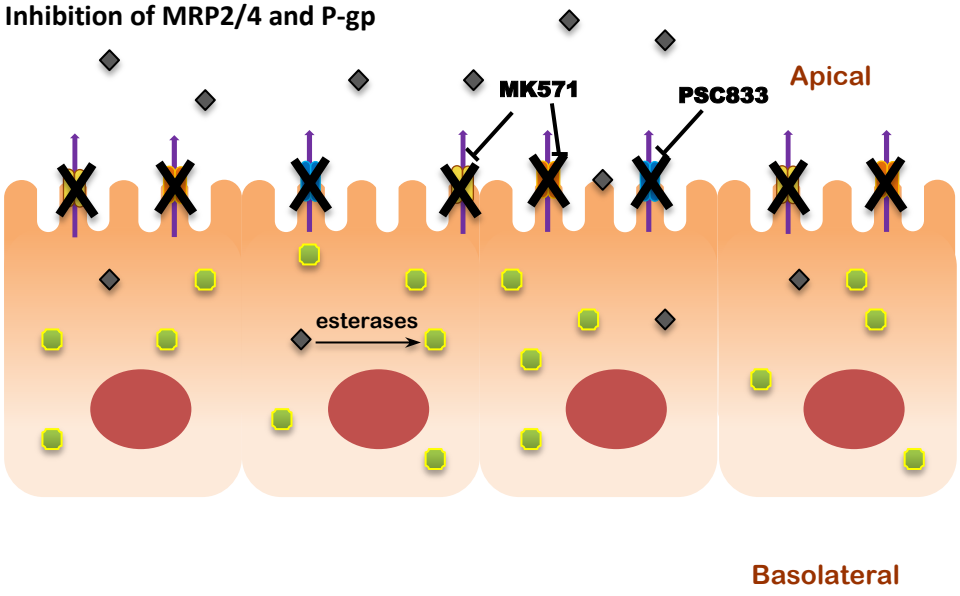

Figure 2.2 Representation of the developments that occur during the CMFDA assay. (A) In normal conditions, the CMFDA dye enters the cells freely, but once inside, esterases transform it into an impermeable fluorescent molecule. Consequently, it can only be pumped out of the cell by specific transporters such as MRP4, MRP2 or P-gp. (B) When inhibitors for P-gp (PSC833) or MRP2/4 (MK571) are added, the cells are unable to excrete the fluorescent CMFDA molecule and the dye gets accumulated in the cytosol. This fluorescent accumulation can be detected and it is an indicator of the functionality of the inhibited transporter/s.

at 33°C and then transferred at 37°C for 5 days. Once these incubations were finished, cells were washed twice in Krebs buffer and the same buffer was used to prepare CMFDA solution at a concentration of 1.25 µM. Then, the buffer was removed and half of the plate was treated with increasing concentrations of MK571 (0 µM, 1.25 µM, 3.13 µM, 6.25 µM, 12.5 µM and 25 µM), which is an inhibitor of MRP transporters (Weiss et al. 2007), in CMFDA solution. The other half was treated with PSC833, which inhibits P-gp transporter (Boesch et al. 1991, Bezombes et al. 1998), in CMFDA solution (0 µM, 0.16 µM, 0.49 µM, 1.48 µM, 4.44 µM and 13.33 µM). The 96-well plate was left at 37°C in the dark for 30 minutes. Then, it was washed with Krebs buffer twice and cells in the dark at 37°C for another 30 minutes. Finally, the fluorescence was recorded using a plate reader (Varioskan, Thermo Scientific).

2.2.20 Hoechst 33342 dye as a method to analyse P-gp and BCRP functionality

The essence of the Hoechst 33342 uptake assay was the same as the CMFDA assay. Hoechst 33342 is a cell-permeable DNA stain that is excited by ultraviolet light and emits blue fluorescence at 460 to 490 nm. Hoechst 33342 is a non-fluorescent substrate for BCRP and P-gp (Shapiro et al. 1997, Scharenberg et al. 2002, Kim et al. 2002). However, it acquires fluorescence when bound to DNA, but not on the aqueous medium. With no inhibitors, the accumulation and therefore the fluorescence increase slowly, as the efflux pumps persistently excrete the dye (Jenkinson et al. 2012). In contrast, when inhibitors are added, it should result in a faster accumulation of Hoechst 33342 and therefore greater fluorescence.

HEK 293, OK cells or ciPTECs were grown in a T75 and left until 90 – 95% confluence. Then, they were split and 1/3 of the total pool of cells was seeded in a 96-well plate (ciPTECs and HEK cells had a concentrations of 9,000 cells/well while OK cells had a concentration of

4,500 cells/well). After 72 h at 37°C, cells were washed twice in Krebs buffer and the same buffer was used to prepare a Hoechst solution at a concentration of 1.25 µM. Then, the buffer was removed and half of the plate was treated with increasing concentrations of KO143 (0 µM, 0.47 µM, 0.94 µM, 1.88 µM, 3.75 µM and 7.5 µM), which is an inhibitor of BCRP (Allen et al. 2002), in Hoechst 33342 solution. The other half was treated with PSC833, which inhibits P-gp transporter (Boesch et al. 1991, Bezombes et al. 1998), in Hoechst 33342 solution (0 µM, 0.16 µM, 0.49 µM, 1.48 µM, 4.44 µM and 13.33 µM). The 96-well plate was left at 37°C in the dark for 30 minutes. Then, it was washed with Krebs buffer twice and the fluorescence was recorded using a plate reader (Varioskan, Thermo Scientific).

2.2.22 Statistical analysis

Statistical analysis of data was performed using StatsDirect software. All results were represented as the mean ± standard error of the mean (SEM) or as the mean ± standard deviation (SD) of three independent experiments. The choice of SEM *vs*. SD was only based on obtaining a better visual representation of the figures. Data was first assayed for normality using the Shapiro-Wilk test. When assaying differences amongst at least three groups, if data was normal, statistical analysis was performed using One Way ANOVA with Dunnet as a post-hoc comparison, as this test is specifically designed to compare each treatment against a single control. If there was no evidence of normality, Kruskal-Wallis test was applied instead. To test for differences amongst two groups, a t-test was performed if data was classified as normal and a Mann-Whitney test when data showed no evidence of normality. Only when p values <0.05 the results were considered significant.

2.3 RESULTS

2.3.1 Validation of self-designed PCR primers

As previously described, HEK 293 cells have been demonstrated as a poor PT model to perform toxicity studies as they lack the expression of key drug transporters, metabolic enzymes and proteins essential for PT specific functions such as organic cation transporters and the Na^+/K^+-ATPase pump (Shaw et al. 2002). To verify this fact, we checked the mRNA expression of PT markers in this cell line through PCR. See Appendix 2 for a full list of gene names and their respective proteins.

Moreover, to make sure the primer design was accurate and they were able to amplify the desired fragment from the gene of choice, we first tested the primers on cDNA re-transcribed from human kidney tissue mRNA (Figure 2.3). In fact, the electrophoresis gel of PCR products revealed that each set of primers amplified only one band and that band was found at the right molecular weight position for each gene (see Table 2.2). For example, LRP2 fragment was located around 600 bp as expected by the amplicon length. Some bands were thicker and brighter than others, indicating qualitatively possible greater mRNA expression of those genes in the kidney tissue sample such as CUBN and OATP4C1. OAT1 showed the lowest expression of all represented by a fainter band. The fact that only one band was amplified per gene indicated the melting temperature was appropriate and the primers showed high specificity, ergo they did not amplify any other cDNA region.

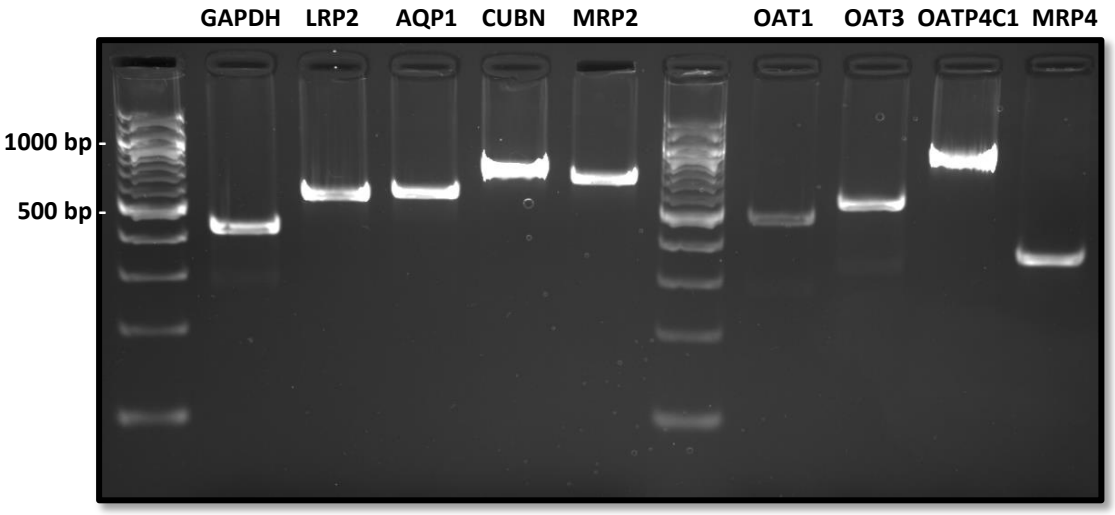

Figure 2.3 PCR products run in agarose gel electrophoresis for the validation of self-designed primers.

The cDNA was retro-transcribed from kidney tissue mRNA, amplified in a PCR reaction for 35 cycles and the resulting amplification products were run in a 2% agarose gel. 5 µl of PCR product and 5 µl of 1x Gel Loading Dye were added per lane. From left to right, the 1st and 7th lanes correspond to the molecular weight ladder and each band has a separation from the next of 100 bp. The gene names that correspond to the amplified fragments are displayed at the top of each lane. Data is representative of n = 3 experiments.

2.3.2 mRNA expression of PT markers in HEK 293 cells

In order to confirm the lack of expression of important PT transporters in HEK 293 cells and use them as a negative control, we isolated mRNA, retro-transcribed it and performed a PCR with the previously validated primers.

The electrophoresis gel in Figure 2.4 showed no mRNA expression of LRP2, AQP1, CUBN, MRP2, OAT1, OAT3 and OATP4C1. A fine line just under 400 bp was detected for MRP4 transporter, which corresponds with MRP4 amplicon length (366 bp) and indicates a low gene expression. A strong band for GAPDH (435 bp) in both electrophoresis gels proved that the PCR worked fine and the lack of bands could definitely be attributed to a lack of expression.

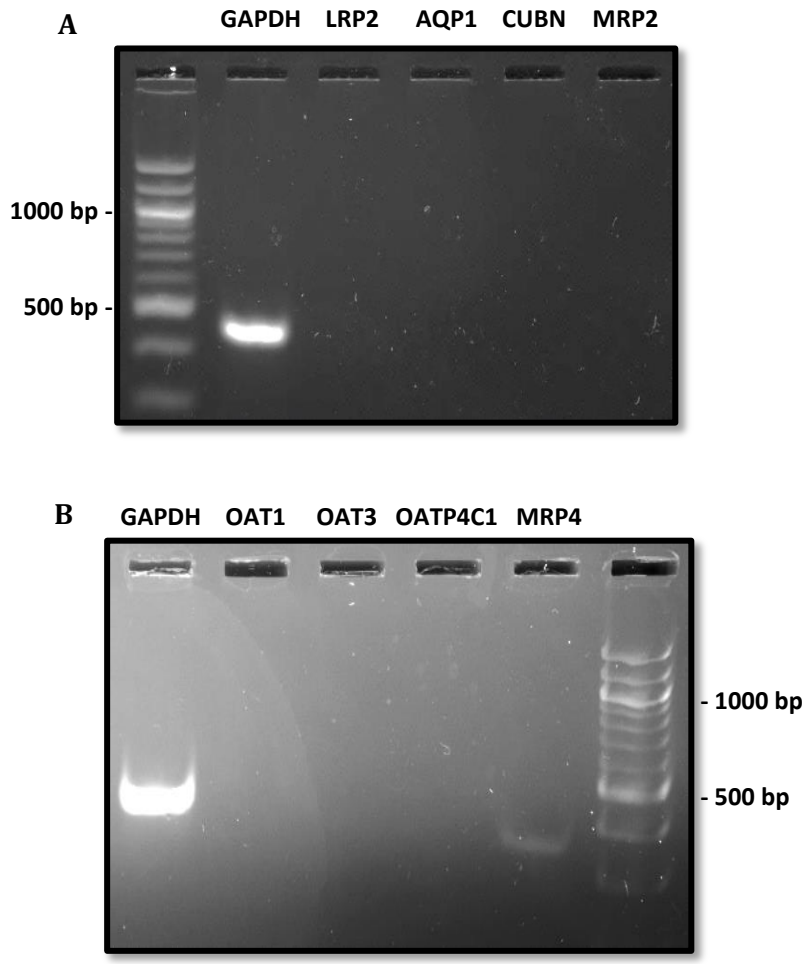

Figure 2.4 PCR products run in agarose gel electrophoresis to detect expression of PT markers in HEK 293 cells.

The cDNA was retro-transcribed from mRNA extracted from HEK 293, amplified in a PCR reaction for 40 cycles and the resulting amplification products were run in a 2% agarose gel. 5 µl of PCR product and 5 µl of 1x Gel Loading Dye were added per lane. The 1st lane of gel A and the 6th lane of gel B correspond to the molecular weight ladder and each band has a separation from the next of 100 bp. The gene names that correspond to the amplified fragments are displayed at the top of each lane. Data is representative of n = 3 experiments.

2.3.3 mRNA expression of different kidney markers in ciPTECs

In contrast to HEK 293 cells, ciPTECs are known to express a variety of PT transporters (Wilmer et al. 2010). To corroborate this fact and to validate the cell line for subsequent studies, a qPCR at both 33°C and 37°C was performed. In this case, the method of choice was qPCR instead of PCR in order to quantify and compare the mRNA expression of different kidney markers.

Figure 2.5 represents the ciPTECs expression of different kidney markers from different kidney cell types normalised to a tubular fraction at passage 2. Therefore, the graph only represents the relative expression of different genes compared to their expression in the tubular fraction. Meaning that, if the value is 1, ciPTECs and the tubular fraction had the same expression, which would be ideal. See Table 2.5 for the actual Ct values to have an idea of cell abundance.

The first 7 genes correspond to PT markers. Only BCRP, OATP4C1 and CUBN showed differences between 33°C and 37°C. BCRP exhibited a higher expression at 33°C and, in contrast, OATP4C1 and CUBN expression was significantly higher at 37°C. Except for MRP2 at 37°C, CUBN at 33°C and AQP1, all PT genes analysed had a greater or similar mRNA expression to the tubular fraction. It was also important to note that the expression of some key PT transporters was not detected, these included LRP2, OAT1 and OAT3.

The expression of some genes that are specific to other parts of the nephron was also evaluated. SYNPO is expressed specifically in podocytes. Therefore, low expression of this marker was expected in this PT cell line. Surprisingly though, compared to the tubular fraction, ciPTECs displayed an increase in expression of 10 fold. Other markers from other nephron segments such as AQP3 (collecting duct) or NCCT (distal convoluted tubule) showed similar or lower mRNA levels compared to the normalised baseline. No significant differences were observed between both temperature conditions.

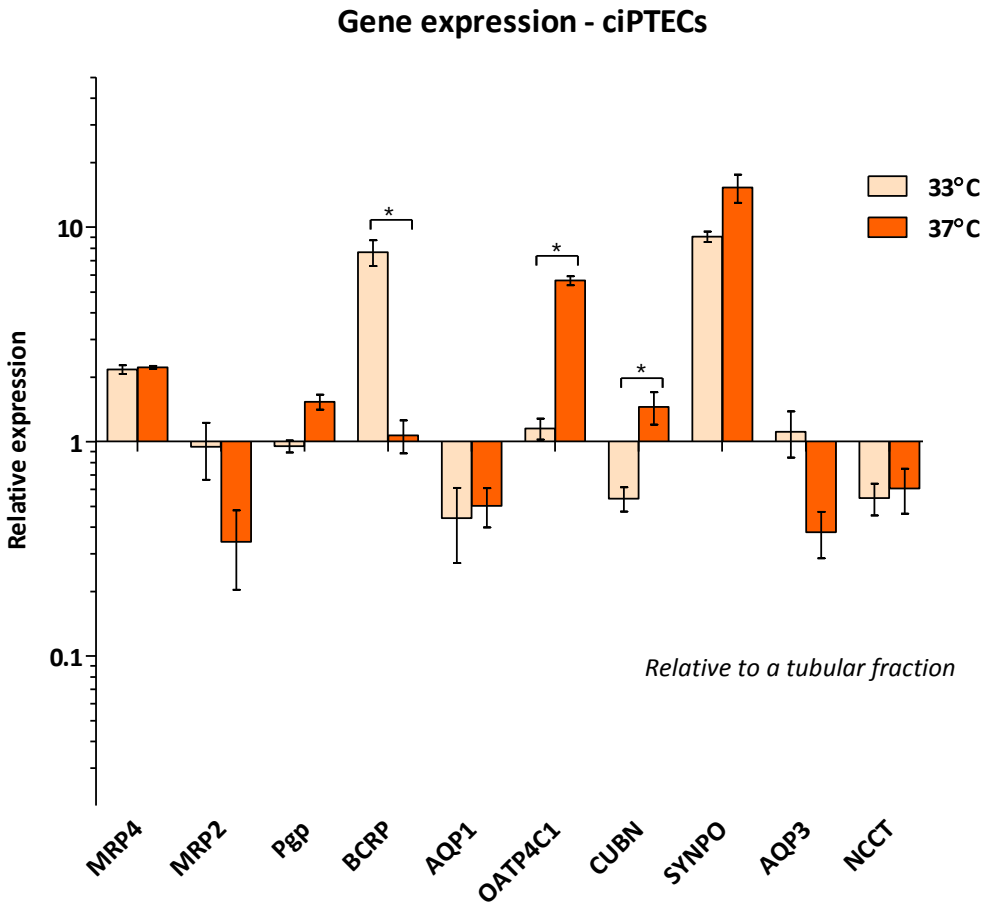

Figure 2.5 Relative expression of kidney markers in ciPTECs.
The relative expression of PT genes as well as other kidney markers in ciPTECs at 33°C and 37°C was analysed by qPCR. Gene names are displayed under each set of bars. Data was normalised against a human tubular fraction at passage 2. Data are mean ± SEM (n = 3). Statistical significance was determined between both temperature conditions by Mann-Whitney test, *p<0.05.

Table 2.5 Ct values of the renal markers analysed by qPCR

	MPR4	MRP2	Pgp	BCRP	AQP1	OATP4C1	CUBN	SYNPO	AQP3	NCCT
33°C Ct value ± SEM	27.52 ± 0.07	37.71 ± 0.55	29.31 ± 0.09	32.84 ± 0.2	34.82 ± 0.51	31.33 ± 0.17	34.25 ± 0.21	27.27 ± 0.08	34.5 ± 0.33	35.81 ± 0.22
37°C Ct value ± SEM	27.54 ± 0.02	39.38 ± 0.58	29.08 ± 0.11	35.04 ± 0.28	35.09 ± 0.32	29.78 ± 0.07	33.56 ± 0.24	26.98 ± 0.23	35.5 ± 0.39	35.56 ± 0.31

Data are mean ± SEM (n = 3)

2.3.4 Failure to upregulate megalin mRNA levels with a PPARα agonist

Although Wilmer *et al*. had previously published in 2010 that ciPTECs expressed megalin at a protein level and it was functional, we could not detect any mRNA expression (Figure 2.5). To see if we could upregulate the expression and therefore have detectable levels of LRP2 mRNA, we dosed ciPTECs with WY 14643, a PPARα agonist known to upregulate LRP2 mRNA expression (Cabezas et al. 2011).

Cells were treated with the PPARα agonist for 24 h at different percentages of FBS (0%, 1%, 5% and 10%) since it has been revealed that high concentrations of albumin can contribute to the downregulated expression of megalin (Gekle et al. 1998). The qPCR results did not display any increase in LRP2 mRNA expression, which remained undetectable for every single condition (Table 2.6). Nevertheless, this fact might not be as surprising since no expression was either found in the tubular fraction at passage 2. We could only detect the presence of LRP2 in mRNA isolated from human kidney tissue (hKid tissue) with a ΔCt of 16.32 ± 3.42.

Table 2.6 Detection of LRP2 mRNA by qPCR in human kidney tissue, in a tubular fraction and in ciPTECs treated with a PPARα agonist.

			ciPTECs 33°C			ciPTECs 37°C		
	hKid tissue	Tubular fraction	1%	5%	10%	1%	5%	10%
ΔCt value ± SD	16.32 ± 3.42	--	--	--	--	--	--	--

Data are mean ± SD (n = 3). Key: hKid indicates human kidney, the percentages refer to the amount of FBS and "—" indicates undetermined value.

2.3.5 Assessment of megalin and cubilin functionality

Even though no LRP2 expression was detected, since we found important levels of CUBN expression and their corresponding receptors function together (see Figure 1.3), we decided to confirm their presence by assessing protein function. To study the functionality of the megalin and cubilin endocytic system, we measured the capacity of ciPTECs to uptake fluorescently labelled albumin: FITC-BSA. Furthermore, to determine how specific the uptake was to this system, we submitted the cells to a competitive inhibition with BSA and to a non-competitive inhibition with simvastatin. Simvastatin is an inhibitor of 3-hydroxy-3-methylglutaryl CoA (HMG-CoA) reductase in the PT, which supresses the conversion of HMG-CoA to mevalonate, a rate limiting step in the sterol pathway. As a result, the cellular sterol pool is depleted and the post-translational modifications of GTP-binding proteins such as Rap1a are blocked (Sidaway et al. 2004, Verhulst et al. 2004).

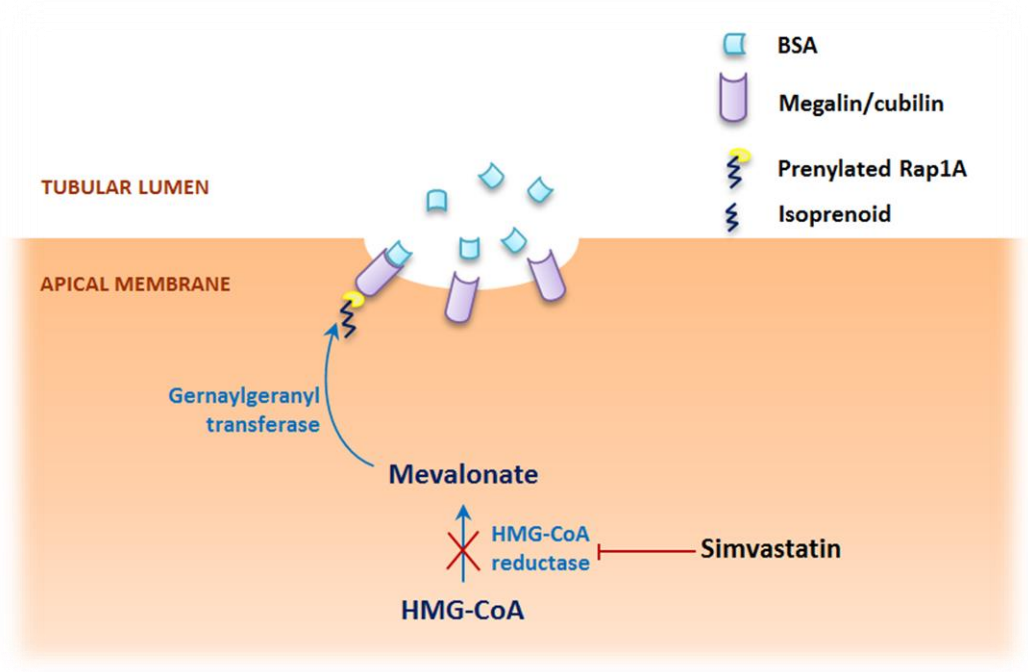

Figure 2.6 Schematic of megalin/cubilin endocytosis inhibition caused by simvastatin.
Renal uptake of albumin is dependent on the interaction between megalin/cubilin system with prenylated GTP-binding proteins such as Rap1A by isoprenoids pyrophosphates from the mevalonate pathway. Therefore, by inhibiting the synthesis of mevalonate we are indirectly inhibiting the albumin uptake.
Key: CoA = coenzyme A; HMG-CoA = hydroxymethylglutaryl coenzyme A.

Without the interaction between Rap1a to megalin/cubilin, the system is not ready to receive ligands. Therefore, simvastatin indirectly inhibits the receptor-mediated endocytosis by increasing the intracellular level of unprenylated GTP-binding proteins (see Figure 2.6).

To determine if the batch of received simvastatin was pharmacologically active, we investigated whether the HMG-CoA reductase inhibitor was still able to inhibit GTP-binding protein (Rap1A) prenylation in ciPTECs (Antoine et al. 2010). Western blotting revealed a clear dose dependent increase of unprenylated Rap1A when ciPTECs were treated with 10 µM of simvastatin for 24 h (Figure 2.7 A). The β-actin blot confirmed an equal loading of protein content. These results were later corroborated by densitometry (Figure 2.7 B). At the two lowest concentrations of simvastatin, the amount of unprenylated Rap1A was nearly indiscernible and, therefore, the relative density was close to 1; as was the control.

After establishing that simvastatin was pharmacologically active, we proceeded to treat the negative control (HEK 293) and the positive control (OK) cell lines with FITC-BSA, FITC-BSA + BSA and FITC-BSA + simvastatin for 15 minutes. Cells were then fixed, the nuclei were stained and the fluorescence was evaluated under the microscope. In HEK 293 cells, no difference was observed amongst all three different conditions (Figure 2.8). Some non-specific fluorescence could still be detected, especially in samples treated only with FITC-BSA, however it was clear that it was not due to megalin or cubilin uptake since the typical dot pattern of endocytosis could not be detected (Ranghini et al. 2013). In contrast, OK cells displayed a clear uptake of FITC-BSA (Figure 2.9 A), with the endocytic vesicles filled with fluorescent albumin clearly visible surrounding the nuclei. In some areas, the amount of accumulated FITC-BSA was so high that the image looked saturated. When BSA or simvastatin were added to the treatment (Figure 2.9 B, C), the general amount of

fluorescence was reduced in both conditions indicating that the competitive and non-competitive inhibitions had taken place as expected.

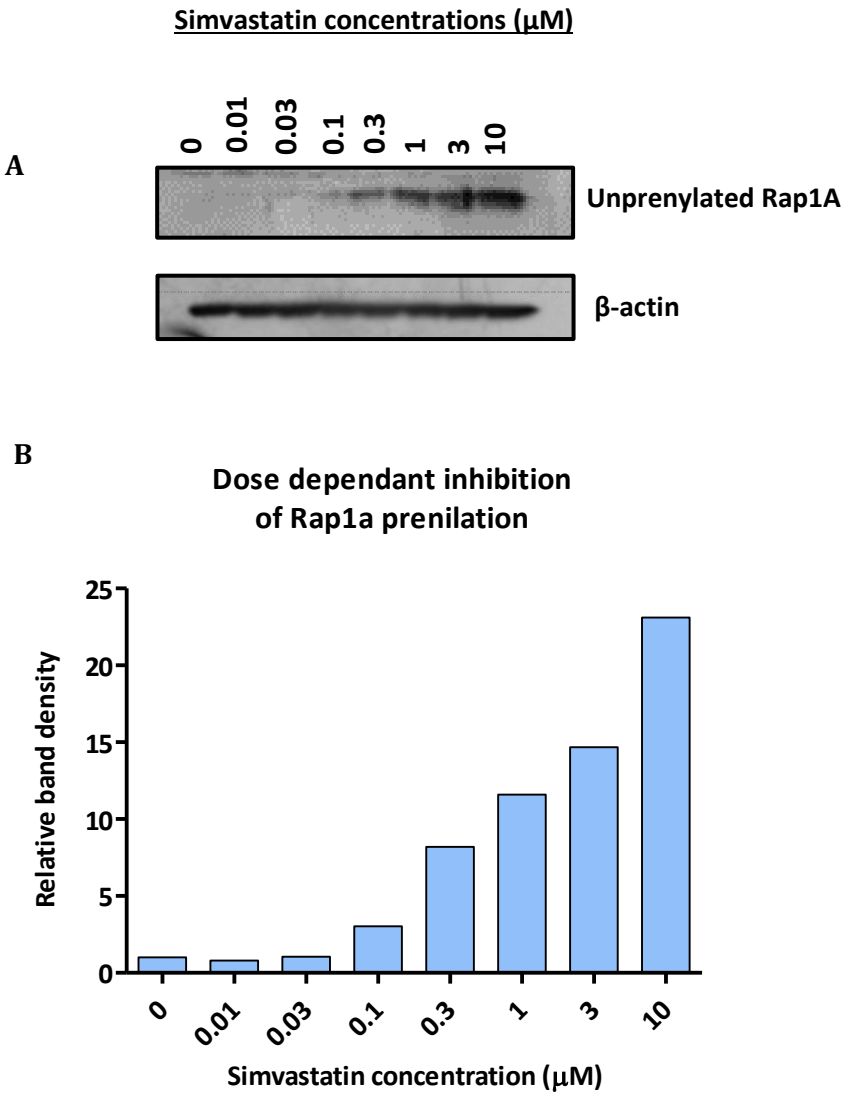

Figure 2.7 Western blotting (A) and densitometry (B) of the amount of unprenylated Rap1A after 24 h of simvastatin treatment in ciPTECs.
ciPTECs were incubated with simvastatin (0 - 10 μM) for 24 h. (A) Equal amounts of protein were separated by SDS-PAGE from whole cell RIPA lysates. The presence of unprenylated Rap1A (22 kDa) was determined by western blot and compared to a β-actin loading control. (B) Densitometry for each simvastatin concentration was performed by ImageJ software and the relative density of the complexes was normalized to the relative density of the corresponding β-actin band (n=1).

A. FITC-BSA

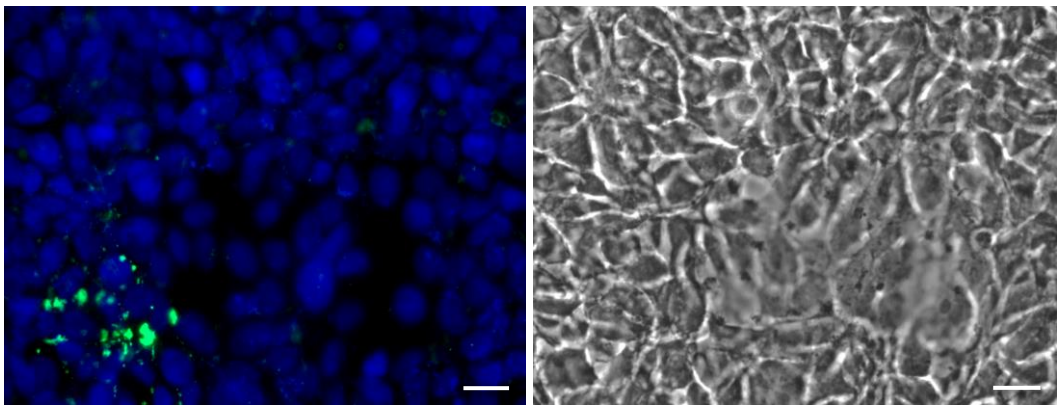

B. FITC-BSA + BSA

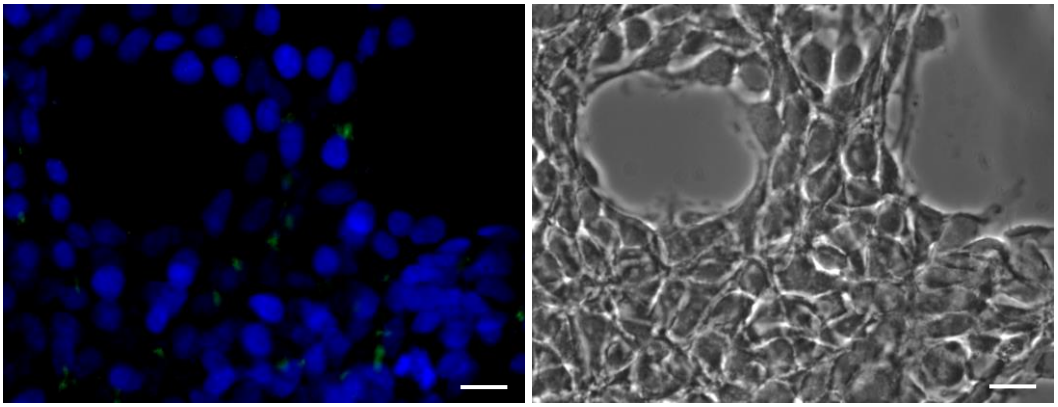

C. FITC-BSA + Simvastatin

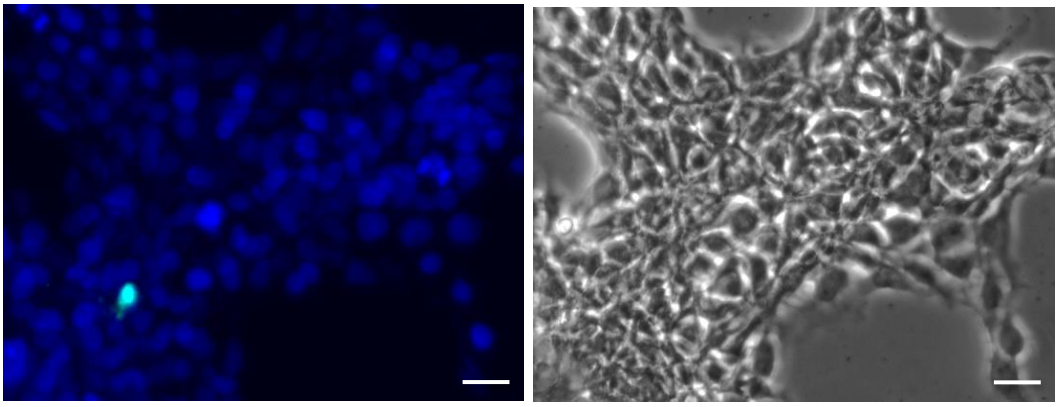

Figure 2.8 Albumin uptake assay in HEK 293 cells.
HEK 293 cells were incubated with (A) FITC-BSA, (B) FITC-BSA + BSA and (C) FITC-BSA + simvastatin for 15 minutes. Nuclei were stained with Hoechst 33342 and FITC-BSA was visualized at 488 nm. A phase contrast image of the same area was also added to locate the cells. Images were taken using a 40x objective. Scale bar is 20 µm. Data is representative of n = 3 experiments.

A. FITC-BSA

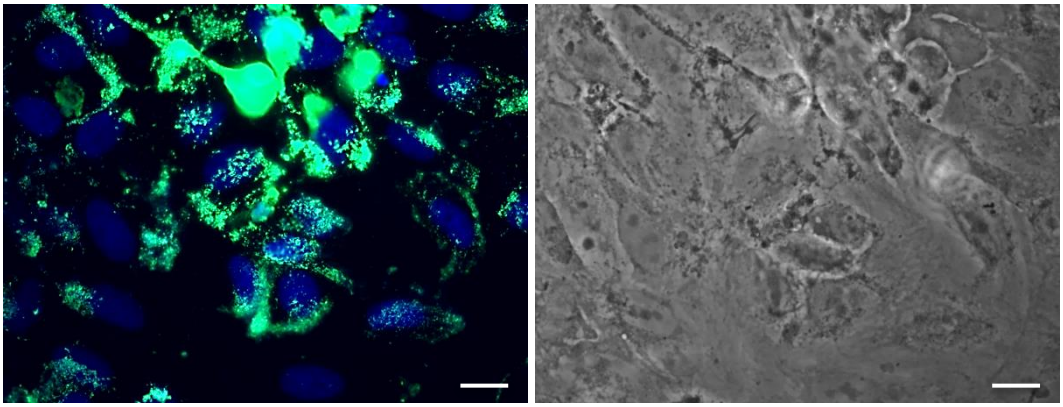

B. FITC-BSA + BSA

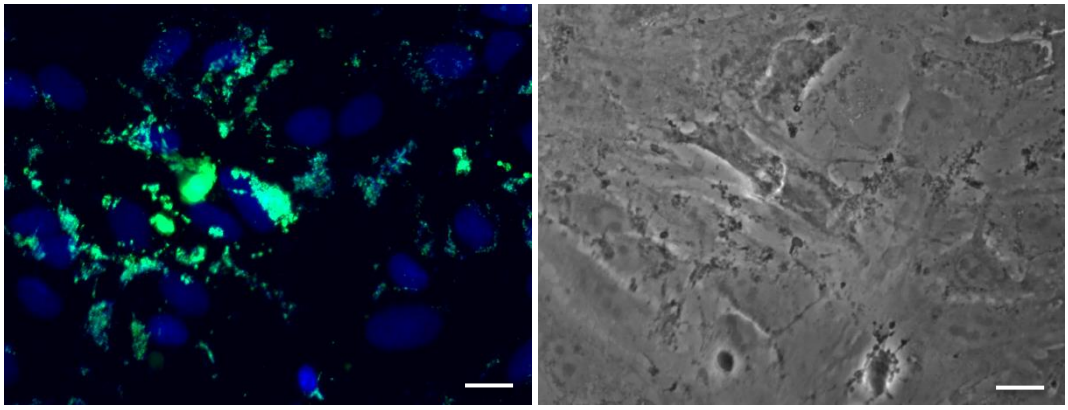

C. FITC-BSA + Simvastatin

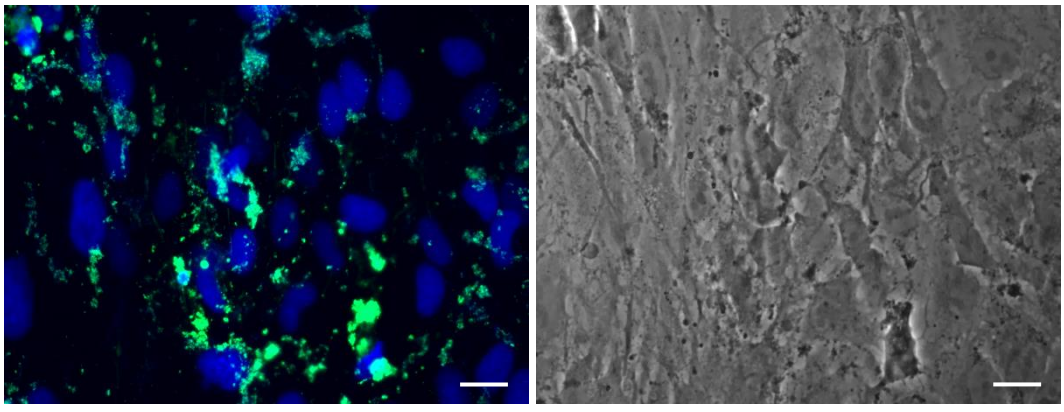

Figure 2.9 Albumin uptake assay in OK cells

OK cells were incubated with (A) FITC-BSA, (B) FITC-BSA + BSA and (C) FITC-BSA + simvastatin for 15 minutes. Nuclei were stained with Hoechst 33342 and FITC-BSA was visualized at 488 nm. A phase contrast image of the same area was also added to locate the cells. Images were taken using a 40x objective. Scale bar is 20 µm. Data is representative of n = 3 experiments.

Once the negative and the positive controls for albumin uptake had been established, the functionality of the megalin and cubilin endocytic system in ciPTECs was assessed. Although the results demonstrated albumin uptake, they were not clearly distinguishable due to a fluorescent background network, most likely due to FITC-BSA stuck in the extracellular matrix (ECM) created by this PT cell line (Figure 2.10 A). This phenomenon was also observed when ciPTECs were incubated with FITC-BSA + BSA (Figure 2.10 B). Based on these data, we did not study the effect of simvastatin using this technique since it seemed ineffective in ciPTECs to evaluate the uptake of FITC-BSA.

A. FITC-BSA

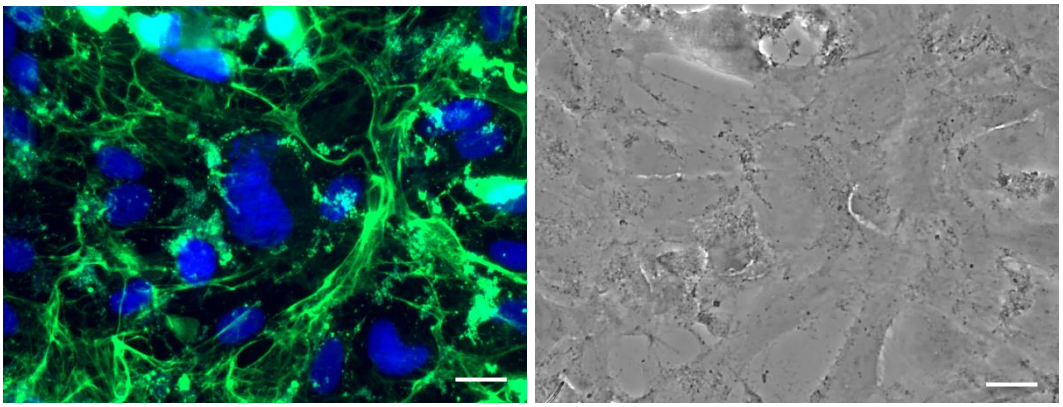

B. FITC-BSA + BSA

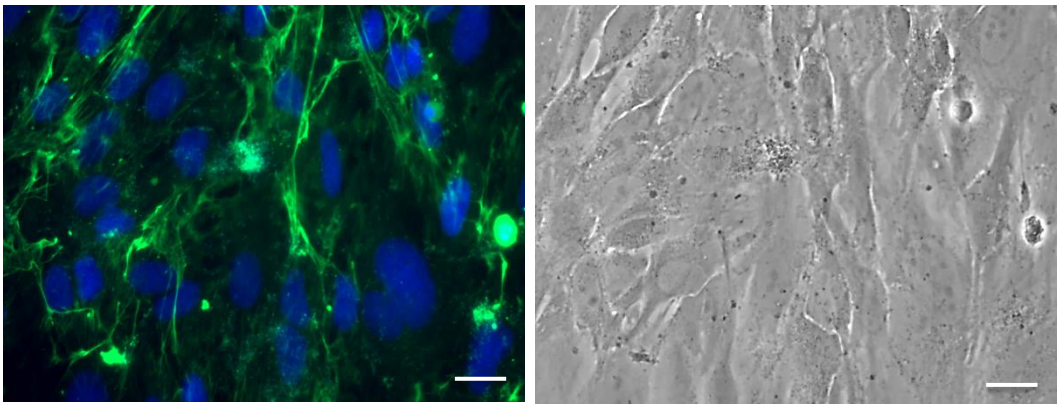

Figure 2.10 Albumin uptake assay in ciPTECs at 33°C.
ciPTECs were incubated with (A) FITC-BSA and (B) FITC-BSA for 15 minutes. Nuclei were stained with Hoechst 33342 and FITC-BSA was visualized at 488 nm. A phase contrast image of the same area was also added to locate the cells. Images were taken using a 40x objective. Scale bar is 20 µm. Data is representative of n = 3 experiments.

Alternatively, to tackle the fluorescent ECM problem in ciPTECs observed by immunocytochemistry (ICC), we decided to analyse the FITC-BSA uptake using flow cytometry. The rationale for this line of methodology is that after tripsinization, the ECM would be dissolved and we would be able to selectively quantify the albumin fluorescence of each cell. The experiment was also repeated in HEK 293 and OK cells.

The flow cytometric analysis for HEK 293 cells did not show any significant difference between the control and cells treated with simvastatin. However, a significant 20% reduction in fluorescence was detected in HEK 293 cells treated with non-labelled BSA (Figure 2.11 A). Note that the fluorescence of the control condition was only represented as 100% to compare the effect of the inhibitions. It is not a reflection of the real percentage of cells containing FITC-BSA. In OK cells, the uptake of fluorescent albumin was significantly reduced to 50% under both inhibitory conditions compared to control (Figure 2.11 B). These data also correlated with the results obtained using the fluorescence microscope (Figure 2.9).

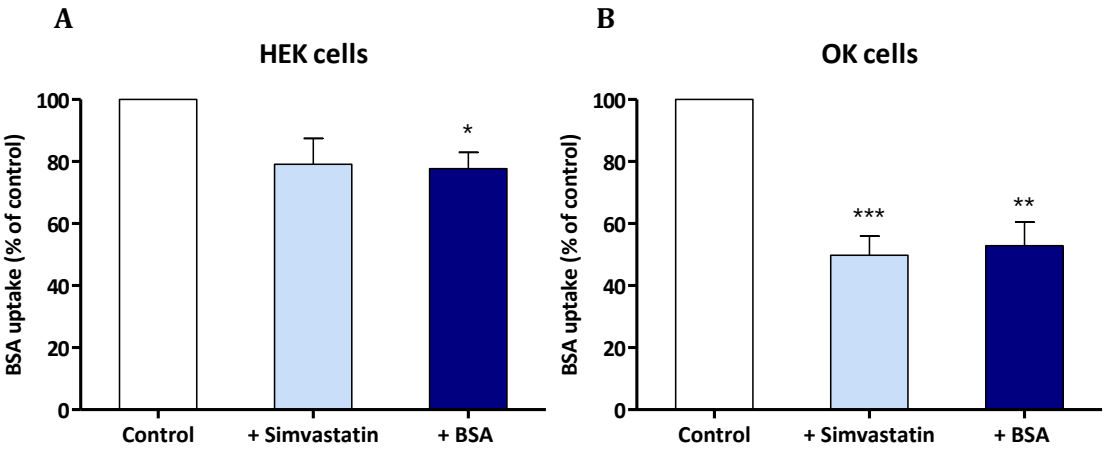

Figure 2.11 Flow cytometric analysis of FITC-BSA uptake.
(A) HEK 293 cells and (B) OK cells were treated with FITC-BSA, FITC-BSA + BSA and FITC-BSA + 10 µM of simvastatin for 15 minutes. Results are expressed as a percentage compared to control. Data are mean ± SEM (n = 3). Statistical significance was determined by One Way ANOVA test, *p<0.05, **p<0.01, ***p<0.001

Finally, the albumin uptake in ciPTECs was analysed. The obtained results were similar to what we had previously seen in OK cells. Simvastatin was able to downregulate the FITC-BSA uptake down to 60% at 33°C and down to 50%-55% at 37°C (Figure 2.12 A, B, C) and the BSA competitive inhibition down to around 40% (Figure 2.12 A, B) or 55% (Figure 2.12 C). In summary, ciPTECs showed similar levels of megalin/cubilin functionality at both temperatures as well as at different incubation treatments.

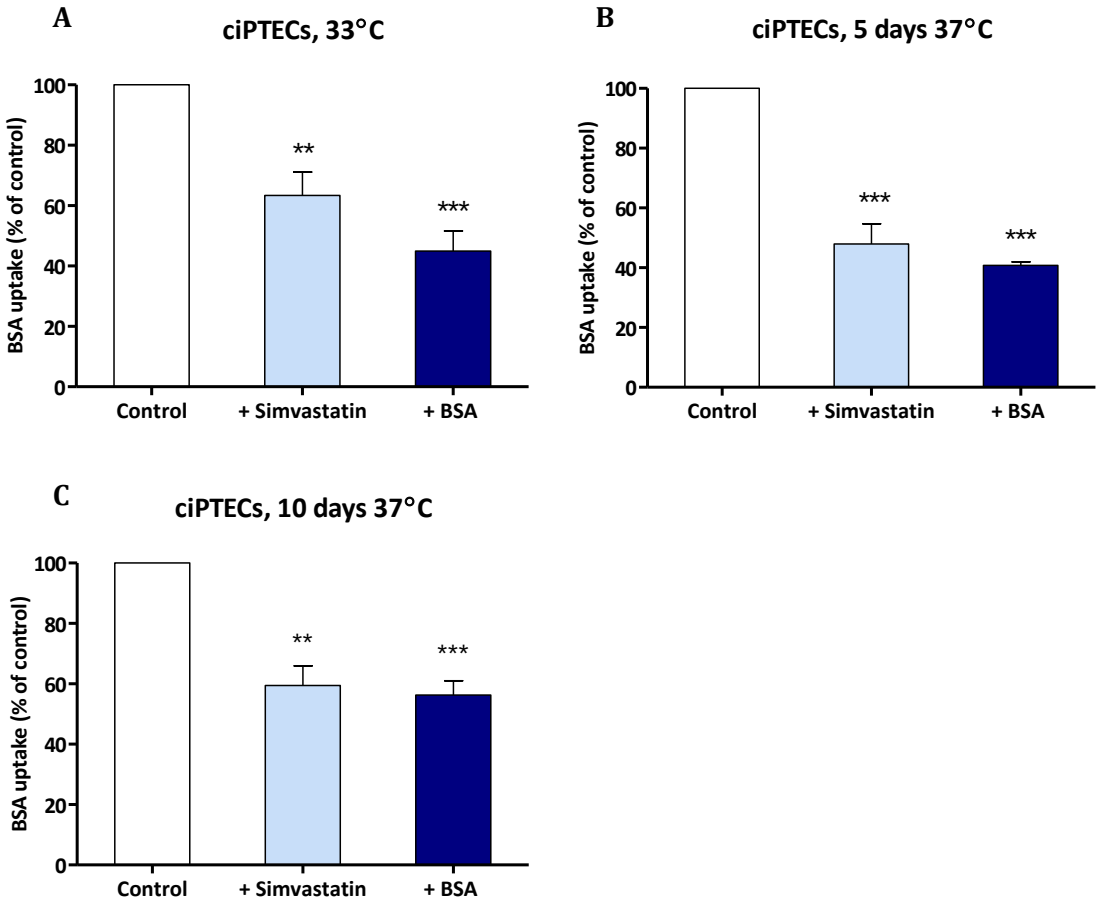

Figure 2.12 Flow cytometric analysis of FITC-BSA uptake.
(A) ciPTECs at 33°C, (B) ciPTECs at 37°C for 5 days and (C) ciPTECs at 37°C for 10 days were treated with FITC-BSA, FITC-BSA + BSA and FITC-BSA + 10 µM of simvastatin for 15 minutes. Results are expressed as a percentage compared to control. Data are mean ± SEM (n = 3). Statistical significance was determined by One Way ANOVA test, *p<0.05, **p<0.01, ***p<0.001

2.3.6 CMFDA as a tool to study MRP2, MRP4 and P-gp functionality in ciPTECs

As represented in Figure 2.2, CMFDA dye can enter the cells through the cell membrane but once inside, the molecule is cleaved by esterases, becoming fluorescent and impermeable. As MRP2, MRP4 and P-gp are capable of excreting the impermeant dye, we hypothesized that if these transporters were functional and were inhibited with MK571 or PSC833, an increase in fluorescence would be detected due to CMFDA accumulation inside the cells (Jenkinson et al. 2012). On the other hand, if the transporters were not present or functional, the addition of inhibitors would not affect the intracellular fluorescence.

When MK571 was added in HEK 293 cells, no increase in CMFDA fluorescence was detected in the two lowest concentrations. However, from 6.25 μM a small but significant increase was observed (Figure 2.13 A). Instead, when HEK 293 cells were dosed with PSC833 no changes were seen (Figure 2.14 A). As expected, HEK 293 cells showed inexistent or very low levels of functionality.

In OK cells, after inhibiting MRP transporters, the fold in CMFDA fluorescence increased more than 3 times, even at the lowest concentrations of MK571 (Figure 2.13 B). At 25 μM, a minor setback in fluorescence could be observed, which could be due to changes in pH as CMFDA dye is very sensitive to it. P-gp inhibition also caused a rise in fluorescence, duplicating at 1.48 μM of PSC833 and reaching values 4 times higher at 4.44 μM and 13.33 μM (Figure 2.14 B).

The results for ciPTECs were very similar at both temperatures investigated. A dose dependent increase in CMFDA fluorescence was detected for both inhibitors. MK571 triggered a fold increment of 3 at the two highest concentrations (Figure 2.13 C, D), which was comparable to the highest values obtained in OK cells. However, PSC833 only induced a significant 1.7 fold change peaking at 13.33 μM (Figure 2.14 C) as well as 4.44 μM (Figure 2.14 D). In summary, these fold increases observed were lower than the ones obtained in

OK cells but higher than in HEK 293 cells, indicating that ciPTECs have functional levels of MRP2, MRP4 and P-gp transporters and these are not excessively high as detected in the multidrug resistant OK cell line.

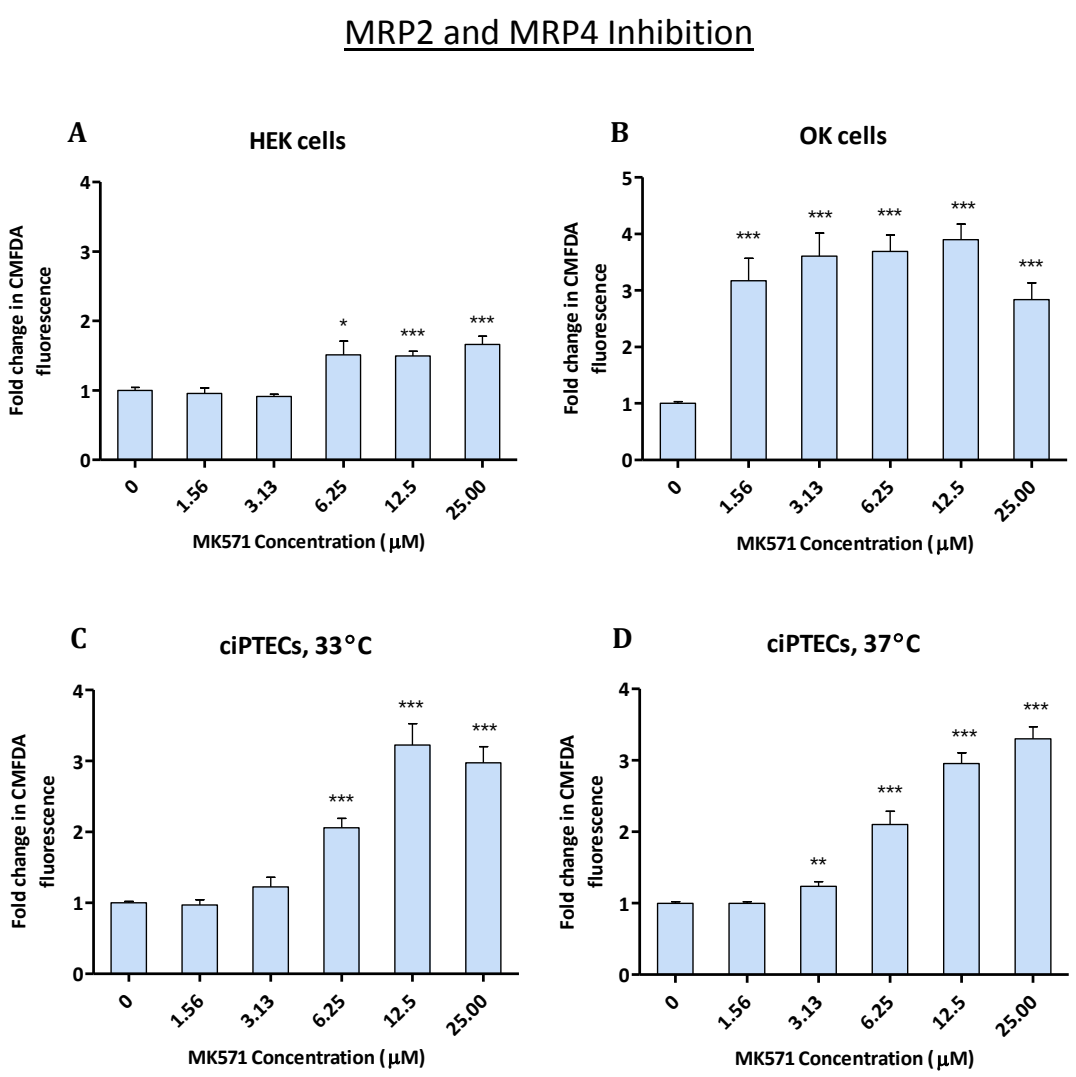

Figure 2.13 Study of MRP2 and MRP4 function using CMFDA dye

(A) HEK 293 cells, (B) OK cells, (C) ciPTECs at 33°C and (D) ciPTECs at 37°C were cultured in CMFDA solution (1.25 µM) at increasing concentrations of MK571 (0 - 25 µM). Data are represented in fold change and compared to the control (0 µM) for each cell type. Data are mean ± SEM (n = 3). Statistical significance was determined by One Way ANOVA test, **p*<0.05, ***p*<0.01, ****p*<0.001

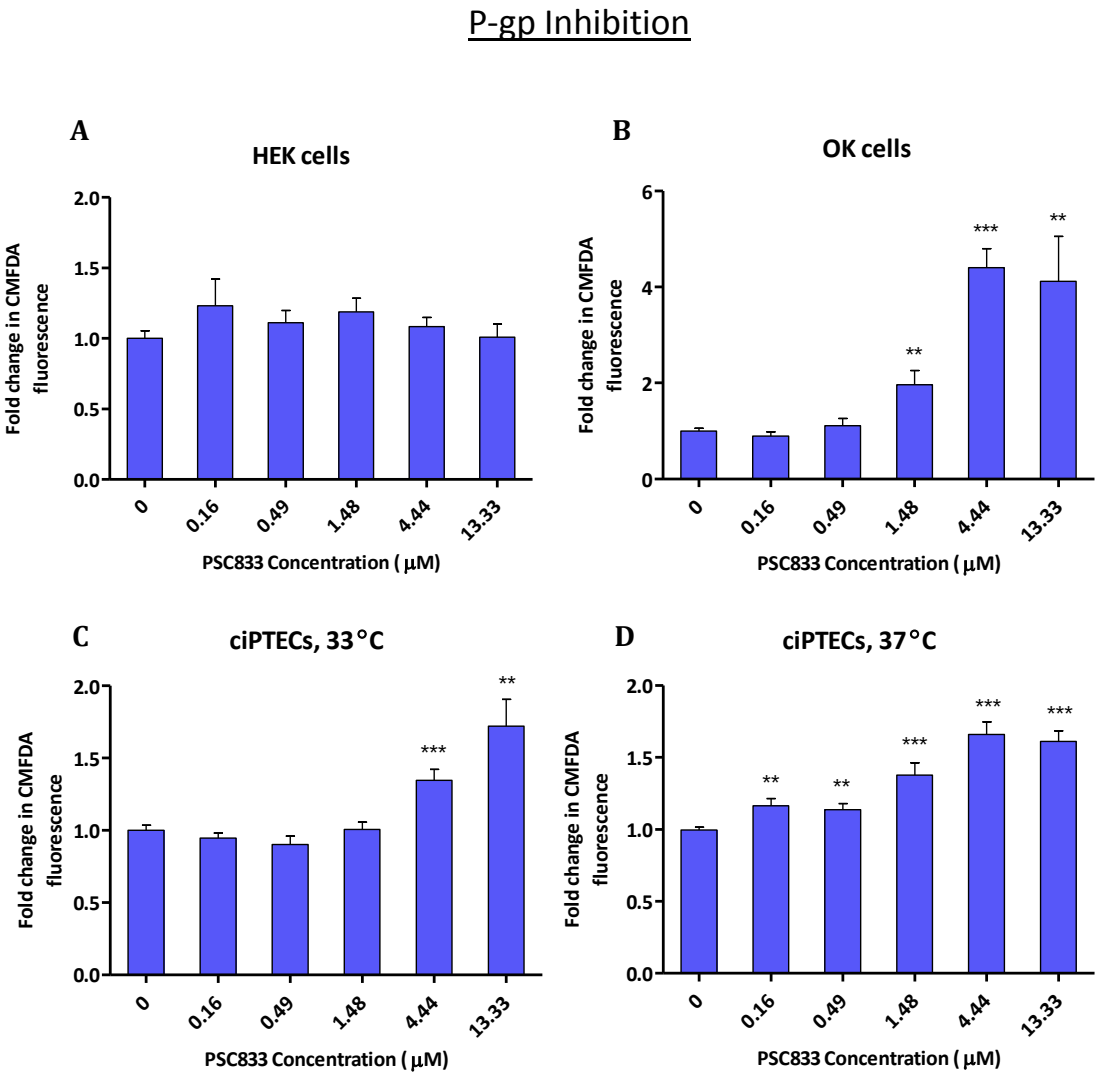

Figure 2.14 Study of P-gp function using CMFDA dye

A) HEK 293 cells, (B) OK cells, (C) ciPTECs at 33°C and (D) ciPTECs at 37°C were cultured in CMFDA solution (1.25 µM) at increasing concentrations of PSC833 (0 - 13.33 µM). Data are represented in fold change and compared to the control (0 µM) for each cell type. Data are mean ± SEM (n = 3). Statistical significance was determined by One Way ANOVA test, **p*<0.05, ***p*<0.01, ****p*<0.001

2.3.7 Hoechst 33342 uptake does not offer functional information

In order to acquire a further understanding about ciPTECs transporters, we used Hoechst 33342 to study BCRP function. Hoechst 33342 is a substrate of BCRP but also of P-gp (Jenkinson et al. 2012), thus P-gp was additionally analysed and used as an assay reference by comparing the results to the ones obtained for the same transporter using CMFDA.

The results obtained with HEK 293 showed no upregulation of Hoechst 33342 fluorescence after inhibiting neither BCRP (Figure 2.15 A) nor P-gp (Figure 2.16 A), which correlated with the data obtained with CMFDA and it could be translated into an absence of these two transporters in this particular cell line. Nevertheless, even though we were expecting to detect higher levels of functionality in OK cells, when they were dosed with the BCRP inhibitor (Figure 2.15 B) or the P-gp inhibitor (Figure 2.16 B) we could not observe any significant increment in fluorescence.

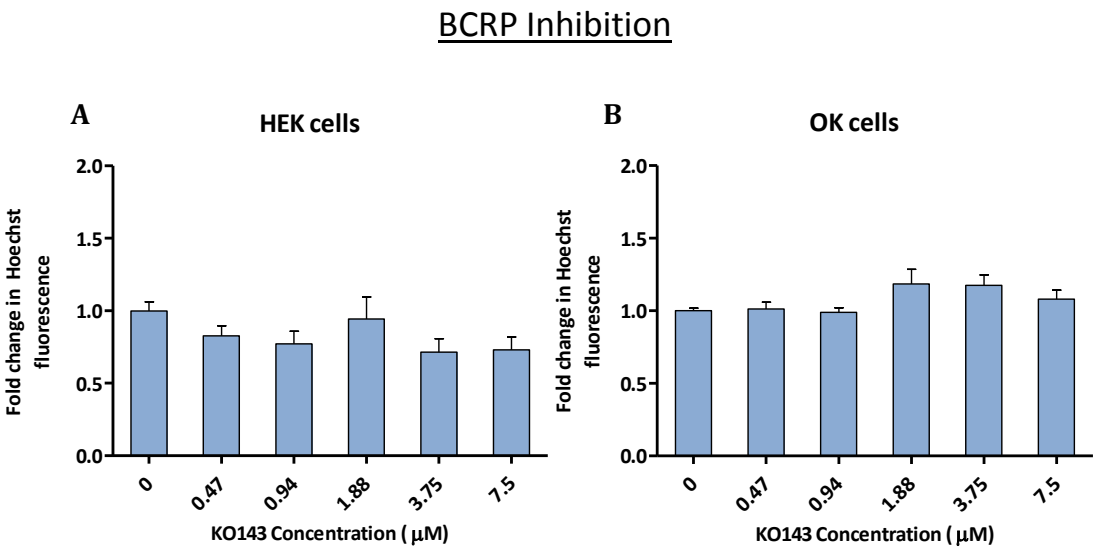

Figure 2.15 Study of BCRP function using Hoechst 33342
A) HEK 293 cells and (B) OK cells were cultured in Hoechst solution (1.25 µM) at increasing concentrations of KO143 (0 - 7.5 µM). Data are represented in fold change and compared to the control (0 µM) for each cell type. Data are mean ± SEM (n = 3). Statistical significance was determined by One Way ANOVA test, **p*<0.05, ***p*<0.01, ****p*<0.001

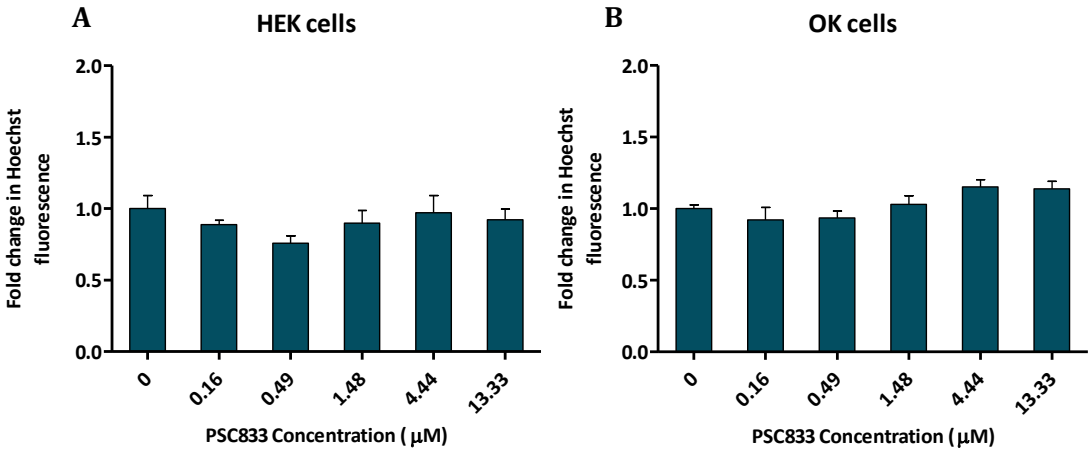

Figure 2.16 Study of P-gp function using Hoechst 33342
(A) HEK 293 cells and (B) OK cells were cultured in Hoechst 33342 solution (1.25 μM) at increasing concentrations of PSC833 (0 - 13.33 μM). Data are represented in fold change and compared to the control (0 μM) for each cell type. Data are mean ± SEM (n = 3). Statistical significance was determined by One Way ANOVA test, *p<0.05, **p<0.01, ***p<0.001.

To determine if the reason why no difference in fold change could be detected was the achievement of a plateau in fluorescence, we cultured OK cells in increasing concentrations of Hoechst 33342 with no inhibitors, with PSC833 at 13.33 μM and with KO143 at 7.5 μM (Figure 2.17). The data evidenced that no plateau had been attained as cells could accumulate greater levels of fluorescence than observed with cells in the presence of 1.25 μM of Hoechst 33342 (Figure 2.17 A). Moreover, a plateau was only starting to become discernible at the highest concentrations of the dye (20 μM to 25 μM). A closer look of Hoechst 33342 fluorescence can be observed in Figure 2.17 B. At 1.25 μM, the difference of accumulated dye between all three conditions was small, but it seemed to increase around 6.25 μM. Furthermore, although the differences between Km were not significant, the concentration of Hoechst 33342 needed to reach the maximal fluorescence intensity in the presence of inhibitors was considerably reduced (Table 2.7). As a result, the Hoechst 33342

functional assay was repeated, increasing the concentration of the dye to 6.25 µM, to see if this could lead to a detectable fold difference.

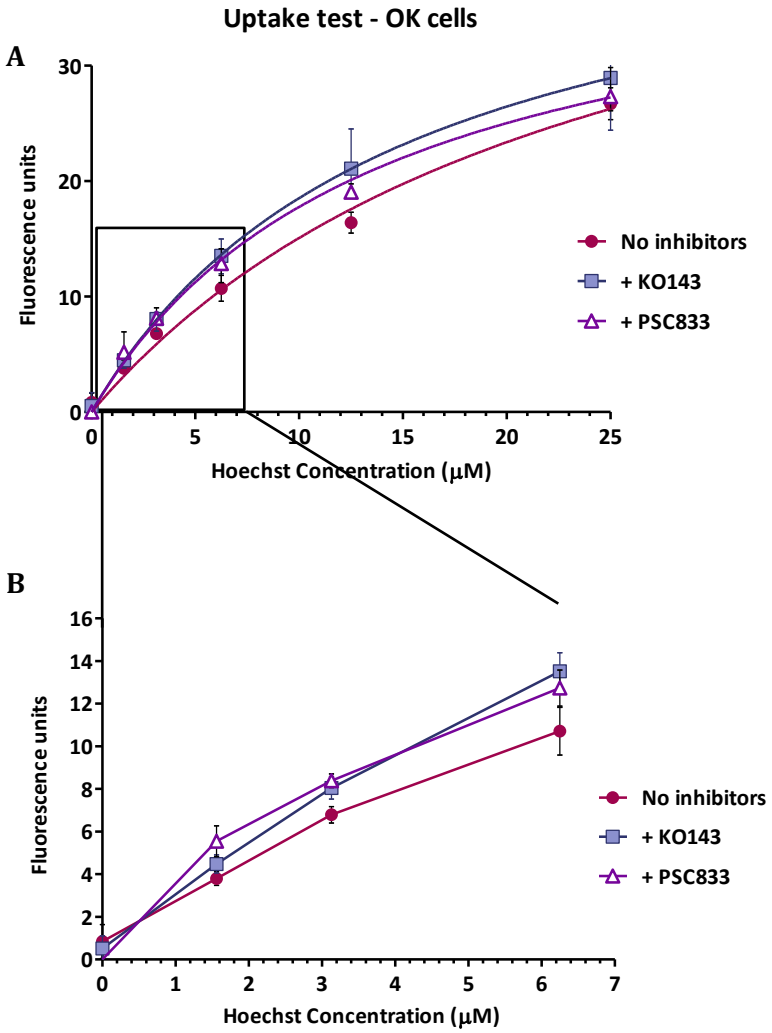

Figure 2.17 Dose dependent uptake of Hoechst 33342 in OK cells.
OK cells were cultured in Hoechst 33342 solution at different concentrations (0 - 25 µM) with no inhibitors, with PSC833 at 13.33 µM and with KO143 at 7.5 µM. Graph B is an amplified version of graph A. Data are represented in fluorescence units. Data are mean ± SEM (n = 3).

Table 2.7 Comparison of Km values obtained from a non-linear analysis of Hoechst 33342 retention in OK cells.

	No Inhibitors	+ KO143	+ PSC833
Km ± SD	24.5 ± 5.4 µM	14.9 ± 3.6 µM	13.8 ± 1.8 µM
***p* value**	--	N.S.	N.S.

Data are mean ± SD (n = 3). *p* value indicates significance ($p<0.05$) to control (No Inhibitors) by One Way ANOVA. Key: N.S. indicates not significant.

In summary, OK cells were treated again with increasing concentrations of KO143 (Figure 2.18 A) and PSC833 (Figure 2.18 B) in Hoechst 33342 solution (6.25 µM). Once more, no differences in fluorescence were observed after the addition of any inhibitor, with even more stable readings than the experiments previously performed at a lower concentration.

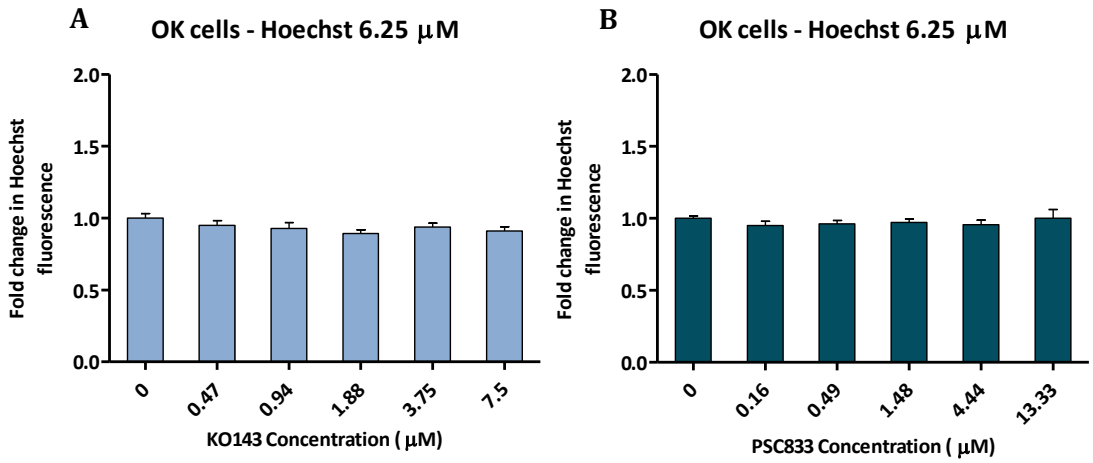

Figure 2.18 Study of BCRP and P-gp function using Hoechst 33342 in OK cells.
OK cells were cultured in Hoechst 33342 solution (6.25 µM) at increasing concentrations of (A) KO143 (0 - 7.5 µM) and (B) PSC833 (0 - 13.33 µM). Data are represented in fold change and compared to the control (0 µM). Data are mean ± SEM (n = 3). Statistical significance was determined by One Way ANOVA test, **p*<0.05, ***p*<0.01, ****p*<0.001

2.4 DISCUSSION

In this chapter, the initial objective was to perform a phenotypical characterisation of ciPTECs and to compare the results obtained with other cell lines such as HEK 293 and OK. PCR and qPCR data elucidated how, in fact, HEK 293 do not represent an ideal PT model due to an evident lack of transporters involved in drug-induced nephrotoxicity such as the OATP4C1 (uptake transporter) or MRP2 (efflux pump) (International Transporter et al. 2010, Nagai and Takano 2010). Therefore, drug toxicity studies in HEK 293 cells would not be representative. In contrast, ciPTECs expression profile was very similar to freshly isolated tubular cells at passage 2. This was the first time that such a large gene expression characterisation was performed in this cell line and results have been compared to freshly isolated renal tubular cells (Jansen et al. 2014, Wilmer et al. 2010). Additionally, comparing the results to HK-2 expression profile (Jenkinson et al. 2012) it became evident that ciPTECs overcome HK-2 cells as a PT model.

Regarding differences at 33°C and 37°C, only three genes stood out. One of the big changes was the upregulation of BCRP, a transporter associated with breast cancer (Doyle and Ross 2003), at 33°C, which could be due to the immortalisation cancer-like process induced at this temperature. CUBN and OATP4C1 were upregulated at 37°C instead, which could be either a sign of final cell differentiation or an upregulation due to cell contact stimuli (Sakairi et al. 2010a). However, no expression of OAT1, OAT3 or LRP2 was detected in ciPTECs or in the tubular fraction, which all play an important role in drug-induced toxicity studies (International Transporter et al. 2010, Nagai and Takano 2010). But since mRNA and protein levels do not always correlate directly, we could hypothesise that even with undetectable mRNA levels, they could still be present in protein form. Other markers like SYNPO showed high levels of mRNA. However, this does not mean that SYNPO is highly

expressed in ciPTECs, it just means that its expression in ciPTECs was 10 times higher than in the compared tubular fraction.

The absent gene expression in HEK 293 cells was also supported by functional data such as megalin/cubilin uptake assays. In contrast, the albumin accumulation in OK cells correlated with previous studies that showed the colocalization of both multiligand receptors and their ability to uptake albumin (Zhai et al. 2000, Gekle et al. 1998, Gekle 2005). Finally, and despite the lack of detectable megalin mRNA, successful FITC-BSA uptake in ciPTECs matched the already published data for ciPTECs (Wilmer et al. 2010) as well as other data published in primary human kidney tubular cells (Verhulst et al. 2004). Moreover, the uptake inhibition through simvastatin indicated that the protein absorption was receptor specific and it was carried out via megalin/cubilin-mediated endocytosis. Simvastatin was the inhibitor of choice, instead of RAP (Christensen and Birn 2002), because it offers a potential therapeutic strategy for further studies against aminoglycoside-induced nephrotoxicity (Antoine et al. 2010) in our conditionally immortalised PT model.

The OK cell line has been described to present multidrug resistant characteristics due to a much higher expression of xenobiotic transporters, such as MRP2, than other PT cell lines (Notenboom et al. 2006, Malstrom et al. 1987, Takano et al. 1996). Thus, as seen in the results, it could be predicted that they would have hold great levels of MRP and P-gp functional transporters. The functionality levels of MRP2, MRP4 and P-gp exhibited in ciPTECs confirmed that the received cell line exhibited the same properties and correlated to the experiments published by our collaborative partners (Wilmer et al. 2010). Therefore, we can conclude that the received ciPTECs are fit for purpose to study nephrotoxicity.

BCRP functionality assay using the uptake method published by Jenkinson *et al*. in 2012 in HK-2 cells proved unsuccessful. However, since P-gp results did not match the ones obtained in CMFDA, the problem could only be attributed to the assay basis (levels of background were too high) or to the performance. Nevertheless, the Km in the presence of these inhibitors decreased and the control Km was much higher than the one observed in HK-2 cells (Jenkinson et al. 2012). Therefore, a higher Km in ciPTECs could indicate a higher amount of BCRP and/or P-gp transporters than in HK-2 cells, since a larger number of transporters would handicap the accumulation of Hoechst 33342 inside the cells and hence, higher concentrations of the dye would be needed to acquire the maximum level of fluorescence. Furthermore, Jenkinson *et al*. barely detected a decrease in Km (around 16 µM) in the presence of KO143 but had a significant decrease when they used cyclosporin A (CSA), which inhibits P-gp. Then, the usage of more potent inhibitors might be an option to measure the functionality of P-gp and BCRP transporters using the Hoechst 33342 uptake assay.

To further explore the functionality of other transporters and develop a better confidence in the ciPTECs as a nephrotoxicity model, additional transport assays could be considered. For instance, an organic anion uptake assay could be performed to test OAT1 and OAT3 function by using probencebid, a potent OAT inhibitor, and the fluorescent anion 6-carboxyfluorecein (6-CF) (Lawrence et al. 2015). Other interesting assays could be an organic anion efflux assay as well as an organic cation uptake assay.

On a final note, it is important to consider that ciPTECs cultured at 33°C have proven to present very similar levels of functionality compared to ciPTECs cultured at 37°C for 5 or 10 days. These data challenges the statements made by Wilmer *et al*., where they only performed functional assays after 8 - 10 days at 37°C as they reasoned that it was the time required to achieve a mature state, which also correlates with the cease of oncogene

expression. However, our results suggest that this is not the case, ciPTECs had very similar levels of expression and functionality at both temperatures and therefore further experiments will not need to be performed after ciPTECs have undergone “maturation”.

In summary, it was confirmed that ciPTECs express the necessary functional transporters to be a potentially valuable and specific physiologically based model to study nephrotoxicity *in vitro*. Based on the data presented from the investigations of this chapter, ciPTECs will be the cell line of choice to perform the mechanistic nephrotoxicity studies within Chapters 3 and 4.

Chapter Three

Development of a novel human-derived conditionally immortalised proximal tubule epithelial cell line model to screen for renal mitotoxicity based on intracellular biochemical modulation

CONTENTS

3.1 INTRODUCTION

In culture, evaluating drug-induced renal mitochondrial dysfunction is a challenging task. As discussed previously, newly immortalised cell lines, of human origin, such as ciPTECs have become the current state of the art alternative to assess cell function *in vitro* and potentially mechanistic drug-induced nephrotoxicity (Wilmer et al. 2010, Wieser et al. 2008). This cell line was characterised in Chapter 2, in which the expression and functionality of some important drug transporters was confirmed. Nonetheless, it has been shown that cancer and immortalised cell lines are metabolically adapted to proliferate in supraphysiological levels of glucose and therefore prone to fall into the Crabtree effect and hence complicates the interpretation on toxicants that might mechanistically operate via intracellular bioenergetic pathways. The Crabtree phenomenon is based on a downregulation of the mitochondrial oxidative phosphorylation (OXPHOS) route to mainly rely on glycolysis for cell energy production (Figure 3.1) (Rodriguez-Enriquez et al. 2001, Guppy et al. 1993, Dell' Antone 2012). Consequently, even though cells are cultured in

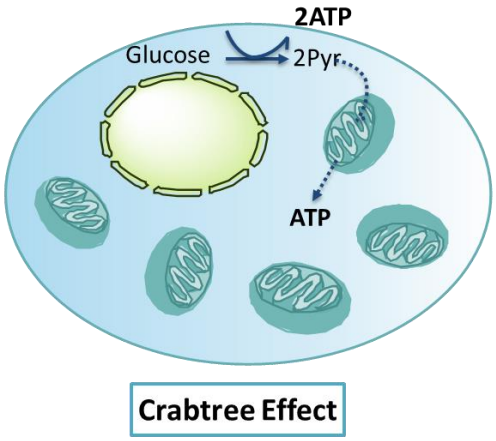

Figure 3.1 Simple representation of the Crabtree effect
The Crabtree effect is a phenomenon observed *in vitro* that consists of cells deriving almost all their energy from glycolysis instead of OXPHOS. The conversion of glucose to pyruvate (Pyr) generates only two net ATP molecules (2ATP). However, in high concentrations of glucose as a substrate, glycolysis flux rate can be radically accelerated to overcome the low efficiency in ATP production. The mitochondria still remain slightly active but only around 5% of the glucose carbon enters the citric acid cycle.

abundant O_2 and hold perfectly healthy mitochondria, since these organelles are not essential for cell energy production, cells can potentially become resistant to mitotoxins and stop representing a relevant model to evaluate mechanistic mitochondrial toxicity.

To bypass the Crabtree effect and increase the potential susceptibility to mitotoxins *in vitro*, Marroquin *et al*. replaced glucose for galactose in the medium. They proved that after 8 weeks in culture, this change in energy source forces anaerobically poised cells to rely on OXPHOS. Metabolically, when galactose becomes the main carbohydrate, the glycolytic activity becomes downregulated with barely any glycolytic intermediates detectable in the cells. Instead, almost all the galactose carbon is metabolised through the pentose phosphate cycle, a metabolic pathway parallel to glycolysis, yielding very little or no energy. Therefore, galactose plays an anabolic role rather than a catabolic one. However, cells are still able to grow at a constant rate, thus the energy has to come from an alternative source: L-glutamine (Figure 3.2). Along with sugar, L-glutamine is the most abundant carbon in the medium and can provide half of the energy in the presence of glucose and

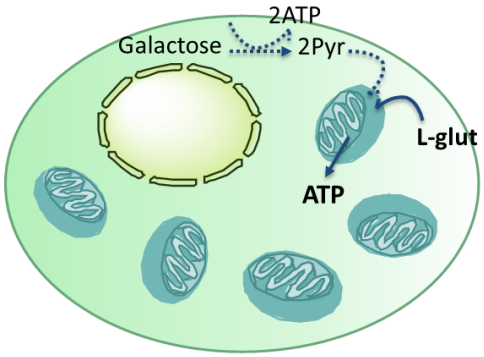

Figure 3.2 Representation of metabolic energy changes when galactose is the main carbohydrate in the medium.
Circumventing the Crabtree effect by substituting glucose for galactose promotes a downregulation of glycolysis, with only very few of galactose molecules following this route. Therefore, cells are forced to use L-glutamine as their main source of energy. L-glutamine skips glycolysis and it is directly incorporated into the citric acid cycle. As a result, OXPHOS is upregulated.

more than 98% of the energy in galactose conditions (Reitzer LJ 1979). This amino acid directly enters the citric acid cycle metabolism, avoiding glycolysis and stimulating mitochondrial OXPHOS (Figure 3.3).

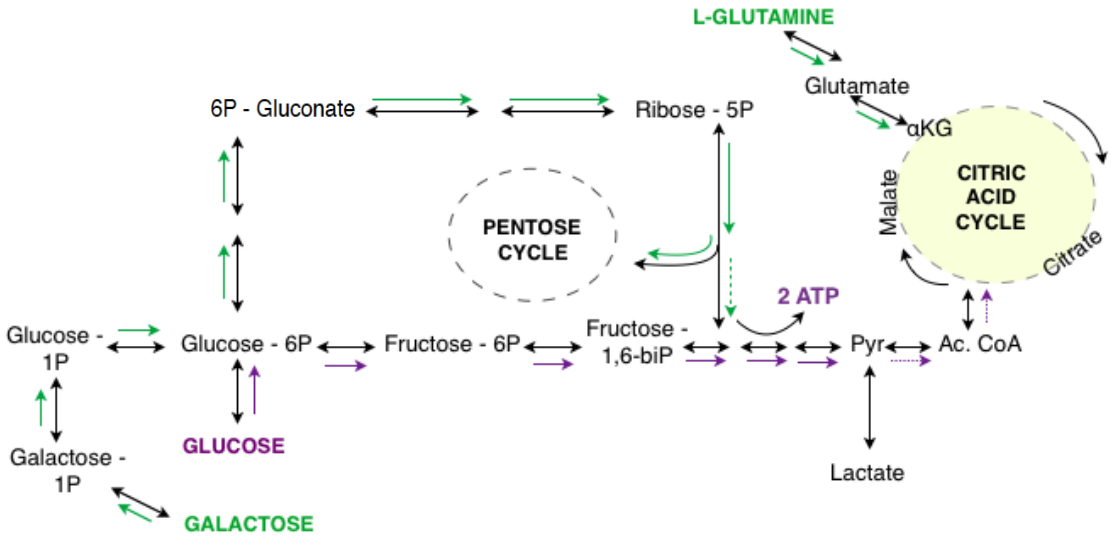

Figure 3.3 Summarized diagram of the biochemical pathways followed by each energetic substrate (Reitzer LJ 1979).
Glucose route of ATP production is delineated in green. When the glucose in the media is replaced by galactose, the ATP production pathway changes and it follows the purple route.

The media change technique based on replacing glucose for galactose, was first implemented in HepG2 cells and later repeated with human primary muscle cells (Marroquin et al. 2007, Aguer et al. 2011). It was also later modified by Kamalian, *L., et al.* (2015) (with whom we were able to collaborate), as they shortened the pre-treatment in both media conditions from 8 weeks to 4 h. The results showed an acceleration of O_2 consumption that reflected the metabolic shift towards mitochondrial respiration and a greater vulnerability in front of mitotoxins such as oligomycin, FCCP and rotenone. Furthermore, they also suggested that a comparison with respiration data between glucose and galactose conditions could be useful as a toxicity screen that would also offer mechanistic insight. Hence, if cytotoxicity is observed in galactose grown but not in glucose grown cells, that would provide an evidence for mitochondrial impairment as the

predominant pathway leading to cell death and toxicity. In contrast, when no difference could be detected, alternative pathways would most likely dictate the cell toxicity (Marroquin et al. 2007).

3.1.1 Aims and hypothesis

Hypothesis:

We hypothesised that if ciPTECs were under the Crabtree effect, by implementing the glucose/galactose media change strategy we would be able to drive them to a higher aerobic metabolic state and use them as a model to evaluate *in vitro* renal mitochondrial impairment.

The aims of this Chapter were to:

- Metabolically characterise ciPTECs in glucose and galactose media conditions to assess if ciPTECs had fallen under the Crabtree effect following the media change strategy reported by Kamalian, L*., et al.*
- Check the vulnerability of ciPTECs to model mitochondrial toxins in glucose *vs.* galactose conditions.
- Test potential mitotoxic and nephrotoxic compounds in the established glucose *vs.* galactose PT cell model to validate its potential in discerning compounds that have mitochondria as its main toxicity target. Hence, validating its potential to be the first renal model able to screen for clinically relevant mitochondrial liabilities.

3.2 MATERIALS AND METHODS

3.2.1 Materials

The OK cell line was purchased from the European Collection of Cell Cultures (ECACC). ciPTECs were obtained from the Department of Pharmacology and Toxicology in Radboud University Nijmegen (Nijmegen, Netherlands). Tissue culture reagents DMEM/F-12 (1:1), FBS, dialyzed fetal bovine serum (DFBS), PBS, MitoSOX™ Red Mitochondrial Superoxide Indicator, Hoechst 33342 and ProLong® Gold Antifade Mountant were purchased from Life Technologies (Paisley, UK). DMEM – F12 without glucose was purchased from Biowest (Nuaillé, France). Seahorse consumables were purchased from Seahorse Biosciences (North Billerica, MA, USA). Cover slides (13 mm ∅) were purchased from VWR (Lutterworth, UK) and microscope slides were obtained from Thermo Fisher Scientific (Loughborough, UK). Gold Star liquid scintillation cocktail was purchased from Meridian Biotechonologies (Surrey, UK) and scintillation vials were obtained from Simport (Beloeil, Canada). Cytotoxicity Detection Kit was purchased from Roche Diagnostics Ltd (West Sussex, UK). CellTiter-Glo Luminescent Cell Viability Assay and CellTiter 96 Aqueous Non-Radioactive Cell Proliferation Assay were purchased from Promega (Southampton, UK). TFV was obtained from Toronto Research Chemicals Inc. (Toronto, Canada) and tritium labelled TFV was purchased from Moravek Biochemicals, Inc. (Brea, California). All other reagents and chemicals were purchased from Sigma Aldrich (Dorset, UK).

3.2.2 Cell culture

OK cells and ciPTECS were cultured as stated in Chapter 2.2.2.

3.2.3 Bioenergetic profile assessment in ciPTECs using Seahorse technology

3.2.3.1 ciPTECs cultured at 33°C

ciPTECs were plated on a XF 96-well microplate at $1x10^4$ cells/well to determine the bioenergetic profile at 33°C. 24 h later, we defined four separate quarters in the microplate dedicated to four different conditions (see Figure 3.4). In two of them, media was changed: in one quarter the media was replaced by the original growth medium using DFBS (10% v/v) instead FBS and in the other quarter the media was replaced by ciPTECs galactose medium. The galactose medium was prepared with DMEM – F12 (1:1) without glucose supplemented with L-glutamine (2 mM), DFBS (10% v/v) and the rest of the cell culture supplements listed in the cell culture section (33°C, 5% CO_2). The media of the other untreated two quarters was replaced following the same arrangement 20 h later:

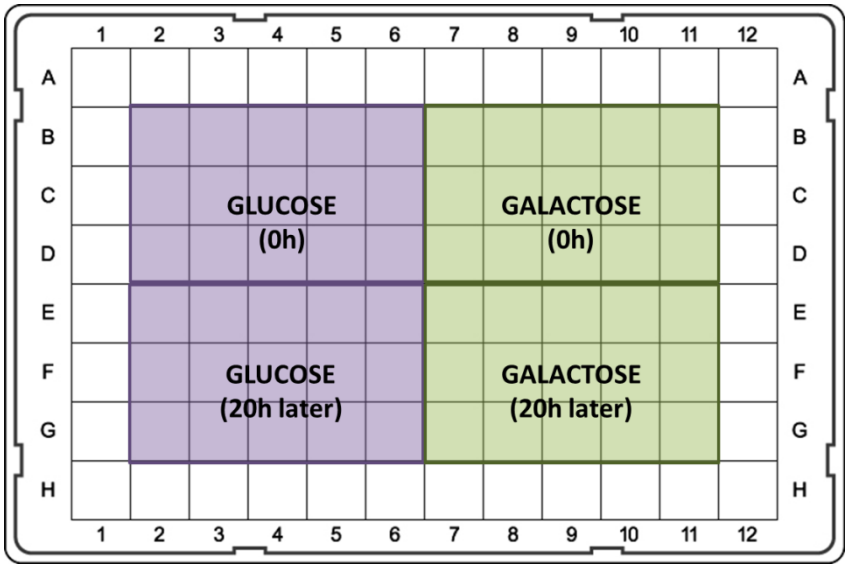

Figure 3.4 Schematic of the plate design.
The 96-well plate was divided into four sectors. The two sectors on the top had the media changed at 0 h and the ones on the bottom had the media changed 20 h later. Results were analysed 24 h after the first change in media.

At 24 h after the first media change, the plate was washed twice with XF Base Medium supplemented with L-glutamine (1% v/v), sodium pyruvate (1 mM) and 25 mM glucose or 10 mM galactose for glucose and galactose based media respectively and then 175 µl of

glucose or galactose medium were added to the respective wells; media pre-warmed to 37°C and pH adjusted to 7.4. Cells were left in a CO_2 free incubator at 37°C for 1 h while 25 µl of 8 µM rotenone stock were loaded/well to the sensor cartridge (final concentration 1 µM) and the optical sensors were calibrated by the Seahorse machine. After loading the cell microplate, basal oxygen consumption rate (OCR) and extracellular acidification rate (ECAR) were measured three times (OCR is reported in units of pmol/minute and ECAR in mpH/minute). Then rotenone was pneumatically injected into the media in each well. After gentle mixing, OCR and ECAR were measured three more times.

3.2.3.2 ciPTECs cultured at 37°C for 5 days

CiPTECs were plated on a XF 96-well microplate at 5000 cells/well and maintained at 33°C. After 24 h, the microplate was transferred to 37°C and cultured for 5 days at this temperature (5% CO_2). After this period, the same protocol for glucose and galactose dosing from section 3.2.3.1 was followed.

3.2.4 Normalization of Seahorse data by BCA assay

To normalize the Seahorse experiment data, ciPTECs were washed twice with cold PBS and 15 µl of RIPA buffer were added per well. A standard curve ranging from 0.125 – 2 mg/ml of albumin was prepared in separate tubes and 9 µl of each concentration was transferred in duplicate into a new 96-well plate as well as 9 µl of dH_2O (blank) and 9 µl of lysed cells from each well. Freshly prepared BCA reagent solution was added into each well (200 µl/well) and the plate was incubated for 35 minutes at 37°C. The absorbance was read at 570 nm on a plate reader (Varioskan, Thermo Scientific). The blank reading (dH_2O with BCA reagent) was subtracted from all sample and standard readings. Protein concentration in the samples was calculated using values obtained from the standard curve.

3.2.5 MitoSOX mitochondrial staining

Four 13 mm ∅ cover slides were placed in the wells of a 24-well plate and coated with 0.5% of gelatine for 30 minutes. The gelatine was removed and ciPTECs were seeded at a density of $4x10^4$ cells/well. After 24 h, the medium was substituted for DFBS glucose medium on two cover slides and ciPTECs galactose medium on the other two. The cells were cultured at 33°C for another 2 days and then transferred to 37°C for 5 days before the staining. When the ciPTECs were ready, they were washed twice with PBS and incubated with a 5 µM MitoSOX solution, also prepared in PBS, for 10 minutes protected from light. Then, the cells were washed 3x in warm PBS and fixed with 2% PFA for 15 minutes at RT in the dark. Two more washes with PBS were performed after cells had been fixed. Then, the nuclei were stained with 2 µg/ml of Hoechst 33342 for 10 minutes at RT protected from light. Finally, after three more washes with PBS, the cover slides were mounted onto a microscope slide with Prolong Gold. Results were visualized at 63x magnification using an inverted fluorescence microscope (Axio Observer.Z1, Zeiss).

3.2.6 Rotenone - complex I inhibition

ciPTECs were plated in four 24-well plates the day before the experiment at $8x10^4$ cells/well and cultured at 33°C (5% CO_2). After 24 h, cells were washed with PBS. Then, the media of two plates was replaced by the original growth medium using DFBS (10% v/v) instead of FBS and the media of the other two plates was replaced by ciPTECs galactose medium (33°C, 5% CO_2). Rotenone concentrations were prepared in DMSO (final solvent concentration lower than 1% v/v) and 4 h after the media replacement, cells were dosed with rotenone for 2 h and 24 h in both glucose and galactose conditions, respectively (Figure 3.5).

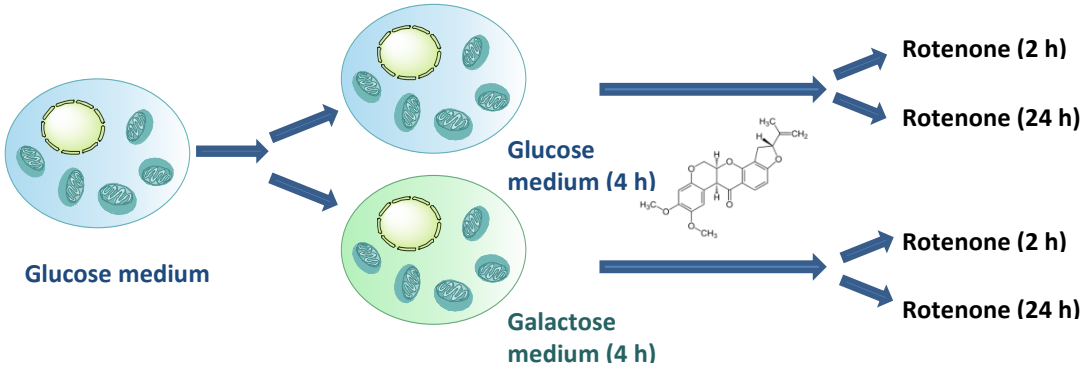

Figure 3.5 Schematic design of the dosing strategy.
Before each dosing, the media is changed for glucose with DFBS or ciPTECs galactose medium 4 h in advance. Then, cells are treated with the mitotoxic compound maintaining the same media composition during the treatment.

3.2.7 Measurement of ATP levels to evaluate cell viability

ATP content was assessed using the CellTiter-Glo Luminescent Cell Viability Assay. Briefly, 25 µl of the CellTiter-Glo Reagent were added per well of a 24-well plate, the plate was placed in a shaker for 1 minute (750 rpm), left in the dark for 5 minutes and 50 µl of the mixture from each well were transferred to a 96-well opaque-wall plate per triplicate. ATP levels were defined as a percentage compared to control. Luminescence was recorded using a plate reader (Varioskan, Thermo Scientific).

3.2.8 Cytotoxicity assessment by measuring LDH content

The LDH content inside the cells and leakage into the medium was measured using the Cytotoxicity Detection Kit. In summary, 50 µl of the media were transferred to a new 96-well plate. The rest of the media was removed from the wells and 200 µl of 1% Triton X-100 solution in DMEM/F-12 serum free medium was added per well to lysate the cells. The cell lysate was also transferred into a new 96-well plate diluted 1/5 (final volume 50 µl). Finally, 50 µl of the reaction mixture were added per well to the 96-well plates and they were incubated at RT protected from light for 30 minutes. Absorbance was measured at 490 nm (Varioskan, Thermo Scientific).

3.2.9 Tritium radiolabelled TFV uptake

This experiment was performed with OK cells and ciPTECs. OK cells were seeded in three wells of a 12-well plate at $1x10^5$ cells/well and cultured for 48 h at 37°C (5% CO_2) in DMEM/F-12 (1:1) medium supplemented with FBS (10% v/v) and penicillin-streptomycin solution (1% v/v). To evaluate the uptake of radiolabeled TFV in ciPTECs at 33°C and 37°C with glucose or galactose medium, four different conditions were set up. The ones that were assessed at 33°C were seeded at $1x10^5$ cells/well and cultured for 48 h at 33°C (5% CO_2). The cells that were evaluated at 37°C were seeded at $8x10^4$ cells/well, cultured at 33°C for 24 h and then transferred to 37°C (5% CO_2) for 5 days. At 24 h prior to the experiment, the medium was changed for either glucose or ciPTECs galactose medium (both containing DFBS). Three wells were analysed per condition. To perform the radiolabelled TFV uptake, cells were dosed with a solution of hot TFV (final concentration 0.3 µCi/well) and TFV (final concentration 10 µM) and incubated for 1 h at 37°C (5% CO_2). Then, 100 µl of each well were collected and placed into three scintillation vials. The rest of the media was removed, cells were washed with PBS twice and 100 µl of tap water were added to lyse the cells. The lysates were collected and 4 ml of scintillation cocktail were added into each scintillation vial, mixed upside down and the tritium radioactivity was measured using a scintillation analyser (Tri-Carb 3100TR, PerkinElmer).

3.2.10 Toxicity screening of different compounds using the glucose *vs*. galactose method

For antimycin A and cisplatin treatments, ciPTECs were seeded and dosed with these two compounds following the same indications and dosing strategy from section 3.2.6. The different concentrations were also prepared in DMSO and the results analysed after 2 h and 48 h respectively. When ciPTECs were dosed with gentamicin (stock prepared in dH_2O) and adefovir (stock prepared in DMSO) they were seeded at $4x10^4$cells/well in 24-well plates. The same media change strategy from section 3.2.6 was also followed and ciPTECs were

dosed for 4 and 3 days correspondingly. Lastly, ciPTECs were seeded at $1x10^4$ cells/well in 24-well plates to be dosed with TFV (stock prepared in dH_2O). Again, 3.2.6 section glucose and galactose dosing strategy was used and cells were dosed for 48 h, 8 days and 15 days with TFV changing the medium every two days. Note that every concentration was analysed in triplicate and all final solvent concentrations were lower than 1% v/v.

3.2.11 Assessment of cell growth after gentamicin exposure

ciPTECs were seeded at $1x10^5$cells/well in a 24-well plate and maintained at 33°C (5% CO_2). After 24 h, cells were dosed with different concentrations of gentamicin in glucose medium and cultured for 72 h. Then, a scratch with the tip of a 200 µl pipette was performed in each well and a picture was taken using an inverted microscope (Eclipse TS100, Nikon). Cells were incubated for another 18 h at 33°C and pictures were taken at the end of this period (Figure 3.6). ImageJ was used to analyse the amplitude of the scratch after 18 h and results were compared to the initial amplitude.

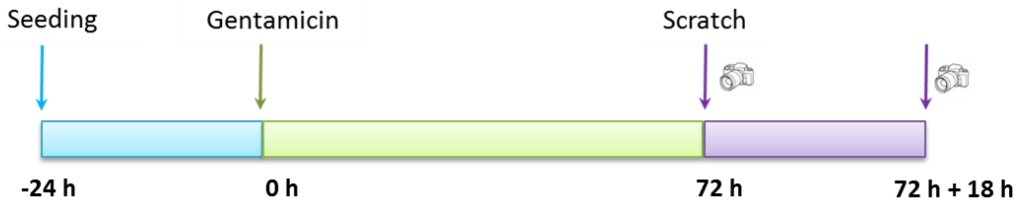

Figure 3.6 Simple representation of the study design.
Cells were seeded and dosed with gentamicin after 24 h. Then, after 72 h of gentamicin treatment, a scratch through the center of the wells was performed and pictures were taken. ciPTECs were left to recover in the same medium and another set of pictures were taken 18 h after the scratches.

3.2.12 Statistical analysis

Statistical analysis of data was performed using StatsDirect software. All results were represented as the mean ± SEM or as the mean ± SD of three independent experiments. The choice of SEM *vs*. SD was only based on obtaining a better visual representation of the

figures. Data was first assayed for normality using the Shapiro-Wilk test. When assaying differences amongst at least three groups, if data was normal, statistical analysis was performed using One Way ANOVA with Dunnet as a post-hoc comparison, as this test is specifically designed to compare each treatment against a single control. If there was no evidence of normality, Kruskal-Wallis test was applied instead. To test for differences amongst two groups, a t-test was performed if data was classified as normal and a Mann-Whitney test when data showed no evidence of normality. Only when p values <0.05 the results were considered significant.

3.3 RESULTS

3.3.1 Determination of ciPTECs bioenergetic profile and the Crabtree effect: glucose *vs.* galactose medium

To assess any differences in energetic metabolism when cells were cultured in galactose medium (without glucose) and to investigate the hypothesis that ciPTECs are under the Crabtree effect, the OCR and ECAR were measured in both glucose and galactose conditions.

The first assessment was performed at the growing temperature of the cells (33°C) at 4 h and 24 h after changing the media. At basal conditions, two different phenotypes could be detected. OCR was significantly upregulated in galactose cultured cells and it was also complemented with a reduction in the ECAR (Figure 3.7 A, B). When rotenone (complex I inhibitor) was added, oxygen consumption levels dropped drastically. Glucose grown ciPTECs also had a distinctive increase in medium acidification (ECAR values were doubled). In contrast, ECAR was maintained within similar parameters for galactose ciPTECs. All the changes seen at 24 h could also be detected at 4 h (Figure 3.7 A, B).

The same energetically metabolic pattern seen at 33°C was also displayed at 37°C (Figure 3.7 C, D). Therefore, disregarding the culturing temperature, switching to a galactose based medium induced ciPTECs to transition into a higher oxidative bioenergetic configuration.

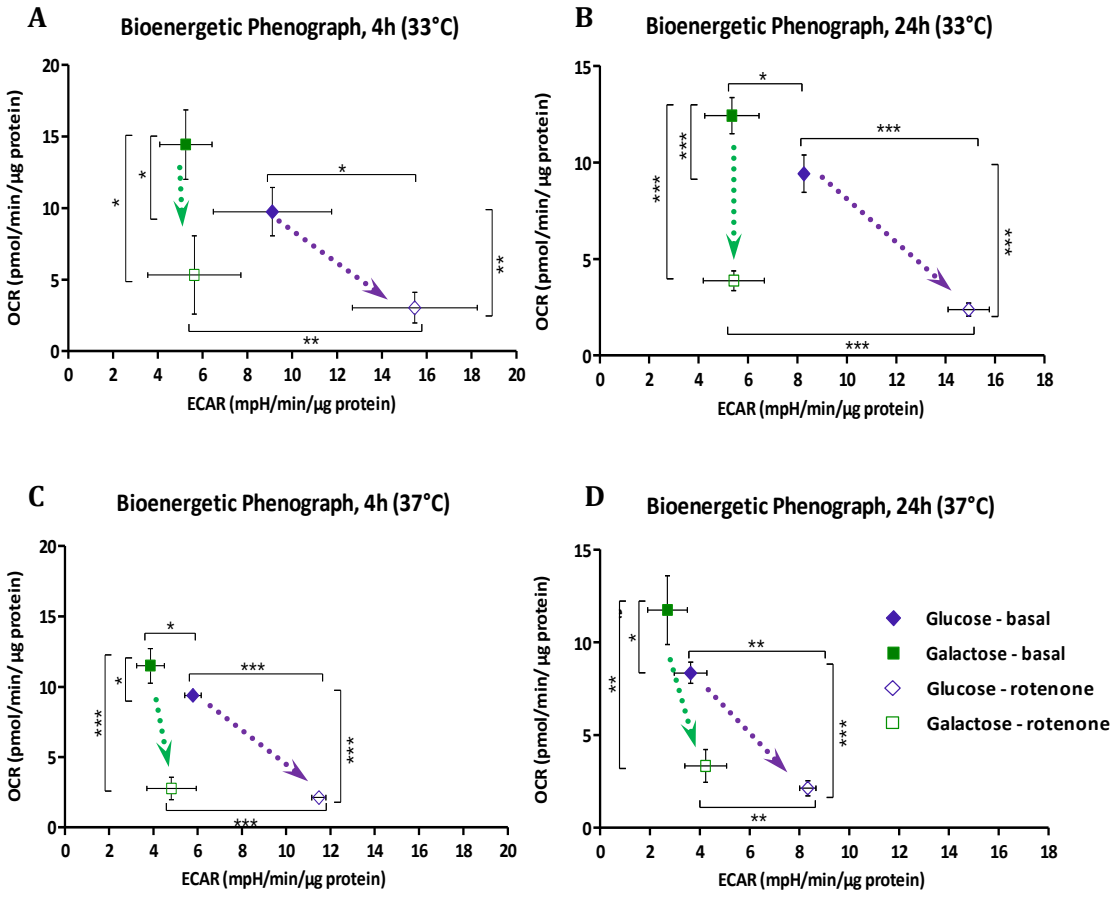

Figure 3.7 Bioenergetic profile of ciPTECs measuring OCR and ECAR at basal conditions and after rotenone exposure.

The Seahorse experiment was performed 4 h and 24 h of changing the medium. Three basal measurements were recorded before rotenone was injected and three more after the injection. The third value was used in each case because it represents the most stable measure. Arrows mark the shift in energy metabolism after ciPTECs are dosed with rotenone. Results have been normalised to the amount of protein per well. Data are mean ± SD (n = 3). Statistical significance was determined by t-test, *p<0.05, **p<0.01, ***p<0.001.

3.3.2 Assessment of mitochondrial distribution in galactose culture conditions

In order to investigate if culturing ciPTECs in galactose instead of glucose would affect mitochondrial distribution, we stained the cells with a mitochondrial specific superoxide indicator (MitoSOX) (Figure 3.8). At both conditions, mitochondria appeared denser around the nucleus, becoming more scattered at the extremities. Mitochondrial number, even though more difficult to gauge, looked qualitatively similar and so did the organelle size. In summary, no major differences could be appreciated amongst both culture conditions.

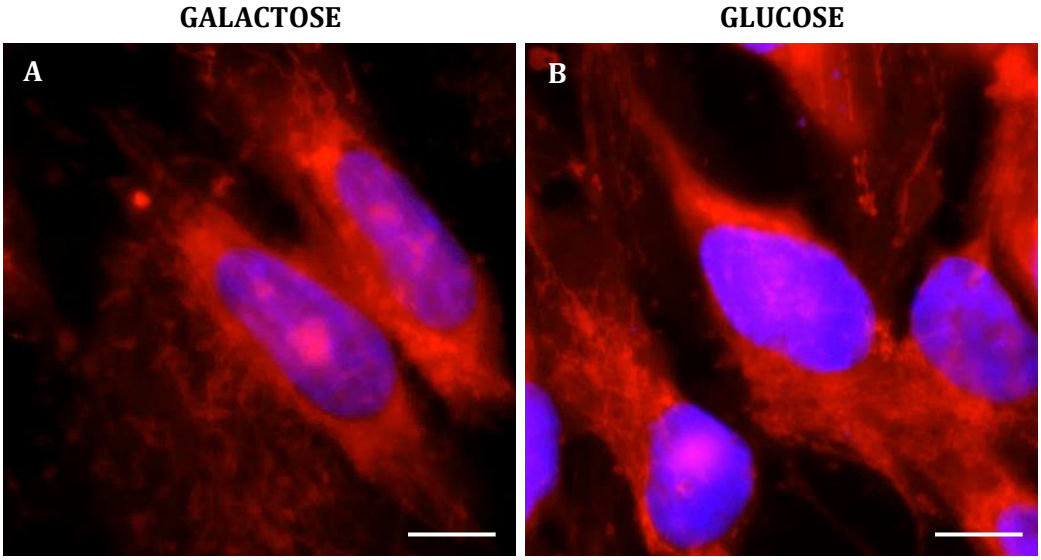

Figure 3.8 Mitochondrial distribution in glucose *vs*. galactose conditions.
Mitochondria were stained with MitoSOX (visualized at 594 nm) and Hoechst after 7 days in ciPTECs galactose medium (A) and after 7 days in glucose medium (B). Images were taken using a 63x objective. Scale bar is 10 µm. Data is representative of n = 3 experiments.

3.3.3 Greater susceptibility to mitotoxins detected in galactose cultured ciPTECs

Previous results (Figure 3.7) showed how after a mitotoxic insult, galactose cultured ciPTECs were unable to activate glycolysis as a compensatory mechanism (ECAR values were maintained). In theory, this would render galactose cultured ciPTECS a more sensitive *in vitro* model to detect potential renal mitochondrial toxicity. To investigate this hypothesis, both glucose or galactose cultured ciPTECs were dosed with rotenone, a well-defined mitotoxin, at concentrations ranging from 0.01 µM to 100 µM. Cell viability was assessed measuring ATP levels and LDH leakage. After a 2 h incubation, a marked decrease in ATP levels was observed in galactose conditions between 0.01 µM and 0.1 µM (Figure 3.9 A). However, no variation in ATP content was detected in normal glucose medium (Figure 3.9 C). LDH leakage into the medium was not detectable in either case, which implies that cell death had not occurred yet. A longer incubation of 24 h was also performed. In this case, galactose ciPTECs suffered a decrease in ATP levels at the same concentration range observed in the shorter incubation, but a dose dependant increase in LDH leakage was detected after 0.1 µM (Figure 3.9 B). In contrast, glucose-grown ciPTECs showed stable levels of ATP and no LDH leakage when exposed to rotenone concentrations up to 100 µM (Figure 3.9 D).

All these data supports the above-mentioned hypothesis and confirms that galactose cultured ciPTECs are more vulnerable to mitotoxins, as they cannot sustain their basal energy needs once the mitochondria have been damaged.

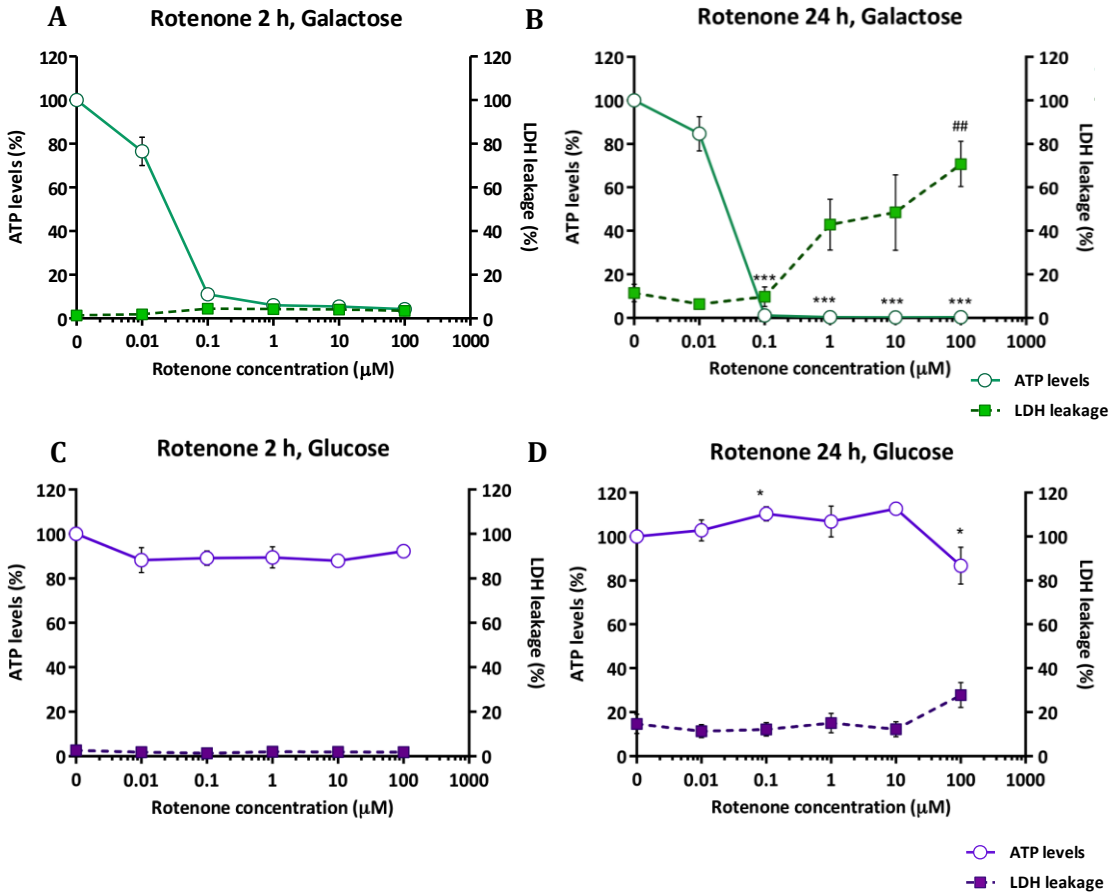

Figure 3.9 Dose responses after 2 h and 24 h of rotenone exposure for glucose grown ciPTECs and galactose cultured ciPTECs.

Cells were pre-cultured for 4 h in glucose or galactose conditions and then dosed with rotenone for (A,C) 2 h or (B,D) 24 h. ATP levels are represented in the left Y axis and LDH leakage in the right Y axis. Data are mean ± SEM (n = 3). Statistical significance in ATP levels (*) and LDH leakage (#) compared to the control (0 μM) was determined by One Way ANOVA test, *p<0.05, **p<0.01, ***p<0.001.

3.3.4 Validation of glucose *vs*. galactose mitotoxicity method in ciPTECs

To reassure the validity of the recently established model to detect mitotoxicity in PT cells, we dosed ciPTECs with another well-defined mitotoxin (antimycin A) as a positive control and two nephrotoxic compounds (cisplatin and gentamicin) as test compounds. Antimycin A is a potent inhibitor of the mitochondrial respiratory chain that binds to complex III (Huang et al. 2005), hence we would expect similar results to the observed response with rotenone. On the other hand, even though in the cisplatin and gentamicin toxicity mechanism mitochondria play an important role, alternative pathways have been postulated to be the critical mechanisms leading to cell death (Servais et al. 2008). Therefore, it would be anticipated that no differences should be detected in the glucose *vs.* galactose model.

As seen with rotenone (Figure 3.10 A), antimycin A produced a severe drop in ATP levels from 0.01 μM in galactose conditions after 2 h (Figure 3.10 B). Cells cultured in glucose conditions did not show any decrease in ATP content. However, a small increase was detected at the highest concentration. After the cisplatin incubation for 48 h, a very similar dose response curve was observed for both conditions (Figure 3.10 C). No differences were observed after 4 days of gentamicin treatment between glucose and galactose media (Figure 3.10 D). In summary, the model was able to correctly discern between compounds that have mitochondria as the main toxicity target from compounds where mitochondria only play a secondary role in the toxicity pathway.

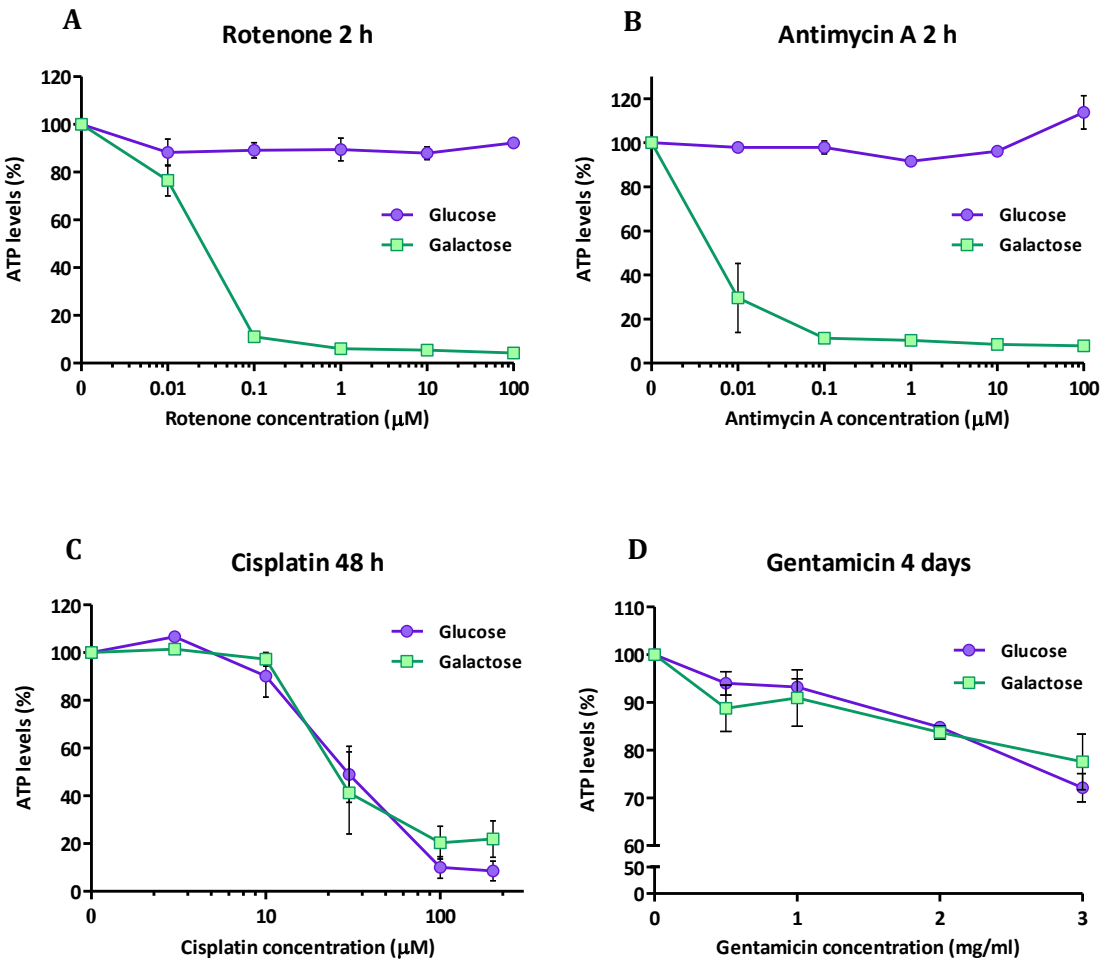

Figure 3.10 Effect of mitotoxic and nephrotoxic compounds on ATP levels in ciPTECs. Dose response curves after exposure of (A) rotenone for 2 h, (B) antimycin A for 2 h, (C) cisplatin for 48 h and (D) gentamicin for 4 days in ciPTECS. The experiments were performed in glucose grown *vs.* galactose cultured ciPTECs. (A) and (B) represent the positive controls whilst (C) and (D) are nephrotoxic negative controls. Data are mean ± SEM (n = 3).

3.3.5 Gentamicin impairs ciPTECs cell growth

Based on the balance of current literature evidence, ciPTECs are thought to be one of the best *in vitro* models to detect nephrotoxicity. Although gentamicin is a potent nephrotoxic agent in man and in animal models (Lopez-Novoa et al. 2011), in the results presented in section 3.3.4, exposure to gentamicin did not result in severe levels of cytotoxicity. Nevertheless, we have proven previously that ciPTECs possess satisfying levels of functional gentamicin transporters (Chapter 2, Figure 2.12). Here we then investigated whether gentamicin had other deleterious effects on ciPTECs such as cell growth impairment that may lead to cytotoxicity.

The control wells showed nearly a full recovery of cell density 18 h after the scratch assay was performed (Figure 3.11 B). ciPTECs practically repopulated the whole area that had been scraped cell free. Similar results were observed at 0.5 mg/ml (Figure 3.11 C). At 1 mg/ml of gentamicin, the scraped area was slightly wider (Figure 3.11 D), which became more obvious at 2 mg/ml and 3 mg/ml of gentamicin (Figure 3.11 E, F). After quantifying the scratch width, we could appreciate a significant delay in cell growth that was proportional to gentamicin dosage (Figure 3.12).

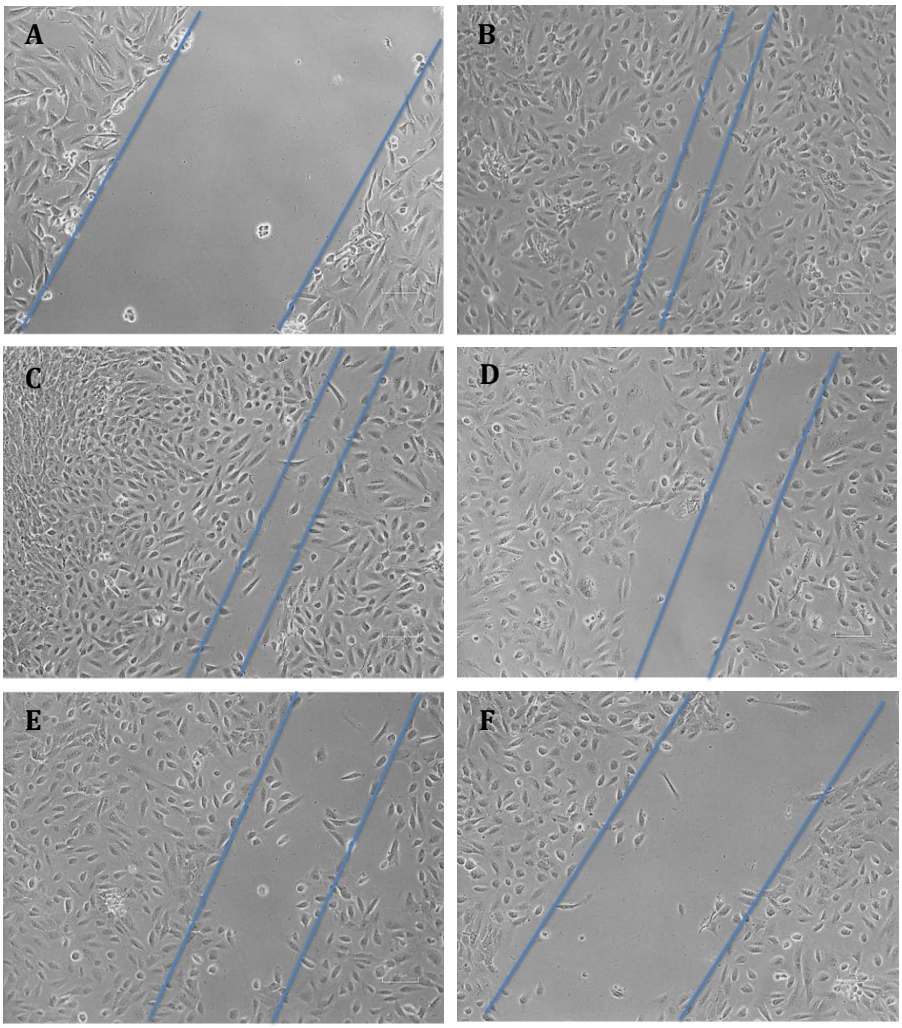

Figure 3.11 Assessment of cell growth after gentamicin exposure.
ciPTECs were treated with gentamicin at concentrations ranging from 0 to 3 mg/ml for 72 h and wells were scratched to analyse cell growth. (A) Scratch at 72 h + 0 h. 72 h + 18 h pictures correspond to: (B) 0 mg/ml, (C) 0.5 mg/ml, (D) 1 mg/ml, (E) 2 mg/ml and (F) 3 mg/ml of gentamicin.

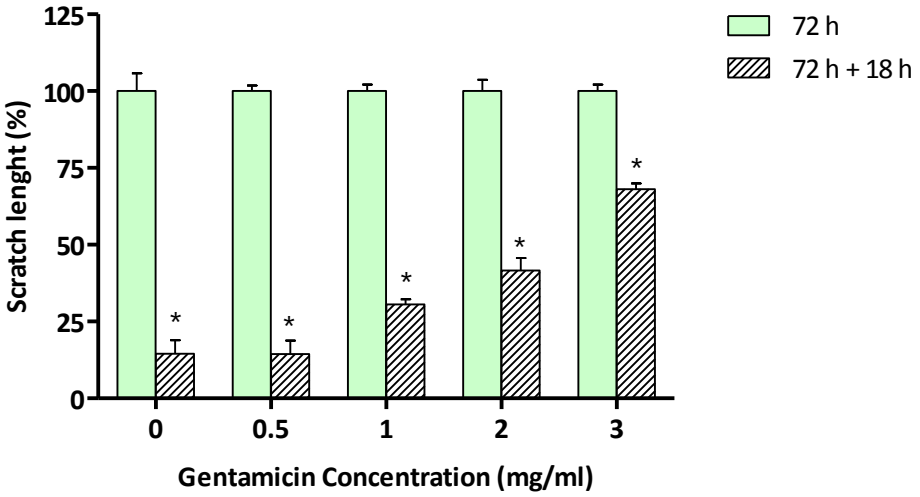

Figure 3.12 Quantified assessment of cell growth after gentamicin exposure.
ciPTECs were treated with gentamicin at concentrations ranging from 0 to 3 mg/ml for 72 h and wells were scratched to analyse cell growth. Data from 72 h refers to the initial amplitude of the scratch represented in percentage (%). 72 h + 18 h data plots the scratch amplitude (%) after 18 h of recovery. Data are mean ± SD (n = 3). Statistical significance was determined by Mann-Whitney test, *p<0.05.

3.3.6 Galactose cultured ciPTECs are more sensitive to adefovir triggered toxicity

Once the mitochondrial toxicity model had been initially validated, we were interested to see if the glucose *vs.* galactose method could detect any differential toxicity when the ciPTECs were treated with adefovir. This NtRTI is still used in controlled doses to treat Hepatitis B patients but although never demonstrated *in vitro*, it is known to induce renal dysfunction (Ha et al. 2009).

After 3 days of adefovir exposure, the dose response curves that corresponded to the two different medium conditions could be distinctively distinguished (Figure 3.13). ATP depletion in galactose cultured cells started around 0.3 µM, whilst ATP depletion for glucose cultured ciPTECs was not detectable until 5 µM. Although the effect was not as prominent as we had previously seen with rotenone (Figure 3.10 A), galactose cultured PT cells suffered a drop in ATP levels ahead of glucose grown cells. In other words, they were able to reveal adefovir toxicity earlier on (Figure 3.13).

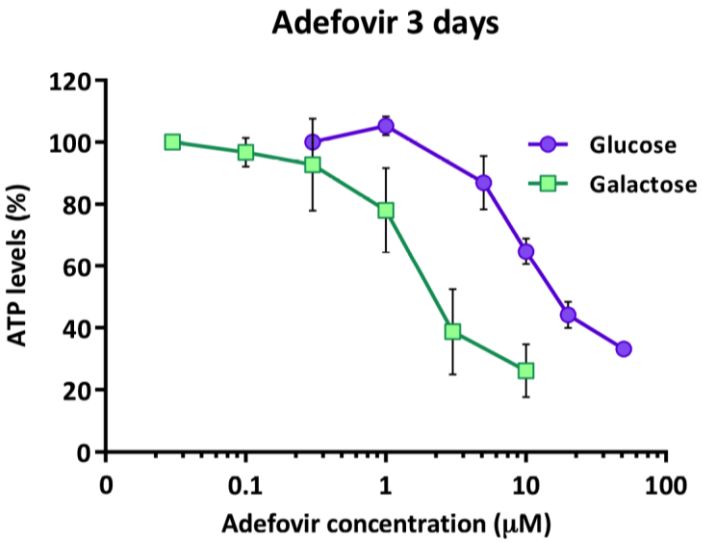

Figure 3.13. The effect of adefovir on ATP levels in galactose cultured *versus* glucose grown ciPTECs.
Galactose cultured and glucose grown ciPTECs dose response curves after adefovir exposure for 3 days at different concentrations (0.1 - 100 µM). ATP levels are represented as a percentage (%) and the results are compared to the control (0 µM) for each medium condition, expressed as 100%. Data are mean ± SEM (n = 3).

3.3.7 TFV mitochondrial toxicity evaluation using the glucose *vs*. galactose model

To further investigate the mitochondrial implication in NtRTIs toxicity, the glucose *vs.* galactose experiment was repeated using TFV. This compound is a lower toxic analogue of adefovir with a higher relevance in the clinic since it is broadly used to treat HIV patients. However, although with a lower incidence, it has been reported to induce PT dysfunction but no clear toxicity pathway has been identified yet (Hall 2013, Herlitz et al. 2010).

First, glucose grown and galactose cultured ciPTECs were exposed to TFV for 48 h (Figure 3.14 A). ATP levels remained at 100% for both conditions throughout all concentrations investigated. A longer incubation of 8 days was then performed (Figure 3.14 B). Although not significantly, a slight variation between glucose and galactose ATP levels was detected. In glucose grown ciPTECs, ATP content had a 10% reduction at the last two highest concentrations of TFV. Finally, a much longer TFV treatment of 15 days was performed in which cells spent 5 days at 33°C and 10 days at 37°C (Figure 3.14 C). Glucose grown ciPTECs expressed lower ATP levels compared to control and to galactose cultured cells. In general, the energy content for both conditions was below 100% and above 65% and lower than any of the prior treatments with the NtRTI.

To confirm that ciPTECs were able to uptake the compound, cells were incubated with tritium radiolabelled TFV for 1 h and the amount of intracellular radioactivity was measured (Figure 3.14 D). The results were compared with the intracellular uptake in OK cells. TFV internalisation values varied from 20% to 30% amongst the two cell lines and the different temperature and medium conditions.

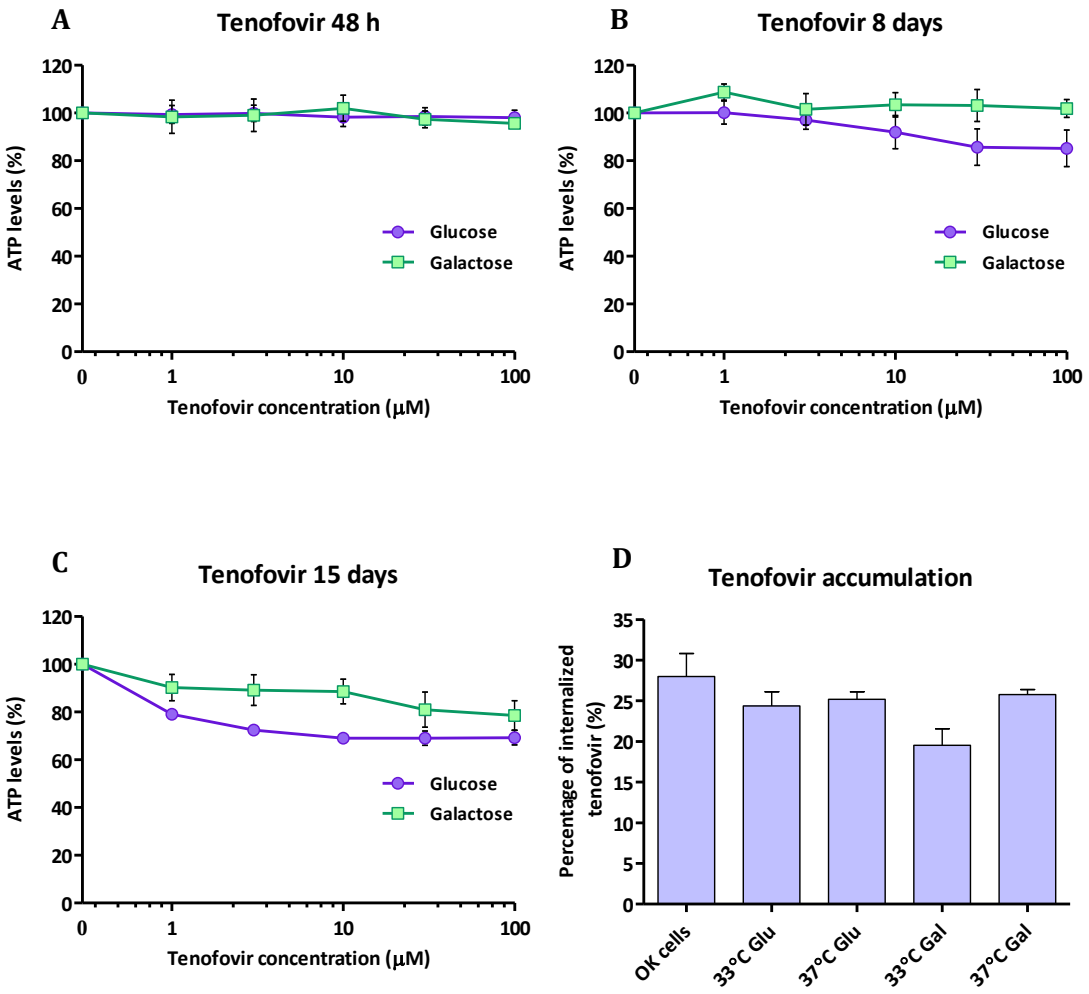

Figure 3.14. TFV uptake and cytotoxic impact on ciPTECs over time.

The uptake was analysed at 33°C and 37°C in glucose (Glu) and galactose (Gal) conditions. ATP levels were measured in ciPTECs and represented as a percentage (%) compared to the control (0 µM) after TFV treatment for (A) 48 h, (B) 8 days and (C) 15 days). TFV concentrations ranged from 1 µM to 100 µM. (D) Tritium radiolabelled TFV uptake in OK cells and ciPTECs. Data are mean ± SEM (n = 3).

3.3.8 Mitochondrial rearrangements after TFV exposure

In order to detect if TFV had affected the mitochondria at a structural or morphological level, ciPTECs were stained with MitoSOX after they had been dosed with TFV for 15 days at 100 µM. Since no important differences had been detected with the different media conditions, this time the experiment was only carried out in glucose medium. The control images (0 µM) showed evenly spread mitochondria. A slight tendency to accumulate around the nuclei could be appreciated, but mitochondria can clearly be seen in cytoplasmic elongations (Figure 3.15 A). In contrast, after 15 days of TFV exposure, not only some cells looked bigger but also the mitochondria had changed distribution. The accumulation around the nuclei appeared more obvious and some cells had lost the evenly spread arrangement seen at 0 µM. The mitochondrial density at the edges of the cytoplasm had also notably decreased (Figure 3.15 B).

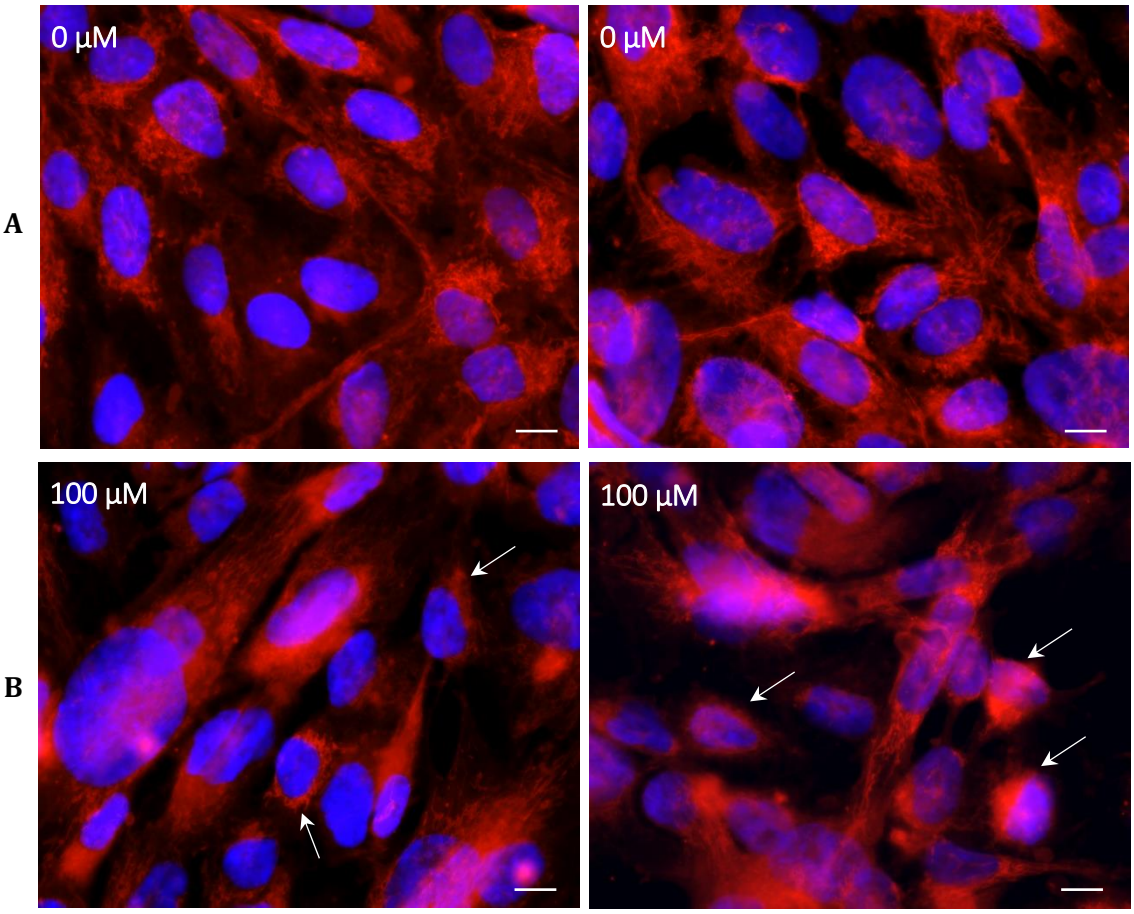

Figure 3.15 Mitochondrial distribution after 15 days of TFV treatment.
ciPTECs were stained with MitoSOX (visualised at 594 nm) and Hoechst after 15 days (A) in glucose medium and (B) 15 days of TFV treatment (100 µM). The arrows mark mitochondrial distribution changes compared to 0 µM. Images were taken using a 63x objective. Scale bar is 10 µm. Data is representative of n = 3 experiments.

3.3.9 Classification of mitotoxic and non-mitotoxic compounds

Interestingly, it is known that the determination of ATP levels can unmask if a compound has potential to induce mitochondrial impairment long before cell death occurs (Kamalian et al. 2015). To specifically detect drug-induced mitochondrial toxicity, a cell viability assay was first established with a bone marrow cell line (K562 cells) (Swiss et al. 2013) and later published with a liver cell line (HepG2 cells) (Kamalian et al. 2015) by calculating the EC_{50}ATP (compound concentration that causes a 50% drop in ATP levels) in glucose and galactose medium from dose response curves (Swiss et al. 2013). If the ratio value of EC_{50}ATPglu divided by EC_{50}ATPgal was ≥ 2 and the difference between the EC_{50}ATP for both conditions was statistically significant (One Way ANOVA, *p* values lower than 0.05), then the compound was defined as mitotoxic (Swiss et al. 2013). Here, we apply the same rationale to our PT glucose *vs.* galactose model to classify the compounds previously tested (Table 3.1).

The previously described method successfully classified rotenone (EC_{50}ATPglu /EC_{50}ATPgal > 3125, $p < 0.0001$) and antimycin A (EC_{50}ATPglu /EC_{50}ATPgal > 14925, $p < 0.0001$) as mitotoxins in ciPTECs. Cisplatin and gentamicin, two known nephrotoxins, were used as negative controls. Cisplatin was correctly classified as non mitotoxic after 48 h of dosing with an EC_{50}ATPratio of 0.976. However, after 4 days of gentamicin exposure, ciPTECs ATP depletion was not enough to calculate the EC_{50}ATP and this was established as > 6.5 µM. A similar scenario happened after 15 days of TFV treatment (redosed every 3 days), both glucose and galactose EC_{50}ATP were established as >100 µM. Nonetheless, adefovir was categorised for the first time *in vitro* as a mitotoxin with an EC_{50}ATPgal 6.12 times lower than EC_{50}ATPglu ($p = 0.0049$).

Table 3.1 List of compounds that are known to cause nephrotoxicity plus rotenone and antimycin A as positive controls for mitotoxicity

	EC_{50}ATP (μM) ± SD		EC_{50}ATPglu / EC_{50}ATPgal	*P* value	Incubation time
	Glucose	Galactose			
Rotenone	> 100	0.032 ± 0.016	> 3125	< 0.0001	2 h
Antimycin A	> 100	0.0067 ± 0.0064	> 14925	< 0.0001	2 h
Cisplatin	24.7 ± 12.3	25.3 ± 11.6	0.976	N.S.	48 h
Gentamicin	> 6.5	> 6.5	1	N.S.	4 days
Adefovir	15.3 ± 3.7	2.5 ± 1.4	6.12	0.0049	3 days
TFV	> 100	> 100	1	N.S.	15 days

Data are mean ± SD (n = 3). P value indicates significance ($p<0.05$) between EC_{50}ATPglu and EC_{50}ATPgal values as tested by One Way ANOVA. Key: N.S. indicates not significant.

3.4 DISCUSSION

As hypothesised, the bioenergetic profiles confirmed that ciPTECs were under the Crabtree effect and were mainly synthetizing ATP via glycolysis. The OCR was significantly upregulated in galactose conditions, hence galactose cultured ciPTECs were considerably more reliable on respiration at both 33°C and 37°C. Glycolytic activity, measured by looking at the ECAR, was also higher in glucose conditions. This is consistent with a higher ATP production anaerobically, as this pathway generates lactate in the cytosol and induces medium acidification. This trend is detectable at 24 h as well as 4 h after changing the medium. This suggests that in 4 h ciPTECs were able to readapt to the new energy source and modify their energetic metabolism correspondingly, which confirms that Kamalian, L., *et al.*'s variation of the medium replacement approach is also valid for our immortalised PT cell model. Subsequently, we can say that galactose medium confers the ability to bypass the Crabtree effect to ciPTECs in a short period of 4 h. Furthermore, the higher ECAR values observed at 33°C are most likely an indication that, at this temperature, ciPTECs need to derive even more energy from glycolysis as a quick ATP production route to maintain the high energy needs of rapid cell growth. In contrast, at 37°C the promoters that induce cell division are inactivated (Wilmer et al. 2010) and ciPTECs cell energy demand is downregulated.

To take the metabolic characterisation further, the impact of rotenone on ciPTECs bioenergetic profile was analysed. The severe drop in OCR observed in glucose and galactose cultured ciPTECs indicated that rotenone could efficiently inhibit OXPHOS, as well as trigger a significant upregulation of glycolysis in glucose conditions. Conversely, no effect on the ECAR was detected in galactose cultured cells. Therefore, it can be reasoned that in normal glucose conditions and when respiration is inhibited, ciPTECs are able to upregulate

glycolysis as a compensatory mechanism to produce ATP. However, when lacking a profitable energetic source for glycolysis, galactose cultured cells cannot activate the anaerobic pathway to produce ATP. This will rapidly cause a breach in the basal energetic threshold and lead them to cell death. Therefore, in theory, galactose cultured ciPTECs should show an upgraded vulnerability to mitochondrial toxins compared to glucose conditions. It is also worth noting that other cell lines such as HepG2 did not show significant differences between both conditions until rotenone was added (Kamalian et al. 2015). In contrast, here two significantly different bioenergetics configurations were discerned at basal conditions. Thus, ciPTECs have the potential to be and advantageous and highly reliable model to detect mitochondrial toxicity.

Variations in mitochondrial distribution or morphology due to changes in energetic metabolism were also assessed. However, even though the mitochondria were more active in galactose conditions, no differences were observed using MitoSOX. This suggests that mitochondria do not need to adopt any rearrangements to increase their activity. Nonetheless, it has been proven before that this is not the case. In fact, Schmitt,S*. et al*. showed how “galactose mitochondria” from McA 777 cells appeared with increased matrix space and with better defined cristae structures, resembling typical rat liver mitochondria (Schmitt et al. 2013). It is also important to consider that although MitoSOX is advertised as a dye specifically targeted to mitochondria, it has been published that its selectivity is complicated due to autooxidation as well as other intracellular oxidation processes (Robinson et al. 2006). Therefore, electron microscopy should be applied to confirm any structural changes in the mitochondria.

In light of addressing the second aim of this chapter and checking if galactose ciPTECs are more vulnerable to mitochondrial toxins, cell viability was analysed after rotenone exposure. As expected, when galactose ciPTECs were exposed to the complex I inhibitor,

ATP levels dropped significantly due to no alternative system to generate ATP. Moreover, extended exposure induced cell death due to a prolonged failure to sustain oxidative phosphorylation to meet basal energy needs. In contrast, since glucose grown cells can upregulate glycolysis as a compensatory mechanism of energy production, glucose ciPTECs remained perfectly healthy. Only after 24 h at the highest concentration, minor changes were detected that indicated the start of cell energy compromise. Previous studies have also shown similar glucose/galactose differences in other cell types (Kamalian et al. 2015). In summary, it was confirmed that galactose cultured ciPTECs are more vulnerable to mitotoxins, as they cannot sustain their basal energy needs once the mitochondria have been damaged.

To validate rotenone results, antimicyin A (complex III inhibitor) was tested in the glucose *vs.* galactose model. Cisplatin and gentamicin were also tested as negative controls, as it is known that mitochondria play a role in their nephrotoxic mechanism but it is not the main toxicity target (Servais et al. 2008, Lopez-Novoa et al. 2011). Although it has been published that dissolving cisplatin in DMSO results in ligand displacement and reduces the cytotoxicity (Massart et al. 1993, Dernell et al. 1998), we still detected significant levels of ATP depletion. Cisplatin and gentamicin ATP dose response curves were completely overlapped compared to rotenone and antimycin A ATP curves. Therefore, the data confirmed that our glucose *vs.* galactose mitotoxicity model is able to discriminate between drugs that specifically target the mitochondria from other renal compounds that cause mitochondrial damage as a reflection of other detrimental pathways.

Although gentamicin has been characterised as nephrotoxic and it is known that mitochondria play a role in its nephrotoxic mechanism (Servais et al. 2008, Lopez-Novoa et al. 2011), ATP levels did not reach 50% depletion after 4 days in culture. However, we have

demonstrated that gentamicin causes toxicity by impairing PT cell growth in a dose dependant manner.

Once the model validation was concluded, we chose to submit TFV and its higher toxic analogue adefovir to mitochondrial toxicity evaluation. Both NtRTIs are known to cause PT toxicity with enlarged and dysmorphic mitochondria (Herlitz et al. 2010, Tanji et al. 2001). Therefore, these clinically relevant and presumable mitotoxic compounds were tested in our glucose *vs.* galactose model.

First, adefovir toxicity was assessed in glucose *vs.* galactose conditions. Cells cultured in galactose medium demonstrated a significantly higher sensitivity in front of adefovir, as ATP levels dropped at a lower concentration of the drug. Comparing these data with the data obtained from rotenone or antimycin A, a similar but less pronounced tendency was observed. This suggests that adefovir is not only a PT toxin but also has mitochondria as one of the main toxicity targets. There is not yet any *in vitro* evidence showing this result. From these findings, a new thesis objective was established aiming to use the developed model to study the molecular mechanistic pathways leading to the observed mitotoxicity. Therefore, putative toxicity pathways will be discussed in Chapter 4 by investigating changes in mitochondrial respiration and OXHPOS complexes.

After successfully identifying adefovir as a mitotoxic drug, a similar strategy was applied to detect TFV mitotoxicity. Although no changes were seen up to 8 days, after 15 days a small reduction in ATP content was observed, however it was not strong enough to confirm a clear cytotoxicity. Since *in vivo* renal toxicity only appears after prolonged TFV treatments (Hall 2013), these results were not unforeseen. Hence, longer incubations might be needed but these might not be compatible with *in vitro* cultures. A deeper analysis of TFV mitochondrial toxicity will be performed in Chapter 4.

TFV enters the cell through the same mechanisms as adefovir (Uwai et al. 2007) and therefore it was postulated that, although no toxicity had been previously detected, ciPTECs were uptaking the drug. In fact, the theory was confirmed by using a tritium radiolabelled version of the compound. However, this information is only relevant to confirm the uptake of the compound; data is not comparable between conditions because internalisation is dependent on cell number and cell volume and these two parameters vary for each situation and cell type.

Mitochondrial distribution was reassessed after 15 days of TFV treatment in glucose medium. IF images showed some cells with localised mitochondria around the nucleus that had also lost the typical elongated tubules that formed an interconnecting network in healthy cells. When cells are under stress or before apoptosis is being triggered, mitochondrial fission is activated (Suen et al. 2008). Furthermore, any changes in mitochondrial dynamics such as fission/fusion could influence cell bioenergetics and could be interpreted as an early sign of cell stress (Picard et al. 2013, Chen and Chan 2009). More in detail results using electron microscopy would better elucidate structural and morphological changes.

Finally, the classification established by Swiss, R. *et al.*, was applied to the developed PT mitotoxicity model. Rotenone and antimycin A were correctly classified as mitochondrial toxins and cisplatin was also correctly categorised as not mitotoxic (EC_{50}ATPglu/EC_{50}ATPgal < 2). As discussed before, gentamicin ATP levels did not reach 50% depletion and as a result the ratio was defined as 1. Similar results were found with TFV after 15 days of dosing. Nevertheless, the method significantly classified adefovir again as a mitochondrial toxin; with an EC_{50}ATPglu/EC_{50}ATPgal ratio = 6.12 (p = 0.0049).

In conclusion, these findings represent a step forward towards refining *in vitro* models and eventually developing robust *in vivo* predictions that could be used during drug development to avoid organ specific toxicities.

Future work should focus on further validating ciPTECs glucose *vs.* galactose mitotoxicity model by screening a larger pool of nephrotoxic as well as mitotoxic compounds. Swiss, R. *et al*, classification should be then applied to finally confirm that galactose cultured ciPTECs are a highly reliable model to identify renal mitochondrial toxicity. Moreover, it would also be interesting to use it as a tool to investigate the mechanism of toxicity for several drugs. Adefovir and TFV will be subjected to deeper evaluation in Chapter 4 in order to bring some mechanistic insight into their putative mitotoxicity pathways.

Chapter Four

Assessing the role of cellular bioenergetics on susceptibility to renal drug-induced mitotoxicity *in vitro*

CONTENTS

4.1 INTRODUCTION

Within the previous chapter, we developed a screen using ciPTECs that was capable of detecting whether or not a compound will have a potential mitochondrial liability. This method was able to provide evidence, for the first time *in vitro*, that adefovir has mitotoxic potential. We also investigated this concept as part of the mechanism associated with TFV, a compound with a lower incidence of nephrotoxicity in man. We noted a slight downregulation in ATP levels but no clear cytotoxicity in this model. Therefore, more mitochondrial specific studies in ciPTECs could deliver important information about adefovir's mitotoxicity pathway and help identify any signs of TFV mitochondrial impairment in our *in vitro* model.

Causes of mitochondrial dysfunction are variable and include mtDNA depletion, generation of ROS, impairment of protein synthesis in the organelle, ETC inhibition and induction of mitochondrial permeability amongst others (Figure 4.1) (Dykens and Will 2007). Nonetheless, all of these mechanisms display the very same feature: an alteration in the

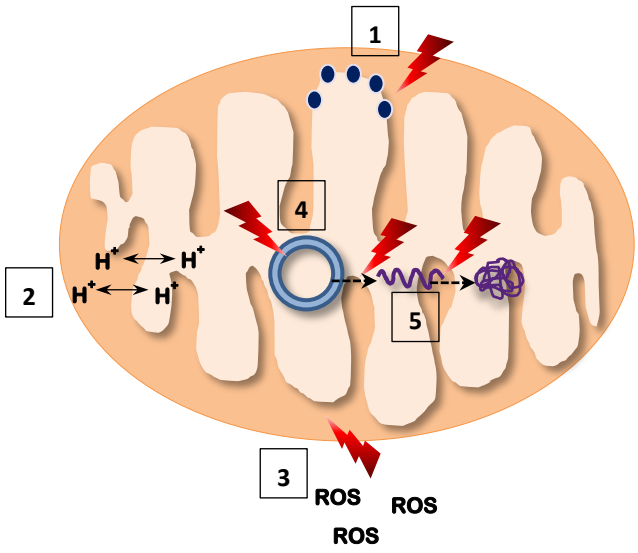

Figure 4.16 Representation of some critical mitochondrial toxicity pathways.
Mitochondrial function can be modulated in different ways, such as (1) electron transport chain inhibition, (2) induction of mitochondrial permeability, (3) generation of ROS, (4) mtDNA depletion or (5) impairment of protein synthesis.

respiratory parameters. As a consequence, mitotoxicity can be detected analysing changes in respiration, however, not all mitotoxic pathways affect the respiratory parameters equally and this must therefore be considered in a quantitative way.

Studying the basic respiratory parameters can give insights from different aspects of mitochondrial function that may be applicable to understanding drug safety in man. Therefore, different mechanisms affecting mitochondrial toxicity will have a diverse impact on mitochondrial respiration, which will be represented as a modified cellular bioenergetic profile. The bioenergetic profile is built using a mitochondrial stress test, which is able to define mitochondrial function by a sequential addition of ETC inhibitors (Figure 4.2).

The respiratory parameters forming the bioenergetic profile are:

- **Basal respiration**: is the standard amount of oxygen used by cells in regular culture conditions. Variations in this parameter will be due to changes in ATP linked OCR, proton leak or non-mitochondrial respiration.

- **ATP linked respiration**: is the amount of oxygen consumed to produce ATP. Changes in ATP linked respiration will indicate changes in ATP demand, which can be due to substrate availability or OXPHOS damage.

- **Proton leak**: is the background level of protons (H^+) that cross through the inner mitochondrial membrane. Proton leak can be affected by an uncoupling protein, impairment of the inner mitochondrial membrane or increased ion transport, which would dissipate the proton gradient.

- **Maximal Respiration**: is the maximal OCR level that a particular cell line could reach if all mitochondria were functioning at 100% of their capacity. From here **spare respiratory capacity** can be derived**,** this is defined as the difference between

maximal respiration and basal respiration. Variations in this parameter could indicate changes in mitochondrial mass or integrity. Specifically, when a decrease is detected, it tends to be one of the first signs of mitochondrial impairment, as this parameter is closely linked to bioenergetic health.

- **Non-mitochondrial respiration (NMR)**: is the amount of oxygen consumed by external mitochondrial processes such as NADPH oxidases or lipoxygenases. An increase in NMR would indicate ROS formation in the cytosol, which could

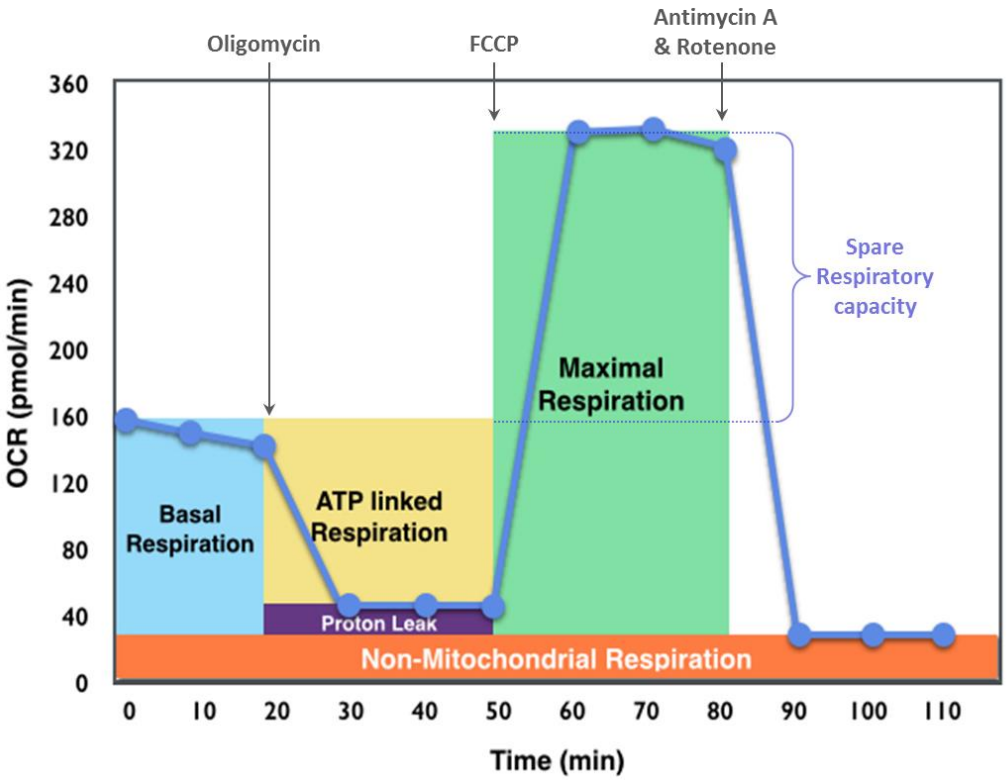

Figure 4.2 Schematic of the cellular bioenergetic profile.
Time course representation of the mitochondrial stress test and breakdown into mitochondrial respiratory parameters. The first inhibitor added is oligomycin, which inhibits ATP synthesis by blocking the proton channel of complex V. Therefore, the OCR drops due to no ATP linked respiration. The second injection is FCCP, an uncoupling agent that permeates the inner mitochondrial membrane, giving free pass to protons (H^+) and collapsing the membrane potential. This leads to a rapid consumption of energy and oxygen, without the generation of ATP. The third injection is a combination of rotenone (complex I inhibitor) and antimycin A (complex III inhibitor). This combination shuts down mitochondrial respiration and enables both the mitochondrial and non-mitochondrial fractions contributing to respiration to be calculated. Each dot represents an OCR and ECAR measurement.

eventually cause mitochondrial dysfunction by targeting ETC complexes (Chacko et al. 2014, Hill et al. 2012).

Another important mitochondrial parameter is the **coupling efficiency**, which measures the amount of ATP turnover in the mitochondria, compared to a baseline reading. If the coupling efficiency is depleted, that could be interpreted as a downregulated efficiency of the ETC complexes to produce ATP. Therefore, that would be translated into a loss of functionality from one or more OXPHOS complexes.

4.1.1 Aims and hypothesis

Hypothesis:

The hypothesis under investigation within this chapter is that the molecular events underpinning both adefovir and TFV-induced mitotoxcity in ciPTECs could be determined by a thorough interrogation of cellular bioenergetics profiling.

The aims of this chapter were to:

- Implement the mitochondrial stress test in ciPTECs using Seahorse technology.
- Use the information from the cellular bioenergetic profile to investigate the impact of adefovir on mitochondrial respiration.
- Identify the molecular initiating events (MIEs) of adefovir-induced mitotoxicity.
- Assess the bioenergetic profile after TFV exposure and see if there is any detectable mitochondrial damage.

4.2 MATERIALS AND METHODS

4.2.1 Materials

ciPTECs were obtained from the Department of Pharmacology and Toxicology in Radboud University Nijmegen (Nijmegen, Netherlands). Tissue culture reagents DMEM/F-12 (1:1), FBS, DFBS, PBS, MitoSOX™ Red Mitochondrial Superoxide Indicator, Hoechst 33342 and ProLong® Gold Antifade Mountant were purchased from Life Technologies (Paisley, UK). DMEM – F12 without glucose was purchased from Biowest (Nuaillé, France). Cover slides (13 mm ∅) were purchased from VWR (Lutterworth, UK) and microscope slides were obtained from Thermo Fisher Scientific (Loughborough, UK). Seahorse consumables were purchased from Seahorse Biosciences (North Billerica, MA, USA). Precision Plus Kaleidoscope Standards (molecular weight markers) and non-fat milk were purchased from Bio-Rad Laboratories Ltd (Hemel Hempstead, UK). Amersham Hybond ECL membrane and Amersham Hyperfilm ECL were purchased from GE Healthcare (Little Chalfont, UK). Western Lightning Plus-ECL was purchased from Perkin Elmer (Beaconsfield, UK). Total OXPHOS Human WB antibody cocktail was purchased from Abcam (Cambridge, UK). TFV was obtained from Toronto Research Chemicals Inc. (Toronto, Canada). All other reagents and chemicals were purchased from Sigma Aldrich (Dorset, UK) or Fisher Scientific (Loughborough, UK).

4.2.2 Cell culture

ciPTECs were cultured as described in Chapter 3.2.2.

4.2.3 Cell dosing strategies

Before performing the mitochondrial stress test, ciPTECs were dosed with different drugs. The selected time points were shorter than the ones used previously for ATP content since

mitochondrial impairment occurs before energy decline and the Seahorse-based technology works optimally with a monolayer to measure OCR and ECAR parameters accurately. Cisplatin was used as a model nephrotoxin that could act as a negative control for mitochondrial toxicity. Cells were seeded on a XF 96-well microplate in glucose growth medium with DFBS at 10,000 cells/well and dosed 24 h later with cisplatin for 24 h (0 µM, 10 µM, 30 µM, 100 µM, 200 µM) in the same medium. The exact same seeding and dosing design was applied for adefovir and ciPTECs were dosed with 0 µM, 1 µM, 3 µM, 10 µM, 30 µM and 100 µM of the compound. A different strategy was used for TFV. Cells were seeded in glucose growth medium with dialysed FBS at 500 cells/well and dosed 24 h later with TFV (0 µM, 10 µM, 50 µM, 100 µM, 200 µM, 300 µM) in glucose growth medium with DFBS. The medium was changed 4 h prior to dosing for glucose growth medium with DFBS. The cells were dosed for 15 days, the first 5 days ciPTECs were cultured at 33°C and the last 10 days they were transferred to 37°C to induce differentiation, which as a result gradually stops division (Wilmer et al. 2010). For TFV treatment, cells were re-dosed every 2 days. All final solvent concentrations were lower than 1% v/v.

4.2.4 Mitochondrial stress test

After dosing the cells (see 4.2.3 section) with cisplatin, adefovir or TFV, the medium was removed and the wells were washed x2 with pre-warmed XF Base Medium supplemented with L-glutamine (1% v/v), sodium pyruvate (1 mM) and 25 mM glucose; pH of 7.4. Then, a final volume of 175 µl of the same medium were added per well. Cells were left in a CO_2 free incubator at 37°C for 1 h while 25 µl of 8 µM oligomycin were loaded to port A, 25 µl of 4.5 µM FCCP were loaded to port B and 25 µl of 10 µM rotenone and antimycin A solution were loaded to port C of each well of the sensor cartridge. Immediately after loading, the sensor cartridge was placed in the Seahorse instrument to calibrate. The calibration takes 30 minutes and finished when the cells were ready to be analysed. When both the sensor

cartridge and the cell microplate were in the Seahorse instrument, the OCR and ECAR measurements started and were executed every 7 minutes. Three basal measurements were performed at the start. The oligomycin solution was then injected (port A) to the cells, followed by FCCP solution (port B) and finally rotenone and antimycin A solution (port C). Three measurements were recorded after each injection (Figure 4.2).

4.2.5 Normalization of Seahorse data by BCA assay

Seahorse data was normalised as described in Chapter 3.2.4.

4.2.6 Seahorse data collection and analysis

Data was recorded using Wave software from Seahorse Bioscience. Then, an Excel Macro-Enabled Workbook was downloaded from the Seahorse Bioscience web page that allows to extract the data from the instrument and at the same time compute the respiration parameters. The third measurement after each injection was the one used to do the calculations as it is the most stable reading. Respiration parameters were calculated according to Table 4.1.

Table 4.2 Description or formula for each respiration parameter

PARAMETER	DESCRIPTION / FORMULA
Non mitochondrial respiration (NMR)	= OCR 12th reading
Basal respiration	= OCR 3rd reading – NMR
Proton leak	= OCR 6th reading – NMR
ATP linked respiration	= Basal respiration - Proton leak
Maximal respiration	= 9th reading - NMR
Spare respiratory capacity	= Maximal respiration – Basal respiration
Coupling efficiency (%)	= (1 – (Proton leak/Basal respiration))x100

4.2.7 Western blotting – whole cell lysates

For the measurement of the ETC complexes, ciPTECs were seeded in a 6-well plate at $5x10^5$ cells/well for adefovir treatment and at $5x10^4$ cells/well for TFV treatment. ciPTECs were cultured at 33°C and dosed with different concentrations of adefovir (from 0 µM to 100 µM) for 24 h. For TFV, ciPTECs were cultured for 5 days at 33°C in different concentrations of the NtRTI (from 0 µM to 300 µM) re-dosing every 2 days and then transferred to 37°C for 10 days. After the drug treatment, cells were washed twice with 1 ml of cold PBS before lysis in 100 µl of RIPA buffer.

4.2.8 Western blotting – protein quantification

The total protein content of whole cell lysates was measured using the BCA assay. See Chapter 2.2.12.

4.2.9 Western blotting

To analyse the presence of the respiratory chain complexes after adefovir and TFV treatment, 20 µg of cell lysate from each condition were mixed with reducing agent and sample buffer and then denatured at 85°C for 5 minutes. Samples were then loaded onto 10% acrylamide gels and proteins separated by electrophoresis in a Tris-Glycine running buffer. Proteins were then electro-transferred onto a nitrocellulose membrane using 20% MeOH buffer for 1 h at 80 V. Successful transfer and even loading was then checked using Ponceau Red. Membranes were washed with 0.1% Tween-TBS and blocked with 10% non-fat milk overnight with shaking at 4°C. Next day, the membrane was incubated for 2 h at RT with a cocktail of mouse monoclonal antibodies for the OXPHOS complexes (1/500 in 10% milk). The membrane was then washed (4x 5 minutes) with 0.1% Tween-TBS before addition of secondary antibody anti-mouse IgG (1/10,000 in 10% milk) and incubation for 1

h at RT. The membrane was washed again with 0.1% Tween-TBS and treated with ECL reagent for 1 minute. Proteins were visualised using exposure to X-ray film. After developing, films were scanned using a densitometry scanner (GS800, Bio-Rad).

4.2.10 Stripping and reprobing for β-actin

To probe for β-actin (41.7 kDa), the membrane needs to be stripped first because the band would overlap with complex III (48 kDa). To do so, the membrane was submerged in stripping buffer and incubated for 30 minutes at 50°C. Then the membrane was washed (3x 10 minutes) with 0.1% Tween-TBS and blocked with 10% non-fat milk for 1 h at RT. Incubation with mouse monoclonal anti-actin (1/10,000 in 10% milk) was performed for 1 h. Membrane was then washed (4x 5 minutes) with 0.1% Tween-TBS and the secondary antibody anti-mouse IgG (1/10,000 in 10% milk) was incubated for 1 h also at RT. The membrane was washed again with 0.1% Tween-TBS and treated with ECL reagent for 1 minute. Proteins were visualised using exposure to X-ray film. After developing, films were scanned using a densitometry scanner (GS800, Bio-Rad).

4.2.11 Densitometry

Densitometry was performed as described in section 2.2.14.

4.2.12 ROS analysis - DHE incubation

Cells were seeded at $4x10^4$ cells/well in a 24-well plate and incubated at 33°C (5% CO_2). 2 days later, they were dosed with adefovir (0 µM, 0.5 µM, 1 µM, 10 µM, 50 µM) for 48 h at the same temperature. Then ciPTECs were washed with PBS and trypsinized to get a single cell suspension. Cells were washed with PBS and then resuspended with a 10 µM solution of dihydroethidium (DHE) and incubated at 37°C for 10 minutes protected from light.

Finally, the cell solution was transferred to FACS tubes and placed on ice protected from light.

4.2.13 ROS analysis – Flow cytometry

DHE fluorescence was analysed at 488 nm (excitation wavelength) and 512 nm (emission wavelength), which corresponds to the FL1-H channel on the flow cytometer instrument (FACSCalibur, BD Biosciences, Singapore). See Chapter 2.2.17 and 2.2.18 sections for further details.

4.2.14 Detection of mitochondrial ROS

MitoSOX was used to detect mitochondrial ROS levels after adefovir incubation. Cover slides (13 mm ∅) were placed in wells of a 24-well plate and coated with 0.5% of gelatine for 30 minutes. The gelatine was removed and ciPTECs were seeded at $4x10^4$ cells/well and incubated at 33°C (5% CO_2). After 48 h, they were dosed with adefovir (0 µM, 5 µM, 50 µM) for another 48 h. After the drug treatment, cells were washed twice with PBS and incubated with a 5 µM MitoSOX solution, also prepared in PBS, for 10 minutes protected from light. Then, the cells were washed 3x in warm PBS and fixed with 2% PFA for 15 minutes at RT in the dark. Two more washes with PBS were performed after cells had been fixed. Finally, the cover slides were mounted on a microscope slide with Prolong Gold. Results were visualized at 63x magnification using an inverted fluorescence microscope (Axio Observer.Z1, Zeiss) with ApoTome (optical sectioning using structured illumination). In this experiment, samples could not be stained with DAPI or Hoechst to visualize the nuclei because the 396 nm excitation wavelength applied to visualise the MitoSOX compound would have also excited the nuclei dyes and both emission spectras would have overlapped.

4.2.15 Statistical analysis

Statistical analysis of data was performed using StatsDirect software. All results were represented as the mean ± SEM or as the mean ± SD of three independent experiments. The choice of SEM *vs*. SD was only based on obtaining a better visual representation of the figures. Data was first assayed for normality using the Shapiro-Wilk test. When assaying differences amongst at least three groups, if data was normal, statistical analysis was performed using One Way ANOVA with Dunnet as a post-hoc comparison, as this test is specifically designed to compare each treatment against a single control. If there was no evidence of normality, Kruskal-Wallis test was applied instead. To test for differences amongst two groups, a t-test was performed if data was classified as normal and a Mann-Whitney test when data showed no evidence of normality. Only when p values <0.05 the results were considered significant.

4.3 RESULTS

4.3.1 Validation of ciPTECs mitochondrial respiration parameters

Before analysing the mitochondrial effect of drugs based on changes in the respiratory parameters, a validation of the mitochondrial stress test was performed in normal conditions to confirm that ciPTECs would respond and follow the expected OCR pattern. One batch of cells was cultured for 24 h at 33°C and another one was cultured for 24 h at 33°C plus 5 days at 37°C before performing the mitochondrial stress test. The validation time points were selected accordingly with previous experiments performed in Chapters 2 and 3.

The results confirmed that ciPTECs responded successfully to the injections of the different OXPHOS inhibitors and the OCR pattern was representative of a typical mitochondrial stress test (Figure 4.2). At both temperatures, the initial OCR had very similar levels (60 – 65 pmol/min). After the addition of oligomycin (4^{th} point), there was a marked decrease in OCR that was stable until FCCP was injected (7^{th} point). Here, ciPTECs that had been cultured for 5 days at 37°C showed a greater maximal respiration, 25 pmol/min higher than at 33°C. Finally, when antimycin A and rotenone were added (10^{th} point), the respiratory chain stopped working and oxygen consumption levels fell again leaving only a baseline of OCR resultant from oxidative procedures outside the mitochondria (Figure 4.3).

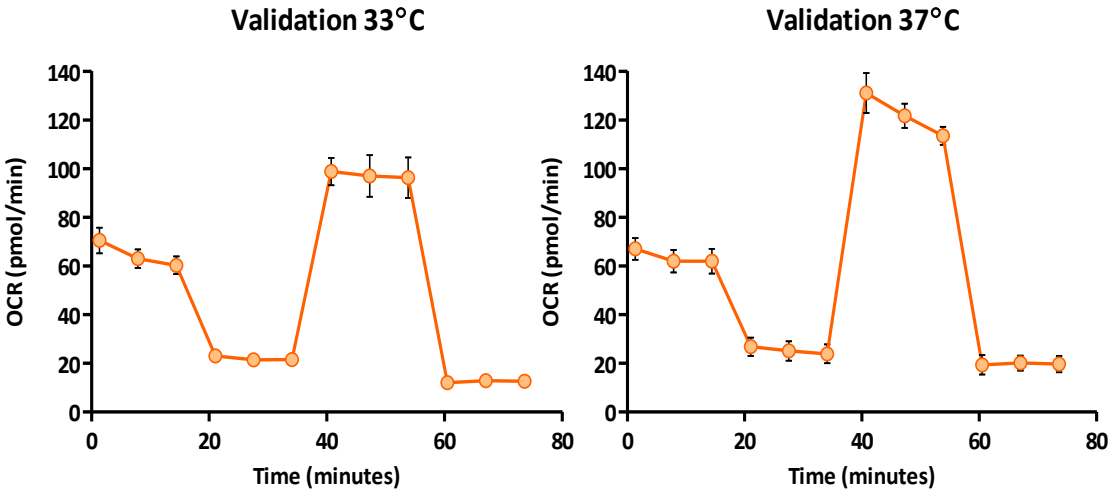

Figure 4.3 Mitochondrial stress test validation at 33°C and 37°C.
ciPTECs were cultured at 33°C for 24 h and at 37°C for 5 days before performing the mitochondrial stress test with the Seahorse instrument. OCR is represented in pmol/min and readings were taken every 7 minutes. Oligomycin was added after the 3rd measurement, FCCP was added after the 6th measurement and antimycin A and rotenone were added after the 9th measurement. Data are mean ± SD (n = 3).

4.3.2 Effect of cisplatin toxicity on the respiratory chain

Cisplatin (cis-diamminedichloroplatinum II) was chosen as a negative control to evaluate how a non-mitochondrial nephrotoxin would affect the established respiration parameters. However, although cisplatin causes toxicity through formation of DNA adducts and interfering with DNA synthesis (Wang and Lippard 2005), the mitochondria is believed to be a secondary target (Servais et al. 2008). The fact that possible mitochondrial impairment does not drive cisplatin toxicity was proven in Chapter 3 (Table 3.1).

The Seahorse instrument requires a high level of cell confluence to measure OCR and ECAR parameters accurately. Therefore, the experiment was designed accordingly by dosing ciPTECs with cisplatin for 24 h at different concentrations; longer incubations would trigger cell death and loss of confluence. Furthermore, it was demonstrated in Chapter 3 that changes in ATP levels, and therefore mitochondrial respiration, happen before cell death. Hence we should be able to detect respiration changes with shorter dosing treatments.

The respiratory parameters in Figure 4.4 were calculated following Table 4.1 guidelines and results were normalised to cell protein content. OCR due to ATP production was maintained around 5 pmol/min/µg protein up until 30 µM of cisplatin but the levels fell drastically to 2 pmol/min/µg at higher concentrations (Figure 4.4 A). The spare respiratory capacity followed a similar pattern and oxygen consumption was significantly reduced at 100 µM and 200 µM (Figure 4.4 B). In contrast, the levels of consumed oxygen related to proton leak remained fairly stable for every single dose (Figure 4.4 C). No significant differences were observed in the coupling efficiency either (Figure 4.4 D).

Finally, the results at the 3rd point of the mitochondrial stress test were represented in a bioenergetic phenograph (Figure 4.5) to study the cell energetic metabolism in terms of ECAR. The data also corroborates that no significant changes in OCR or in ECAR could be

detected from 0 µM to 30 µM of cisplatin. However, at 100 µM or higher the oxygen consumption drops significantly but it is not followed by any modifications in ECAR.

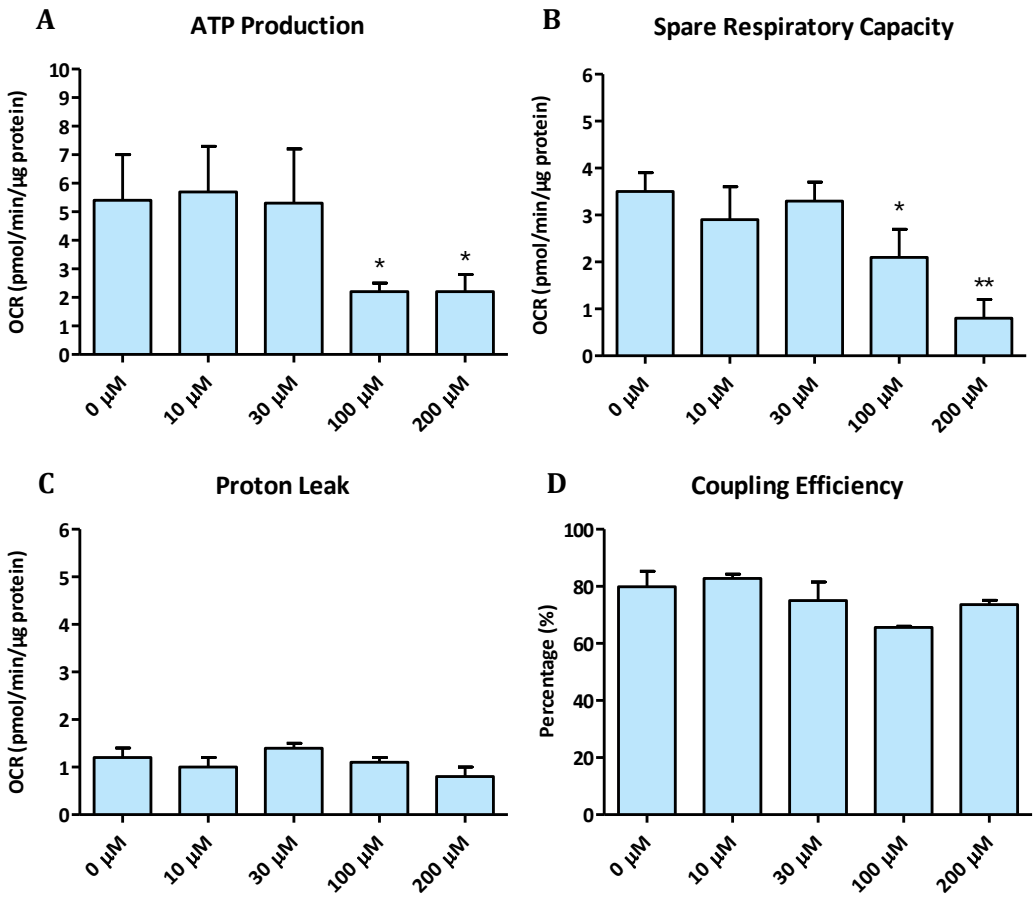

Figure 4.4 Representation of mitochondrial respiration parameters after cisplatin exposure.

ciPTECs were dosed with cisplatin for 24 h (0 - 200 µM) and then Seahorse technology was used to perform a mitochondrial stress test. The amount of consumed oxygen linked to ATP production (A), spare respiratory capacity (B) and proton leak (C) are represented in pmol/min/µg protein. The coupling efficiency (D) was also determined and it is represented as a percentage (%). Data are mean ± SD (n = 3). Statistical significance was determined by One Way ANOVA test, **p*<0.05, ***p*<0.01, ****p*<0.001.

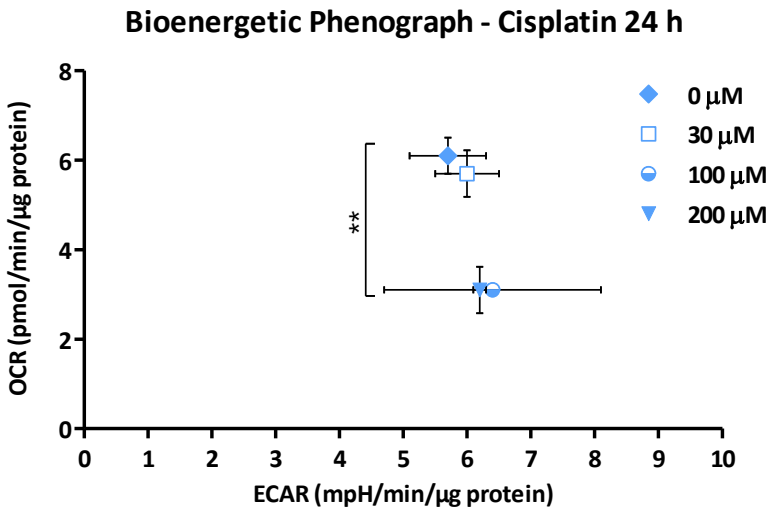

Figure 4.5 Bioenergetic profile of ciPTECs measuring OCR and ECAR at basal conditions after cisplatin exposure.

Data was taken from the 3rd point in the mitochondrial stress test (basal conditions). A 24 h exposure with cisplatin had taken place before the experiment. Only data from ciPTECs treated with 0 - 200 µM of cisplatin has been plotted to simplify the graph. OCR is represented in pmol/min/µg protein and ECAR is represented in mpH/min/µg protein. Data are mean ± SEM (n = 3). Statistical significance was determined by One Way ANOVA test, *p<0.05, **p<0.01, ***p<0.001.

4.3.3 Assessment of adefovir-induced mitochondrial perturbation via Seahorse analysis

In Chapter 3, it was demonstrated using the glucose *vs.* galactose *in vitro* model that adefovir treatment of cells displays the typical characteristics of a mitotoxin. To find out a little bit more about adefovir's toxicity mechanism in a PT cell line, ciPTECs were dosed with an adefovir dose response for 24 h and changes in the mitochondrial respiration parameters were analysed using the Seahorse instrument. Again, a 24 h experiment rather than the 3 day experiment from Chapter 3, was executed to avoid cell death and measure OCR and ECAR accurately. Although the incubation was shorter, it should be possible to detect alterations in the OCR as they appear before cells reach energetic compromise. The experiment was carried out in glucose conditions since, even though at a lower degree, the mitochondria are still producing ATP and also the presence of glucose in the medium allows to measure changes in the ECAR.

Table 4.1 definitions were used to calculate the respiratory parameters in Figure 4.6 and data was normalised to protein content. The amount of oxygen used to produce ATP decreased proportionally with increasing adefovir concentration, becoming significant between 30-100 µM. The basal OCR decreased from 4.5 to 1 pmol/min/µg protein from 0 to 100 µM, respectively (Figure 4.6 A). Moreover, the spare respiratory capacity did not show a clear dose response but a significant drop in OCR was observed at 10 µM as well as 100 µM of adefovir. Surprisingly, oxygen consumption levels at 30 µM were not different from the control (Figure 4.6 B). As observed previously with cisplatin, the amount of oxygen fated for proton leak processes was stable (Figure 4.6 C). Nevertheless, the coupling efficiency was significantly reduced from 80% to less than 60% from control cells to 100 µM, respectively (Figure 4.6 D).

Data from the 3rd time point in the mitochondrial stress test was plotted to generate a bioenergetic profile: OCR *vs.* ECAR (Figure 4.7). At basal conditions, a dose-dependent

decrease in OCR was detected, which correlated with the tendency seen for OCR linked to ATP production (Figure 4.6 A). However, instead of detecting no change in ECAR, as it was observed with cisplatin (Figure 4.5) or an increase as observed with rotenone (Figure 3.6), a non-significant tendency towards ECAR downregulation was detected (Figure 4.7).

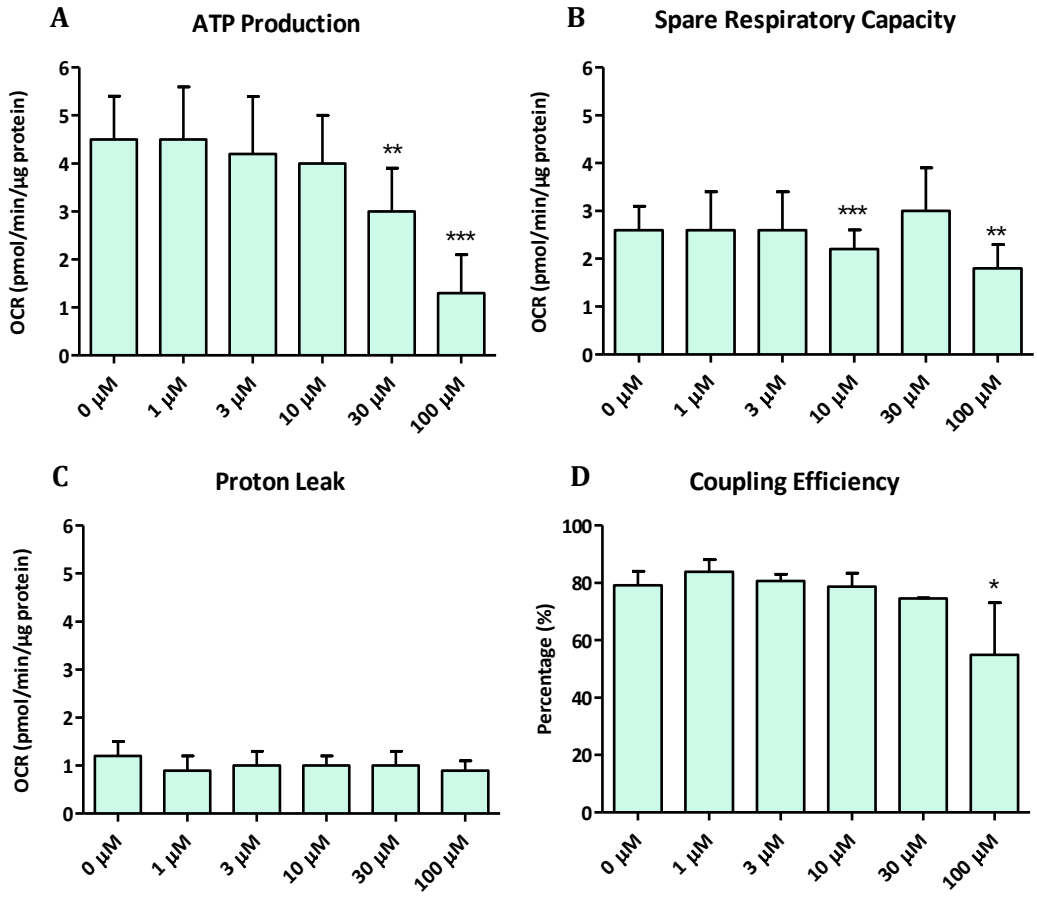

Figure 4.6 Representation of mitochondrial respiration parameters after adefovir exposure.

CiPTECs were dosed with adefovir for 24 h (0 - 100 µM) and then Seahorse technology was used to perform a mitochondrial stress test. The amount of consumed oxygen linked to ATP production (A), spare respiratory capacity (B) and proton leak (C) are represented in pmol/min/µg protein. The coupling efficiency (D) was also determined and it is represented as a percentage (%). Data are mean ± SD (n = 3). Statistical significance was determined by One Way ANOVA test, *p<0.05, **p<0.01, ***p<0.001.

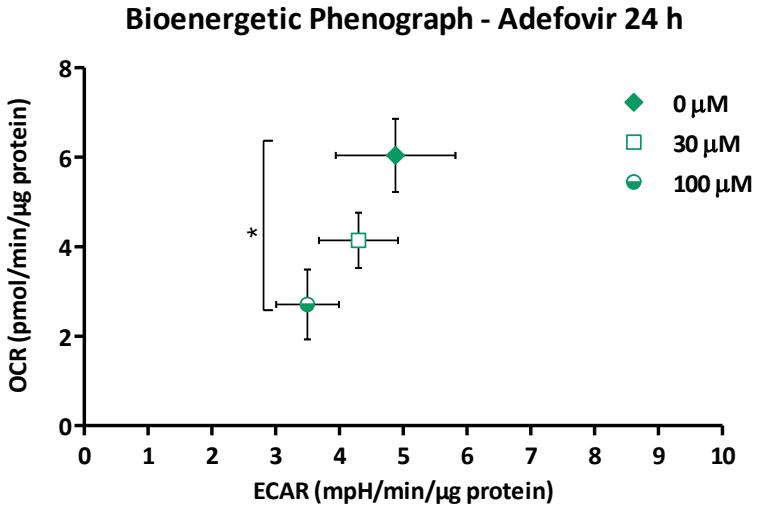

Figure 4.7 Bioenergetic profile of ciPTECs measuring OCR and ECAR at basal conditions after adefovir exposure.

Data was taken from the 3rd point in the mitochondrial stress test (basal conditions). A 24 h exposure with adefovir had taken place before the experiment. Only data from ciPTECs treated with 0 µM, 30 µM and 100 µM of adefovir has been plotted to simplify the graph. OCR is represented in pmol/min/µg protein and ECAR is represented in mpH/min/µg protein. Data are mean ± SEM (n = 3). Statistical significance was determined by One Way ANOVA test, **p*<0.05, ***p*<0.01, ****p*<0.001.

4.3.4 Quantification of respiratory chain complexes after adefovir treatment

In light of the downregulation in ATP linked respiration and the decrease in coupling efficiency demonstrated with adefovir treatment, we decided to look at the protein level of various mitochondrial respiratory chain complexes. Coupling efficiency was defined as a measure for the ATP turnover. Therefore, impairment in this parameter would indicate that one or more OXPHOS complexes have been targeted as part of the mechanism. To check if the altered functionality is due to a quantitative depletion of the mitochondrial redox carriers, a western blot was performed.

After the 24 h treatment with adefovir, the western blotting results demonstrated no obvious differences in protein expression of complex V, III or II compared with the control. No noticeable differences could be observed for complex IV either. Nevertheless, complex I expression was qualitatively lower at 30 µM and 100 µM compared to control (0 µM) (Figure 4.8 A). Complex I results were corroborated by densitometry (Figure 4.8 B), where a 50% decrease in band density was determined. Moreover, a slight depletion of complex IV levels was also detected at 30 µM and 100 µM (15-20% reduction).

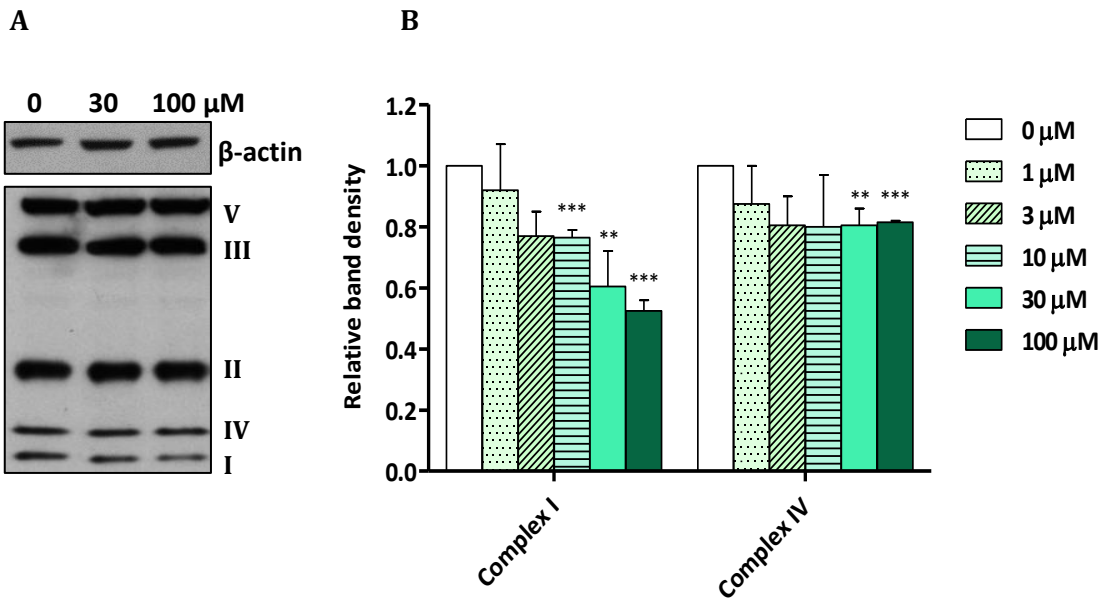

Figure 4.8 Western blotting (A) and densitometry (B) of the electron transport chain complexes after 24 h of adefovir treatment in ciPTECs.

CiPTECs were incubated with adefovir (0 - 100 µM) for 24 h. Equal amounts of protein were separated by SDS-PAGE from whole cell RIPA lysates. The presence of OXPHOS complex I (18 kDa), complex II (29 kDa), complex III (48 kDa), complex IV (22 kDa) and complex V (54 kDa) was determined by western blot and compared to a β-actin loading control (A). Densitometry of complex I and IV was performed by ImageJ software and the relative density of the complexes was normalized to the relative density of the corresponding β-actin band. Data are mean ± SEM (n = 3). Statistical significance was determined by One Way ANOVA test, **p*<0.05, ***p*<0.01, ****p*<0.001.

4.3.5 Investigating the role of ROS in adefovir-induced mitotoxicity

To further explore the mechanism of adefovir-induced mitotoxicity, we decided to determine whether or not ROS could be generated by the treatment of ciPTECs with this compound. Drug-induced oxidative stress has been implicated as a key contributor for mechanistically different toxicities such as cisplatin or azidothymidine toxicity, a nucleoside reverse transcriptase inhibitor (Deavall et al. 2012). Therefore, it would be plausible to think that adefovir exposure could elevate cellular ROS and cause oxidative stress that could eventually lead to mitochondrial dysfunction and cell death.

ROS levels in glucose and galactose conditions were analysed using 10 µM of DHE after cells were treated with adefovir for 48 h (Figure 4.9). A dose-dependent increase in ROS was observed reaching values greater than 2-fold between 10 - 50 µM adefovir in glucose cultured cells. In galactose medium, ciPTECs also had a dose-dependent increase up to 3-fold of ROS compared to basal glucose levels and up to 2-fold compared to basal galactose levels. It was also worth noting that under control conditions (0 µM), ciPTECs produced a significantly higher amount of ROS in galactose conditions compared to glucose.

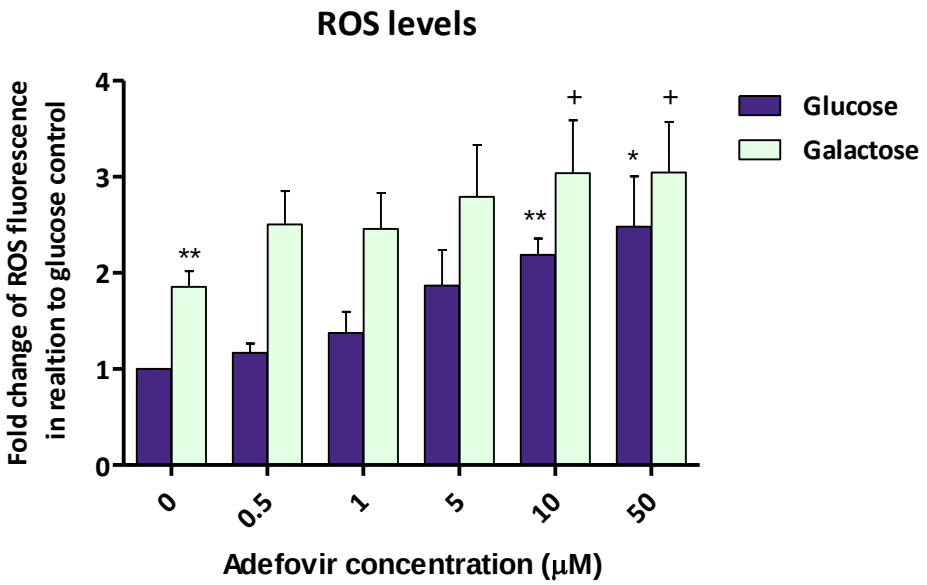

Figure 4.9 Analysis of ROS levels by DHE fluorescence.
ROS levels were determined after 48 h with adefovir (0 - 50 μM) in glucose and galactose conditions. Glucose data and galactose at 0 μM are compared to glucose control (*). Galactose data is compared to galactose control (+). Data are mean ± SD (n = 3). Statistical significance was determined by One Way ANOVA test when data was compared to the control and a t-test to analyse the significance between both controls (0 μM), *p<0.05, **p<0.01, ***p<0.001.

4.3.6 Mitochondrial ROS assessment

Having identified elevated cellular levels of ROS during adefovir exposure and knowing that oxidative stress can also cause mitochondrial dysfunction, we decided to specifically look at ROS accumulation inside the mitochondria itself.

ciPTECs were cultured for 48 h with exposure to adefovir at 0 µM (Figure 4.10) and 5 µM (Figure 4.11) in glucose conditions and later stained with MitoSOX (mitochondrial superoxide indicator). Two different excitation wavelengths were used to visualise superoxide ($O_2^{\cdot-}$) production. Cells were excited with a traditional 510 nm wavelength, according to manufacturer's guidelines, and with a 396 nm wavelength to improve the selectivity of superoxide-oxidised MitoSOX (Robinson et al. 2006). No differences were observed between 0 and 5 µM at 510 nm in terms of fluorescence intensity. However, when looking at the images taken at 396 nm, distinctive colour intensification was detected at 5 µM of adefovir, which should correspond to an increase in mitochondrial superoxide levels. Unexpectedly though, the fluorescence pattern observed at 396 nm was different from 510 nm. At 510 nm it was distinguishable where the nuclei would fit in as a roundish less fluorescent area was appreciated in each cell. Instead, at 396 nm the fluorescence was more intense at the same nuclei area, which questions the specificity of the results.

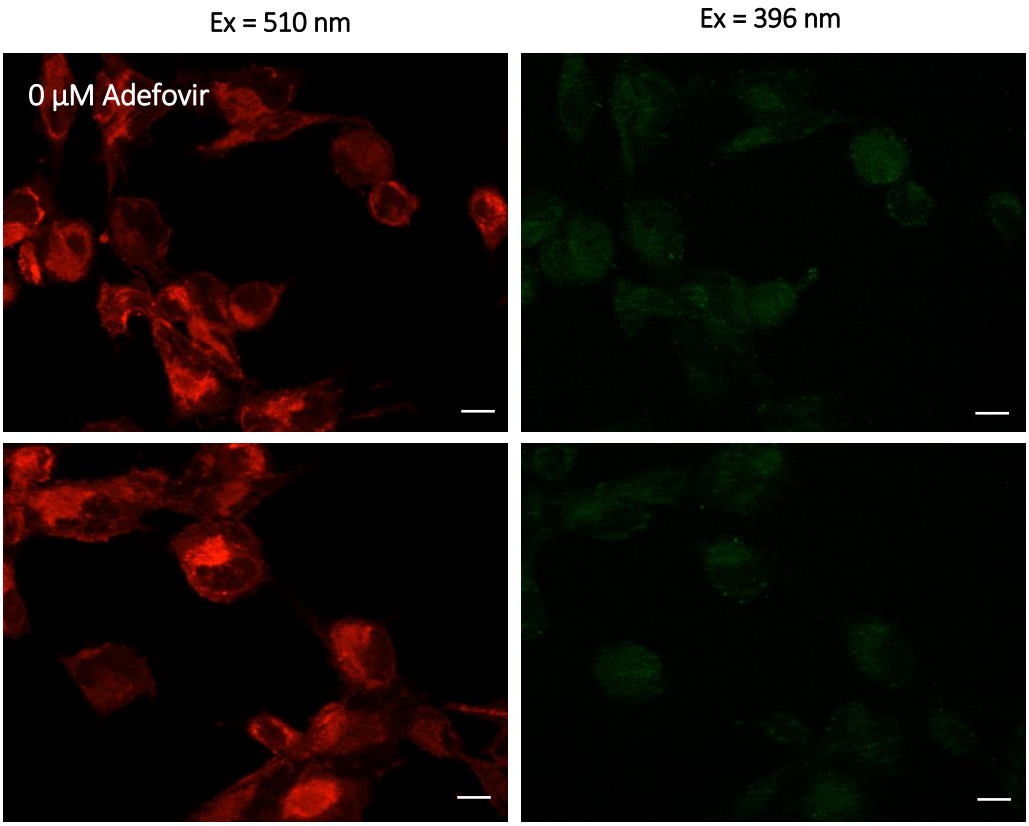

Figure 4.10 Detection of mitochondrial superoxide in control conditions.
ciPTECs were cultured without adefovir for 48 h and then stained with MitoSOX. Cells were visualised at 510 nm and 396 nm excitation wavelength. Images were taken using a 63x objective with the ApoTome. Scale bar is 10 µm. Data is representative of n = 3 experiments.

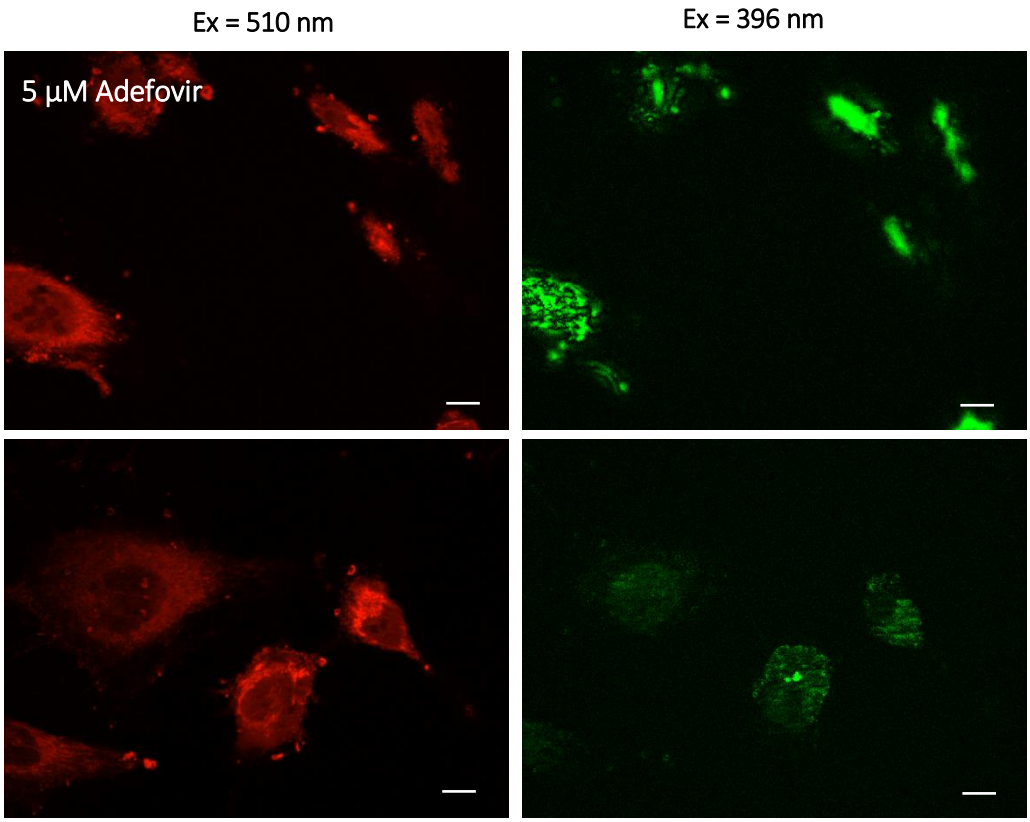

Figure 4.11 Detection of mitochondrial superoxide after 48 h with adefovir (5 µM). ciPTECs were cultured with 5 µM of adefovir for 48 h and then stained with MitoSOX. Cells were visualised at 510 nm and 396 nm excitation wavelength. Images were taken using a 63x objective with the ApoTome. Scale bar is 10 µm. Data is representative of n = 3 experiments.

4.3.7 Effect of cisplatin and adefovir in mitochondrial biogenesis *in vitro*

Mitochondrial biogenesis can be triggered after an episode of oxidant injury that has led to mitochondrial loss (Rasbach and Schnellmann 2007), which as a result accelerates the return of mitochondrial functions (Funk et al. 2010). As we have previously demonstrated, adefovir caused oxidative stress in ciPTECs after 48 h of treatment; therefore we reasoned that mitochondrial biogenesis could also be induced as a counteractive mechanism of cellular oxidant damage.

Here, we applied the strategy of Beeson *et al*. in ciPTECs to use Seahorse technology as a high-throughput respirometric assay to assess the role of mitochondrial biogenesis. Their method is based on using FCCP-uncoupled OCRs as a marker of mitochondrial biogenesis by comparing them with basal OCRs. Ergo, a stable basal OCR after compound exposure but with an enhanced FCCP-uncouple OCR would indicate that cells possess a higher spare respiratory capacity as a result of increased mitochondrial number (Beeson et al. 2010).

A negative control experiment was first performed with cisplatin (Figure 4.12). Cells were dosed with cisplatin for 24 h and then analysed with Seahorse. No significant differences between FCCP-uncoupled OCRs were identified at 10 µM or 30 µM compared to the control. A decrease in basal OCR was seen at 30 µM and a strong reduction of both OCRs was seen at 100 µM (Figure 4.12).

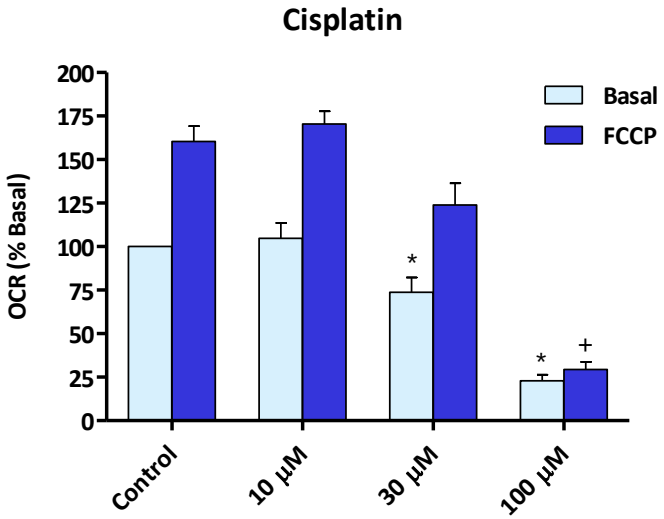

Figure 4.12 Respirometric measurement of mitochondrial biogenesis after cisplatin exposure.

A 24 h cisplatin treatment was performed in ciPTECs (0 - 100 µM). Basal and FCCP-uncoupled OCRs (in pmol/min/µg protein) were analysed with Seahorse technology and normalized to basal OCR of untreated wells. Results are expressed as a percentage (%) compared to the basal. Data are mean ± SEM (n = 3). Statistical significance was determined by Kruskal–Wallis test, *p<0.05. An asterisk (*) represents a statistically significant difference from control basal. A cross (+) represents a statistically significant difference from control FCCP-uncoupled.

Based on these findings and to evaluate mitochondrial biogenesis after adefovir treatment, we followed the same protocol used with cisplatin. Cells were dosed with adefovir for 24 h and then changes in respiration were analysed with Seahorse. At the lowest concentrations (1 - 10 µM), no significant differences were observed in basal OCRs compared to the control and the same result was detected for FCCP-uncoupled OCRs compared to their control (Figure 4.13). The only significant changes were seen at 30 µM, where both basal and FCCP-uncoupled OCRs suffered a substantial reduction. In summary, the lack of enhanced FCCP-uncoupled OCRs indicated that no mitochondrial biogenesis was taking place after adefovir exposure.

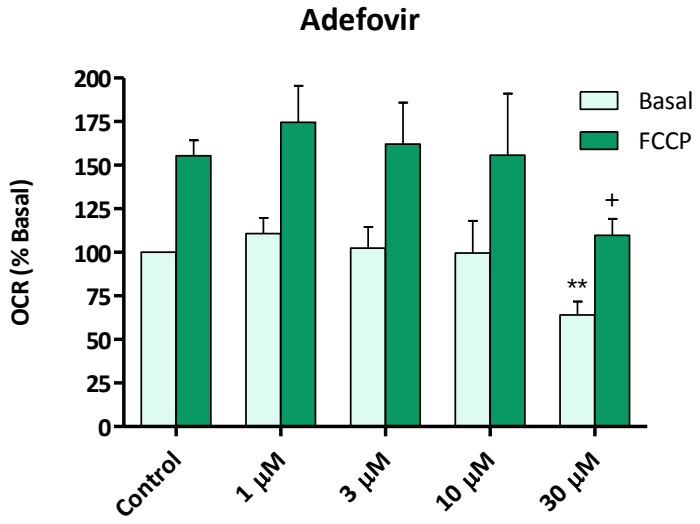

Figure 4.13 Respirometric measurement of mitochondrial biogenesis after adefovir exposure.

A 24 h adefovir treatment was performed in ciPTECs (0 - 30 µM). Basal and FCCP-uncoupled OCRs (in pmol/min/µg protein) were analysed with Seahorse technology and normalized to basal OCR of untreated wells. Results are expressed as a percentage (%) compared to the basal. Data are mean ± SEM (n = 3). Statistical significance was determined by Kruskal–Wallis test, *p<0.05. An asterisk (*) represents a statistically significant difference from control basal. A cross (+) represents a statistically significant difference from control FCCP-uncoupled.

4.3.8 Investigating TFV toxicity using Seahorse technology – early signs of mitochondrial dysfunction?

In Chapter 3 we established that no signs of mitotoxicity could be detected after 15 days of TFV incubation in the glucose *vs.* galactose ciPTECs model. We observed a 20% -25% downregulation of cellular ATP levels at the highest concentration investigated (100 μM). To further explore the mechanistic basis of potential mitochondrial involvement in TFV toxicity, we measured in ciPTECs potential variations on the respiration parameters and on the ECAR after 15 days of TFV treatment using the Seahorse technology.

The definitions described in Table 4.1 were used to calculate the respiratory parameters in Figure 4.14 and data was normalised to protein content. At every concentration, respiration linked to ATP production (Figure 4.14 A) was much lower than the values obtained after 24 h with adefovir (Figure 4.6 A). Furthermore, the amount of oxygen consumed remained stable over the investigated TFV dose response (Figure 4.14 A). No substantial changes were observed on the spare respiratory capacity, proton leak or coupling efficiency (Figure 4.14 B, C, D). The first two parameters (Figure 4.14 A, B) also displayed lower oxygen consumption levels than in adefovir dose response treatment (Figure 4.6).

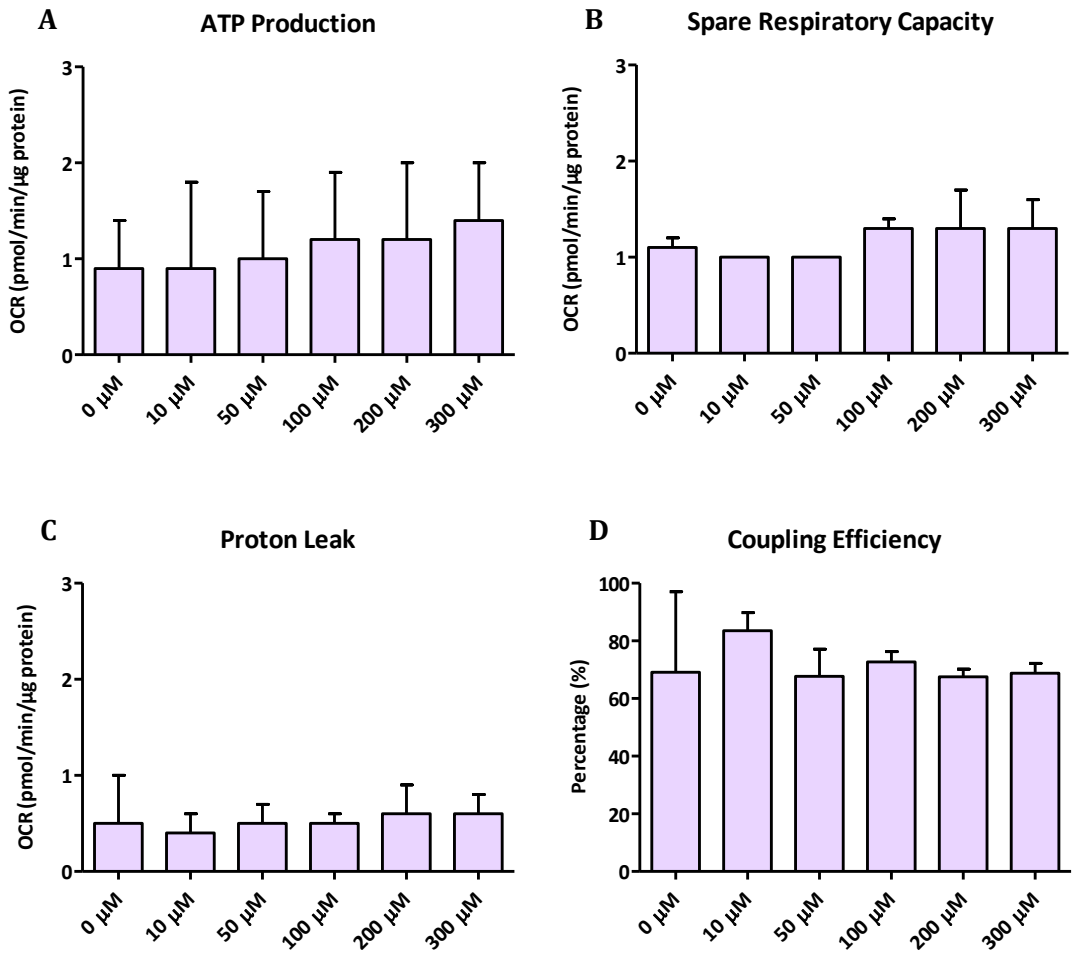

Figure 4.14 Representation of mitochondrial respiration parameters after TFV exposure in glucose conditions.

ciPTECs were dosed with tenofovir for 15 days (0 - 300 µM) and then Seahorse technology was used to perform a mitochondrial stress test. The amount of consumed oxygen linked to ATP production (A), spare respiratory capacity (B) and proton leak (C) are represented in pmol/min/µg protein. The coupling efficiency (D) is represented as a percentage (%). Data are mean ± SD (n = 3). Statistical significance was determined by One Way ANOVA test, **p*<0.05, ***p*<0.01, ****p*<0.001

The typical respiration parameters did not confer any extra information regarding possible mitochondrial toxicity. Nonetheless, in Figure 4.15 a dose-dependent increase on ECAR values could be identified, which were preserved for the duration of the Seahorse experiment. Specifically, at 200 µM of TFV the ECAR was around 1.5 units (mpH/min/µg protein) higher than the control cells, which provides some evidence that TFV treated cells developed a higher glycolytic activity.

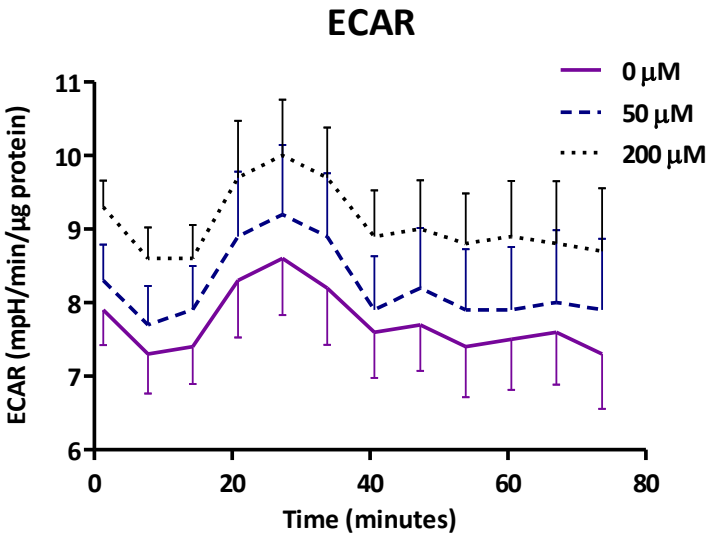

Figure 4.15 Measurement of ECAR throughout Seahorse experiment after TFV exposure.
ciPTECs were dosed with tenofovir for 15 days at different concentrations (here only represented 0 µM, 50 µM and 200 µM) and then Seahorse technology was used to perform a mitochondrial stress test. The extracellular acidification rate was measured throughout the test and it is represented in mpH/min/µg protein. Data are mean ± SEM (n = 3).

4.3.9 Quantification of respiratory chain complexes after TFV treatment

Having analysed the activity and respiration parameters derived from the OXPHOS complexes, we examined if we could detect any quantitative variations at a protein level after TFV exposure as we had observed with adefovir. The western blotting results (Figure 4.16) did not reveal any alterations in protein content for any respiratory chain complex along the different TVF concentrations. β-actin levels confirmed a stable loading.

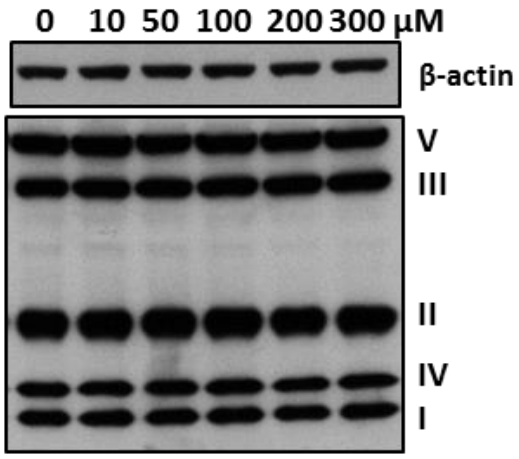

Figure 4.16 Western blotting of the ETC complexes after 15 days of TFV treatment in ciPTECs.
ciPTECs were incubated with TFV (0 µM - 300 µM) for 15 days. Equal amounts of protein were separated by SDS-PAGE from whole cell RIPA lysates. The presence of OXPHOS complex I (18 kDa), complex II (29 kDa), complex III (48 kDa), complex IV (22 kDa) and complex V (54 kDa) was determined by western blot and compared to a β-actin loading control. Data are representative of three independent experiments.

4.4 DISCUSSION

Cellular bioenergetics have been previously investigated using Seahorse technology in other cell types such as HepG2 cells to demonstrate their importance in mitochondrial toxicity (Kamalian et al. 2015). However, this was the first time that a PT line such as ciPTECs was successfully energetically interrogated.

Based on the OCR pattern described at both 33°C and 37°C, ciPTECs energetic metabolism in basal conditions was concordant with other established cell lines (Dott et al. 2014, Chacko et al. 2014). However, as highly aerobically poised cells, *in vivo* energy requirements of PT cells would probably differ from the pattern observed and present a much higher FCCP stimulated rate (Hill et al. 2012).

Before looking into the perturbation of respiratory parameters by adefovir and TFV, we analysed the bioenergetic changes triggered by a renal non-mitotoxic compound such as cisplatin. Even though ATP-linked OCR and spare respiratory capacity were affected, that could be attributed to OXPHOS damage caused by ROS and activation of the apoptotic intrinsic pathway (Servais et al. 2008). In contrast, since the anticancer drug has not been described to have uncoupling effects or to target a particular complex, it was expected that mitochondrial permeability and coupling efficiency would be unaffected. Moreover, the observed failure to upregulate glycolysis by ciPTECs after cisplatin treatment might be an indication that the apoptotic mechanism had already been activated and the cell energetic metabolism was focused on other pathways (Brdiczka et al. 2006).

In light of addressing which mitochondrial mechanism was responsible for adefovir mitotoxicity, ciPTECs cellular bioenergetics were thoroughly interrogated. Although the repercussions in respiratory parameters were quite similar to the ones observed in the

negative control, a distinctive decrease in the coupling efficiency indicated that one or more respiratory complexes had been hampered and the ETC efficiency downregulated as a result. Protein levels of the ETC complexes showed that, in fact, the decrease in coupling efficiency could be due to a lower protein content of complexes I and IV. It is known that electron transport chain complexes have a mix of nuclear and mitochondrial encoded subunits (Figure 4.17), and in particular complex I and complex IV are the only two complexes with an important mtDNA encoded core (Schon et al. 2012). Therefore, if adefovir was either targeting mtDNA as Tanji *et al*. postulated (Tanji et al. 2001) or mitochondrial protein synthesis as other NRTIs (Dykens and Will 2007), the most affected complexes would most likely be complex I and IV, as the lack of mitochondrial subunits would not allow protein assembling and they would be degraded by the mitochondrial protein quality control system (Amm et al. 2014, Fox 2012). To confirm which of the two hypotheses is actually taking place, further experiments would be required. Levels of mtDNA could be measured by qPCR as well as levels of mitochondrial mRNA. Furthermore, ciPTECs could be dosed with a mitochondrial protein synthesis inhibitor, such as

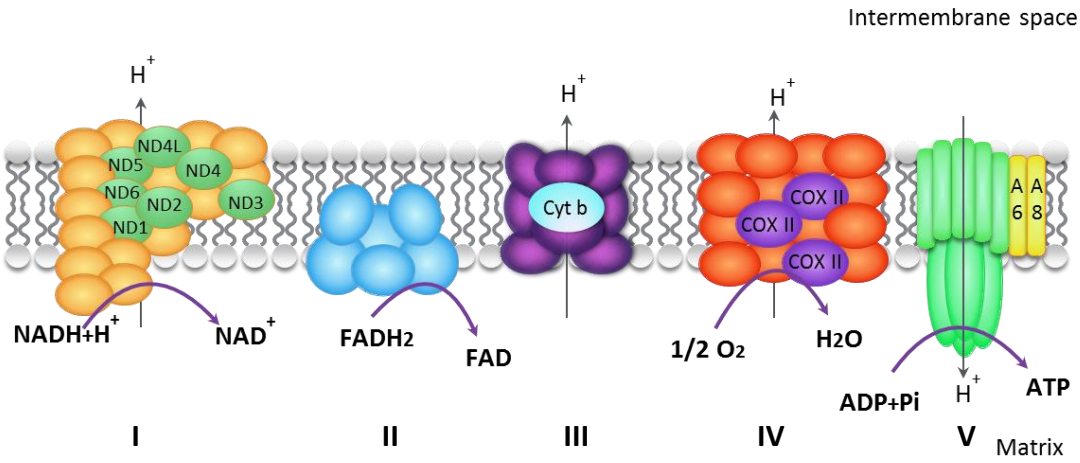

Figure 4.17 Mitochondrial encoded subunits of the ETC complexes.
The ETC complexes are encoded by nuclear and mitochondrial DNA. The subunits encoded by mtDNA are represented in a different colour and the names have been added. Complex I has 7 mtDNA subunits compared to 39 from the nDNA (7/39), complex II has 0/4, complex III has 1/10, complex IV has 3/10 and complex V has 2/14 (Schon et al. 2012).

oxazolidinones (McKee et al. 2006), and western blotting results should be compared with the ones obtained after adefovir exposure.

As seen with other retroviral agents (Deavall et al. 2012), DHE results confirmed that oxidative stress via ROS production also plays a role in adefovir toxicity. In addition, the galactose-dependent increase in ROS levels corroborated a greater activity of the ETC (Brand et al. 2004). In most cell types, mitochondria are one of the highest contributors to the generation of ROS through the generation of unpaired electrons in OXPHOS, which interact with oxygen and form superoxide ions (Duchen 2004). However, the specificity of the IF results was questionable due to a higher nuclei fluorescence at 396 nm and ROS increased production could not be directly associated to the mitochondria. Other experiments using new methods for mitochondrial ROS detection such as hydroxylamine spin probes could be applied to tackle this problem (Dikalov and Harrison 2014). Additionally, to test the significance of ROS in adefovir toxicity, it would be interesting to incubate ciPTECs, prior and during adefovir exposure, with clinically relevant ROS scavengers such as N-acetyl cysteine (NAC) (Sun 2010, Bavarsad Shahripour et al. 2014) and measure if a delay in toxicity or ATP levels depletion could be detected. Moreover, to take things a step further, the type of ROS, such as superoxide or peroxides, responsible for oxidative stress could be identified using ROS fluorescent sensors (Dikalov and Harrison 2014).

It is known that, after an event of oxidative stress that leads to mitochondrial loss, a cell response can be activated capable of inducing mitochondrial biogenesis to recover full organelle functionality (Rasbach and Schnellmann 2007, Funk et al. 2010). Although we previously showed that adefovir induces oxidative stress, no mitochondrial biogenesis was detected. We followed the same dosing strategy as Beeson *et al.,* when he showed some compounds capable of inducing biogenesis after 24 h. Nevertheless, adefovir might need a

longer exposure time (48 h) to produce a strong enough oxidant injury to ciPTECs and some recovery time for the cells to react and induce mitochondrial biogenesis.

The impact of TFV, a less toxic nucleotide analogue of adefovir but highly used in the clinic (Herlitz et al. 2010), on the respiratory parameters was also assessed. Even though the effect of TFV on ATP levels was investigated in Chapter 3 without any clear indication of mitotoxicity, we were interested in determining whether we could detect any changes at a molecular level. The stable level of ETC complexes supported the theory that some NtRTIs might induce mitochondrial injury through a mechanism that is distinct from inhibiting DNA polymerase-γ (Ross 2014). However, to confirm this hypothesis, mtDNA should be quantified through qPCR. Moreover, Seahorse results did not match the slight ATP reduction observed in Chapter 3. Instead, levels of ATP-linked OCR were quite low and no variations compared to control were detected. One theory to explain it would be that TFV hampers cell growth, and that is why the not normalised results from Chapter 3 showed lower amounts of total ATP. Hence, when the results are normalised to protein content the difference disappears. However, if what TFV actually hinders is protein synthesis (Zhang et al. 2015), normalising the Seahorse results to protein content would show misleading information. Specifically, in this case, it would look like ciPTECs were producing more ATP than they actually were. To address this issue, a simple solution would be to normalise the data against cell number. For the same reason, western blotting results might have not been representative. If ciPTECs are in fact not generating enough ATP, the shift towards higher levels of ECAR (dependant on TFV concentration) to upregulate glycolysis energy production fits with the metabolic energetic scenario.

In summary, these results represent the first step to perform further mitotoxicity related studies and to explore different mitochondrial toxicity pathways from other nephrotoxic compounds. Therefore, future studies will be designed to elucidate some key features of

the adefovir and TFV metabolism and toxicity. Uptake and metabolism of both NtRTIs could be assessed through mass spectrometry, which would give an idea of the concentration inside the cells compared to the extracellular dose. It would also be interesting to look at changes in membrane potential using a fluorescent probe (JC-1) or to analyse cytochrome c release with IF. Moreover, a collaboration has been established with the intention of repeating these experiments on ciPTECs that overexpress human OAT1 and OAT3, which are the key transporters involved in adefovir and TFV uptake (Uwai et al. 2007).

Chapter Five

Isolation and characterisation of UPCs as preliminary steps to establish a novel patient-specific model of nephrotoxicity

CONTENTS

5.1 INTRODUCTION

The existence of a distinct stem cell population in the kidney that would be responsible for repopulating the damaged tubule area after injury is highly controversial. It was first accepted that the source of the cells capable of repairing injured nephrons was intrinsic and not derived from other niches such as bone marrow-derived stem cells (Vogetseder et al. 2008, Humphreys et al. 2008). Nonetheless, it was unclear if the repopulating cells were differentiated PT cells that were able to dedifferentiate and start proliferating to repair the damage, or alternatively, there was a latent progenitor/stem cell population responsible for the repair. Using a co-labelling strategy, Humphreys *et al*. brought some light on the matter by confirming that any surviving cell was able to proliferate and restore the tubules (Humphreys et al. 2011). However, the same year, another study appeared to contradict this work by demonstrating that there was a scattered population of PT cells within the tubules that co-expressed CD24 and CD133 and displayed stem/progenitor characteristics *in vitro* (Lindgren et al. 2011). In addition, it was later shown that when SCID mice with acute tubular injury were injected intravenously with CD24 and CD133 positive cells, these double positive cells would engraft into the kidney, help tubular repair and cause a significant improvement in renal function (Angelotti et al. 2012).

Since the isolation of the first designated progenitor cells from urine (Zhang et al. 2008), other groups have claimed that they were able to isolate urine-derived stem cells (USCs) of kidney origin (Wu et al. 2011, Bharadwaj et al. 2011). Even though Bharadwaj and colleagues confirmed the presence of cells at varying stages of differentiation in human urine, which supports the concept described by Humphreys *et al*., they were able to differentiate the urine-derived cells into the three germinal lineages, including neurogenic and urothelial cells. These data therefore demonstrated that these cells had stem cell

features (Bharadwaj et al. 2013). Furthermore, the simple cost-effective isolation technique, their high reprogramming efficiency and their excellent differentiation potential, promoted the generation of induced pluripotent stem cells (iPSCs) from urine-derived progenitor cells (UPCs) (Zhou et al. 2012, Zhou et al. 2011).

The studies described in the preceding chapters were first designed to use the already characterised ciPTECs in Chapter 2 as a control for future pharmacological assays in newly developed PT lines. These new PT cell lines were supposed to have originated from kidney stem/progenitor cells (KSPCs) isolated from kidney tissue that had been differentiated using specific medium treatments and biomaterials into PT cells. However, the isolation of KSPCs using CD133 and CD24 markers and their differentiation by collaborative groups within our Institution suffered several unexpected delays. Despite this inconsistency, we decided to follow the published protocol of Zhang *et al*. to pursue the isolation of progenitor/stem cells from urine to later differentiate them into PT cells that may ultimately be utilised as predictive *in vitro* toxicological models (Figure 5.1). Although differentiation experiments have been previously performed in these types of cells (Bharadwaj et al. 2013), the possibility to attain a PT fate had not been explored. To do so, we chose to follow a protocol designed for human embryonic stem cells (Narayanan et al. 2013).

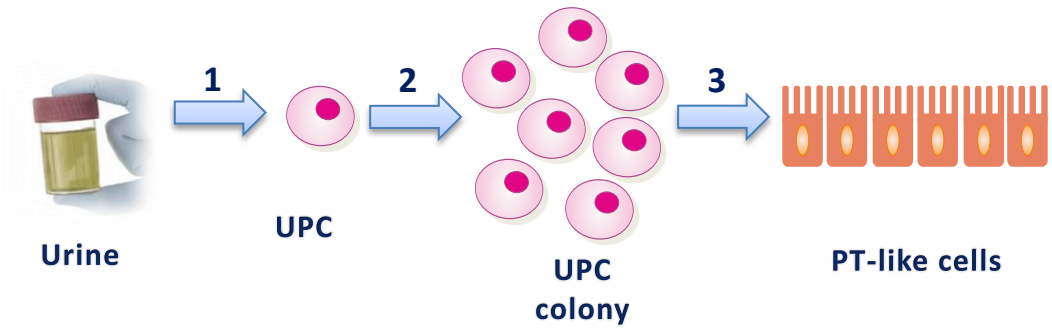

Figure 5.1 Schematic of the strategy to develop a patient-specific proximal tubule model from urine cultures.
The first step (1) would consist of isolating the cells from a urine sample and culture them to get a single urine-derived progenitor cell (UPC) in one well, which is key to generate a clonal cell line. Then, (2) after detecting a colony formation, UPCs would be expanded and characterised. Finally, (3) a proximal tubule (PT) differentiation treatment should be applied to obtain PT-like cells, which would be functionally tested against ciPTECs.

We postulated that if the isolation and differentiation treatment were successful, given that individuals often respond differently to the same drug, the differentiated PT-like cells might become a powerful tool to analyse patient-specific nephrotoxicity. In comparison, the published ciPTEC lines, and their pharmacological/toxicological response, previously used in preceding chapters may only be typical of a subset of the human population. Additionally, autologous urine-derived progenitor/stem differentiated PT cells could potentially be obtained from patients in whom renal injury can be anticipated, and hence be used in the future for the development of personalised medicine.

5.1.1 Aims and hypothesis

Hypothesis:

Many published and developed renal cell lines available poorly predict *in vivo* toxicity due to low metabolic competence and low transporter expression. Over recent years, this problem has been circumvented to some extent by the generation of conditionally immortalised PTCs (ciPTECs). Nevertheless, urine is also a good and non-invasive source of kidney cells as well as UPCs. Therefore, we aim to test the hypothesis that UPCs can be derived and differentiated into PT cells from different donors and retain efficient transporter expression that can be used to establish patient-specific models for *in vitro* nephrotoxicity exploration.

The aims of this chapter were to:

- Isolate and characterise UPCs from different donors.
- Direct the differentiation of isolated UPCs towards PT cells.
- After differentiation, perform a phenotypical characterisation and apply the functional assays developed in Chapter 2 to evaluate if the PT differentiated UPCs have acquired functionality levels similar to ciPTECs.

5.2 MATERIALS AND METHODS

5.2.1 Materials

Urine was obtained from healthy volunteers with informed ethical consent obtained for studies to be conducted within the Centre for Drug Safety Science, University of Liverpool. Conditionally immortalised podocytes were obtained from Saleem *et al*. group in Bristol, UK. RNA from human kidney tissue was obtained from the Department of Cellular and Molecular Physiology, University of Liverpool (Liverpool, UK). Tissue culture reagents Hamm's F12 medium, keratinocyte serum free medium, FBS, bovine pituitary extract, PBS as well as Hoechst 33342, ProLong® Gold Antifade Mountant, CellTracker™ Green CMFDA Dye, BMP2, BMP7, qPCR reagents and primers, DNase treatment, reverse transcription reagents, Alexa Fluor® 594 Goat Anti-Mouse IgG2b and Alexa Fluor® 488 Goat Anti-Rabbit IgG were purchased from Life Technologies (Paisley, UK). QIAzol Lysis Reagent was purchased from QIAGEN (Manchester, UK). Cover slides (13 mm ∅) were purchased from VWR (Lutterworth, UK). Microscope slides, chloroform, isopropyl alcohol (IPA) and absolute ethanol were obtained from Thermo Fisher Scientific (Loughborough, UK). Renal epithelial cell growth medium (REGM) Bulletkit was purchased from Lonza (Slough, UK). Activin A was purchased from R&D Systems (Abingdon, UK). CD133/1 and CD24 antibodies for flow cytometry were purchased from Miltenyi Biotec (Surrey, UK). Synaptopodin mouse monoclonal antibody was obtained from PROGEN (Heidelberg, Germany). Podocin rabbit monoclonal antibody was purchased from Abcam (Cambridge, UK). Megalin mouse monoclonal antibody was obtained from Acris (Herford, Germany). All other reagents and chemicals were purchased from Sigma Aldrich (Dorset, UK).

5.2.2 Cell culture

Urine derived cells were cultured in a mixture of keratinocyte serum free medium and progenitor cell medium in a 1 : 1 ratio (Zhang et al. 2008), that we will refer to as urine stem cells medium. Keratinocyte medium was supplemented with EGF (5 ng/ml), bovine pituitary extract (50 ng/ml), cholera toxin (30 ng/ml) and penicillin-streptomycin solution (1% v/v). Progenitor medium is a mixture of 75% DMEM and 25% Hamm's F12 medium and it was also supplemented with FBS (10% v/v), hydrocortisone (0.4 μg/ml), cholera toxin (10^{-10} M), insulin (5 ng/ml), adenine (1.8x 10^{-4} M), transferrin (5 μg/ml), 3,39,5-triiodo-L-tyronine (2x 10^{-9} M), epidermal growth factor (10 ng/ml) and penicillin-streptomycin solution (1% v/v).

5.2.3 Isolation of urine derived cells

Sterile fresh mid-stream urine samples (50 – 200 ml) were collected from a total of 5 healthy volunteers aged from 18 to 30 years old. No morning urine was used and the volunteers were asked to drink 500 ml of water before sample collection to favour cell shedding (Zhou et al. 2012). The isolation of urinary cells was performed using a combination of Zhou *et al*. (2012) and Bharadwaj, S*. et al.* (2013) procedures. Briefly, immediately after collection, urine was transferred to 50 ml falcon tubes and spun down at 1000 rpm for 5 minutes inside a sterile environment. Carefully, the supernatant was aspirated leaving around 1 ml of urine in the tube. The pellets were gently resuspended and then pooled down to a single 50 ml falcon tube. Cells were later washed twice by adding PBS up to 50 ml and centrifuged at 1000 rpm for 5 minutes. Finally, the supernatant was discarded, leaving only around 0.2 ml of PBS, the pellet was gently resuspended and 6 – 12 ml (depending on the pellet size) of the urine stem cells medium was added. Straight after, 0.5 ml of the cell solution were seeded per well in a 24-well plate and left at 37°C (in 5% CO_2) for 3 days (Figure 5.2).

5.2.4 Cell cloning and proliferation

After 3 days in culture, the medium was changed for fresh urine stem cell medium and after that it was changed again every other day. Differentiated squamous epithelial cells did not stick to the well surface. Therefore, they were eventually washed away and only putative progenitor cells would remain, which in our study represented less than 1% of the total cell pellet obtained from urine. Colonies did not start appearing until a week later.

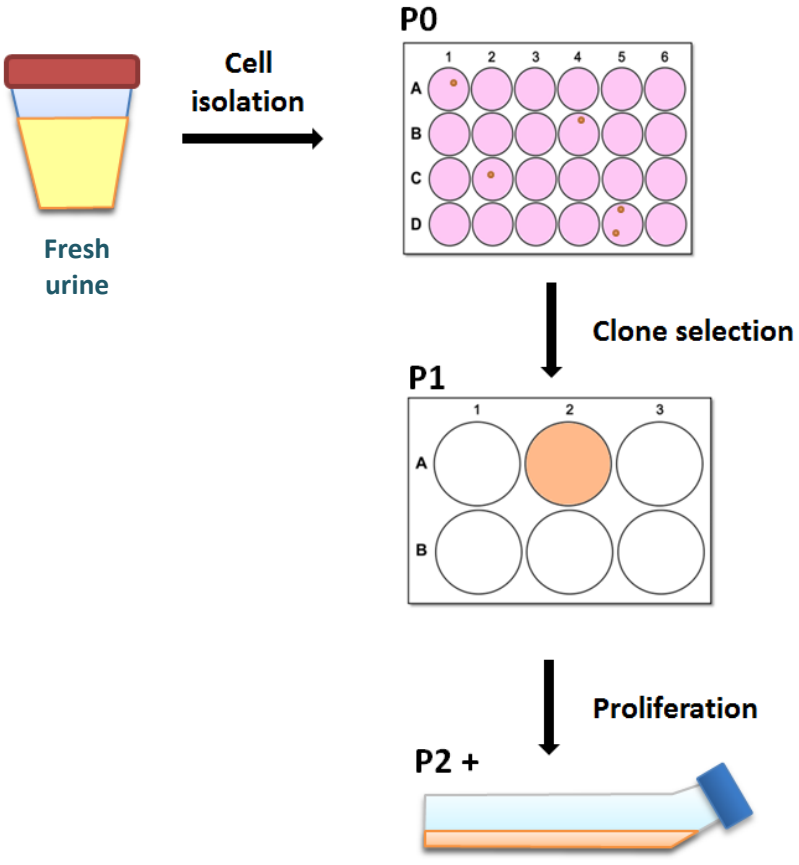

Figure 5.2 Schematic of the isolation process and propagation of UPCs.
The first step was a sterile isolation of cells contained in urine followed by an initial culture in urine stem cells medium. Colonies started appearing a week later. In this stage, colonies were at passage 0 (P0). The next step was a clone selection, where only the wells that contained one colony were transferred to a 6-well plate. This was considered passage 1 (P1). Finally, a last step of propagation for each colony was performed by transferring the colony to a T75 flask. From passage 2 (P2) onwards, urine progenitor cells were propagated in T75 flasks.

Once spotted, they were left to grow until they occupied at least half of the well in the 24-well plate. Only wells that contained a single colony were harvested by trypsin collection and then transferred to one well of a 6-well plate. Since colonies come from a single cell, this can be considered a cloning step. Once the cells occupied 90% of the well, they were transferred to a T75 flask. After that, cells were split in ¼ to different T75 every time the confluence reached 90% (Figure 5.2).

5.2.5 Clonogenicity assay

To detect the capacity of urine-derived progenitor colonies to generate a colony from a single cell, a single cell solution was prepared (1 cell/100 µl) and 100 µl/well were added in a 96-well plate. The urine stem cell medium was changed 2 days later and after that changed every other day. Wells that contained no cells or more than one cell were not used. After 10 days, we counted the wells that had a colony of cells and divided them by the total number of wells initially containing 1 cell. Finally, clonogenicity was expressed as a percentage. Other studies call it plating efficiency (PE) but the formula used is the same (Franken et al. 2006):

$$\text{Clonogenicity} = \frac{\text{no. colonies formed}}{\text{no. cells seeded} - \text{no. failed wells}} \times 100\%$$

5.2.6 Preparation of UPCs for flow cytometry

UPCs were detached to form a cell suspension and distributed in various microfuge tubes (around $2x10^5$ cells in each) to analyse different characterisation markers. The cells with the microfuge tubes were spun down at 2000 rpm for 3 minutes. The supernatant was aspirated and the pellet was resuspended in 30 µl of FACS buffer (0.1% of NaN_3 and 1% BSA in PBS). Then, 3 µl per antibody were added (if analysing co-expression they were added together) and samples were incubated for 10 minutes in the dark at 4°C. After incubation,

200 µl of FACS buffer was added per microfuge tube and samples were centrifuged again (2000 rpm, 3 minutes). The supernatant was carefully aspirated and cells were resuspended in 100 µl of FACS buffer and transferred to FACS tubes. Samples were finally analysed in the flow cytometer (FACSCalibur, BD Biosciences).

5.2.7 Flow cytometry data analysis

Data was analysed using Flowing Software. From the general cloud of particles, the population that represented single cells was selected, excluding debris and duplets of cells. Then, the percentage of cells expressing a determined marker was calculated by representing the control population (no antibodies added) in a histogram and selecting an area on the right edge of the control peak. Next, the sample incubated with antibodies was represented in the same histogram and the cells that fell into this area were considered positive for the analysed marker. Finally, the software was able to plot them in a combined dot plot and expresses each marker as a percentage from the single cell population.

5.2.8 RNA isolation

See methods described in Chapter 2.2.3.

5.2.9 DNase treatment of RNA

See methods described in Chapter 2.2.4.

5.2.10 Reverse transcription

See methods described in Chapter 2.2.5.

5.2.11 Quantitative real-time PCR (qPCR)

See methods described in Chapter 2.2.9.

5.2.12 Differentiation towards a PT state

The PT differentiation medium used was based on that published by Narayanan, K. *et al*. (2013). The medium was composed of renal epithelial cell growth medium (REGM) plus Bulletkit supplements and it was additionally supplemented with BMP2 (10 ng/ml), BMP7 (2.5 ng/ml), activin A (10 ng/ml) and retinoic acid (0.1 µM).

UPCs in a T75 flask were split 1/9 and seeded in T25 flasks. After 24 h, the medium was changed for PT differentiation medium in one T25 and for urine stem cells medium in another T25, this was established as day 0. A third T25 was used to isolate the mRNA from day 0. The medium was changed every day and on day 3 mRNA was isolated from both flasks.

5.2.13 Assessment of MRP2/4 and P-gp function using CMFDA dye

UPCs in a T75 flask were split 1/3 and seeded in a 96-well plate. After 24 h, the medium was changed for PT differentiation medium in one plate and for urine stem cells medium in another plate. The medium was changed again every 24 h for 3 days. On the last day, an experiment using CMFDA dye was performed to analyse the function of MRP2, MRP4 and P-gp. See Chapter 2.2.19 section for the assay details.

5.2.14 Immunofluorescence (IF)

Cover slides (13 mm ∅) were placed in wells of a 24-well plate and coated with 0.5% of gelatine for 30 minutes. The gelatine was removed and cells were seeded at $4x10^4$ cells/well. The plate was incubated for 72 h at 37°C (5% CO_2). Cells were washed 3x in warm

PBS and fixed with 4% PFA for 10 minutes at RT. Then, cells were washed again with PBS 3x and later permeabilised with PBS containing 0.2% Triton X-100 for 10 minutes at RT. Cells were washed 2x with PBS and blocked for 1 h with 10% serum (from the animal the 2nd antibody had been raised in) diluted in PBS. Primary antibodies were then added in PBS solution containing 10% serum and 0.1% Triton X-100 O/N at 4°C in the dark using the following dilutions:

- Megalin mouse monoclonal (1/300)
- Podocin rabbit monoclonal (1/500)
- Synaptopodin mouse monoclonal (no dilution)

After an overnight incubation, cells were washed 3x with PBS and later incubated with the secondary antibodies in PBS solution containing 10% serum and 0.1% Triton X-100 for 2 h at 4°C in the dark using the following dilutions:

- Goat anti-mouse (1/500, 594 nm)
- Goat anti-rabbit (1/500, 488 nm)

After the incubation, 3x washes with PBS were applied and then the nuclei were stained with 2 µg/ml of Hoechst 33342 for 10 minutes at RT protected from light. Finally, after 3 more washes with PBS, the cover slides were mounted onto a microscope slide with Prolong Gold. Results were visualized at 40x magnification using an inverted fluorescence microscope (Axio Observer.Z1, Zeiss).

5.2.15 Statistical analysis

Statistical analysis of data was performed using StatsDirect software. All results were represented as the mean ± SEM or as the mean ± SD of three independent experiments. The choice of SEM *vs*. SD was only based on obtaining a better visual representation of the figures. Data was first assayed for normality using the Shapiro-Wilk test. When assaying differences amongst at least three groups, if data was normal, statistical analysis was

performed using One Way ANOVA with Dunnet as a post-hoc comparison, as this test is specifically designed to compare each treatment against a single control. If there was no evidence of normality, Kruskal-Wallis test was applied instead. To test for differences amongst two groups, a t-test was performed if data was classified as normal and a Mann-Whitney test when data showed no evidence of normality. Only when p values <0.05 the results were considered significant.

5.3 RESULTS

5.3.1 Morphological characterization and evolution of UPC colonies over passages

In order to isolate UPCs, different urine collections were performed as described previously. Published methods have shown that the success rate to isolate this type of cell was very low (Zhang et al. 2008). These observations were also supported by our analysis showing that the vast majority of isolated colonies (90%) were incapable of continual proliferation past passage 5. However, based on their cobblestone-like morphology and high growth rates, we identified 3 colonies from 3 different healthy individuals that displayed progenitor-like qualities and could be kept in culture for up to 10 - 11 passages.

One of the typical features described for a progenitor colony was a uniform and compact cluster of cells at the origin of the colony formation (Zhang et al. 2008). To analyse the morphology of different colonies at their generation and at later passages, phase contrast images were taken with an inverted microscope (Eclipse TS100, Nikon). Colonies A and C (Figure 5.3 A and Figure 5.5 A) were good examples of a compact cell formation, both showed how the origin of the clone was a compact cluster of cells that displayed smooth and well-defined edges. These features were in concordance with what had been defined in a previous report as type I colonies (Zhou et al. 2012). Particularly, the image from Figure 5.3 A was taken after 6 days of seeding and no more than 20 cells could be counted at that stage. The daily monitoring of the wells allowed us to establish that the colony had originated from a single cell, as such a cell cluster could not be detected after the initial seeding. Colony A yielded millions of cells passages later. In the same image, remaining squamous cells could still be observed. They were not attached to the well and did not divide; they were eventually washed away after consecutive medium changes (Suppl. Figure 5.1). Figure 5.5 A was taken 2 weeks after seeding, just before splitting the cells to the next passage, and a much bigger cluster of cells could be appreciated. The formation of

colony B occurred close to the edge of the well and the picture was therefore not as clear due to light refraction limitations (Figure 5.4 A). However, a more scattered arrangement could still be seen, which would classify the colony as type II (Zhou et al. 2012). The two different cell morphology classifications were also detected on the formation of other colonies (Suppl. Figure. 5.2 - 5.3), which stopped proliferating before passage 5.

Regarding the general morphology of these 3 clonal cell lines, after passage 0 they all exhibited a slightly elongated rice grain shape but became cobblestone-like when confluent, forming a compact monolayer (Figure 5.3 – 5.5). Cells stayed small in size up until passage 8. After this stage, they started to slow down division and become bigger by increasing the area of the cytoplasm. At passage 10, nearly all the cells had stopped division and were clearly bigger compared to other passages (Figure 5.3 E, 5.4 E and 5.5 E). Exceptionally, in some areas a subpopulation of smaller cells were detected and although they were still able to divide and resembled the same cells at a lower passage, they ultimately differentiated (Figure 5.4 E).

The population doubling times represented in Table 5.1 were very similar for all 3 colonies (32.1 h to 33.6 h).

Colony A

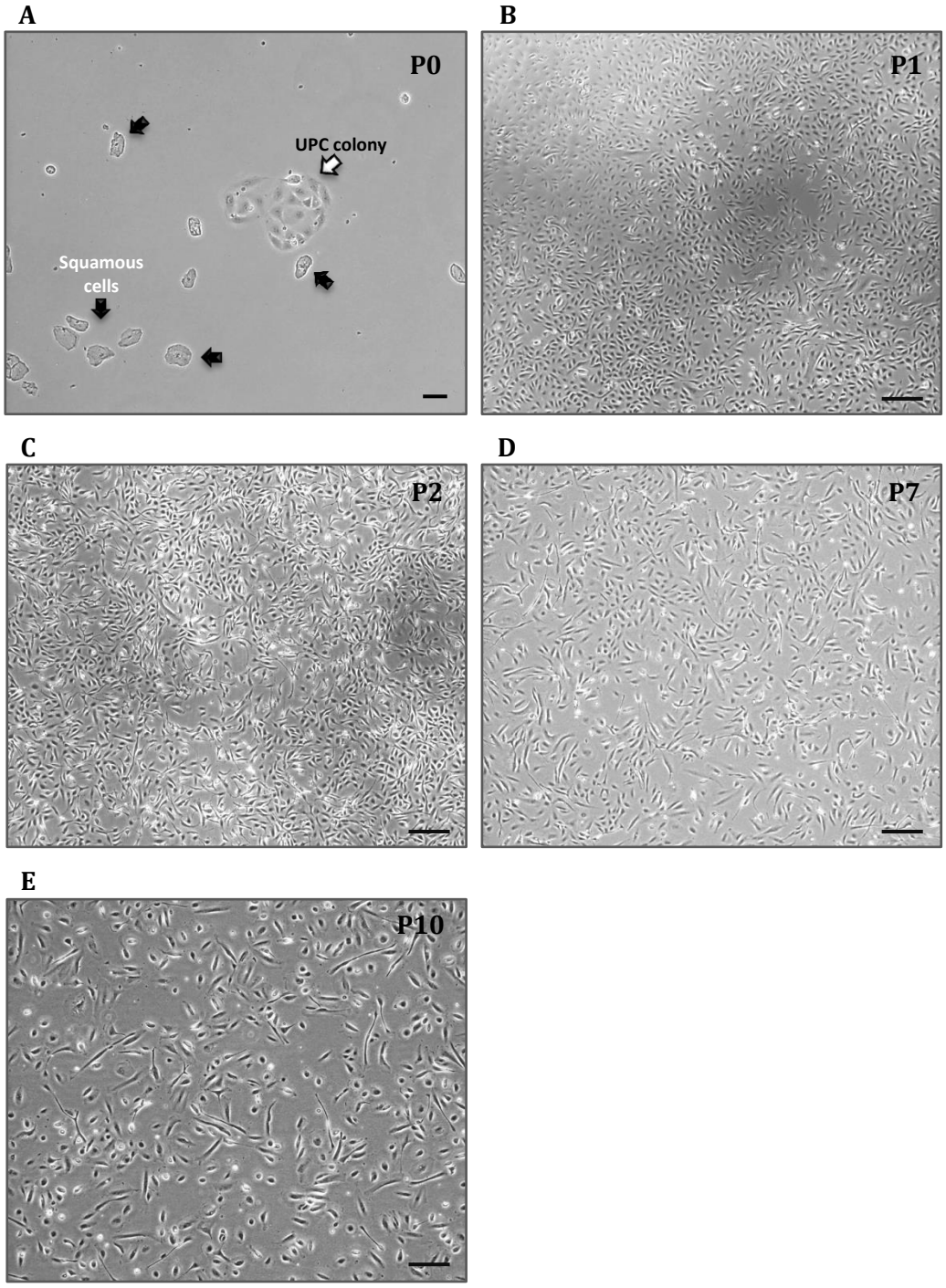

Figure 5.3 Evolution of colony A morphology.

These phase contrast images were taken just before splitting the colony. (A) The image regarding the formation of the colony at passage 0 was taken using a 10x objective. Black arrows mark squamous cells and the white arrow marks the urine progenitor-like colony. Scale bar is 100 µm. The other images were taken at (B) passage 1, (C) passage 2, (D) passage 7 and (E) passage 10 using a 4x objective. Scale bar is 100 µm.

Colony B

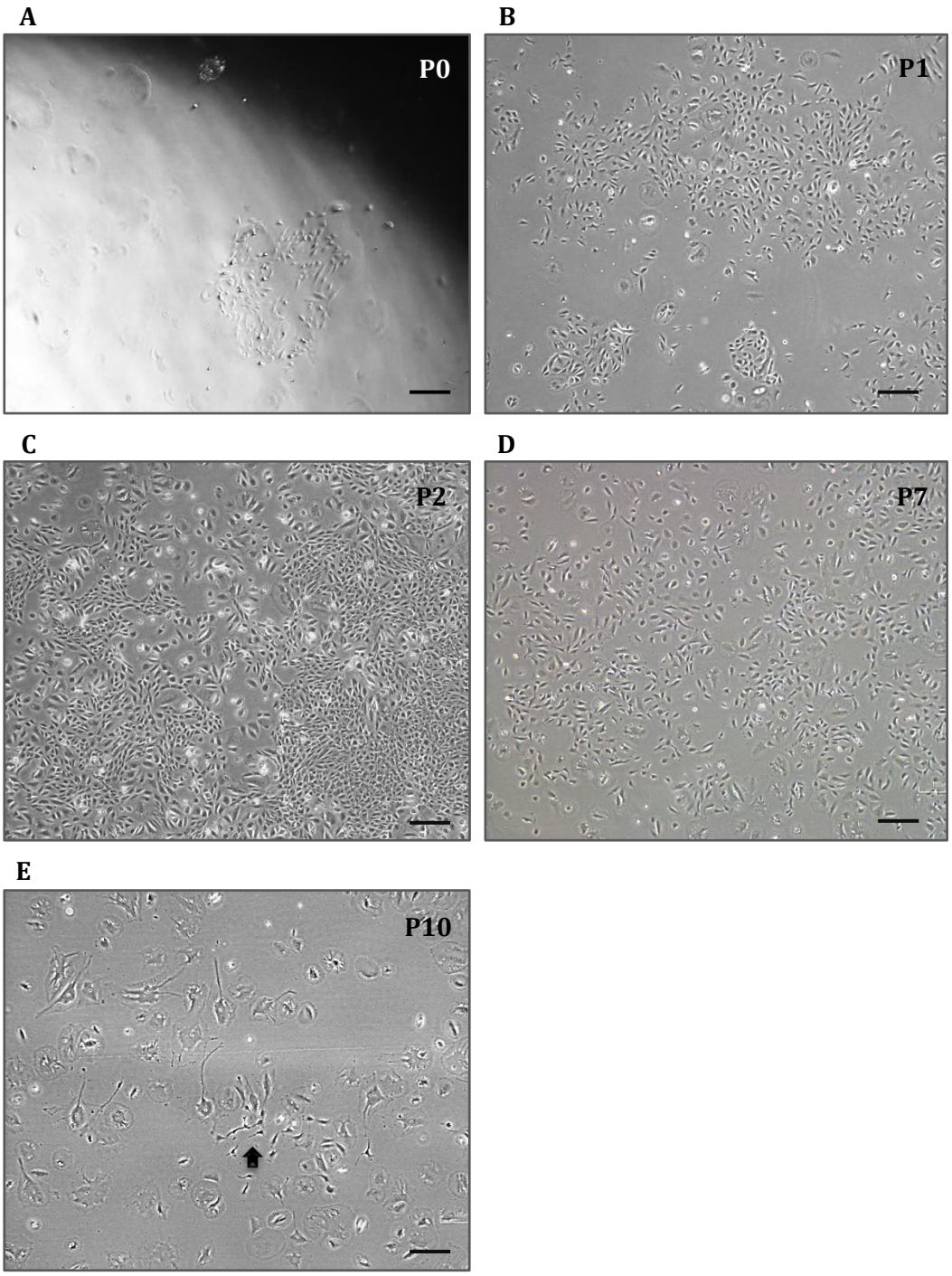

Figure 5.4 Evolution of colony B morphology

These phase contrast images were taken just before splitting the colony. Image (A) captures the formation of the colony and the other images were taken at (B) passage 1, (C) passage 2, (D) passage 7 and (E) passage 10 using a 4x objective. (E) The arrow marks a subpopulation of smaller cells. Scale bar is 100 µm.

Colony C

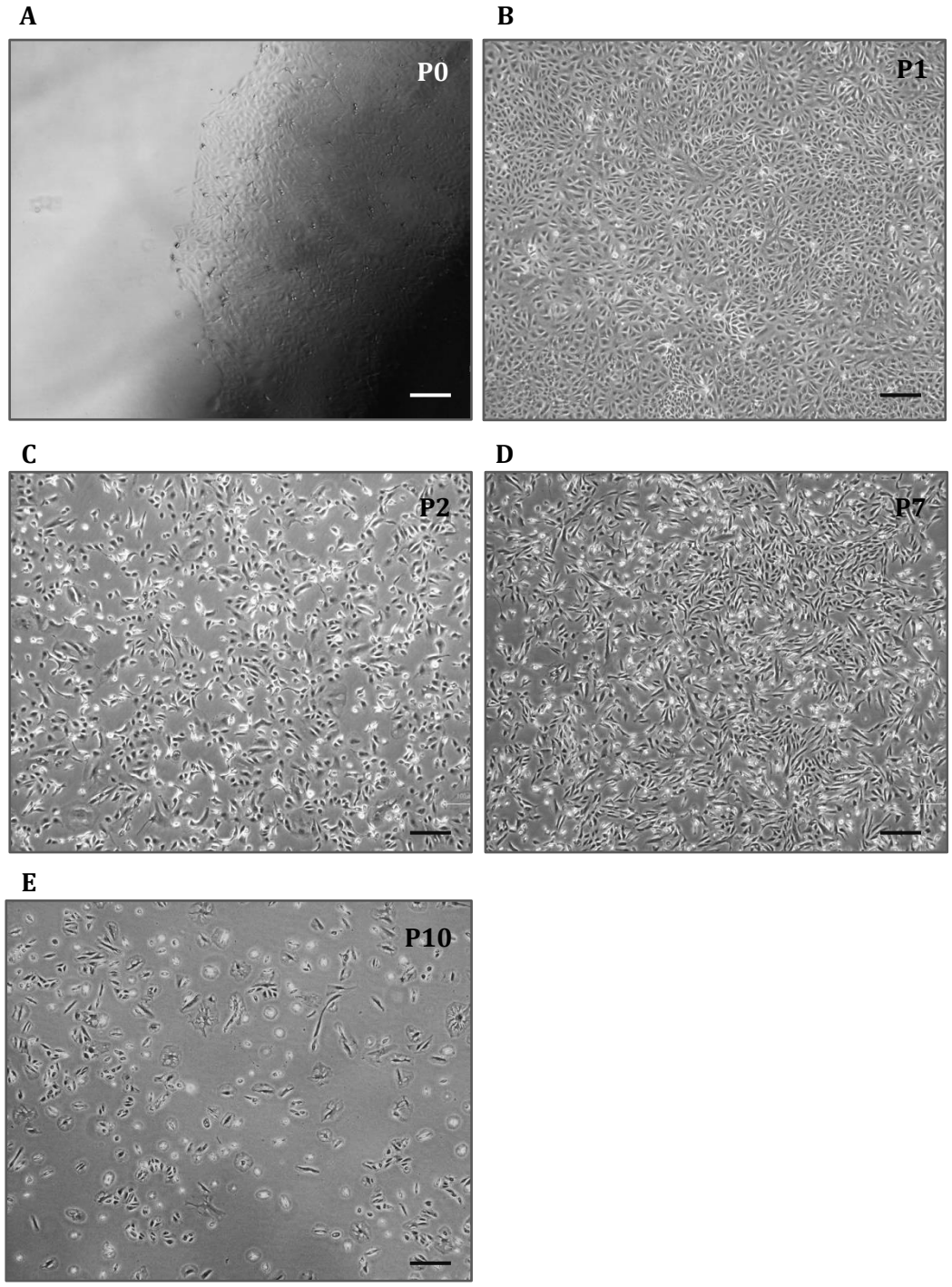

Figure 5.5 Evolution of colony C morphology

These phase contrast images were taken just before splitting the colony. Images were taken at (A) passage 0, (B) passage 1, (C) passage 2, (D) passage 7 and (E) passage 10 using a 4x objective. Scale bar is 100 µm.

Table 5.1 Cell growth parameters calculated from passage 2 to passage 8.

	Average cell split rate (splits/week)	Split ratio	Population doubling time
Colony A	1.25	1/4	33.6 h
Colony B	1.31	1/4	32.1 h
Colony C	1.27	1/4	33.1 h

5.3.2 Clonogenic capacity of UPCs

Clonogenicity represents the ability of a single cell within a population to self-renew and undergo unlimited division. This capacity of self-renewal is one of the key features that define stem cells, whereas progenitor cells only preserve the clonogenic properties for a limited number of passages. Our previous results highlighted that the isolated colonies were not able to proliferate past passage 10 or 11, therefore we decided to calculate how the clonogenic capacity declined over passages.

Cells were diluted to obtain a single cell solution and seeded in a 96-well plate. A week later, the number of colonies were counted and expressed as a percentage of clonogenicity (Table 5.2). While the cell growth was still exponential (passage 6), colony B presented a clonogenicity percentage of 31.91%. Nevertheless, at higher passages this percentage decreased considerably. At passage 8, colony A displayed a clonogenic capacity of 8.23% and only 3.37% of colony C cells retained the capacity to produce colonies at passage 9.

Table 5.2 Overview of clonogenic capacity (%) over passages.

	Clonogenicity (%)	Colonies/valid wells
Colony A (P8)	8.23%	7/85
Colony B (P6)	31.91%	30/94
Colony C (P9)	3.37%	3/89

5.3.3 Isolated urine progenitor colonies have a kidney origin

To rule out the possibility that the isolated urine colonies were of urothelial origin instead of originating from the kidney, we analysed the expression of UPK1A via qPCR. UPK1A is expressed in the urothelium which comprises ureter, bladder and urethra, but not in the kidneys (Wu et al. 2009).

cDNA from ureter cells was isolated and used as a positive control to evaluate UPK1A expression. A ΔCt value of 12.28 ± 0.046 was obtained in these cells. Instead, no UPK1A expression was detected in the tubular fraction or in any of the isolated colonies (Table 5.3).

Table 5.3 UPK1A mRNA detection by qPCR in ureter cells, in a tubular fraction and in colonies A, B and C.

	Ureter cells	Tubular fraction	Colony A	Colony B	Colony C
ΔCt value ± SD	12.28 ± 0.046	--	--	--	--

Data are mean ± SD (n = 3). Key: "--" indicates undetermined value.

5.3.4 Assessment of CD133 and CD24 co-expression

Co-expression of CD133 and CD24 has been previously linked to a population of renal stem/progenitor cells in the human adult kidney (Lindgren et al. 2011). CD133 is a glycoprotein widely expressed in immature cells as well as in differentiated cells. However, we used an antibody for the human glycosylated epitope CD133/1, which has only been detected in immature cells (Corbeil et al. 2000, Kemper et al. 2010). In contrast, CD24 is only detected in immature cells and absent in differentiated ones (Shirasawa et al. 1993). To assess if these 2 markers were also expressed in our UPC colonies, we used flow cytometry to screen for the presence of both markers on the cell surface at different passages.

Flow cytometry was performed for each colony at passage 6 and passage 9 to assess any variations in the co-expression of both markers at a high proliferative state compared to the cell growth plateau.

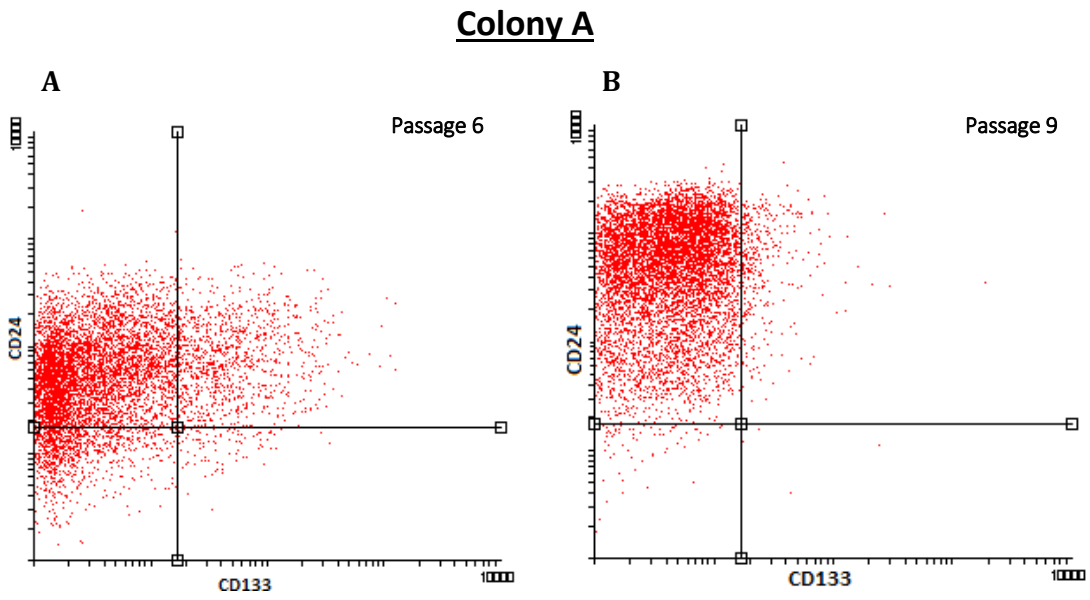

Figure 5.6 Flow cytometric analysis of CD24 *vs*. CD133 in colony A.
Cells from colony A at (A) passage 6 and (B) passage 9 were represented in a combined dot plot divided in 4 quarters. The top left quarter represents cells only positive for CD24 ($CD24^+$), the bottom left quarter represents negative cells, the bottom right quarter holds the cells only positive for CD133 ($CD133^+$) and the top right quarter contains the double positive cells ($CD24^+$ and $CD133^+$).

Table 5.4 Statistics data from colony A flow cytometric analysis.

	CD24$^+$	CD133$^+$	CD133$^+$ & CD24$^+$
Passage 6	70.93%	1.25%	13.87%
Passage 9	94.51%	0.06%	4.53%

A very high percentage of colony A cells were CD24$^+$ at both passages. However, only 1.25% were single positive for CD133 and a 13.87% were double positive. This decreased to 0.87% and 4.53% respectively at passage 9 (Table 5.4). Therefore, cells lost their CD133 expression at the highest passage, while increasing their expression of CD24. This shift in the markers expression can be clearly observed in Figure 5.6.

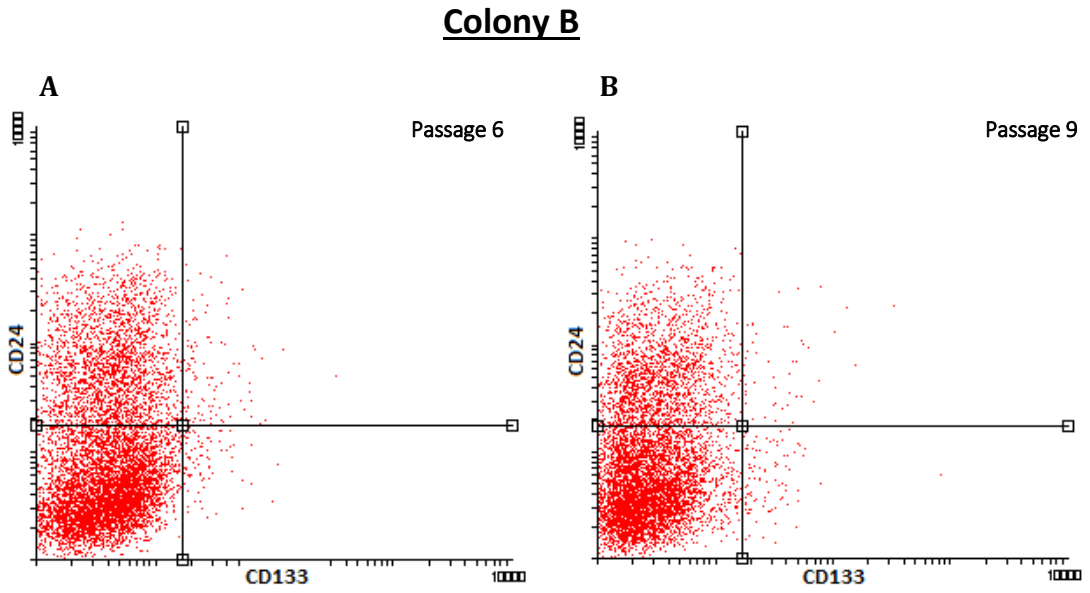

Figure 5.7 Flow cytometric analysis of CD24 *vs.* CD133 in colony B.
Cells from colony B at (A) passage 6 and (B) passage 9 were represented in a combined dot plot divided in 4 quarters. The top left quarter represents cells only positive for CD24 (CD24$^+$), the bottom left quarter represents negative cells, the bottom right quarter holds the cells only positive for CD133 (CD133$^+$) and the top right quarter contains the double positive cells (CD24$^+$ and CD133$^+$).

Table 5.5 Statistics data from colony B flow cytometric analysis.

	CD24$^+$	CD133$^+$	CD133$^+$ & CD24$^+$
Passage 6	31.29%	1.96%	1.37%
Passage 9	29.31%	2.36%	0.75%

The expression of CD133 and CD24 in colony B was quite different from colony A. Double negative cells comprised the 72.4 – 73.8% of the whole cell population and only around 1% of cells were CD24$^+$ and CD133$^+$ (Table 5.5). Moreover, the expression barely changed between passages (Figure 5.7). Around 30% of the cells were only CD24 positive and around 2% only CD133 positive (Table 5.5).

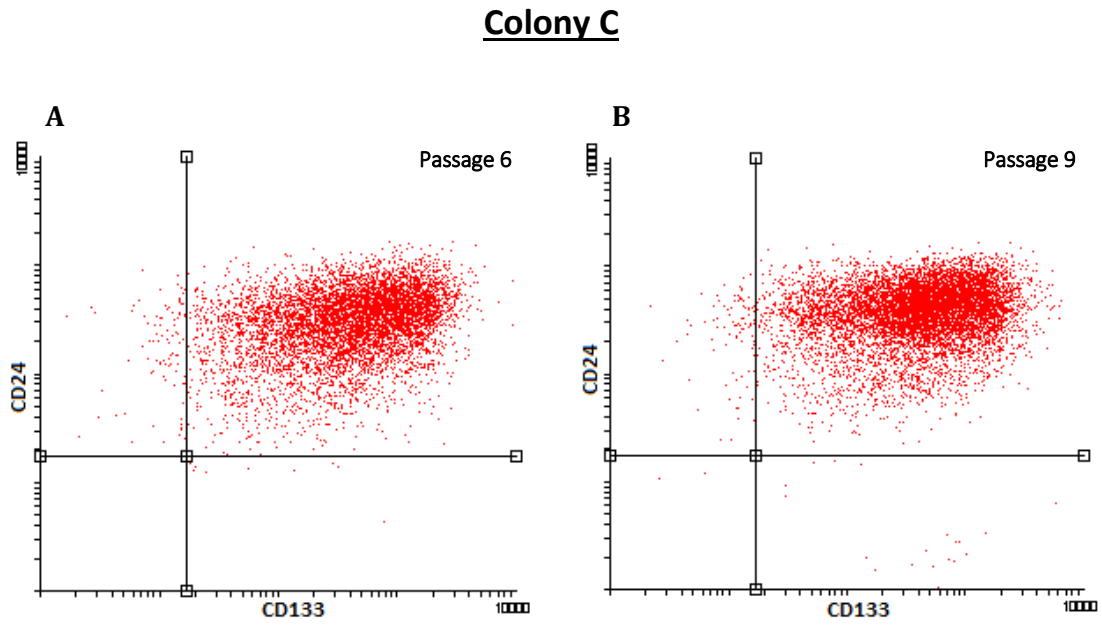

Figure 5.8 Flow cytometric analysis of CD24 *vs.* CD133 in colony C.
Cells from colony C at (A) passage 6 and (B) passage 9 were represented in a combined dot plot divided in 4 quarters. The top left quarter represents cells only positive for CD24 (CD24$^+$), the bottom left quarter represents negative cells, the bottom right quarter holds the cells only positive for CD133 (CD133$^+$) and the top right quarter contains the double positive cells (CD24$^+$ and CD133$^+$).

Table 5.6 Statistics data from colony C flow cytometric analysis.

	$CD24^+$	$CD133^+$	$CD133^+$ & $CD24^+$
Passage 6	1.05%	0.21%	98.53%
Passage 9	1.29%	0.12%	98.58%

Finally, colony C was the only one with a very high percentage of double positive cells. Precisely, 98.53% of cells co-expressed $CD24^+$ and $CD133^+$ at passage 6 and 98.58% of cells co-expressed $CD24^+$ and $CD133^+$ at passage 9. Scarcely any cells were positive for only one of the markers (Table 5.6). As it can be appreciated in Figure 5.8, the expression pattern was maintained even when the cell growth rate slowed down (passage 9).

5.3.5 Changes in kidney markers expression throughout passages

To check if there were any differences in gene expression at different stages of the *in vitro* culture, we assessed the mRNA levels of different kidney markers over passages. We theorised that, as progenitors, the colonies might start differentiating towards the cell type that they were programmed to be and this would be reflected in a time-dependent manner by the expression of specific markers.

RNA was isolated from every other passage, starting at passage 1 for colony A and passage 3 for colonies B and C. After retrotranscription to cDNA, qPCR was performed using the same TaqMan Gene Expression Assays from Chapter 2. Genes that gave no amplification signal were not represented. Amongst them there was WT1, a gene linked to kidney progenitor cells during development (Kreidberg 2010), the expression of which could not be detected in colony A (Figure 5.9) and only at passage 3 in colony C (Figure 5.11). In colony A, the expression of most of the tested genes remained the same, but a significant increase in the expression levels of *AQP1* and *SYNPO* was observed over time, while the expression levels of *AQP3* decreased. In colony B, WT1 expression was more than a 100 times higher than the expression from the tubular fraction (Figure 5.10). In conjunction with P-gp and AQP3, WT1 expression visibly decreased over passages. On the other hand, OATP4C1 mRNA levels increased. In colony C, MRP2 expression significantly decreased over passages and although not significantly, so did BCRP. P-gp levels decreased and later recovered at passage 9. In contrast, a general increasing tendency was detected for AQP1, CUBN and SYNPO (Figure 5.11). See Appendix 6 for Ct numbers.

Furthermore, at the first passage, 4 out of 7 PT markers in colony A had similar mRNA levels compared to the PT fraction at passage 2. The mRNA expression was higher when analysed at passage 3. In this case, 5 out of 7 markers showed a similar expression for colony A and B, however in colony C the expression of the analysed PT genes was equal or even higher

than the tubular fraction. Additionally, even though SYNPO levels appeared elevated compared to the levels detected in the cells from the tubular fraction, a similar expression level was detected for ciPTECs in Chapter 2 (Figure 2.5).

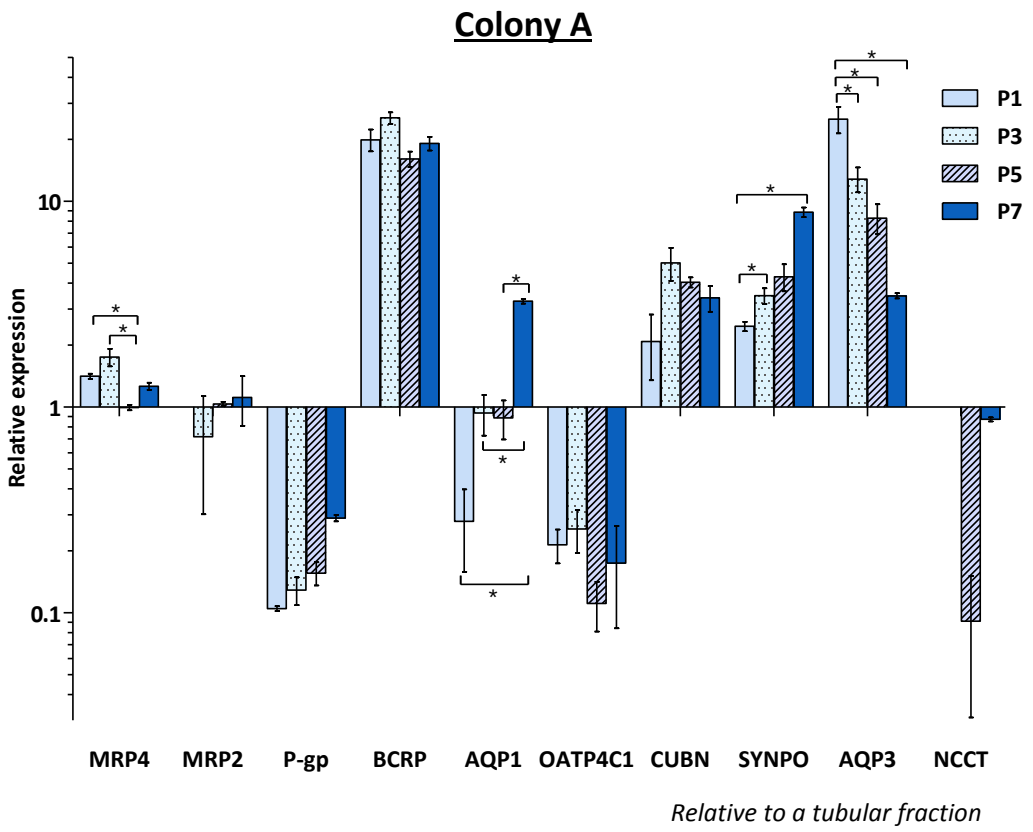

Figure 5.9 Relative expression of kidney markers in colony A throughout passages.
The relative expression of PT genes as well as other kidney markers in colony A was analysed by qPCR at passage 1 (P1), passage 3 (P3), passage 5 (P5) and passage 7 (P7). Gene names are displayed under each set of bars. Data was normalised against a human tubule fraction at passage 2 (P2). Data are mean ± SEM (n = 3). Statistical significance was determined amongst passages by Mann-Whitney test, *p<0.05.

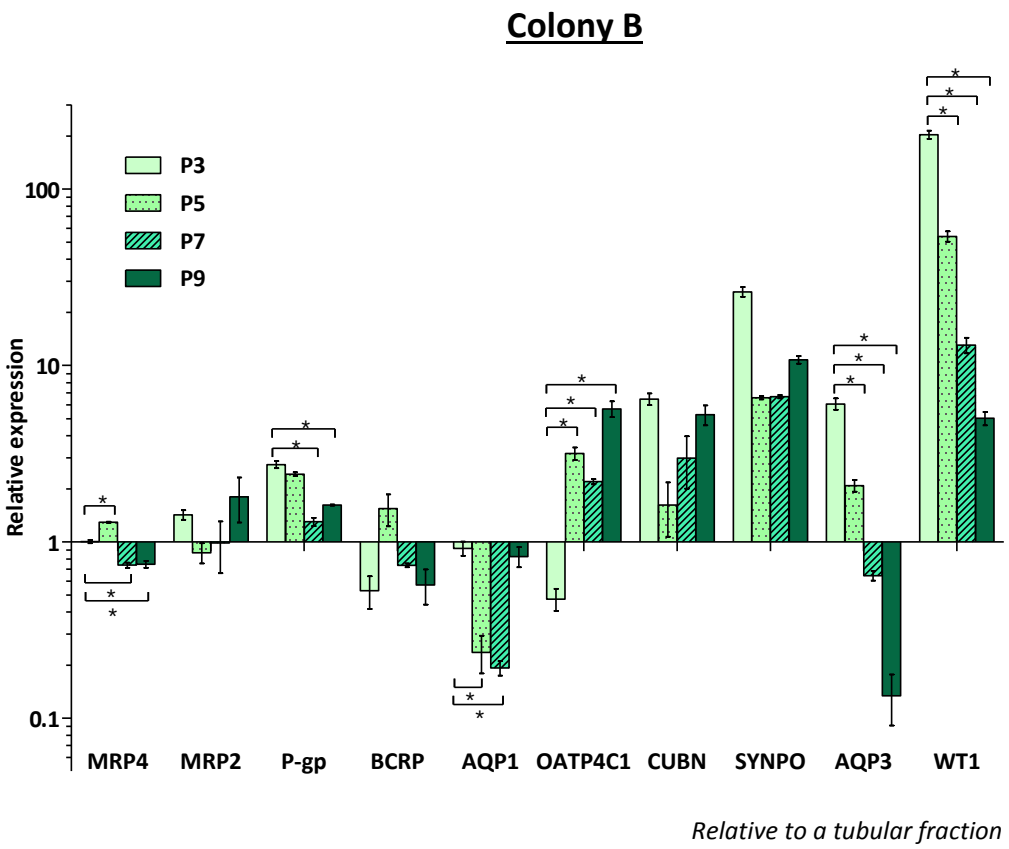

Figure 5.10 Relative expression of kidney markers in colony B throughout passages.
The relative expression of PT genes as well as other kidney markers in colony B was analysed by qPCR at passage 3 (P3), passage 5 (P5), passage 7 (P7) and passage 9 (P9). Gene names are displayed under each set of bars. Data was normalised against a human tubule fraction at passage 2. Data are mean ± SEM (n = 3). Statistical significance was determined amongst passages by Mann-Whitney test, *p<0.05.

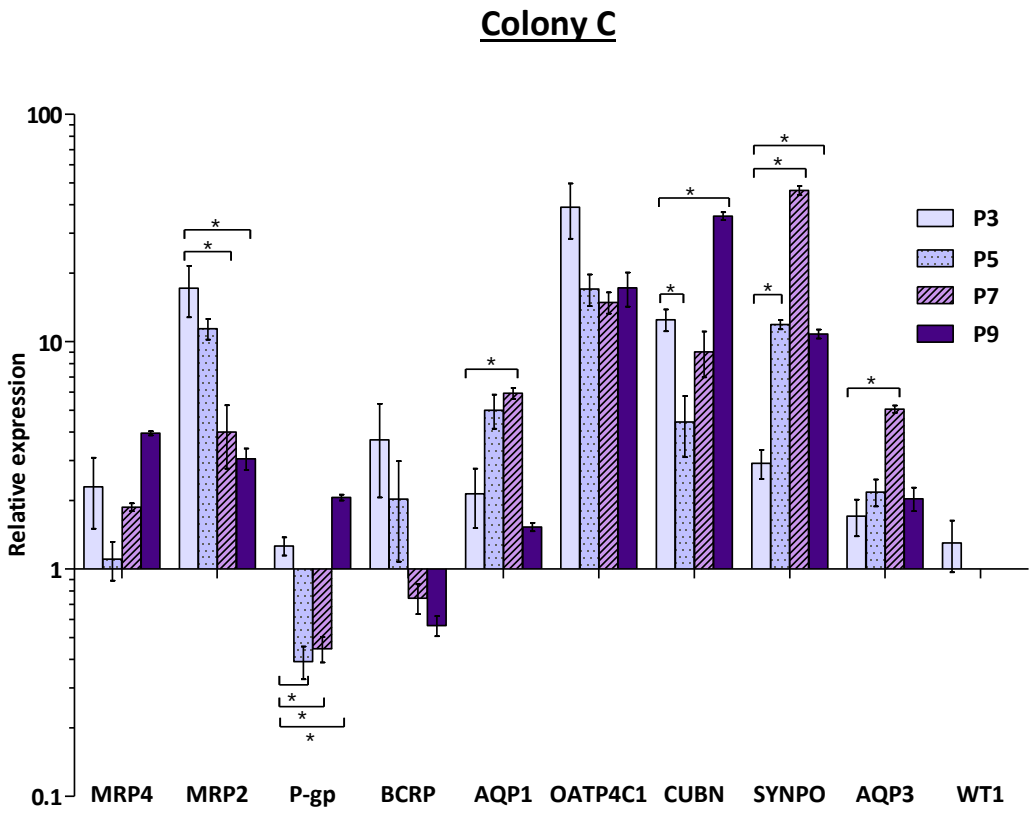

Figure 5.11 Relative expression of kidney markers in colony C throughout passages.
The relative expression of PT genes as well as other kidney markers in colony C was analysed by qPCR at passage 3 (P3), passage 5 (P5), passage 7 (P7) and passage 9 (P9). Gene names are displayed under each set of bars. Data was normalised against a human tubule fraction at passage 2. Data are mean ± SEM (n = 3). Statistical significance was determined amongst passages by Mann-Whitney test, *p<0.05.

5.3.6 Effect of PT differentiation: random or colony specific?

After analysing the gene expression of all 3 colonies, we decided to investigate whether or not the fate of these cells could be directed towards better differentiated PT cells. Considering that in their basal medium quantitatively good expression of PT genes was observed (Figure 5.9 - 5.11), we hypothesised that these progenitor colonies might have already been committed to the PT lineage and the differentiation treatment would, therefore, be more effective.

Cells from all 3 colonies at passage 6 were cultured for 3 days in the PT differentiation medium used by Narayanan *et al*. for human embryonic stem cells and compared to the same cells cultured for 3 days in their urine stem cell medium (control). After the treatment, all 3 isolated urine colonies in differentiation media exhibited a much more elongated morphology (Figure 5.12 A, Figure 5.13 A, Figure 5.14 A) compared to control cells, which had a more cobblestone-like shape (Figure 5.12 B, Figure 5.13 B, Figure 5.14 B). Nevertheless, the expression of PT markers showed extensive variation between colonies. Successfully, in colony A the expression of MRP4, P-gp, BCRP and OATP4C1 was significantly upregulated in differentiated cells compared to control cells at day 0 and at day 3. MRP2 was also significantly upregulated compared to day 0 (Figure 5.12 C). The other PT genes had no significant changes in their mRNA levels.

With respect to colony B, only MRP2 and CUBN were upregulated and WT1 downregulated, compared to day 0. No significant positive changes were seen at day 3 between both conditions. In contrast, P-gp and OATP4C1 mRNA levels were significantly higher in control cells at day 3 (Figure 5.13 C).

Finally, colony C data showed that only BCRP was significantly upregulated after 3 days in PT compared to both controls. MRP4, OATP4C1 and CUBN were also upregulated in both

medium conditions after 3 days compared to day 0. Instead, P-gp and AQP1 expression was significantly upregulated in day 3 control cells (Figure 5.14 C).

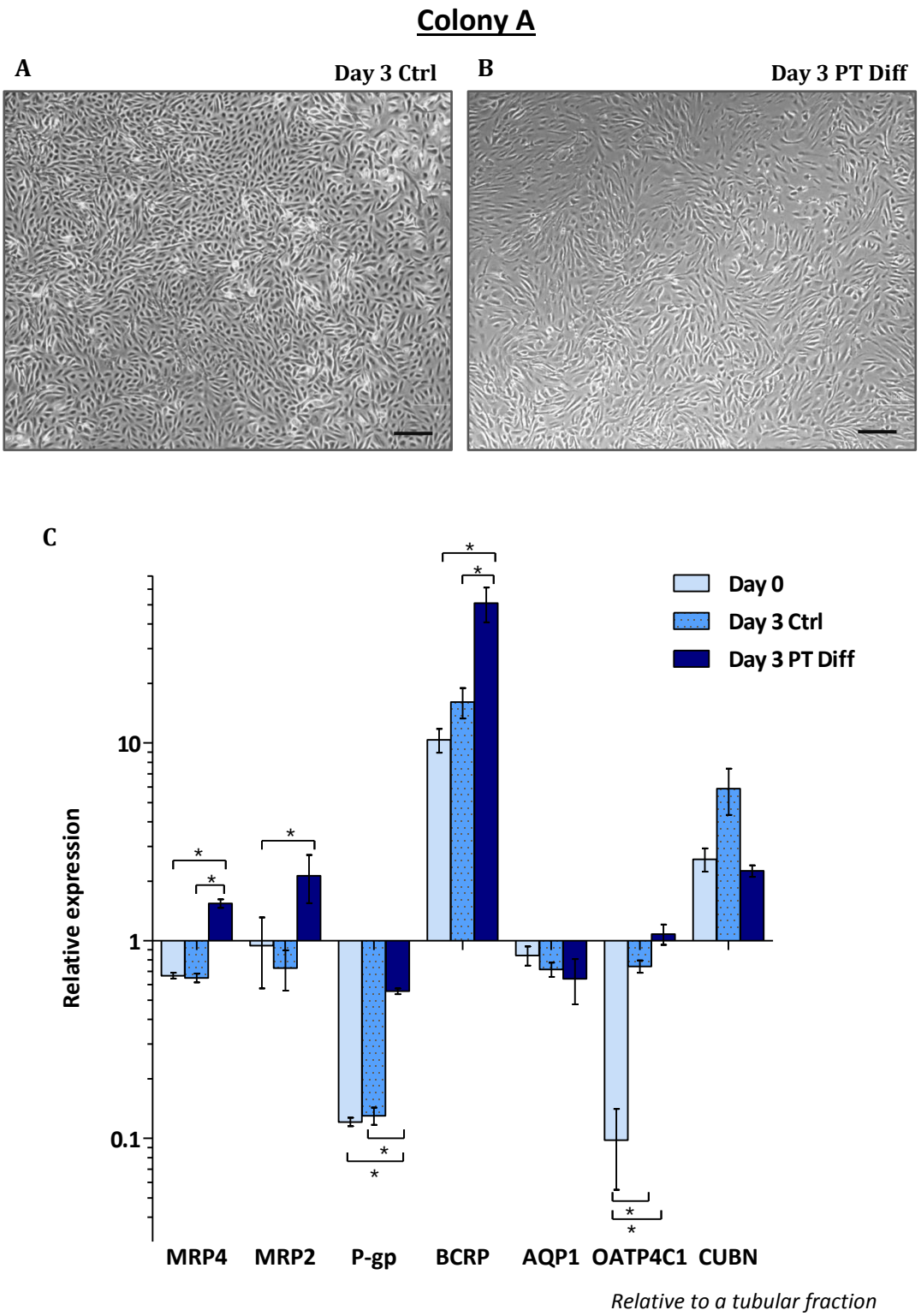

Figure 5.12 Differentiation of colony A towards a PT state.

UPCs from colony A at passage 6 were cultured for 3 days in a medium that induces differentiation towards a PT state. Pictures were taken at (A) day 3 in control medium and (B) day 3 in PT differentiation medium using a 4x objective. Scale bar is 100 µm. (C) qPCR analysis of the relative expression of PT genes at day 0, day 3 in control medium and day 3 in PT differentiation medium compared to a tubular fraction (P2). Statistical significance was determined by Mann-Whitney test, *p<0.05.

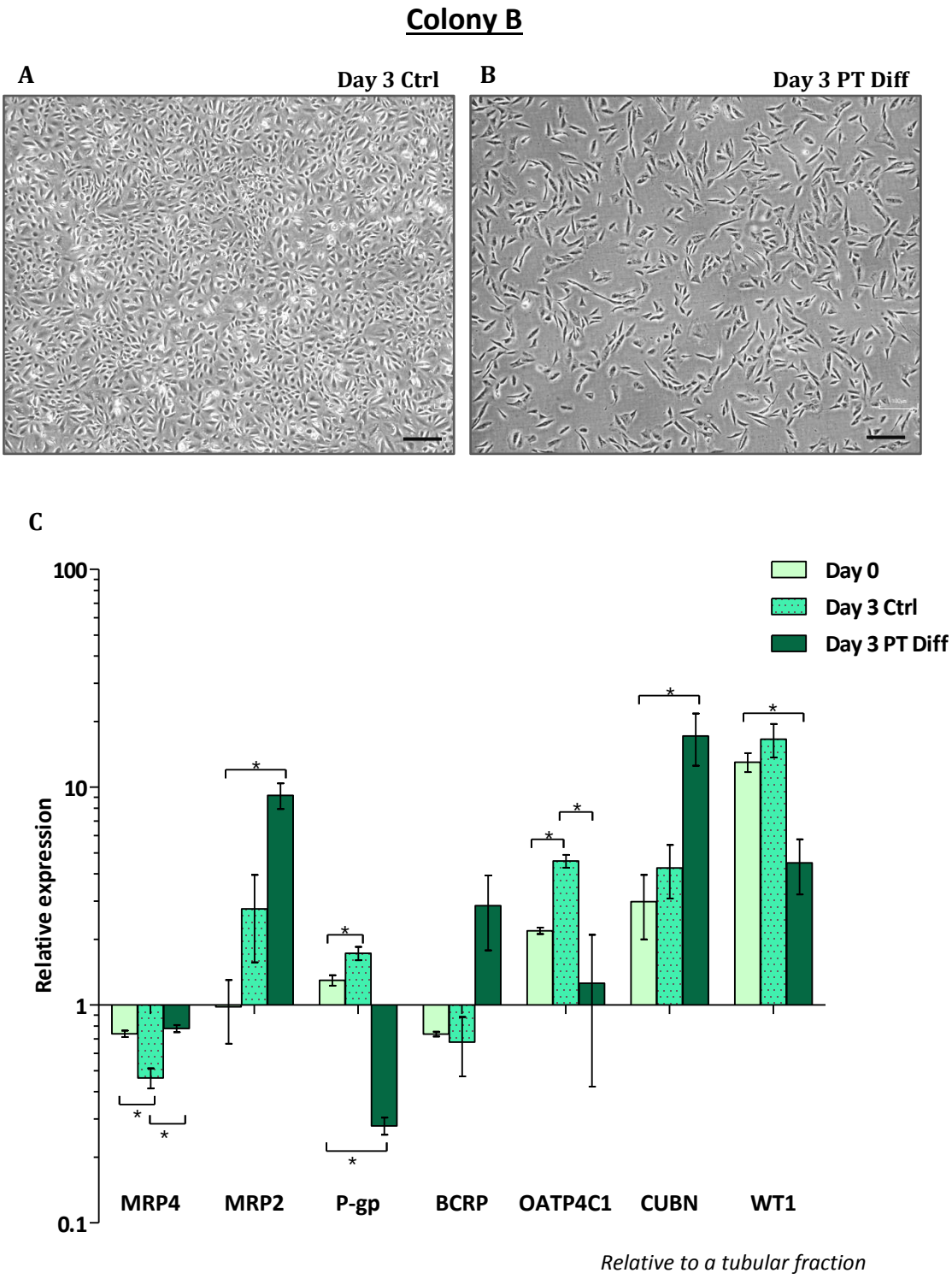

Figure 5.13 Differentiation of colony B towards a PT state.

UPCs from colony B at passage 6 were cultured for 3 days in a medium that induces differentiation towards a PT state. Pictures were taken at (A) day 3 in control medium and (B) day 3 in PT differentiation medium using a 4x objective. Scale bar is 100 µm. (C) qPCR analysis of the relative expression of PT genes at day 0, day 3 in control medium and day 3 in PT differentiation medium compared to a tubular fraction (P2). Statistical significance was determined by Mann-Whitney test, *p<0.05.

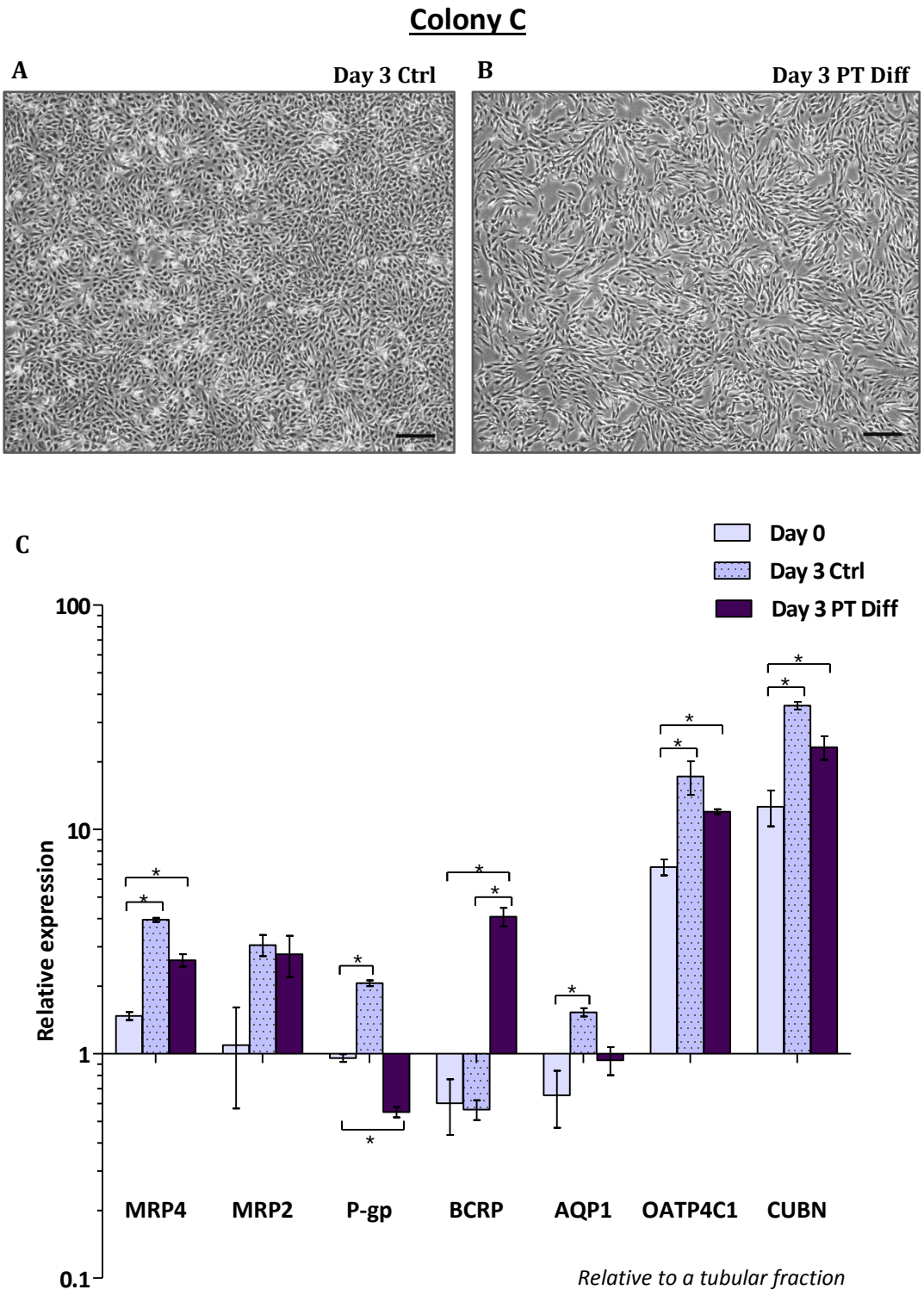

Figure 5.14 Differentiation of colony C towards a PT state.

UPCs from colony C at passage 6 were cultured for 3 days in a medium that induces differentiation towards a PT state. Pictures were taken at (A) day 3 in control medium and (B) day 3 in PT differentiation medium using a 4x objective. Scale bar is 100 µm. (C) qPCR analysis of the relative expression of PT genes at day 0, day 3 in control medium and day 3 in PT differentiation medium compared to a tubular fraction (P2). Statistical significance was determined by Mann-Whitney test, *p<0.05.

5.3.7 Analysis of PT transporters activity

Using the same CMFDA assay developed for the ciPTECs in Chapter 2, we assessed whether or not isolated UPCs exhibited any functionality for MRP2, MRP4 and P-gp transporters after 3 days in their growth medium and after 3 days in PT differentiation medium.

All 3 isolated colonies generated a significant increase in CMFDA accumulation after the addition of both inhibitors in control and PT differentiated cells, which confirmed the presence and functionality of MRP2/4 and P-gp in these cell lines (Figure 5.15 – 5.17). Whereas the levels of fluorescence were low and did not surpass 2-fold in any case, the P-gp results were very similar to the ones observed for ciPTECs in Chapter 2 (Figure 2.14). Furthermore, although the control *vs* differentiated fluorescence was similar in all graphs, colony A differentiated cells demonstrated a slightly greater functionality levels of MRP2/4 at 1.56 μM and 3.13 μM of MK571 (Figure 5.15 A) and colony B differentiated cells displayed a higher function for P-gp at 1.48 μM, 4.44 μM and 13.33 μM of PSC833 (Figure 5.16 B). At the highest concentration of MK571, an unexpected decrease in fluorescence could be detected in all 3 UPCs, but not for PSC833 inhibitor. Overall, the differentiated cells did not exhibit greater levels of PT transporters functionality compared to their control.

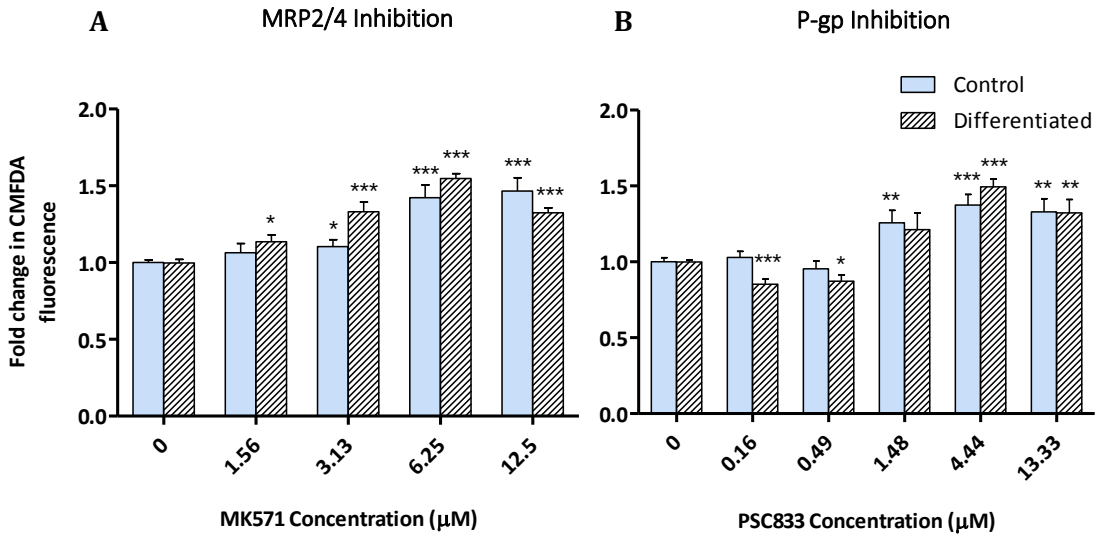

Figure 5.15 Study of MRP2, MRP4 and P-gp function in colony A.

One set of colony A cells were cultured in their own medium for 3 days and another set in PT differentiation medium also for 3 days. Then they were both incubated in CMFDA solution (1.25 μM) with (A) increasing concentrations of MK571 (MRP inhibitor) or (B) increasing concentrations of PSC833 (P-gp inhibitor). Data are represented in fold change and compared to the control (0 μM). Data are mean ± SEM (n = 3). Statistical significance was determined by One Way ANOVA test, **p*<0.05, ***p*<0.01, ****p*<0.001.

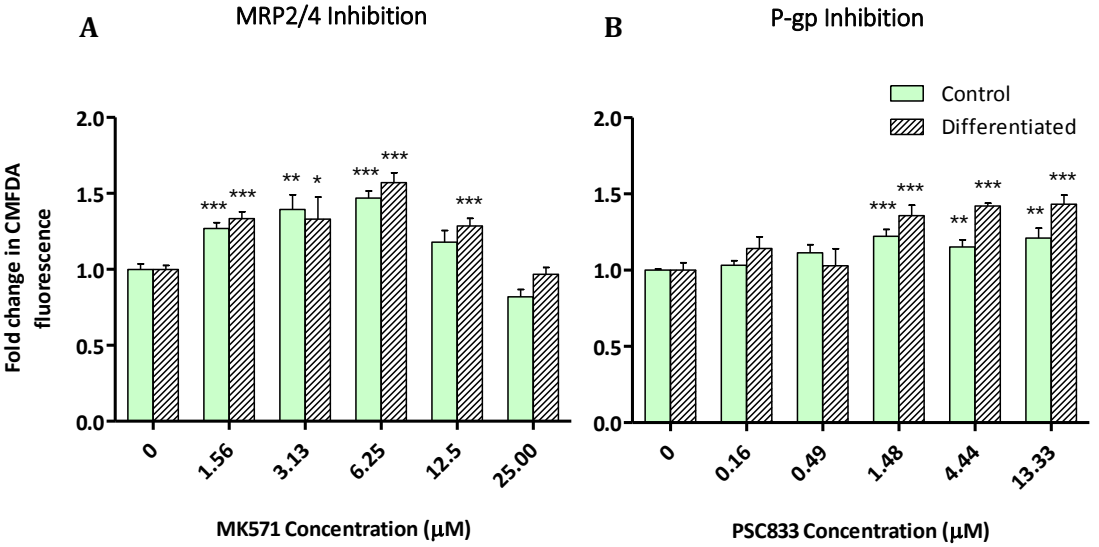

Figure 5.16 Study of MRP2, MRP4 and P-gp function in colony B.

One set of colony B cells were cultured in their own medium for 3 days and another set in PT differentiation medium also for 3 days. Then they were both incubated in CMFDA solution (1.25 μM) with (A) increasing concentrations of MK571 (MRP inhibitor) or (B) increasing concentrations of PSC833 (P-gp inhibitor). Data are represented in fold change and compared to the control (0 μM). Data are mean ± SEM (n = 3). Statistical significance was determined by One Way ANOVA test, **p*<0.05, ***p*<0.01, ****p*<0.001.

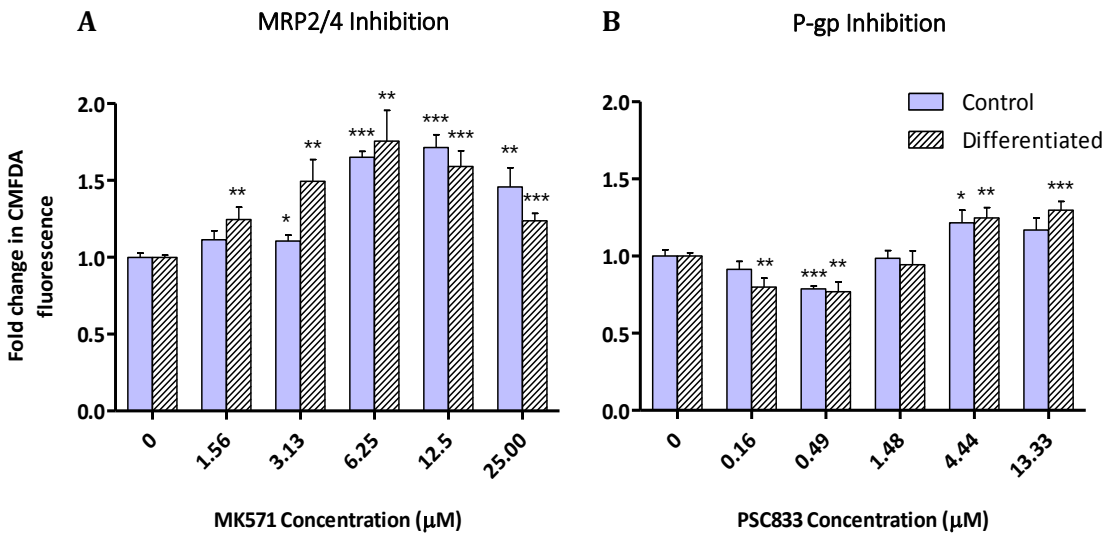

Figure 5.17 Study of MRP2, MRP4 and P-gp function in colony C.

One set of colony C cells were cultured in their own medium for 3 days and another set in PT differentiation medium also for 3 days. Then they were both incubated in CMFDA solution (1.25 μM) with (A) increasing concentrations of MK571 (MRP inhibitor) or (B) increasing concentrations of PSC833 (P-gp inhibitor). Data are represented in fold change and compared to the control (0 μM). Data are mean ± SEM (n = 3). Statistical significance was determined by One Way ANOVA test, **p*<0.05, ***p*<0.01, ****p*<0.001.

5.3.8 Spontaneous podocyte differentiation or pre-established fate?

As previously mentioned, not all the isolated colonies displayed progenitor characteristics. In fact, most of the cells stopped dividing before passage 5 and exhibited an enlarged cytoplasm that mirrored a podocyte morphology (Shankland et al. 2007). From colony D to H, we could observe flat cells with interdigitating processes and different sizes of arborized cytoplasms (Figure 5.18 – 5.22). Some cells reached nearly 400 µm in diamater (it has been shown that they can reach 500 µm diameter *in vivo* (Saleem et al. 2002)). Moreover, some of the cells were multinucleated, (marked by arrows in Figure 5.19 and Figure 5.20). It is important to note that no specific medium treatment was performed; cells suddenly slowed down division and stopped proliferating once they adopted a podocyte phenotype. This development occurred at different points during tissue culture. For instance, colony G cells started the podocyte differentiation at passage 4 (Figure 5.21), while cells from colony H started differentiation towards podocytes as soon as passage 1 (Figure 5.22).

Colony D

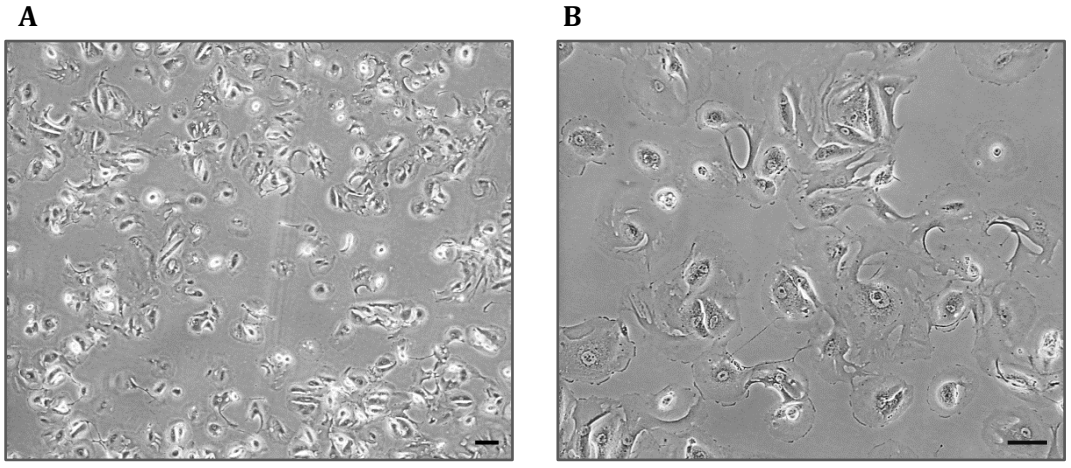

Figure 5.18 Colony D revealed podocyte-like features at passage 3.
The colony stopped division at passage 3 and changed its morphology resembling podocyte-like cells. Images were taken using (A) 4x and (B) 10x objectives. Scale bar is 100 µm.

Colony E

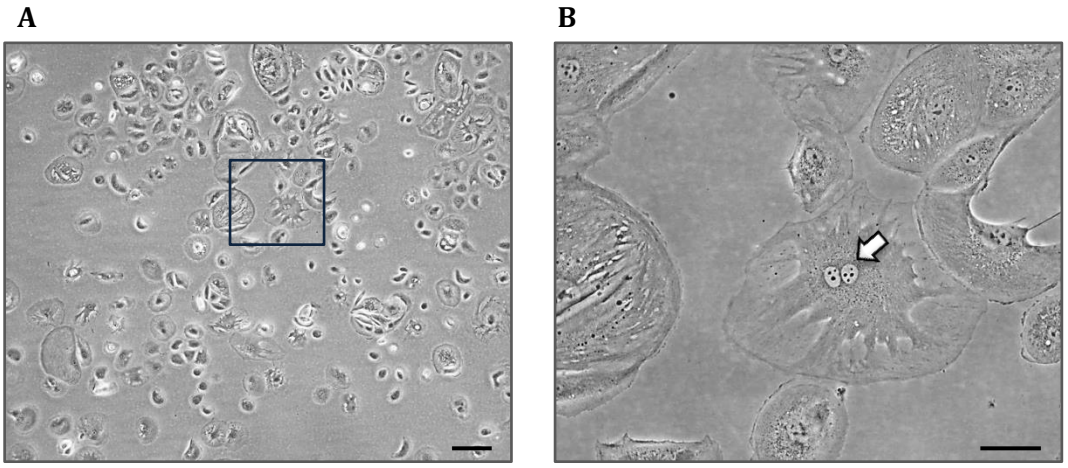

Figure 5.19 Colony E revealed podocyte-like features at passage 4.
The colony stopped division at passage 4 and changed its morphology resembling podocyte-like cells. Picture B is an amplified image of the delineated square in A. The arrow marks a binucleated cell. Images were taken using (A) 4x (scale bar is 100 µm) and (B) 20x objectives (scale bar is 50 µm).

Colony F

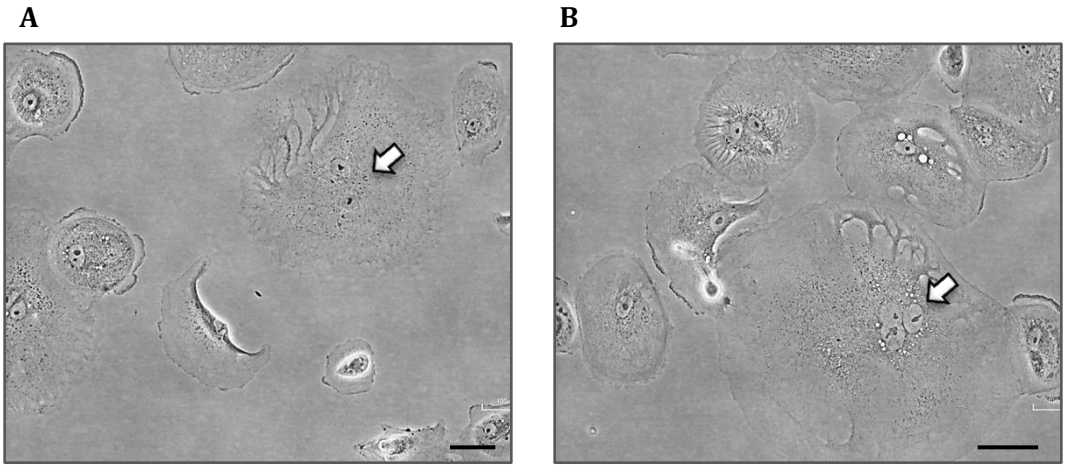

Figure 5.20 Colony F revealed podocyte-like features at passage 4.
The colony stopped division at passage 4 and changed its morphology resembling podocyte-like cells. The arrows mark cells with more than 1 nucleus. Images were taken using a 20x objective. Scale bar is 50 µm.

Colony G

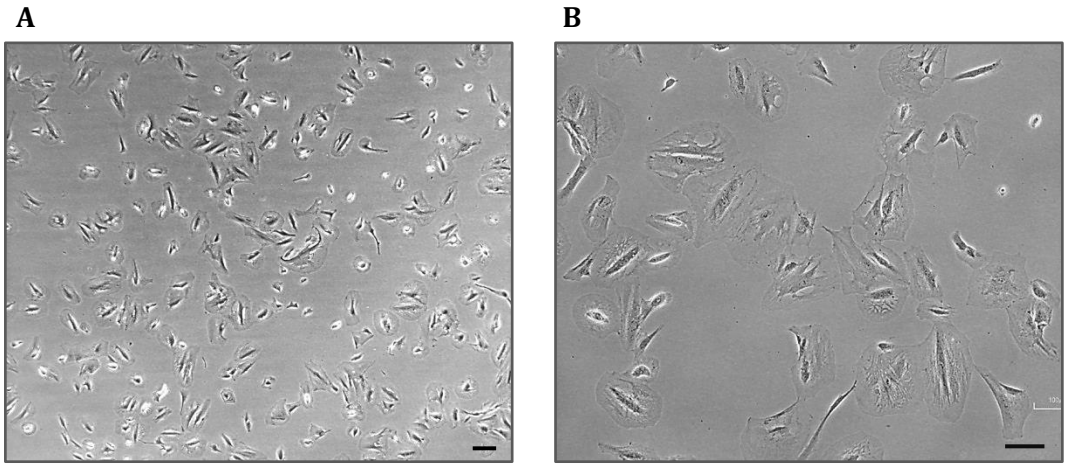

Figure 5.21 Colony G revealed podocyte-like features at passage 4.
The colony stopped division at passage 4 and changed its morphology resembling podocyte-like cells. Images were taken using (A) 4x and (B) 10x objective. Scale bar is 100 µm.

Colony H

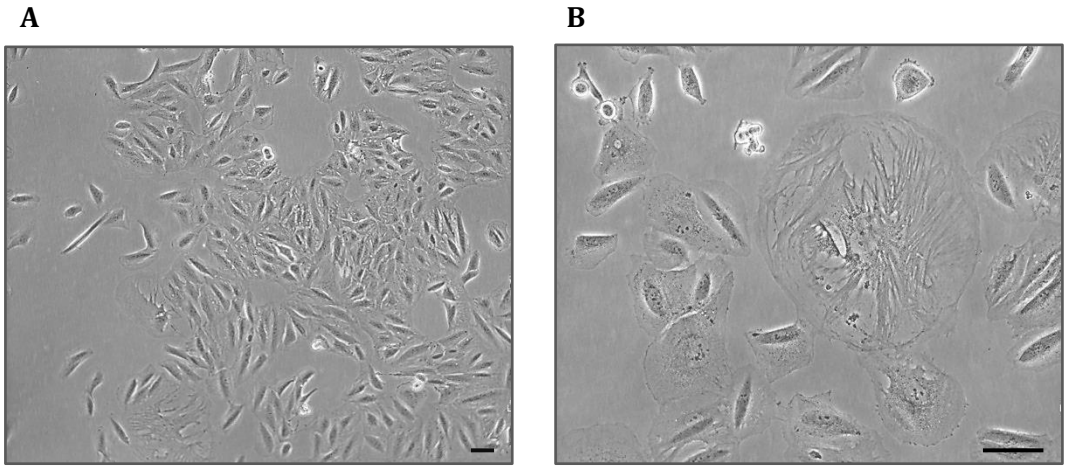

Figure 5.22 Colony H revealed podocyte-like features at passage 1.
The colony stopped division at passage 1 and changed its morphology resembling podocyte-like cells. Images were taken using (A) 10x (scale bar is 100 µm) and (B) 20x objective (scale bar is 50 µm).

We pursued some further characterisation of colonies D and E to assess if the podocyte morphology was also supported by the expression of podocyte markers. We performed IF for podocin and synaptopodin as well as qPCR to analyse the mRNA expression of some podocyte genes.

The IF images revealed the presence of podocyte markers in the two colonies that we assessed. Colony D was only stained with podocin, whereas colony E was stained for podocin and synaptopodin. Podocin plays a key role in the glomerular slit diaphragm (Mollet et al. 2009) while synaptopodin is an actin-associated protein found in differentiated podocytes and specifically localised in the cytoskeleton of foot processes (Mundel et al. 1997a, Garovic et al. 2007). Podocin was detected in all the podocyte-like cells from colony D at passage 3, even the ones with a less expanded cytoplasm (Figure 5.23). Although slightly more irregular, a similar pattern for podocin expression was identified in colony E at passage 4. Furthermore, these urine cells also had good expression levels of synaptopodin, with bigger cells displaying higher fluorescence for this marker (Figure 5.24). Binucleated cells could also be detected in both colonies throughout the population.

Colony D

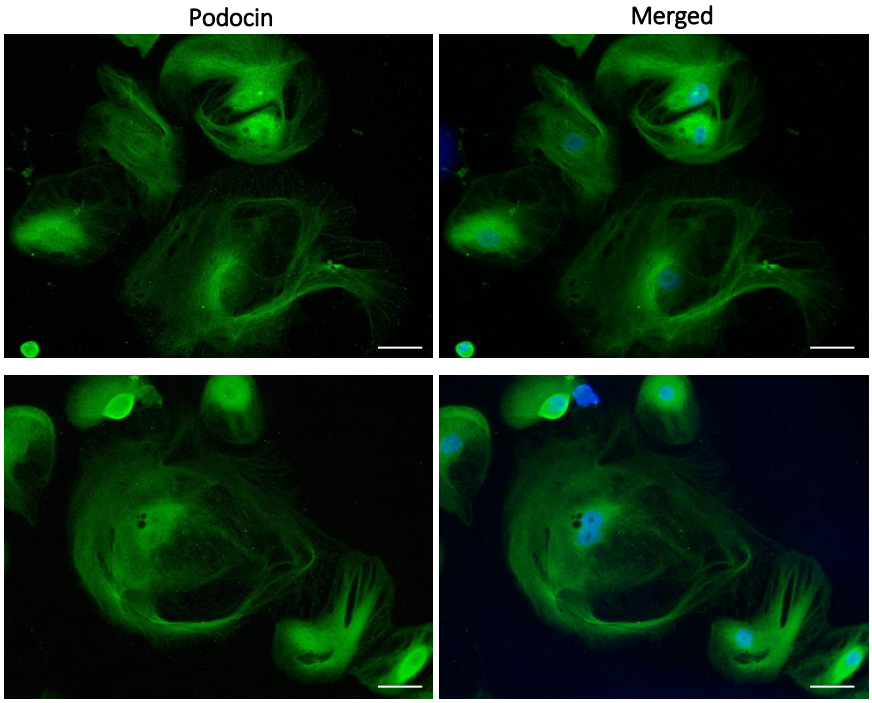

Figure 5.23 Podocin IF staining in colony D at passage 3.
Cells were stained for podocin (green) and the DNA was stained using Hoechst 33342 (blue). Images were taken using a 40x objective and they were representative of the whole cell population. Scale bar is 20 µm.

Colony E

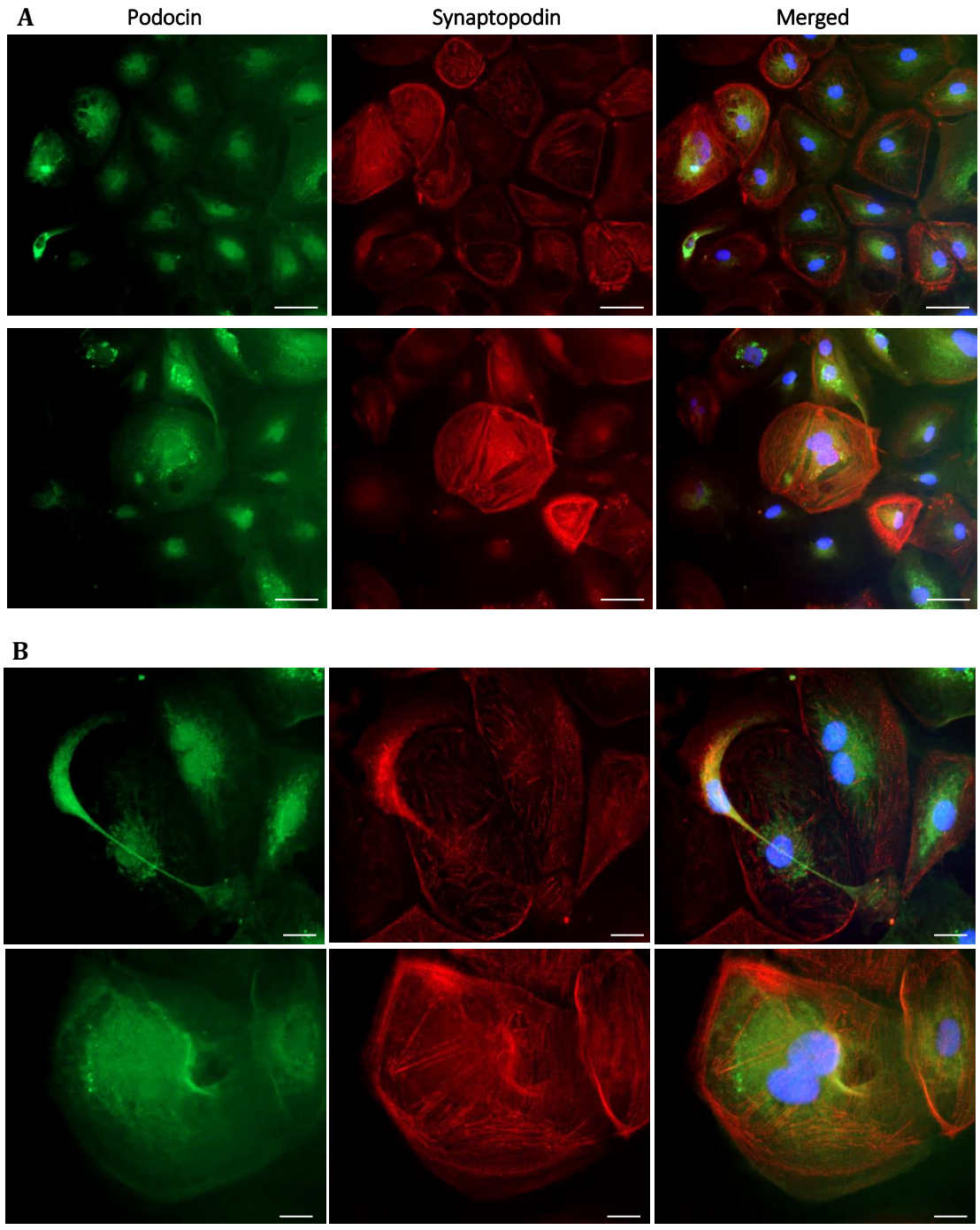

Figure 5.24 Podocin IF staining in colony E at passage 4.
Cells were stained for podocin (green) and synaptopodin (red). The DNA was stained using Hoechst 33342 (blue). Images were taken using (A) 20x objective (scale bar is 50 µm) and (B) 40x objective (scale bar is 20 µm) and they were representative of the whole cell population.

qPCR results for colony D were compared to the gene expression from a human kidney. No mRNA levels of NPHS1, NPHS2 or WT1 were identified (see Appendix 2 for further details). This observation contrasts with the IF data, where the NPHS2 encoded protein, podocin, was clearly detected. SYNPO expression was present in colony D, a lower relative expression compared to human kidney and no difference was observed between passage 2 and passage 3 (Figure 5.25).

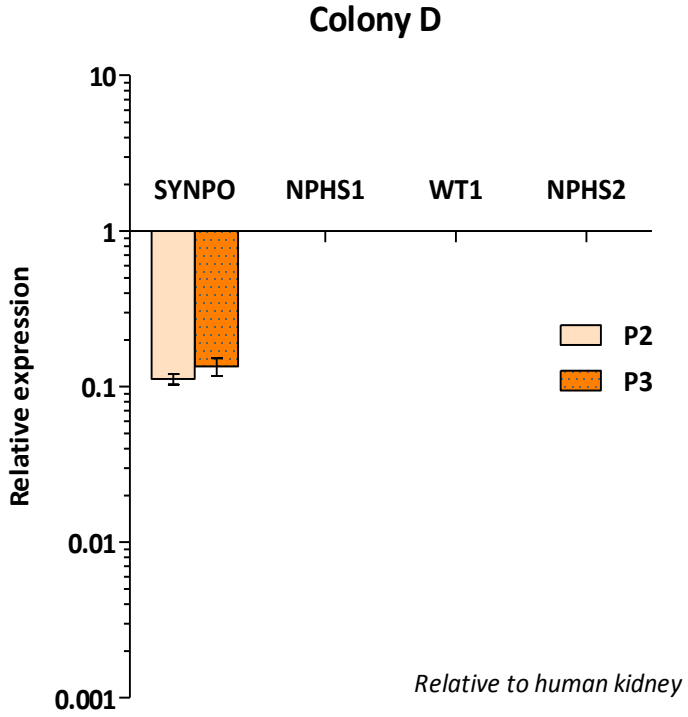

Figure 5.25 Relative expression of podocyte markers plus WT1 in colony D throughout passages.
The relative expression of podocyte genes as well as WT1 in colony D was analysed by qPCR at passage 2 (P2) and passage 3 (P3). Gene names are displayed above each set of bars. Data was normalised against human kidney tissue. Data are mean ± SEM (n = 3). Statistical significance was determined by Mann-Whitney test, *p<0.05.

The gene expression data of cells derived from colony E was compared to the mRNA expression of human kidney tissue (Figure 5.26 A) as well as to the expression of a conditionally immortalised podocyte (ciPodocyte) cell line after 10 days at 37°C (Figure 5.26 B). As previously seen in colony D, no expression of NPHS2 was detected in colony E cells. However, this cell line had detectable levels of SYNPO, NPHS1 and WT1 mRNA (Figure 5.26 A). Furthermore, it was interesting to see how SYNPO expression significantly increased with each passage. WT1 expression in passage 3 was also significantly higher compared to passage 2 but no statistical difference was detected in passage 4. NPHS1 expression could not be found at passage 2, however the mRNA levels became detectable at passage 3 with an increasing trend in expression. Compared to human kidney, the mRNA levels of the assessed genes were lower. Nevertheless, when compared to an already established podocyte cell line such as ciPodocytes (Saleem et al. 2002), SYNPO expression at passage 4 was not statistically different (Figure 5.26 B). Moreover, ciPodocytes did not express NPHS1, the gene encoding nephrin, which was detected in our podocyte-like colony E.

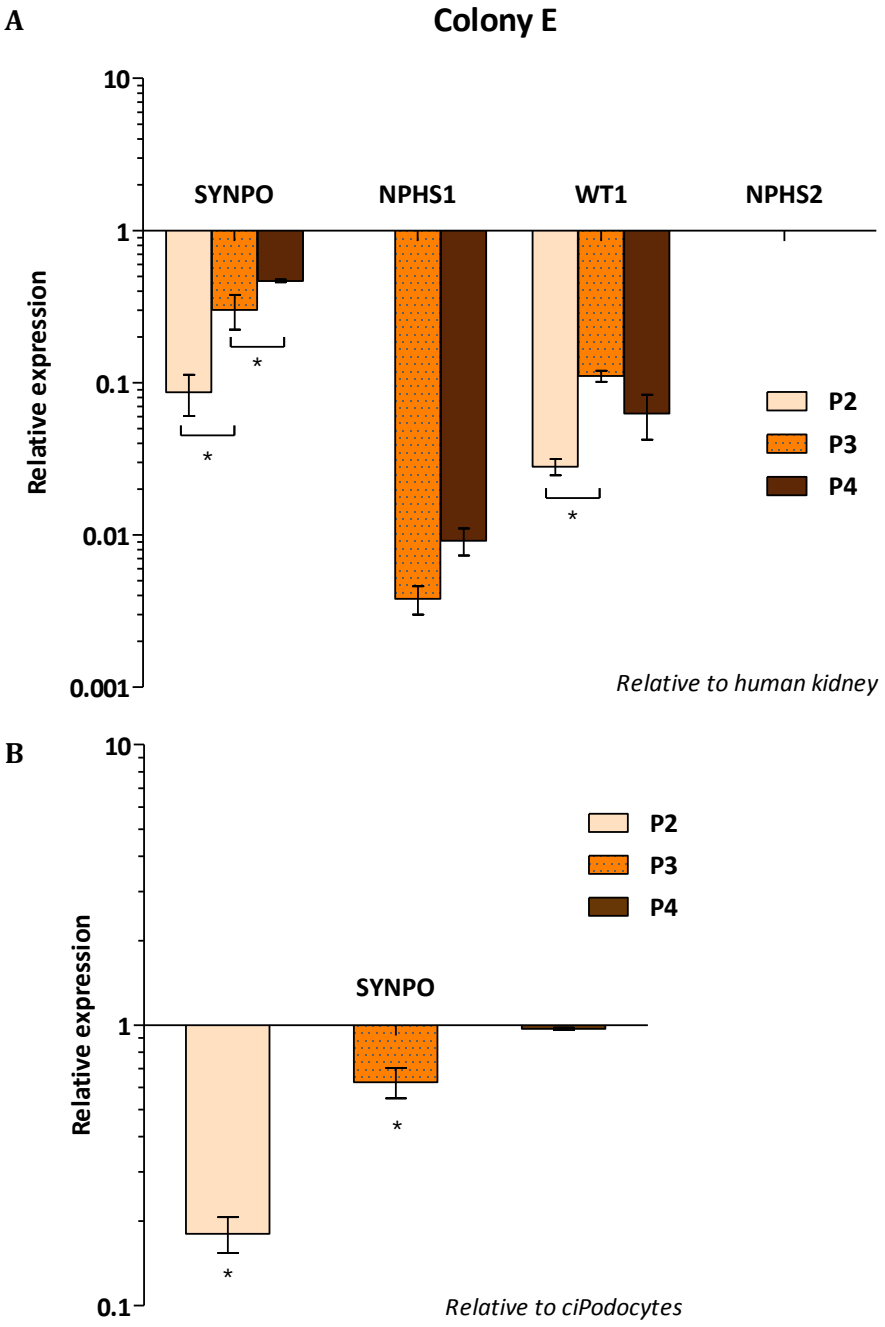

Figure 5.26 Relative expression of podocyte markers plus WT1 in colony E throughout passages.

The relative expression of podocyte genes as well as WT1 in colony D was analysed by qPCR at passage 2 (P2), passage 3 (P3) and passage 4 (P4). Gene names are displayed above each set of bars. Data was normalised against (A) human kidney tissue and (B) a ciPodocyte cell line after 10 days at 37°C. Data are mean ± SEM (n = 3). Statistical significance was by Mann-Whitney test, *p<0.05.

5.4 DISCUSSION

The first aim of this chapter was to detect colony formations of UPCs in urine cultures, isolate them and perform a simple characterisation. Considering that kidney tubule cells isolated from human tissue can only divide *in vitro* for up to 6 passages (Baer et al. 1997) and that from a single cell we obtained a population able to reach passage 10 at a steady growth rate, based on the findings of Zhang *et al.* we defined our isolated cell lines as UPCs. Additionally, the doubling times observed by Zhang et al. were very similar to the ones obtained from colonies A, B and C. The urothelial origin of the cells was ruled out by the lack of expression of UPK1A (Wu et al. 2009) which was in agreement with other published observations (Bharadwaj et al. 2013). Furthermore, clonogenicity values detected during the exponential growth phase were similar to the ones obtained for cancer cell lines using the same clonogenic method (Fedr et al. 2013). Hence, indicating that the division capacity of the isolated urine-derived cells was consistent with progenitor characteristics.

Within this chapter, the expression of the recognised kidney progenitor markers CD133 and CD24 (Lindgren et al. 2011) was assessed, although a screening for general progenitor surface markers such as c-Kit (a stem cell factor receptor) (Matsui et al. 2004) was not performed. The differential expression of both markers in the isolated colonies of UPCs might be an indication that while these two markers are reliable to select kidney progenitors *in vivo* (Romagnani and Remuzzi 2014), *in vitro* culture conditions might trigger aberrant regulation of their expression. As a result, they should not be considered progenitor-specific after *in vitro* culture. If a more in depth characterisation was to be performed, it would be interesting to analyse the expression of other kidney progenitor markers such as NCAM1 (neural cell adhesion molecule 1), which has been linked to

clonogenic potential (Buzhor et al. 2013), or Six2, an early nephron progenitor marker like WT1 (Kobayashi et al. 2008).

Before assessing the expression of kidney markers, and particularly PT markers, prior to and after culture in differentiation-promoting medium, we also analysed the variation in expression of these markers throughout passages. We theorised that if the isolated cells were progenitors and therefore committed to a renal fate, some markers would show an increasing/decreasing trend in mRNA levels with time. An increasing/decreasing trend in markers expression would also be detected if they were dedifferentiated cells instead. Although no general trend was detected amongst donors, the general expression of PT genes was similar to the expression obtained in ciPTECs (Chapter 2). Therefore, these data support the conclusion that the isolated colonies were either PT progenitors or dedifferentiated PT cells (Berger et al. 2014). This observation also supports the recently published concept of nephron segment-restricted progenitors (Bussolati and Camussi 2015) .

In light of the above conclusions and in order to address the second aim, the differentiation protocol (Narayanan et al. 2013) was adapted to 3 days as it was considered that the starting point consisted of cells that still preserved renal characteristics. Moreover, longer incubations than 3 days needed a lower number of cells at the start, which resulted in an imbalance between both conditions (control cells would become over-confluent while treated cells would not reach confluence). The differentiation towards a PT state was not highly successful and the fact that the medium did not trigger the same response in each colony was probably due to specific characteristics of the different colonies. Although some PT features were acquired, a different and more specific medium for UPCs as well as other resources such as biomaterials should be investigated as a more effective method to direct PT differentiation (Chen et al. 2014, Hoppensack et al. 2014). Functional data were also

obtained after presumed PT differentiation and revealed very few differences between control and PT differentiated cells. However, all three isolated colonies displayed functional levels of important renal drug efflux transporters, supporting once more the existence of renal progenitor colonies rather than stem cells.

Through the process of obtaining UPCs, we encountered other colonies, mainly of type II that early differentiated into podocytes. These conclusions were initially confirmed by the observation of morphological features of mature podocytes such as large, branched, arborized and frequently binucleated cells (Mundel et al. 1997b, Krtil et al. 2007). Subsequently, qPCR analysis revealed increasing levels of SYNPO expression throughout passages. *In vivo*, SYNPO expression is specific to postmitotic mature podocytes (Shankland et al. 2007), hence, its detection confirmed a differentiated podocyte phenotype. IF results supported the qPCR data and also showed podocin expression, another specific podocyte marker (Shankland et al. 2007).

To investigate the possibility of spontaneous podocyte differentiation compared with pre-established fate, we reasoned that if the medium used was the cause of the spontaneous podocyte differentiation, then our UPCs should have eventually adopted a podocyte phenotype. However, although they became bigger at the latest passage due to a slowdown in division rate, only colony B displayed podocyte morphology despite expressing important PT markers. Generally, cells from the other two colonies did not become arborized, big and multinucleated. Therefore, although IF for podocyte markers should be performed to confirm final podocyte differentiation, it could be reasoned that results supported pre-established fate over medium-driven differentiation. However, contradictive data for colony B had been previously obtained. While qPCR results would classify colony B as PT progenitor, final morphology suggested a podocyte origin. Functional experiments did not add further evidence to elucidate this matter as P-gp and MRPs are expressed in both

PT cells and podocytes (Zennaro et al. 2014). It is also worth highlighting that colony B was the only colony that maintained expression of WT1. As well as being a renal progenitor marker (Kreidberg 2010), in the adult kidney it is also expressed in podocytes (Mundlos et al. 1993). Consequently, following the theory that colony B might have originated from a progenitor/dedifferentiated podocyte, a differentiation towards this cell type using VRAD (Vitamin D3, retinoic-acid-supplemented DMEM) medium (Ronconi et al. 2009) might have been more effective than the PT differentiation applied and warrants further investigation.

In summary, we were able to isolate UPCs that demonstrated functional levels of some important drug efflux transporters. However, further studies are required to achieve the goal of establishing a patient-specific nephrotoxicity model. Therefore, further characterisation and better selection methods could be used to obtain better UPC lines and develop a deeper understanding of isolated urine-derived colonies. To improve the selection methods and avoid aberrant regulation of renal progenitor markers due to *in vitro* conditions, colonies co-expressing $CD133^+$ and $CD24^+$ surface markers should be selected at passage 0 (Lazzeri et al. 2015). Furthermore, detection of additional surface cell markers described to be linked to segment specific renal progenitors should be considered in order to bring some insight into the origin of the renal progenitors (Bussolati and Camussi 2015) and to select the best differentiation route. For instance, UPCs expressing the initial CD133 and CD24 combination, plus CD106, would most likely proceed from glomerular outgrowths and therefore they would probably respond better on a podocyte differentiation treatment (Angelotti et al. 2012). Other medium compositions used in other published investigations to isolate and culture progenitor cells from kidney tissue could also be explored, which might favour the growth of UPC colonies and delay differentiation (Lazzeri et al. 2015).

In conclusion, we have shown that it is possible to isolate UPCs of kidney origin from urine of healthy subjects that express some PT characteristics. Therefore, the initial stages have

been established to further explore the possibility of a urine-derived PT nephrotoxicity model. In addition to novel models for predictive and mechanistic toxicity, isolated UPCs have potential to be applied as an autologous non-invasive source to pursue regenerative and personalised medicine (Romagnani et al. 2013, Oliveira Arcolino et al. 2015). This has recently been demonstrated for a podocyte model derived from UPCs for the investigation of different genetic glomerular pathologies (Lazzeri et al. 2015).

Chapter Six

Final Discussion

CONTENTS

6.1 INTRODUCTION

Drug-induced mitochondrial dysfunction has lately attracted attention from industry as it has become apparent that it is a key feature to increase the success rate of new compounds under development. This interest originated after it was proven that mitochondrial liabilities are linked to late-stage drug attrition and organ toxicity (Nadanaciva and Will 2011, Dykens et al. 2007, Chan et al. 2005). So far, *in vitro* assays to predict mitotoxicity have only been developed in a bone marrow cell line (K562 cells) (Swiss et al. 2013) and in a liver cell line (HepG2 cells) (Kamalian et al. 2015). However, even though a broad range of nephrotoxins target the mitochondria, there is no equivalent model in a kidney cell line. Therefore, the re-characterised ciPTECs in Chapter 2 were used to establish an *in vitro* model that could better assess drugs that specifically induce renal mitochondrial toxicity.

To facilitate our aims, the medium change approach developed by Marroquin *et al*. and later modified by Kamalian*, L. et al*. was first implemented to ciPTECs as it has been previously done in other cell lines (Aguer et al. 2011, Kamalian et al. 2015). ciPTECs were the renal line of choice since they are a newly developed PT cell line that expresses multiple endogenous organic ion transporters, mimicking renal excretion and reabsorption in the PT (Wilmer et al. 2010). Despite having perfectly healthy mitochondria, it was conceivable that ciPTECs had fallen into the Crabtree effect, which would translate into a high glycolytic activity and a partial inhibition of cellular OXPHOS (Rodriguez-Enriquez et al. 2001). This would therefore diminish ciPTECs susceptibility to mitotoxic compounds. Hence, the implementation of Marroquin *et al*. approach by replacing glucose for galactose in the culture medium resulted in a good strategy to drive cells to a higher OXPHOS state, increasing at the same time their mitotoxic susceptibility.

In parallel with the ciPTECs mitochondrial toxicity model, in Chapter 5 we projected to develop a new renal *in vitro* model from urine. As a non-invasive method, the acquirement of human progenitor cells from urine avoids significant ethical concerns and presents a wide array of possibilities (Zhang et al. 2014, Zhang et al. 2008). Nowadays, *in vitro* nephrotoxicity assessment during drug development, as well as the study of underlying mechanisms of renal toxicity, is limited to the metabolic and genetic characteristics of a specific cell line. To investigate this problem, we proposed that if UPCs could be efficiently differentiated into mature PT cells and podocytes, it would offer the opportunity to perform patient-specific pharmacological and toxicological studies. Specifically, the use of UPCs from different sources could increase the accuracy of the results by carrying interesting donor variability, which would be useful to analyse different individual drug kinetics and metabolism for mechanistic studies (Turner et al. 2015).

6.2 POTENTIAL OF THE NEWLY DEVELOPED PT MITOTOXICITY MODEL IN DRUG DEVELOPMENT

The media replacement strategy performed on ciPTECs in Chapter 3 delivered two significantly distinctive energetic configurations, achieving a higher aerobic metabolic state in galactose conditions. In contrast to other cell lines such as HepG2 cells (Kamalian et al. 2015) or skeletal muslcle cells (Dott et al. 2014), our newly developed renal mitotoxicity model showed higher sensitivity and quicker adaptation, respectively. Therefore, this would translate into a quicker applicability and a much accurate responsiveness for the pharmacological industry in higher throughput screenings. Moreover, since the two distinctive energetic configurations can serve as a predictive tool to detect mitochondrial toxicity, the potential to discover drugs that can interfere with mitochondrial dynamics offered by this model overcomes by far the possibilities of any other renal model. This was demonstrated in this thesis by the classification of adefovir as a mitotoxic compound for

the first time *in vitro*. Therefore, further experiments using a varied panel of renal mitotoxic and non-mitotoxic drugs could provide valuable information about drug-related mitochondrial liabilities and their underlying toxicity mechanisms. Furthermore, as previously mentioned, industry could highly benefit from this PT mitotoxic model, specifically to yield safer drugs in the future. In fact, if this model was to be incorporated in early stages of drug development, it could feedback crucial information about the potential of a particular compound to induce renal mitochondrial dysfunction. Nevertheless, the implementation of a program to screen for mitochondrial toxicity should not be applied to completely discriminate and stop new drugs from being developed, but to gain a deeper understanding of the nephrotoxicity process and help improve safety measures. The mitotoxic results should be backed up with further assessment of the cytotoxic potential to stop a compound from reaching the market.

6.3 ADEFOVIR TOXICITY MECHANSIM AND IMPACT OF NOVEL ASSAYS

Publications have previously described polymerase-γ as a possible adefovir target, causing mtDNA depletion and therefore specific mitochondrial toxicity (Tanji et al. 2001). But recently, Crean *et al*. have demonstrated that adefovir triggers a downregulation of the expression of genes involved in mitochondrial biogenesis (Crean et al. 2015). However, the mechanism is still unclear and it has been shown that other nucleotide reverse transcriptase inhibitors (NtRTIs), such as TFV, do not cause any mtDNA depletion (de Baar et al. 2007). The mechanistic studies performed in Chapter 4, which had the objective to undercover the molecular mechanisms triggering adefovir nephrotoxicity, revealed that this compound is most likely inducing a mitochondrial multifactorial toxicity (Figure 6.1). If adefovir was capable of targeting polymerase-γ, it would only produce an impact on mitochondrial encoded proteins at long term (de Baar et al. 2007). This would not explain

the observed toxicity after 24 h of treatment. However, if adefovir was targeting the mitochondrial redox carriers through another pathway, that could be recapitulated by a quantitative depletion of these proteins. Both hypotheses have been previously linked to adefovir toxicity (Tanji et al. 2001, de Baar et al. 2007, Zhang et al. 2015), however, the fact that we could observe a protein depletion after only 24 h of exposure suggests that adefovir was mainly targeting protein synthesis at that concentration range. Additionally, an increase in ROS was detected. It is worth noting that mitochondria are not only a major source for ROS but also a major target, which includes mtDNA as it is less protected from radical damage than nDNA due to a lack of histones (Duchen 2004). As a consequence, it could be postulated that at high concentrations of adefovir, ROS and depleted mitochondrial encoded proteins drive nephrotoxicity, whereas at lower concentrations and

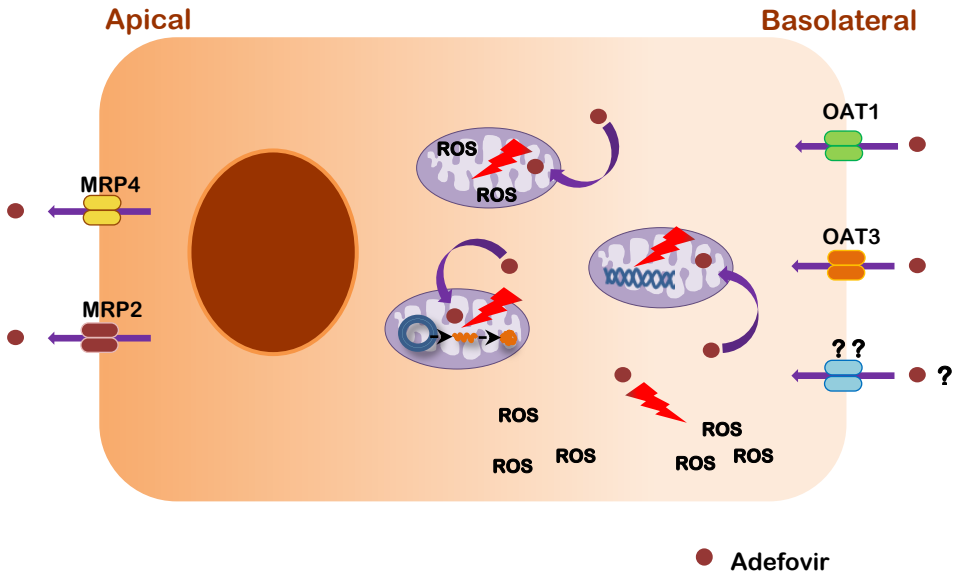

Figure 6.1 Representation of potential toxicity targets of adefovir mitotoxicity mechanism in the PT.
Adefovir enters the PT cell through OAT1 and OAT3 transporters from the basolateral membrane and is excreted via MRP2 and MRP4 to the urine. Once inside, results have shown to induce mitochondrial encoded protein depletion as well as an increase in ROS, which can also target the mitochondria. In addition, other reports have suggested mtDNA as a target. Therefore, the research carried out points towards a multifactorial toxicity.

longer treatments mtDNA depletion combined with persistent levels of slightly upregulated ROS could be responsible for a much milder PT dysfunction. Interestingly, this hypothesis seems to correlate with the situation observed clinically, where adefovir can only be administered at controlled low concentrations due to dose-limiting nephrotoxicity (Jia et al. 2015).

More refined assays and assessment techniques/instruments are being developed and becoming available, which may help to develop safer drugs and treatments. In this thesis, Seahorse technology and the ciPTEC mitotoxicity model have helped to undercover insights into the mechanisms of adefovir-induced mitochondrial toxicity. When the compound was discovered no such data could have been obtainable. Hence, if adefovir was currently pending to go to the market, its unveiled molecular toxicity mechanisms could reduce the nephrotoxicity risk and improve risk/benefit profiles by using controlled doses from the very start. However, better assessment techniques could have also hampered the market approval of the drug. Such implications would be detrimental since adefovir is still an effective treatment for chronic hepatitis B patients (Menendez-Arias et al. 2014). Therefore, new data has to be interpreted very carefully because there is a risk to lose on beneficial compounds from being approved.

6.4 NOVEL CELL MODELS TO PREDICT ANTIVIRAL-INDUCED RENAL TOXICITY

In drug discovery, it still remains a challenge to translate the *in vitro* findings to *in vivo* and clinical outcomes. Undeniable progress has been achieved in developing more relevant cell models and better understanding the properties of drugs (McKim 2010). However, there is still room for improvement in safety prediction during early drug development.

The choice of an appropriate *in vitro* model is essential to obtain translatable cytotoxicity data. In general, cell models have altered expression of metabolic enzymes and transporters, which are usually downregulated. This can influence the cytotoxic response particularly in drugs that are substrates for specific transporters such as adefovir and TFV. To counterbalance this, new toxicity cell models are being developed by transfecting already established cell lines with transporters such as OAT1 and OAT3 (Mandikova et al. 2013, Zhang et al. 2015, Nieskens et al. 2016). However, while cell models with downregulated expression of some transporters might underestimate cytotoxicity, cell lines overexpressing specific transporters run the risk of over-estimating drug-induced cytotoxic potential. Additionally, overexpressing OAT uptake transporters could also cause excessive intracellular accumulation of the drug, triggering a toxicity mechanism that does not reflect the *in vivo* toxicity pathway. An example is the transfected HEK-OAT1 cell line (Zhang et al. 2015), where adefovir and TFV showed very low IC_{50} values and an intracellular drug concentration 10x higher than the initial dose. The applicability of a cell model with these characteristics to score the nephrotoxicity of a compound is highly debatable. For example, the HEK-OAT1 cell line is derived from HEK 293 cells, which are a non-polarised expression system with poor overall predictive power, possibly due to low PT similarity. Furthermore, even though OAT1 has been overexpressed, important efflux transporters remain low or lacking in expression also favouring drug accumulation. Consequently, the predictive value of antiviral toxicity studies in similar overexpressing OAT1 or OAT3 cell lines should be considered low. In contrast, the PT cell model developed during the course of the investigations presented in this thesis to assess drug-induced mitochondrial nephrotoxicity represents a more powerful tool to predict clinical antiviral toxicity. This affirmation is based on the fact that ciPTECs confidently mimic drug absorption and excretion with adefovir EC_{50} values (EC_{50GLU} = 4.18 µg/ml and EC_{50GAL} = 0.68 µg/ml) below the Cmax in

human plasma (Cmax = 4.61 µg/ml) directly after administration of adefovir, which is completely unbound in plasma or serum (Cundy et al. 1995).

Although no mRNA levels of OAT1 and OAT3 transporters were detected, the clear cytotoxic response of ciPTECs to adefovir exposure and the radioactive TFV uptake assay proved that these transporters are present and functional in this PT cell line. Conversely, it was originally thought that ciPTECs lacked these two xenobiotic transporters and a recent publication has revealed the creation of overexpressing ciPTEC-OAT1 and ciPTEC-OAT3 cell lines (Nieskens et al. 2016). Although the conclusions of these reports claim to have developed promising predictive platforms for drug screening, our parental ciPTEC line has shown to be much more sensitive to adefovir toxicity. Furthermore, ciPTEC-OAT1 cell line is surprisingly more sensitive to TFV than to adefovir, suggesting that the spontaneous incorporation into the genome might have perturbed the expression of other transporters as well. In summary, ciPTECs in glucose *vs.* galactose conditions are a highly reliable tool to extrapolate *in vitro* data to clinical outcomes with the added value to screen for specific mitochondrial liabilities.

6.5 PT DIFFERENTIATED UPCS AS A STRATEGY TO STUDY AND CIRCUMVENT RENAL TOXICITY

Worldwide, chronic kidney disease (CKD) is considered a main health problem and affects more than 10% of the population (Eckardt et al. 2013). Therefore, different strategies using renal progenitors to ameliorate and even repair tubule damage have already been put in place (Angelotti et al. 2012, Bussolati et al. 2005). In Chapter 5, the first steps have been attained to obtain a population of UPCs-derived PT cells that can be applied in nephrotoxicity studies, disease modelling and regenerative therapy. All these strategies could help improve renal toxicity and CKD through different routes. However, further

characterisation and better isolation and differentiation protocols are required to optimise the generation of these UPCs-derived PT cells.

A patient specific urine-derived PT nephrotoxicity model could bring valuable information about the impact of a drug on a specific patient, particularly those that are already under medication known to perturb kidney dynamics and function. Specifically, the response of the urine-derived PT nephrotoxicity model could be a useful tool to adjust the dosing treatment and avoid renal toxicity. Moreover, unexpected drug-induced toxicities due to polymorphisms in drug efflux and uptake transporters could also be investigated (Knops et al. 2015, Sprowl et al. 2012). For instance, while an overexpression of MRP2/4 or stronger receptor affinity could enhance adefovir efflux and hence a decrease in drug efficacy, an under-expression or low affinity could lead to drug accumulation and therefore toxicity (Vigano et al. 2011).

Another strategy to model the impact of CKD on drug toxicity could be to establish PT models of genetic disorders such as cystinosis or Dent's disease (Bokenkamp and Ludwig 2011) from differentiated UPCs (Lazzeri et al. 2015). Some genetic PT disorders have already been studied by immortalising urine PT cells (Wilmer et al. 2011, Peeters et al. 2011). However, by isolating progenitors from urine the immortalisation process could be avoided, and so the risk of modifying gene expression due to random insertion of vectors into the DNA. The functional analysis of glomerular pathogenic mutations has already been achieved using UPCs differentiated podocytes as a new research and diagnostic tool (Lazzeri et al. 2015).

Finally, UPCs could promote renal repair in patients suffering from kidney injury (Zhang et al. 2014). Cell therapy studies using $CD133^{+}$ $CD24^{+}$ UPCs and other adult renal progenitor cells have demonstrated to improve renal function in preclinical models of AKI and CKD (Lazzeri et al. 2015, Ronconi et al. 2009, Angelotti et al. 2012, Harari-Steinberg et al. 2013).

Furthermore, both PT differentiated and non-differentiated UPCs could have the potential to contribute to tissue repair via paracrine stimulation and/or tissue engraftment (Bussolati and Camussi 2015).

6.6 CONCLUDING REMARKS

In summary, the results presented in this thesis show that:

- The implementation of the glucose *vs*. galactose strategy in ciPTECs delivered the first renal *in vitro* model capable of specifically identifying mitotoxic compounds.

- In accordance with clinical data, our *in vitro* PT mitotoxicity model was able to classify adefovir as a mitochondrial toxicant, which had not been demonstrated before in preclinical studies.

- The interrogation of bioenergetics and additional mechanistic studies revealed that adefovir nephrotoxicity is multifactorial. In particular, mitochondrial protein depletion and high levels of ROS were identified to drive mitotoxicity at high concentrations of the drug.

- UPCs of kidney origin can be isolated from healthy subjects and, although PT differentiation conditions need to be optimised, they hold the potential to be used as a nephrotoxicity model in personalised medicine and also to pursue regenerative studies.

APPENDIX

Appendix 1

Table showing the list of genes and their TaqMan® Gene Expression Assay used for qPCR:

Gene	Primer ID
MRP4	Hs00988717_m1
MRP2	Hs00166123_m1
P-gp	Hs00184500_m1
BCRP	Hs01053790_m1
AQP1	Hs01028916_m1
OATP4C1	Hs00698884_m1
LRP2	Hs00189742_m1
CUBN	Hs00153607_m1
OAT1	Hs00537914_m1
OAT3	Hs00188599_m1
PEPT 1	Hs00953898_m1
SYNPO	Hs00702468_s1
AQP3	Hs01105469_g1
NCCT	Hs01027568_m1
WT1	Hs01103751_m1
UPK1A	Hs00199638_m1
GAPDH	Hs02758991_g1
18S	Hs03003631_g1
RPLP0	Hs99999902_m1

Appendix 2

Table listing the genes studied in PCR and qPCR experiments and their protein names.

Gene name(s)	Encoded protein	Site of expression in the urinary system	Function
MRP2 ; ABCC2	MRP2	PT	Efflux pump located in the apical membrane
MRP4 ; ABCC4	MRP4	PT	Efflux pump located in the apical membrane
P-gp ; MDR1; ABCB1	P-glycoprotein; P-gp	PT	Efflux pump located in the apical membrane
BCRP ; ABCG2	BCRP	PT	Efflux pump located in the apical membrane
OAT1 ; SLC22A6	OAT1	PT	Involved in the uptake of organic anions from blood
OAT3 ; SLC22A8	OAT3	PT	Involved in the uptake of organic anions from blood
OATP4C1 ; SLCO4C1	OATP4C1	PT	Involved in the uptake of organic anions
LRP2	Megalin	Podocytes and PT	Cubilin endocytic co-transporter that plays a role in lipoprotein uptake
CUBN	Cubilin	Podocytes and PT	Megalin endocytic co-transporter that plays a role in lipoprotein uptake
AQP1	Aquaporin 1 ; AQP1	PT	Water channel protein
PEPT1 ; SLC15A1	Peptide transporter 1 ; PEPT1	PT	Proton-dependant oligopeptide transporter
SYNPO	Synaptopodin	Podocytes	Shape and motility modulator of podocyte foot processes
NPHS1	Nephrin	Podocytes	Regulates glomerular vascular permeability
NPHS2	Podocin	Podocytes	Regulates of glomerular permeability
NCCT ; NCC **;** SLC12A3	Na-Cl co-transporter	Distal tubules	Key mediator of sodium and chloride reabsorption
AQP3	Aquaporin 3 ; AQP3	Collecting duct	Water channel protein
WT1	Wilms tumor protein	Podocytes, developing nephron	Transcription factor involved in cellular development and survival
UPK1A	Uroplakin-1a ; UPKa	Urothelial cells	Component of the asymmetric unit membrane

* *Source: UniProtKB website / References: (International Transporter et al. 2010, Obermuller et al. 1995, Hall et al. 2005)*

Appendix 3

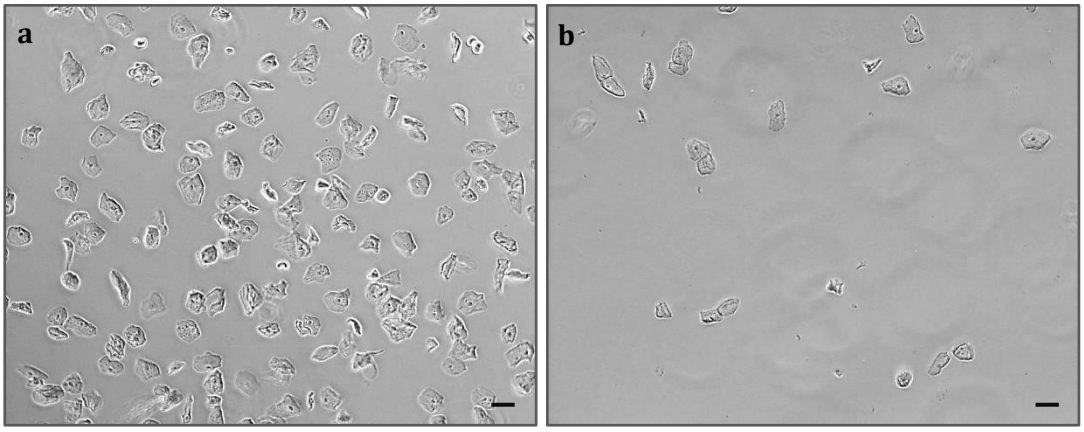

Figure showing the depletion of squamous cells over consecutive medium changes.
(a) After seeding the cells from urine in a 24-well plate, 99% of the cells were fully differentiated epithelial cells (called squamous cells) that did not adhere to the well surface. (b) After the second change in medium, the population of squamous cells was reduced significantly. Images were taken using a 10x objective. Scale bar is 200 µm.

Appendix 4

Type I colonies

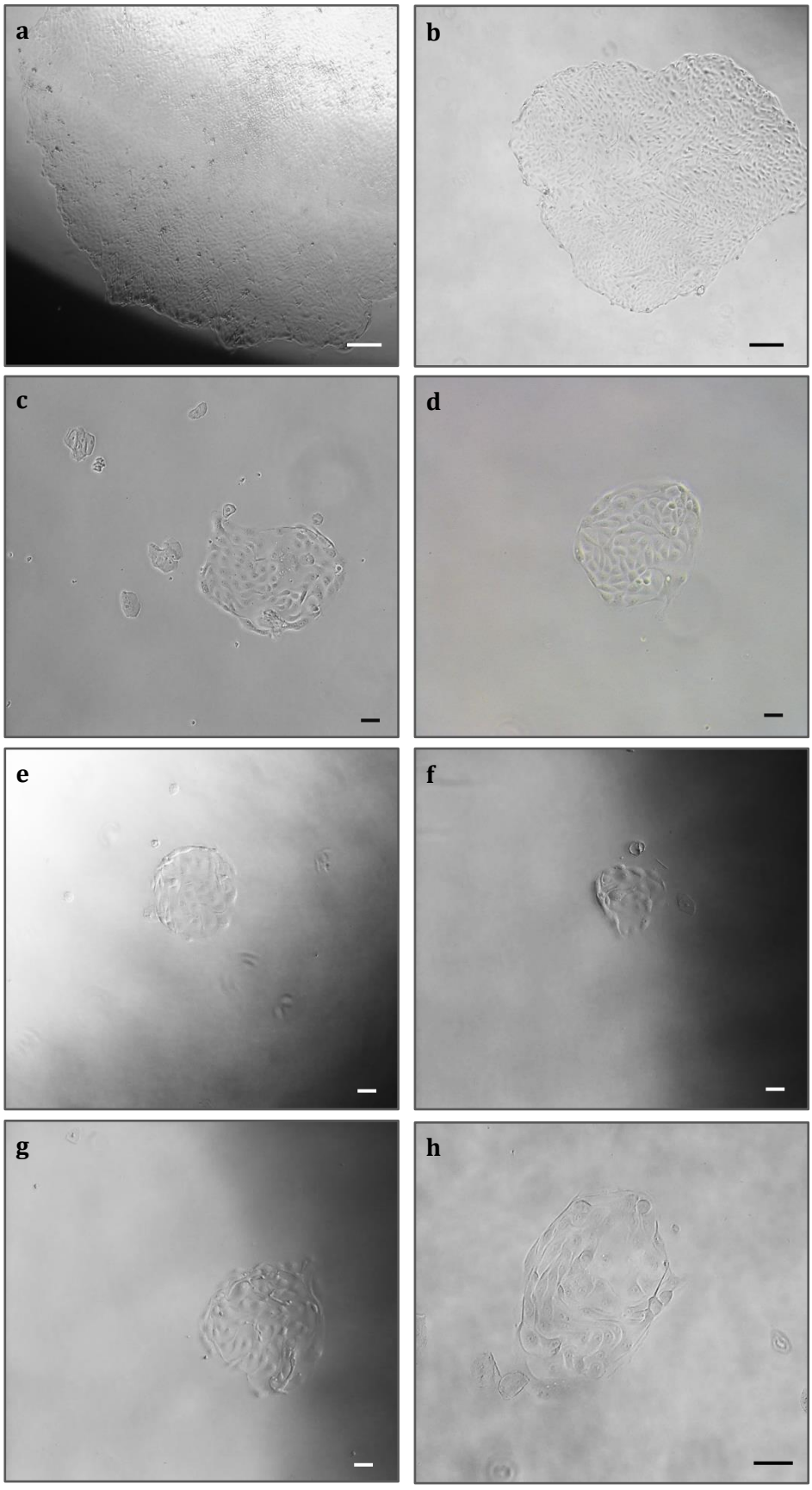

Continued Appendix 4

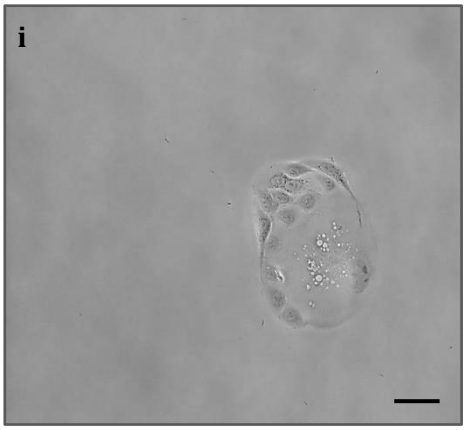

Figure showing examples of type I colonies isolated from urine.
Type I colonies show well-defined edges, compact and cobblestone-like cells. Pictures (a-b) were taken using a 4x objective (scale bar is 100 µm), (c-g) were taken using a 10x objective (scale bar is 100 µm) and (h-i) were taken using a 20x objective (scale bar is 50 µm).

Appendix 5

Type II colonies

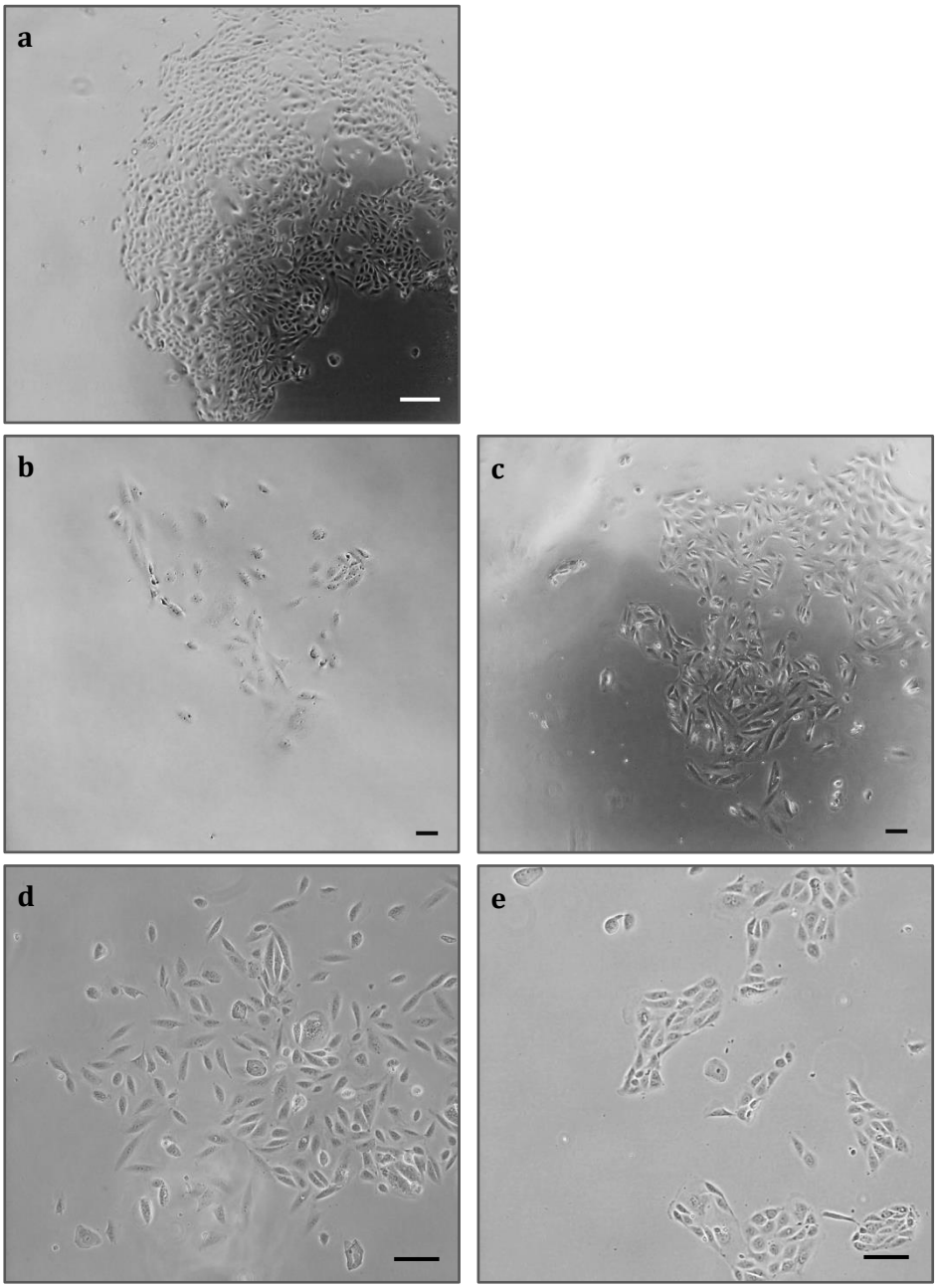

Figure showing examples of type II colonies isolated from urine.
Type II colonies show more scattered arrangement with cells adopting rice grain morphology. Pictures (a-c) were taken using a 4x objective (scale bar is 100 µm) and (d-e) were taken using a 10x objective (scale bar is 100 µm).

Appendix 6

Colony A

Table listing Ct values of the renal markers analysed by qPCR

Ct value ± SEM	MPR4	MRP2	P-gp	BCRP	AQP1	OATP4C1	CUBN	SYNPO	AQP3	NCCT
P1	30.20 ± 0.04	--	34.9 ±0.04	32.8 ± 0.2	38.2 ± 0.7	36.54 ± 0.23	34.21 ±0.54	31.59 ± 0.08	31.39 ± 0.2	--
P3	28.87 ± 0.14	38.94 ±0.51	33.6 ± 0.3	31.39 ±0.09	35.16 ± 0.3	35.3 ± 0.38	32.58 ±0.26	30.07 ± 0.13	31.3 ± 0.2	--
P5	28.21 ± 0.12	37.12 ±0.03	31.89 ± 0.4	30.6 ± 0.2	33.8 ±0.66	35.1 ± 0.5	31.69 ±0.08	28.32 ± 0.46	30.5 ±0.48	--
P7	28.39 ± 0.06	37.35 ±0.61	31.51 ±0.04	30.87 ±0.11	32.35 ±0.04	35.17 ± 0.7	32.64 ±0.22	27.77 ± 0.08	32.24 ±0.04	35.42 ±0.03

Data are mean ± SEM (n = 3)

Colony B

Table listing Ct values of the renal markers analysed by qPCR

Ct value ± SEM	MPR4	MRP2	P-gp	BCRP	AQP1	OATP4C1	CUBN	SYNPO	AQP3	WT1
P3	28.21 ± 0.03	36.70± 0.09	28.04 ±0.07	35.8 ± 0.3	33.9 ±0.14	33.46 ±0.19	31.49 ±0.06	26.08 ± 0.09	31.22 ±0.11	27.6 ±0.08
P5	28.54 ± 0.01	38.14± 0.19	28.92 ±0.04	35.05± 0.34	36.7 ±0.35	31.41 ±0.12	34.81 ±0.42	28.78 ± 0.03	33.46 ±0.11	30.22 ± 0.1
P7	28.51 ± 0.05	37.26± 0.5	28.98 ±0.08	35.2 ±0.04	36.09 ±0.13	31.09 ± 0.05	33.03 ±0.24	27.92 ± 0.03	34.31 ±0.09	31.44 ±0.14
P9	28.73 ± 0.06	36.57± 0.4	28.9 ±0.01	35.88 ±0.34	34.24 ± 0.2	29.97 ± 0.15	32.27 ±0.4	27.46 ± 0.07	36.94 ±0.43	33.05 ±0.13

Data are mean ± SEM (n = 3)

Colony C

Table listing Ct values of the renal markers analysed by qPCR

Ct value ± SEM	MPR4	MRP2	P-gp	BCRP	AQP1	OATP4C1	CUBN	SYNPO	AQP3	WT1
P3	30.89 ±0.46	36.34 ±0.44	32.84 ±0.14	36.99 ±0.73	36.68 ±0.54	30.91± 0.46	36.01 ±0.13	34.4 ±0.22	37.64 ± 0.3	25.62 ±0.85
P5	30.79 ±0.29	35.76 ±0.15	33.50 ±0.26	36.75 ±0.62	34.27 ±0.27	30.95 ±0.25	36.56 ±0.42	31.96 ±0.07	36.87 ±0.19	--
P7	28.54 ±0.06	36.03 ±0.58	31.87 ±0.19	36.51 ±0.24	32.55 ±0.08	29.7 ±0.15	34.06 ±0.32	28.8 ±0.07	34.43 ±0.05	--
P9	28.25 ±0.04	37.37 ± 0.03	30.1 ±0.02	36.29 ±0.57	35.2 ± 0.2	30.18 ± 0.09	32.91 ±0.13	28.88 ±0.06	33.75 ±0.18	--

Data are mean ± SEM (n = 3)

BIBLIOGRAPHY

AGUER C, GAMBAROTTA D, MAILLOUX RJ, MOFFAT C, DENT R, MCPHERSON R AND HARPER ME. 2011. Galactose enhances oxidative metabolism and reveals mitochondrial dysfunction in human primary muscle cells. PLoS One 6: e28536.

ALBERTS B JA, LEWIS J, ET AL. 2002. Molecular Biology of the Cell. n. 18, 4th ed, New York: Garland Science, 289 p.

ALLEN JD, VAN LOEVEZIJN A, LAKHAI JM, VAN DER VALK M, VAN TELLINGEN O, REID G, SCHELLENS JH, KOOMEN GJ AND SCHINKEL AH. 2002. Potent and specific inhibition of the breast cancer resistance protein multidrug transporter in vitro and in mouse intestine by a novel analogue of fumitremorgin C. Mol Cancer Ther 1: 417-425.

AMM I, SOMMER T AND WOLF DH. 2014. Protein quality control and elimination of protein waste: the role of the ubiquitin-proteasome system. Biochim Biophys Acta 1843: 182-196.

ANGELOTTI ML ET AL. 2012. Characterization of renal progenitors committed toward tubular lineage and their regenerative potential in renal tubular injury. Stem Cells 30: 1714-1725.

ANTOINE DJ, SRIVASTAVA A, PIRMOHAMED M AND PARK BK. 2010. Statins inhibit aminoglycoside accumulation and cytotoxicity to renal proximal tubule cells. Biochem Pharmacol 79: 647-654.

BAER PC, NOCKHER WA, HAASE W AND SCHERBERICH JE. 1997. Isolation of proximal and distal tubule cells from human kidney by immunomagnetic separation. Technical note. Kidney Int 52: 1321-1331.

BAGNASCO S, GOOD D, BALABAN R AND BURG M. 1985. Lactate production in isolated segments of the rat nephron. Am J Physiol 248: F522-526.

BARHOUMI R, BOWEN JA, STEIN LS, ECHOLS J AND BURGHARDT RC. 1993. Concurrent analysis of intracellular glutathione content and gap junctional intercellular communication. Cytometry 14: 747-756.

BAVARSAD SHAHRIPOUR R, HARRIGAN MR AND ALEXANDROV AV. 2014. N-acetylcysteine (NAC) in neurological disorders: mechanisms of action and therapeutic opportunities. Brain Behav 4: 108-122.

BEESON CC, BEESON GC AND SCHNELLMANN RG. 2010. A high-throughput respirometric assay for mitochondrial biogenesis and toxicity. Anal Biochem 404: 75-81.

BELZER M, MORALES M, JAGADISH B, MASH EA AND WRIGHT SH. 2013. Substrate-dependent ligand inhibition of the human organic cation transporter OCT2. J Pharmacol Exp Ther 346: 300-310.

BENARD G, BELLANCE N, JAMES D, PARRONE P, FERNANDEZ H, LETELLIER T AND ROSSIGNOL R. 2007. Mitochondrial bioenergetics and structural network organization. J Cell Sci 120: 838-848.

BENDELE RA AND RICHARDSON FC. 2002. Adefovir nephrotoxicity and mitochondrial DNA depletion. Hum Pathol 33: 574.

BENS M AND VANDEWALLE A. 2008. Cell models for studying renal physiology. Pflugers Arch 457: 1-15.

BERGER K, BANGEN JM, HAMMERICH L, LIEDTKE C, FLOEGE J, SMEETS B AND MOELLER MJ. 2014. Origin of regenerating tubular cells after acute kidney injury. Proc Natl Acad Sci U S A 111: 1533-1538.

BEZOMBES C, MAESTRE N, LAURENT G, LEVADE T, BETTAIEB A AND JAFFREZOU JP. 1998. Restoration of TNF-alpha-induced ceramide generation and apoptosis in resistant human leukemia KG1a cells by the P-glycoprotein blocker PSC833. FASEB J 12: 101-109.

BHARADWAJ S, LIU G, SHI Y, MARKERT C, ANDERSSON KE, ATALA A AND ZHANG Y. 2011. Characterization of urine-derived stem cells obtained from upper urinary tract for use in cell-based urological tissue engineering. Tissue Eng Part A 17: 2123-2132.

BHARADWAJ S ET AL. 2013. Multipotential differentiation of human urine-derived stem cells: potential for therapeutic applications in urology. Stem Cells 31: 1840-1856.

BIERMANN J, LANG D, GORBOULEV V, KOEPSELL H, SINDIC A, SCHROTER R, ZVIRBLIENE A, PAVENSTADT H, SCHLATTER E AND CIARIMBOLI G. 2006. Characterization of regulatory mechanisms and states of human organic cation transporter 2. Am J Physiol Cell Physiol 290: C1521-1531.

BLEASBY K ET AL. 2006. Expression profiles of 50 xenobiotic transporter genes in humans and pre-clinical species: a resource for investigations into drug disposition. Xenobiotica 36: 963-988.

BOESCH D, GAVERIAUX C, JACHEZ B, POURTIER-MANZANEDO A, BOLLINGER P AND LOOR F. 1991. In vivo circumvention of P-glycoprotein-mediated multidrug resistance of tumor cells with SDZ PSC 833. Cancer Res 51: 4226-4233.

BOKENKAMP A AND LUDWIG M. 2011. Disorders of the renal proximal tubule. Nephron Physiol 118: p1-6.

BONVENTRE JV, VAIDYA VS, SCHMOUDER R, FEIG P AND DIETERLE F. 2010. Next-generation biomarkers for detecting kidney toxicity. Nature biotechnology 28: 436-440.

BRAND MD, AFFOURTIT C, ESTEVES TC, GREEN K, LAMBERT AJ, MIWA S, PAKAY JL AND PARKER N. 2004. Mitochondrial superoxide: production, biological effects, and activation of uncoupling proteins. Free Radic Biol Med 37: 755-767.

BRDICZKA DG, ZOROV DB AND SHEU SS. 2006. Mitochondrial contact sites: their role in energy metabolism and apoptosis. Biochim Biophys Acta 1762: 148-163.

BROWN CD, SAYER R, WINDASS AS, HASLAM IS, DE BROE ME, D'HAESE PC AND VERHULST A. 2008. Characterisation of human tubular cell monolayers as a model of proximal tubular xenobiotic handling. Toxicol Appl Pharmacol 233: 428-438.

BUSSOLATI B, BRUNO S, GRANGE C, BUTTIGLIERI S, DEREGIBUS MC, CANTINO D AND CAMUSSI G. 2005. Isolation of renal progenitor cells from adult human kidney. Am J Pathol 166: 545-555.

BUSSOLATI B AND CAMUSSI G. 2015. Therapeutic use of human renal progenitor cells for kidney regeneration. Nat Rev Nephrol 11: 695-706.

BUZHOR E, HARARI-STEINBERG O, OMER D, METSUYANIM S, JACOB-HIRSCH J, NOIMAN T, DOTAN Z, GOLDSTEIN RS AND DEKEL B. 2011. Kidney spheroids recapitulate tubular organoids leading to enhanced tubulogenic potency of human kidney-derived cells. Tissue Eng Part A 17: 2305-2319.

BUZHOR E, OMER D, HARARI-STEINBERG O, DOTAN Z, VAX E, PRI-CHEN S, METSUYANIM S, PLENICEANU O, GOLDSTEIN RS AND DEKEL B. 2013. Reactivation of NCAM1 defines a subpopulation of human adult kidney epithelial cells with clonogenic and stem/progenitor properties. Am J Pathol 183: 1621-1633.

CABEZAS F, LAGOS J, CESPEDES C, VIO CP, BRONFMAN M AND MARZOLO MP. 2011. Megalin/LRP2 expression is induced by peroxisome proliferator-activated receptor -alpha and -gamma: implications for PPARs' roles in renal function. PLoS One 6: e16794.

CHACKO BK ET AL. 2014. The Bioenergetic Health Index: a new concept in mitochondrial translational research. Clin Sci (Lond) 127: 367-373.

CHAN K, TRUONG D, SHANGARI N AND O'BRIEN PJ. 2005. Drug-induced mitochondrial toxicity. Expert Opin Drug Metab Toxicol 1: 655-669.

CHEN H AND CHAN DC. 2009. Mitochondrial dynamics--fusion, fission, movement, and mitophagy--in neurodegenerative diseases. Hum Mol Genet 18: R169-176.

CHEN WC, LIN HH AND TANG MJ. 2014. Regulation of proximal tubular cell differentiation and proliferation in primary culture by matrix stiffness and ECM components. Am J Physiol Renal Physiol 307: F695-707.

CHRISTENSEN EI AND BIRN H. 2002. Megalin and cubilin: multifunctional endocytic receptors. Nat Rev Mol Cell Biol 3: 256-266.

CHRISTENSEN EI, VERROUST PJ AND NIELSEN R. 2009. Receptor-mediated endocytosis in renal proximal tubule. Pflugers Arch 458: 1039-1048.

CIHLAR T, BIRKUS G, GREENWALT DE AND HITCHCOCK MJ. 2002. Tenofovir exhibits low cytotoxicity in various human cell types: comparison with other nucleoside reverse transcriptase inhibitors. Antiviral Res 54: 37-45.

COOPER RD, WIEBE N, SMITH N, KEISER P, NAICKER S AND TONELLI M. 2011. Systematic review and meta-analysis: Renal safety of tenofovir disoproxil fumarate in HIV-infected patients (vol 51, pg 496, 2010). Clin Infect Dis 52: 283-283.

CORBEIL D, ROPER K, HELLWIG A, TAVIAN M, MIRAGLIA S, WATT SM, SIMMONS PJ, PEAULT B, BUCK DW AND HUTTNER WB. 2000. The human AC133 hematopoietic stem cell antigen is also expressed in epithelial cells and targeted to plasma membrane protrusions. J Biol Chem 275: 5512-5520.

CREAN D ET AL. 2015. Development of an in vitro renal epithelial disease state model for xenobiotic toxicity testing. Toxicol In Vitro 30: 128-137.

CUI S, VERROUST PJ, MOESTRUP SK AND CHRISTENSEN EI. 1996. Megalin/gp330 mediates uptake of albumin in renal proximal tubule. Am J Physiol 271: F900-907.

CUNDY KC, BARDITCH-CROVO P, WALKER RE, COLLIER AC, EBELING D, TOOLE J AND JAFFE HS. 1995. Clinical pharmacokinetics of adefovir in human immunodeficiency virus type 1-infected patients. Antimicrob Agents Chemother 39: 2401-2405.

DE BAAR MP, DE ROOIJ ER, SMOLDERS KG, VAN SCHIJNDEL HB, TIMMERMANS EC AND BETHELL R. 2007. Effects of apricitabine and other nucleoside reverse transcriptase inhibitors on replication of mitochondrial DNA in HepG2 cells. Antiviral Res 76: 68-74.

DE CLERCQ E AND HOLY A. 2005. Acyclic nucleoside phosphonates: a key class of antiviral drugs. Nat Rev Drug Discov 4: 928-940.

DEAVALL DG, MARTIN EA, HORNER JM AND ROBERTS R. 2012. Drug-induced oxidative stress and toxicity. J Toxicol 2012: 645460.

DELL' ANTONE P. 2012. Energy metabolism in cancer cells: how to explain the Warburg and Crabtree effects? Med Hypotheses 79: 388-392.

DERNELL WS, STRAW RC, WITHROW SJ, POWERS BE, FUJITA SM, YEWEY GS, JOSEPH KF, DUNN RL, WHITMAN SL AND SOUTHARD GL. 1998. Apparent interaction of dimethyl sulfoxide with cisplatin released from polymer delivery devices injected subcutaneously in dogs. J Drug Target 5: 391-396.

DESHMUKH SRWN, W. 2009. The Renal System Explained: An Illustrated Core Text. Nottingham University Press.

DETRISAC CJ, MAYFIELD RK, COLWELL JA, GARVIN AJ AND SENS DA. 1983. In vitro culture of cells exfoliated in the urine by patients with diabetes mellitus. J Clin Invest 71: 170-173.

DIKALOV SI AND HARRISON DG. 2014. Methods for detection of mitochondrial and cellular reactive oxygen species. Antioxid Redox Signal 20: 372-382.

DORRENHAUS A, MULLER JI, GOLKA K, JEDRUSIK P, SCHULZE H AND FOLLMANN W. 2000. Cultures of exfoliated epithelial cells from different locations of the human urinary tract and the renal tubular system. Arch Toxicol 74: 618-626.

DOTT W, MISTRY P, WRIGHT J, CAIN K AND HERBERT KE. 2014. Modulation of mitochondrial bioenergetics in a skeletal muscle cell line model of mitochondrial toxicity. Redox Biol 2: 224-233.

DOYLE L AND ROSS DD. 2003. Multidrug resistance mediated by the breast cancer resistance protein BCRP (ABCG2). Oncogene 22: 7340-7358.

DUCHEN MR. 2004. Mitochondria in health and disease: perspectives on a new mitochondrial biology. Mol Aspects Med 25: 365-451.

DYKENS JA, MARROQUIN LD AND WILL Y. 2007. Strategies to reduce late-stage drug attrition due to mitochondrial toxicity. Expert Rev Mol Diagn 7: 161-175.

DYKENS JA AND WILL Y. 2007. The significance of mitochondrial toxicity testing in drug development. Drug Discov Today 12: 777-785.

DYKENS JA AND WILL Y 2008. Drug-Induced Mitochondrial Dysfunction. Wiley.

ECKARDT KU, CORESH J, DEVUYST O, JOHNSON RJ, KOTTGEN A, LEVEY AS AND LEVIN A. 2013. Evolving importance of kidney disease: from subspecialty to global health burden. Lancet 382: 158-169.

ENDO T AND YAMANO K. 2009. Multiple pathways for mitochondrial protein traffic. Biol Chem 390: 723-730.

ERALY SA ET AL. 2006. Decreased renal organic anion secretion and plasma accumulation of endogenous organic anions in OAT1 knock-out mice. J Biol Chem 281: 5072-5083.

EYRE J, IOANNOU K, GRUBB BD, SALEEM MA, MATHIESON PW, BRUNSKILL NJ, CHRISTENSEN EI AND TOPHAM PS. 2007. Statin-sensitive endocytosis of albumin by glomerular podocytes. Am J Physiol Renal Physiol 292: F674-681.

FEDR R, PERNICOVA Z, SLABAKOVA E, STRAKOVA N, BOUCHAL J, GREPL M, KOZUBIK A AND SOUCEK K. 2013. Automatic cell cloning assay for determining the clonogenic capacity of cancer and cancer stem-like cells. Cytometry A 83: 472-482.

FELIX JS, SUN TT AND LITTLEFIELD JW. 1980. Human epithelial cells cultured from urine: growth properties and keratin staining. In Vitro 16: 866-874.

FOX TD. 2012. Mitochondrial protein synthesis, import, and assembly. Genetics 192: 1203-1234.

FRANK HN 2012. Anatomy of the urinary tract. In*:* CHRISTOPHER, RKJL (Ed.) The Netter Collection of Medical Illustrations: Urinary System: Saunders, p. 2-28.

FRANKEN NA, RODERMOND HM, STAP J, HAVEMAN J AND VAN BREE C. 2006. Clonogenic assay of cells in vitro. Nat Protoc 1: 2315-2319.

FU XZ, OU Y, PEI JY, LIU Y, LI J, ZHOU W, LAN YY, WANG AM AND WANG YL. 2012. Synthesis, anti-HBV activity and renal cell toxicity evaluation of mixed phosphonate prodrugs of adefovir. Eur J Med Chem 49: 211-218.

FUNK JA, ODEJINMI S AND SCHNELLMANN RG. 2010. SRT1720 induces mitochondrial biogenesis and rescues mitochondrial function after oxidant injury in renal proximal tubule cells. J Pharmacol Exp Ther 333: 593-601.

GALLEGOS TF, MARTOVETSKY G, KOUZNETSOVA V, BUSH KT AND NIGAM SK. 2012. Organic anion and cation SLC22 "drug" transporter (Oat1, Oat3, and Oct1) regulation during development and maturation of the kidney proximal tubule. PLoS One 7: e40796.

GAROVIC VD, WAGNER SJ, PETROVIC LM, GRAY CE, HALL P, SUGIMOTO H, KALLURI R AND GRANDE JP. 2007. Glomerular expression of nephrin and synaptopodin, but not podocin, is decreased in kidney sections from women with preeclampsia. Nephrol Dial Transplant 22: 1136-1143.

GEKLE M. 2005. Renal tubule albumin transport. Annu Rev Physiol 67: 573-594.

GEKLE M, MILDENBERGER S, FREUDINGER R AND SILBERNAGL S. 1998. Long-term protein exposure reduces albumin binding and uptake in proximal tubule-derived opossum kidney cells. J Am Soc Nephrol 9: 960-968.

GORVIN CM, WILMER MJ, PIRET SE, HARDING B, VAN DEN HEUVEL LP, WRONG O, JAT PS, LIPPIAT JD, LEVTCHENKO EN AND THAKKER RV. 2013. Receptor-mediated endocytosis and endosomal acidification is impaired in proximal tubule epithelial cells of Dent disease patients. Proc Natl Acad Sci U S A 110: 7014-7019.

GRAHAM FL, SMILEY J, RUSSELL WC AND NAIRN R. 1977. Characteristics of a human cell line transformed by DNA from human adenovirus type 5. J Gen Virol 36: 59-74.

GSTRAUNTHALER G. 1985. Biochemical characterization of renal epithelial cell cultures (LLC-PK1 and MDCK). Am J Physiol 248: F536-F544.

GUNNESS P, ALEKSA K, KOSUGE K, ITO S AND KOREN G. 2010. Comparison of the novel HK-2 human renal proximal tubular cell line with the standard LLC-PK1 cell line in studying drug-induced nephrotoxicity. Can J Physiol Pharmacol 88: 448-455.

GUPPY M, GREINER E AND BRAND K. 1993. The role of the Crabtree effect and an endogenous fuel in the energy metabolism of resting and proliferating thymocytes. Eur J Biochem 212: 95-99.

HA NB, HA NB, GARCIA RT, TRINH HN, VU AA, NGUYEN HA, NGUYEN KK, LEVITT BS AND NGUYEN MH. 2009. Renal dysfunction in chronic hepatitis B patients treated with adefovir dipivoxil. Hepatology 50: 727-734.

HALL AM. 2013. Update on tenofovir toxicity in the kidney. Pediatr Nephrol 28: 1011-1023.

HALL AM, HENDRY BM, NITSCH D AND CONNOLLY JO. 2011. Tenofovir-associated kidney toxicity in HIV-infected patients: a review of the evidence. Am J Kidney Dis 57: 773-780.

HALL AM, UNWIN RJ, PARKER N AND DUCHEN MR. 2009. Multiphoton imaging reveals differences in mitochondrial function between nephron segments. J Am Soc Nephrol 20: 1293-1302.

HALL GD, WEEKS RJ, OLSBURGH J, SOUTHGATE J, KNOWLES MA, SELBY PJ AND CHESTER JD. 2005. Transcriptional control of the human urothelial-specific gene, uroplakin Ia. Biochim Biophys Acta 1729: 126-134.

HARARI-STEINBERG O ET AL. 2013. Identification of human nephron progenitors capable of generation of kidney structures and functional repair of chronic renal disease. EMBO Mol Med 5: 1556-1568.

HEBERT RJAASC 2008. The Kidney: physiology and pathophysiology. Fourth ed: Elsevier.

HERLITZ LC, MOHAN S, STOKES MB, RADHAKRISHNAN J, D'AGATI VD AND MARKOWITZ GS. 2010. Tenofovir nephrotoxicity: acute tubular necrosis with distinctive clinical, pathological, and mitochondrial abnormalities. Kidney Int 78: 1171-1177.

HEUSER M, RINGERT RH, ZOELLER G AND HEMMERLEIN B. 2003. Dynamic assessment of angiogenesis in renal cell carcinoma spheroids by intravital microscopy. J Urol 169: 1267-1270.

HILL BG, BENAVIDES GA, LANCASTER JR, JR., BALLINGER S, DELL'ITALIA L, JIANHUA Z AND DARLEY-USMAR VM. 2012. Integration of cellular bioenergetics with mitochondrial quality control and autophagy. Biol Chem 393: 1485-1512.

HO ES, LIN DC, MENDEL DB AND CIHLAR T. 2000. Cytotoxicity of antiviral nucleotides adefovir and cidofovir is induced by the expression of human renal organic anion transporter 1. J Am Soc Nephrol 11: 383-393.

HOPPENSACK A, KAZANECKI CC, COLTER D, GOSIEWSKA A, SCHANZ J, WALLES H AND SCHENKE-LAYLAND K. 2014. A human in vitro model that mimics the renal proximal tubule. Tissue Eng Part C Methods 20: 599-609.

HUANG LS, COBESSI D, TUNG EY AND BERRY EA. 2005. Binding of the respiratory chain inhibitor antimycin to the mitochondrial bc1 complex: a new crystal structure reveals an altered intramolecular hydrogen-bonding pattern. J Mol Biol 351: 573-597.

HUMPHREYS BD, CZERNIAK S, DIROCCO DP, HASNAIN W, CHEEMA R AND BONVENTRE JV. 2011. Repair of injured proximal tubule does not involve specialized progenitors. Proc Natl Acad Sci U S A 108: 9226-9231.

HUMPHREYS BD, VALERIUS MT, KOBAYASHI A, MUGFORD JW, SOEUNG S, DUFFIELD JS, MCMAHON AP AND BONVENTRE JV. 2008. Intrinsic epithelial cells repair the kidney after injury. Cell Stem Cell 2: 284-291.

IMAOKA T, KUSUHARA H, ADACHI M, SCHUETZ JD, TAKEUCHI K AND SUGIYAMA Y. 2007. Functional involvement of multidrug resistance-associated protein 4 (MRP4/ABCC4) in the renal elimination of the antiviral drugs adefovir and tenofovir. Mol Pharmacol 71: 619-627.

INTERNATIONAL TRANSPORTER C ET AL. 2010. Membrane transporters in drug development. Nat Rev Drug Discov 9: 215-236.

INUI KI, MASUDA S AND SAITO H. 2000. Cellular and molecular aspects of drug transport in the kidney. Kidney Int 58: 944-958.

ITO K. 2008. ABCC2/Abcc2 transport property in different species and its modulation by heterogeneous factors. Drug Metab Pharmacokinet 23: 394-405.

IZZEDINE H, LAUNAY-VACHER V AND DERAY G. 2005. Antiviral drug-induced nephrotoxicity. Am J Kidney Dis 45: 804-817.

JANG KJ, MEHR AP, HAMILTON GA, MCPARTLIN LA, CHUNG S, SUH KY AND INGBER DE. 2013. Human kidney proximal tubule-on-a-chip for drug transport and nephrotoxicity assessment. Integr Biol (Camb) 5: 1119-1129.

JANSEN J, SCHOPHUIZEN CM, WILMER MJ, LAHHAM SH, MUTSAERS HA, WETZELS JF, BANK RA, VAN DEN HEUVEL LP, HOENDEROP JG AND MASEREEUW R. 2014. A morphological and functional comparison of proximal tubule cell lines established from human urine and kidney tissue. Exp Cell Res 323: 87-99.

JEDLITSCHKY G, HOFFMANN U AND KROEMER HK. 2006. Structure and function of the MRP2 (ABCC2) protein and its role in drug disposition. Expert Opin Drug Metab Toxicol 2: 351-366.

JENKINSON SE, CHUNG GW, VAN LOON E, BAKAR NS, DALZELL AM AND BROWN CD. 2012. The limitations of renal epithelial cell line HK-2 as a model of drug transporter expression and function in the proximal tubule. Pflugers Arch 464: 601-611.

JENNINGS P ET AL. 2012. Transcriptomic alterations induced by Ochratoxin A in rat and human renal proximal tubular in vitro models and comparison to a rat in vivo model. Arch Toxicol 86: 571-589.

JIA HY ET AL. 2015. Early kidney injury during long-term adefovir dipivoxil therapy for chronic hepatitis B. World J Gastroenterol 21: 3657-3662.

JONG NN, NAKANISHI T, LIU JJ, TAMAI I AND MCKEAGE MJ. 2011. Oxaliplatin transport mediated by organic cation/carnitine transporters OCTN1 and OCTN2 in overexpressing human embryonic kidney 293 cells and rat dorsal root ganglion neurons. J Pharmacol Exp Ther 338: 537-547.

KAKUDA TN. 2000. Pharmacology of nucleoside and nucleotide reverse transcriptase inhibitor-induced mitochondrial toxicity. Clin Ther 22: 685-708.

KAMALIAN L, CHADWICK AE, BAYLISS M, FRENCH NS, MONSHOUWER M, SNOEYS J AND PARK BK. 2015. The utility of HepG2 cells to identify direct mitochondrial dysfunction in the absence of cell death. Toxicol In Vitro 29: 732-740.

KEMPER K ET AL. 2010. The AC133 epitope, but not the CD133 protein, is lost upon cancer stem cell differentiation. Cancer Res 70: 719-729.

KIM M, TURNQUIST H, JACKSON J, SGAGIAS M, YAN Y, GONG M, DEAN M, SHARP JG AND COWAN K. 2002. The multidrug resistance transporter ABCG2 (breast cancer resistance protein 1) effluxes Hoechst 33342 and is overexpressed in hematopoietic stem cells. Clin Cancer Res 8: 22-28.

KNOPS N, VAN DEN HEUVEL LP, MASEREEUW R, BONGAERS I, DE LOOR H, LEVTCHENKO E AND KUYPERS D. 2015. The functional implications of common genetic variation in CYP3A5 and ABCB1 in human proximal tubule cells. Mol Pharm 12: 758-768.

KOBAYASHI A, VALERIUS MT, MUGFORD JW, CARROLL TJ, SELF M, OLIVER G AND MCMAHON AP. 2008. Six2 defines and regulates a multipotent self-renewing nephron progenitor population throughout mammalian kidney development. Cell Stem Cell 3: 169-181.

KOHLER JJ, HOSSEINI SH, HOYING-BRANDT A, GREEN E, JOHNSON DM, RUSS R, TRAN D, RAPER CM, SANTOIANNI R AND LEWIS W. 2009. Tenofovir renal toxicity targets mitochondria of renal proximal tubules. Lab Invest 89: 513-519.

KOWOLIK CM, LIANG S, YU Y AND YEE JK. 2004. Cre-mediated reversible immortalization of human renal proximal tubular epithelial cells. Oncogene 23: 5950-5957.

KOYAMA H, GOODPASTURE C, MILLER MM, TEPLITZ RL AND RIGGS AD. 1978. Establishment and characterization of a cell line from the American opossum (Didelphys virginiana). In Vitro 14: 239-246.

KREIDBERG JA. 2010. WT1 and kidney progenitor cells. Organogenesis 6: 61-70.

KRTIL J, PLATENIK J, KAZDEROVA M, TESAR V AND ZIMA T. 2007. Culture methods of glomerular podocytes. Kidney Blood Press Res 30: 162-174.

KUO KL, ZHU H, MCNAMARA PJ AND LEGGAS M. 2012. Localization and functional characterization of the rat Oatp4c1 transporter in an in vitro cell system and rat tissues. PLoS One 7: e39641.

LASH LH, PUTT DA AND CAI H. 2006. Membrane transport function in primary cultures of human proximal tubular cells. Toxicology 228: 200-218.

LAWRENCE ML, CHANG CH AND DAVIES JA. 2015. Transport of organic anions and cations in murine embryonic kidney development and in serially-reaggregated engineered kidneys. Sci Rep 5: 9092.

LAZZERI E ET AL. 2015. Human Urine-Derived Renal Progenitors for Personalized Modeling of Genetic Kidney Disorders. J Am Soc Nephrol 26: 1961-1974.

LEE W AND KIM RB. 2004. Transporters and renal drug elimination. Annu Rev Pharmacol Toxicol 44: 137-166.

LEVY MN, BERNE RM, KOEPPEN BM AND STANTON BA 2006. Berne & Levy Principles of Physiology. Elsevier Mosby.

LIANG M, RAMSEY CR AND KNOX FG. 1999. The paracellular permeability of opossum kidney cells, a proximal tubule cell line. Kidney Int 56: 2304-2308.

LINDER D. 1976. Culture of cells from the urine and bladder washings of adults. Somatic Cell Genet 2: 281-283.

LINDGREN D ET AL. 2011. Isolation and characterization of progenitor-like cells from human renal proximal tubules. Am J Pathol 178: 828-837.

LOPEZ-NOVOA JM, QUIROS Y, VICENTE L, MORALES AI AND LOPEZ-HERNANDEZ FJ. 2011. New insights into the mechanism of aminoglycoside nephrotoxicity: an integrative point of view. Kidney Int 79: 33-45.

LOUIS N, EVELEGH C AND GRAHAM FL. 1997. Cloning and sequencing of the cellular-viral junctions from the human adenovirus type 5 transformed 293 cell line. Virology 233: 423-429.

MA T, YANG B, GILLESPIE A, CARLSON EJ, EPSTEIN CJ AND VERKMAN AS. 1998. Severely impaired urinary concentrating ability in transgenic mice lacking aquaporin-1 water channels. J Biol Chem 273: 4296-4299.

MAACK T. 1975. Renal handling of low molecular weight proteins. Am J Med 58: 57-64.

MALSTROM K, STANGE G AND MURER H. 1987. Identification of proximal tubular transport functions in the established kidney cell line, OK. Biochim Biophys Acta 902: 269-277.

MANDIKOVA J, VOLKOVA M, PAVEK P, CESNEK M, JANEBA Z, KUBICEK V AND TREJTNAR F. 2013. Interactions with selected drug renal transporters and transporter-mediated

cytotoxicity in antiviral agents from the group of acyclic nucleoside phosphonates. Toxicology 311: 135-146.

MARROQUIN LD, HYNES J, DYKENS JA, JAMIESON JD AND WILL Y. 2007. Circumventing the Crabtree effect: replacing media glucose with galactose increases susceptibility of HepG2 cells to mitochondrial toxicants. Toxicol Sci 97: 539-547.

MASSART C, LE TELLIER C, GIBASSIER J, LECLECH G AND NICOL M. 1993. Modulation by dimethyl sulphoxide of the toxicity induced by cis-diamminedichloroplatinum in cultured thyrocytes. Toxicol In Vitro 7: 87-94.

MATSUI F, RHEE A, HILE KL, ZHANG H AND MELDRUM KK. 2013. IL-18 induces profibrotic renal tubular cell injury via STAT3 activation. Am J Physiol Renal Physiol 305: F1014-1021.

MATSUI J, WAKABAYASHI T, ASADA M, YOSHIMATSU K AND OKADA M. 2004. Stem cell factor/c-kit signaling promotes the survival, migration, and capillary tube formation of human umbilical vein endothelial cells. J Biol Chem 279: 18600-18607.

MCKEE EE, FERGUSON M, BENTLEY AT AND MARKS TA. 2006. Inhibition of mammalian mitochondrial protein synthesis by oxazolidinones. Antimicrob Agents Chemother 50: 2042-2049.

MCKIM JM, JR. 2010. Building a tiered approach to in vitro predictive toxicity screening: a focus on assays with in vivo relevance. Comb Chem High Throughput Screen 13: 188-206.

MEKAHLI D ET AL. 2012. Polycystin-1 and polycystin-2 are both required to amplify inositol-trisphosphate-induced Ca2+ release. Cell Calcium 51: 452-458.

MENENDEZ-ARIAS L, ALVAREZ M AND PACHECO B. 2014. Nucleoside/nucleotide analog inhibitors of hepatitis B virus polymerase: mechanism of action and resistance. Curr Opin Virol 8: 1-9.

MIKKAICHI T ET AL. 2004. Isolation and characterization of a digoxin transporter and its rat homologue expressed in the kidney. Proc Natl Acad Sci U S A 101: 3569-3574.

MOLLET G ET AL. 2009. Podocin inactivation in mature kidneys causes focal segmental glomerulosclerosis and nephrotic syndrome. J Am Soc Nephrol 20: 2181-2189.

MOTOHASHI H, SAKURAI Y, SAITO H, MASUDA S, URAKAMI Y, GOTO M, FUKATSU A, OGAWA O AND INUI K. 2002. Gene expression levels and immunolocalization of organic ion transporters in the human kidney. J Am Soc Nephrol 13: 866-874.

MUNDEL P, HEID HW, MUNDEL TM, KRUGER M, REISER J AND KRIZ W. 1997a. Synaptopodin: an actin-associated protein in telencephalic dendrites and renal podocytes. J Cell Biol 139: 193-204.

MUNDEL P, REISER J AND KRIZ W. 1997b. Induction of differentiation in cultured rat and human podocytes. J Am Soc Nephrol 8: 697-705.

MUNDLOS S, PELLETIER J, DARVEAU A, BACHMANN M, WINTERPACHT A AND ZABEL B. 1993. Nuclear localization of the protein encoded by the Wilms' tumor gene WT1 in embryonic and adult tissues. Development 119: 1329-1341.

NADANACIVA S AND WILL Y. 2011. New insights in drug-induced mitochondrial toxicity. Curr Pharm Des 17: 2100-2112.

NAGAI J AND TAKANO M. 2010. Molecular-targeted approaches to reduce renal accumulation of nephrotoxic drugs. Expert Opin Drug Metab Toxicol 6: 1125-1138.

NARAYANAN K, SCHUMACHER KM, TASNIM F, KANDASAMY K, SCHUMACHER A, NI M, GAO S, GOPALAN B, ZINK D AND YING JY. 2013. Human embryonic stem cells differentiate into functional renal proximal tubular-like cells. Kidney Int 83: 593-603.

NAUGHTON CA. 2008. Drug-induced nephrotoxicity. Am Fam Physician 78: 743-750.

NIELSEN S, KWON TH, CHRISTENSEN BM, PROMENEUR D, FROKIAER J AND MARPLES D. 1999. Physiology and pathophysiology of renal aquaporins. J Am Soc Nephrol 10: 647-663.

NIESKENS TT ET AL. 2016. A Human Renal Proximal Tubule Cell Line with Stable Organic Anion Transporter 1 and 3 Expression Predictive for Antiviral-Induced Toxicity. AAPS J 18: 465-475.

NOTENBOOM S, WOUTERSE AC, PETERS B, KUIK LH, HEEMSKERK S, RUSSEL FG AND MASEREEUW R. 2006. Increased apical insertion of the multidrug resistance protein 2 (MRP2/ABCC2) in renal proximal tubules following gentamicin exposure. J Pharmacol Exp Ther 318: 1194-1202.

OBERMULLER N, BERNSTEIN P, VELAZQUEZ H, REILLY R, MOSER D, ELLISON DH AND BACHMANN S. 1995. Expression of the thiazide-sensitive Na-Cl cotransporter in rat and human kidney. Am J Physiol 269: F900-910.

OLIVEIRA ARCOLINO F, TORT PIELLA, A., PAPADIMITRIOU E, BUSSOLATI B, ANTONIE DJ, MURRAY P, VAN DEN HEUVEL L AND LEVTCHENKO E. 2015. Human Urine as a Noninvasive Source of Kidney Cells. Stem Cells Int 2015: 362562.

OLSON H ET AL. 2000. Concordance of the toxicity of pharmaceuticals in humans and in animals. Regulatory toxicology and pharmacology : RTP 32: 56-67.

OROSZ DE ET AL. 2004. Growth, immortalization, and differentiation potential of normal adult human proximal tubule cells. In Vitro Cell Dev Biol Anim 40: 22-34.

PEETERS K, WILMER MJ, SCHOEBER JP, REIJNDERS D, HEUVEL LP, MASEREEUW R AND LEVTCHENKO E. 2011. Role of p-glycoprotein expression and function in cystinotic renal proximal tubular cells. Pharmaceutics 3: 782-792.

PERANTONI A AND BERMAN JJ. 1979. Properties of Wilms' tumor line (TuWi) and pig kidney line (LLC-PK1) typical of normal kidney tubular epithelium. In Vitro 15: 446-454.

PFALLER W AND GSTRAUNTHALER G. 1998. Nephrotoxicity testing in vitro--what we know and what we need to know. Environ Health Perspect 106 Suppl 2: 559-569.

PICARD M, SHIRIHAI OS, GENTIL BJ AND BURELLE Y. 2013. Mitochondrial morphology transitions and functions: implications for retrograde signaling? Am J Physiol Regul Integr Comp Physiol 304: R393-406.

QADIR M, O'LOUGHLIN KL, FRICKE SM, WILLIAMSON NA, GRECO WR, MINDERMAN H AND BAER MR. 2005. Cyclosporin A is a broad-spectrum multidrug resistance modulator. Clin Cancer Res 11: 2320-2326.

RACUSEN LC, FIVUSH BA, ANDERSSON H AND GAHL WA. 1991. Culture of renal tubular cells from the urine of patients with nephropathic cystinosis. J Am Soc Nephrol 1: 1028-1033.

RACUSEN LC, WILSON PD, HARTZ PA, FIVUSH BA AND BURROW CR. 1995. Renal proximal tubular epithelium from patients with nephropathic cystinosis: immortalized cell lines as in vitro model systems. Kidney Int 48: 536-543.

RAHMOUNE H, THOMPSON PW, WARD JM, SMITH CD, HONG G AND BROWN J. 2005. Glucose transporters in human renal proximal tubular cells isolated from the urine of patients with non-insulin-dependent diabetes. Diabetes 54: 3427-3434.

RANGHINI E, FUENTE MORA C, EDGAR D, KENNY SE, MURRAY P AND WILM B. 2013. Stem cells derived from neonatal mouse kidney generate functional proximal tubule-like cells and integrate into developing nephrons in vitro. PLoS One 8: e62953.

RASBACH KA AND SCHNELLMANN RG. 2007. Signaling of mitochondrial biogenesis following oxidant injury. J Biol Chem 282: 2355-2362.

RAY AS, CIHLAR T, ROBINSON KL, TONG L, VELA JE, FULLER MD, WIEMAN LM, EISENBERG EJ AND RHODES GR. 2006. Mechanism of active renal tubular efflux of tenofovir. Antimicrob Agents Chemother 50: 3297-3304.

REITZER LJ WB, KENNELL D. 1979. Evidence that glutamine, not sugar, is the major energy source for cultured HeLa cells*. The Journal of Biological Chemistry 254: 2669-2676.

ROBINSON KM, JANES MS, PEHAR M, MONETTE JS, ROSS MF, HAGEN TM, MURPHY MP AND BECKMAN JS. 2006. Selective fluorescent imaging of superoxide in vivo using ethidium-based probes. Proc Natl Acad Sci U S A 103: 15038-15043.

RODRIGUEZ-ENRIQUEZ S, JUAREZ O, RODRIGUEZ-ZAVALA JS AND MORENO-SANCHEZ R. 2001. Multisite control of the Crabtree effect in ascites hepatoma cells. Eur J Biochem 268: 2512-2519.

RODRIGUEZ-NOVOA S, ALVAREZ E, LABARGA P AND SORIANO V. 2010. Renal toxicity associated with tenofovir use. Expert Opin Drug Saf 9: 545-559.

ROMAGNANI P, LASAGNI L AND REMUZZI G. 2013. Renal progenitors: an evolutionary conserved strategy for kidney regeneration. Nat Rev Nephrol 9: 137-146.

ROMAGNANI P AND REMUZZI G. 2014. CD133+ renal stem cells always co-express CD24 in adult human kidney tissue. Stem Cell Res 12: 828-829.

ROMITI N, TRAMONTI G AND CHIELI E. 2002. Influence of different chemicals on MDR-1 P-glycoprotein expression and activity in the HK-2 proximal tubular cell line. Toxicol Appl Pharmacol 183: 83-91.

RONCONI E ET AL. 2009. Regeneration of glomerular podocytes by human renal progenitors. J Am Soc Nephrol 20: 322-332.

ROSS MJ. 2014. Advances in the pathogenesis of HIV-associated kidney diseases. Kidney Int 86: 266-274.

ROSSIGNOL R, GILKERSON R, AGGELER R, YAMAGATA K, REMINGTON SJ AND CAPALDI RA. 2004. Energy substrate modulates mitochondrial structure and oxidative capacity in cancer cells. Cancer Res 64: 985-993.

RUSSEL FG, KOENDERINK JB AND MASEREEUW R. 2008. Multidrug resistance protein 4 (MRP4/ABCC4): a versatile efflux transporter for drugs and signalling molecules. Trends Pharmacol Sci 29: 200-207.

RYAN MJ, JOHNSON G, KIRK J, FUERSTENBERG SM, ZAGER RA AND TOROK-STORB B. 1994. HK-2: an immortalized proximal tubule epithelial cell line from normal adult human kidney. Kidney Int 45: 48-57.

SAKAIRI T, ABE Y, JAT PS AND KOPP JB. 2010a. Cell-cell contact regulates gene expression in CDK4-transformed mouse podocytes. Am J Physiol Renal Physiol 299: F802-809.

SAKAIRI T, ABE Y, KAJIYAMA H, BARTLETT LD, HOWARD LV, JAT PS AND KOPP JB. 2010b. Conditionally immortalized human podocyte cell lines established from urine. Am J Physiol Renal Physiol 298: F557-567.

SALEEM MA, O'HARE MJ, REISER J, COWARD RJ, INWARD CD, FARREN T, XING CY, NI L, MATHIESON PW AND MUNDEL P. 2002. A conditionally immortalized human podocyte cell line demonstrating nephrin and podocin expression. J Am Soc Nephrol 13: 630-638.

SCHARENBERG CW, HARKEY MA AND TOROK-STORB B. 2002. The ABCG2 transporter is an efficient Hoechst 33342 efflux pump and is preferentially expressed by immature human hematopoietic progenitors. Blood 99: 507-512.

SCHINKEL AH AND JONKER JW. 2003. Mammalian drug efflux transporters of the ATP binding cassette (ABC) family: an overview. Adv Drug Deliv Rev 55: 3-29.

SCHMITT S ET AL. 2013. A semi-automated method for isolating functionally intact mitochondria from cultured cells and tissue biopsies. Anal Biochem 443: 66-74.

SCHON EA, DIMAURO S AND HIRANO M. 2012. Human mitochondrial DNA: roles of inherited and somatic mutations. Nat Rev Genet 13: 878-890.

SERVAIS H, ORTIZ A, DEVUYST O, DENAMUR S, TULKENS PM AND MINGEOT-LECLERCQ MP. 2008. Renal cell apoptosis induced by nephrotoxic drugs: cellular and molecular mechanisms and potential approaches to modulation. Apoptosis 13: 11-32.

SHANKLAND SJ, PIPPIN JW, REISER J AND MUNDEL P. 2007. Podocytes in culture: past, present, and future. Kidney Int 72: 26-36.

SHAPIRO AB, CORDER AB AND LING V. 1997. P-glycoprotein-mediated Hoechst 33342 transport out of the lipid bilayer. Eur J Biochem 250: 115-121.

SHAW G, MORSE S, ARARAT M AND GRAHAM FL. 2002. Preferential transformation of human neuronal cells by human adenoviruses and the origin of HEK 293 cells. FASEB J 16: 869-871.

SHIRASAWA T, AKASHI T, SAKAMOTO K, TAKAHASHI H, MARUYAMA N AND HIROKAWA K. 1993. Gene expression of CD24 core peptide molecule in developing brain and developing non-neural tissues. Dev Dyn 198: 1-13.

SIDAWAY JE, DAVIDSON RG, MCTAGGART F, ORTON TC, SCOTT RC, SMITH GJ AND BRUNSKILL NJ. 2004. Inhibitors of 3-hydroxy-3-methylglutaryl-CoA reductase reduce receptor-mediated endocytosis in opossum kidney cells. J Am Soc Nephrol 15: 2258-2265.

SOHN SJ, KIM SY, KIM HS, CHUN YJ, HAN SY, KIM SH AND MOON A. 2013. In vitro evaluation of biomarkers for cisplatin-induced nephrotoxicity using HK-2 human kidney epithelial cells. Toxicology letters 217: 235-242.

SONG MN, HONG MZ, LUO DQ, HUANG WQ, MIN F, FAN RH, WU WB AND ZHANG L. 2012. Efficacy of 3 years of adefovir monotherapy in chronic hepatitis B patients with lamivudine resistance. World J Hepatol 4: 389-393.

SPROWL JA, GREGORC V, LAZZARI C, MATHIJSSEN RH, LOOS WJ AND SPARREBOOM A. 2012. Associations between ABCC2 polymorphisms and cisplatin disposition and efficacy. Clin Pharmacol Ther 91: 1022-1026.

SUEN DF, NORRIS KL AND YOULE RJ. 2008. Mitochondrial dynamics and apoptosis. Genes Dev 22: 1577-1590.

SUN SY. 2010. N-acetylcysteine, reactive oxygen species and beyond. Cancer Biol Ther 9: 109-110.

SUTHERLAND GR AND BAIN AD. 1972. Culture of cells from the urine of newborn children. Nature 239: 231.

SWEET DH, MILLER DS, PRITCHARD JB, FUJIWARA Y, BEIER DR AND NIGAM SK. 2002. Impaired organic anion transport in kidney and choroid plexus of organic anion transporter 3 (Oat3 (Slc22a8)) knockout mice. J Biol Chem 277: 26934-26943.

SWISS R, NILES A, CALI JJ, NADANACIVA S AND WILL Y. 2013. Validation of a HTS-amenable assay to detect drug-induced mitochondrial toxicity in the absence and presence of cell death. Toxicol In Vitro 27: 1789-1797.

TABER SS AND PASKO DA. 2008. The epidemiology of drug-induced disorders: the kidney. Expert Opin Drug Saf 7: 679-690.

TAKANO M, NAGAI J, YASUHARA M AND INUI K. 1996. Regulation of p-aminohippurate transport by protein kinase C in OK kidney epithelial cells. Am J Physiol 271: F469-475.

TANJI N, TANJI K, KAMBHAM N, MARKOWITZ GS, BELL A AND D'AGATI V D. 2001. Adefovir nephrotoxicity: possible role of mitochondrial DNA depletion. Hum Pathol 32: 734-740.

THIEBAUT F, TSURUO T, HAMADA H, GOTTESMAN MM, PASTAN I AND WILLINGHAM MC. 1987. Cellular localization of the multidrug-resistance gene product P-glycoprotein in normal human tissues. Proc Natl Acad Sci U S A 84: 7735-7738.

THOMAS P AND SMART TG. 2005. HEK293 cell line: a vehicle for the expression of recombinant proteins. J Pharmacol Toxicol Methods 51: 187-200.

TRAMONTI G, ROMITI N, NORPOTH M AND CHIELI E. 2001. P-glycoprotein in HK-2 proximal tubule cell line. Ren Fail 23: 331-337.

TURNER RM, PARK BK AND PIRMOHAMED M. 2015. Parsing interindividual drug variability: an emerging role for systems pharmacology. Wires Syst Biol Med 7: 221-241.

UWAI Y, IDA H, TSUJI Y, KATSURA T AND INUI K. 2007. Renal transport of adefovir, cidofovir, and tenofovir by SLC22A family members (hOAT1, hOAT3, and hOCT2). Pharm Res 24: 811-815.

VAIDYA VS ET AL. 2010. Kidney injury molecule-1 outperforms traditional biomarkers of kidney injury in preclinical biomarker qualification studies. Nature biotechnology 28: 478-485.

VALLE R AND HARAGSIM L. 2006. Nephrotoxicity as a complication of antiretroviral therapy. Adv Chronic Kidney Dis 13: 314-319.

VENKATACHALAM MA, BERNARD DB, DONOHOE JF AND LEVINSKY NG. 1978. Ischemic damage and repair in the rat proximal tubule: differences among the S1, S2, and S3 segments. Kidney Int 14: 31-49.

VERHULST A, D'HAESE PC AND DE BROE ME. 2004. Inhibitors of HMG-CoA reductase reduce receptor-mediated endocytosis in human kidney proximal tubular cells. J Am Soc Nephrol 15: 2249-2257.

VIGANO M, LAMPERTICO P AND COLOMBO M. 2011. Drug safety evaluation of adefovir in HBV infection. Expert Opin Drug Saf 10: 809-818.

VLAMING ML, LAGAS JS AND SCHINKEL AH. 2009. Physiological and pharmacological roles of ABCG2 (BCRP): recent findings in Abcg2 knockout mice. Adv Drug Deliv Rev 61: 14-25.

VOGETSEDER A, PICARD N, GASPERT A, WALCH M, KAISSLING B AND LE HIR M. 2008. Proliferation capacity of the renal proximal tubule involves the bulk of differentiated epithelial cells. Am J Physiol Cell Physiol 294: C22-28.

WANG D AND LIPPARD SJ. 2005. Cellular processing of platinum anticancer drugs. Nat Rev Drug Discov 4: 307-320.

WANG Q, LU Y AND MORRIS ME. 2007. Monocarboxylate transporter (MCT) mediates the transport of gamma-hydroxybutyrate in human kidney HK-2 cells. Pharm Res 24: 1067-1078.

WANG T. 2006. Flow-activated transport events along the nephron. Curr Opin Nephrol Hypertens 15: 530-536.

WEINBERG JM AND MOLITORIS BA. 2009. Illuminating mitochondrial function and dysfunction using multiphoton technology. J Am Soc Nephrol 20: 1164-1166.

WEISS J, THEILE D, KETABI-KIYANVASH N, LINDENMAIER H AND HAEFELI WE. 2007. Inhibition of MRP1/ABCC1, MRP2/ABCC2, and MRP3/ABCC3 by nucleoside, nucleotide, and non-nucleoside reverse transcriptase inhibitors. Drug Metab Dispos 35: 340-344.

WIESER M, STADLER G, JENNINGS P, STREUBEL B, PFALLER W, AMBROS P, RIEDL C, KATINGER H, GRILLARI J AND GRILLARI-VOGLAUER R. 2008. hTERT alone immortalizes epithelial cells of renal proximal tubules without changing their functional characteristics. Am J Physiol Renal Physiol 295: F1365-1375.

WILMER MJ, KLUIJTMANS LA, VAN DER VELDEN TJ, WILLEMS PH, SCHEFFER PG, MASEREEUW R, MONNENS LA, VAN DEN HEUVEL LP AND LEVTCHENKO EN. 2011. Cysteamine restores glutathione redox status in cultured cystinotic proximal tubular epithelial cells. Biochim Biophys Acta 1812: 643-651.

WILMER MJ, SALEEM MA, MASEREEUW R, NI L, VAN DER VELDEN TJ, RUSSEL FG, MATHIESON PW, MONNENS LA, VAN DEN HEUVEL LP AND LEVTCHENKO EN. 2010. Novel conditionally immortalized human proximal tubule cell line expressing functional influx and efflux transporters. Cell Tissue Res 339: 449-457.

WILMES A ET AL. 2013. Application of integrated transcriptomic, proteomic and metabolomic profiling for the delineation of mechanisms of drug induced cell stress. Journal of proteomics 79: 180-194.

WITZGALL R. 2008. Are renal proximal tubular epithelial cells constantly prepared for an emergency? Focus on "the proliferation capacity of the renal proximal tubule involves the bulk of differentiated epithelial cells". Am J Physiol Cell Physiol 294: C1-3.

WRIGHT EM. 2001. Renal Na(+)-glucose cotransporters. Am J Physiol Renal Physiol 280: F10-18.

WU S, LIU Y, BHARADWAJ S, ATALA A AND ZHANG Y. 2011. Human urine-derived stem cells seeded in a modified 3D porous small intestinal submucosa scaffold for urethral tissue engineering. Biomaterials 32: 1317-1326.

WU XR, KONG XP, PELLICER A, KREIBICH G AND SUN TT. 2009. Uroplakins in urothelial biology, function, and disease. Kidney Int 75: 1153-1165.

YAMAGUCHI H, SUGIE M, OKADA M, MIKKAICHI T, TOYOHARA T, ABE T, GOTO J, HISHINUMA T, SHIMADA M AND MANO N. 2010. Transport of estrone 3-sulfate mediated by organic anion transporter OATP4C1: estrone 3-sulfate binds to the different recognition site for digoxin in OATP4C1. Drug Metab Pharmacokinet 25: 314-317.

YAO X, PANICHPISAL K, KURTZMAN N AND NUGENT K. 2007. Cisplatin nephrotoxicity: a review. Am J Med Sci 334: 115-124.

ZENNARO C, ARTERO M, DI MASO V AND CARRARO M. 2014. Small molecule membrane transporters in the mammalian podocyte: a pathogenic and therapeutic target. Int J Mol Sci 15: 21366-21380.

ZHAI XY, NIELSEN R, BIRN H, DRUMM K, MILDENBERGER S, FREUDINGER R, MOESTRUP SK, VERROUST PJ, CHRISTENSEN EI AND GEKLE M. 2000. Cubilin- and megalin-mediated uptake of albumin in cultured proximal tubule cells of opossum kidney. Kidney Int 58: 1523-1533.

ZHANG D, WEI G, LI P, ZHOU X AND ZHANG Y. 2014. Urine-derived stem cells: A novel and versatile progenitor source for cell-based therapy and regenerative medicine. Genes Dis 1: 8-17.

ZHANG QJ, HE J, NI W, LIN X, YAO XP, LIN MT, MURONG SX, WANG N AND CHEN WJ. 2013. Noninvasive urine-derived cell lines derived from neurological genetic patients. Neuroreport 24: 161-166.

ZHANG X, WANG R, PIOTROWSKI M, ZHANG H AND LEACH KL. 2015. Intracellular concentrations determine the cytotoxicity of adefovir, cidofovir and tenofovir. Toxicol In Vitro 29: 251-258.

ZHANG Y, MCNEILL E, TIAN H, SOKER S, ANDERSSON KE, YOO JJ AND ATALA A. 2008. Urine derived cells are a potential source for urological tissue reconstruction. J Urol 180: 2226-2233.

ZHOU T ET AL. 2012. Generation of human induced pluripotent stem cells from urine samples. Nat Protoc 7: 2080-2089.

ZHOU T ET AL. 2011. Generation of induced pluripotent stem cells from urine. J Am Soc Nephrol 22: 1221-1228.